Investigations into *Streptomyces azureus* Thiostrepton-resistance rRNA Methyltransferase and its Cognate Antibiotic

by

Pei Chun Hang

A thesis
presented to the University of Waterloo
in fulfillment of the
thesis requirement for the degree of
Doctor of Philosophy
in
Chemistry

Waterloo, Ontario, Canada, 2008

AUTHOR'S DECLARATION

I hereby declare that I am the sole author of this thesis. This is a true copy of the thesis, including any required final revisions, as accepted by my examiners.

I understand that my thesis may be made electronically available to the public.

ABSTRACT

Thiostrepton (TS: TS; $C_{72}H_{85}N_{19}O_{18}S_5$) is a thiazoline antibiotic that is effective against Gram-positive bacteria and the malarial parasite, *Plasmodium falciparum*. Tight binding of TS to the bacterial L11-23S ribosomal RNA (rRNA) complex of the large 50S ribosomal unit inhibits protein biosynthesis. The TS producing organism, *Streptomyces azureus*, biosynthesizes thiostrepton-resistance methyltransferase (TSR), an enzyme that uses *S*-adenosyl-L-methionine (AdoMet) as a methyl donor, to modify the TS target site. Methylation of A1067 (*Escherichia coli* ribosome numbering) by TSR circumvents TS binding.

The *S. azureus tsr* gene was overexpressed in *E. coli* and the protein purified for biochemical characterization. Although the recombinant protein was produced in a soluble form, its tendency to aggregate made handling a challenge during the initial stages of establishing a purification protocol. Different purification conditions were screened to generate an isolation protocol that yields milligram quantities of protein with little aggregation and sufficient purity for crystallographic studies.

Enzymological characterization of TSR was carried out using an assay to monitor AdoMet-dependent ([methyl-^{3}H]-AdoMet) methylation of the rRNA substrate by liquid scintillation counting. During the optimization of assay, it was found that, although this method is frequently employed, it is very time and labour intensive. A scintillation proximity assay was investigated to evaluate whether it could be a method for collecting kinetic data, and was found that further optimization is required.

Comparative sequence analysis of TSR has shown it to be a member of the novel Class IV SpoUT family of AdoMet-dependent MTases. Members of this class possess a non-

canonical AdoMet binding site containing a deep trefoil knot. Selected SpoUT family proteins were used as templates to develop a TSR homology model for monomeric and dimeric forms. Validation of the homology models was performed with structural validation servers and the model was then used as the basis of ongoing mutagenesis experiments.

The X-ray crystal structure of TSR bound with AdoMet (2.45 Å) was elucidated by our collaborators, Drs. Mark Dunstan and Graeme Conn (University of Manchester). This structure confirms TSR MTase's membership in the SpoUT MTase family with a deep trefoil knot in the catalytic domain. The AdoMet bound in the crystal structure is in an extended conformation not previously observed in SpoUT MTases. RNA docking simulations revealed some features that may be relevant to binding and recognition of TSR to the L11 binding domain of the RNA substrate.

Two structure-activity studies were conducted to investigate the TS-rRNA interaction and TS solubility. Computational analyses of TS conformations, molecular orbitals and dynamics provided insight into the possible modes of TS binding to rRNA. Single-site modification of TS was attempted, targeting the dehydroalanine and dehydrobutyrine residues of the antibiotic. These moieties were modified using the polar thiol, 2-mercaptoethanesulfonic acid (2-MESNA). Similar modifications had been previously used to improve solubility and bioavailability of antibiotics. The resulting analogue was structurally characterized (NMR and mass spectrometry) and showed antimicrobial activity against *Bacillus subtilis* and *Staphylococcus aureus*.

ACKNOWLEDGEMENTS

I would like to offer my sincerest gratitude to my supervisor, Dr. John Honek, for his constant support and guidance. Not only did he give his time and expertise generously, but his constant encouragement, motivation and faith in the most challenging times of this degree was a source of stability, hope and light for which I am forever appreciative. Thank you John.

I also wish to thank the members of my thesis advisory committee, Drs. Thorsten Dieckmann, Michael Palmer and Mario Monteiro, for their valuable advice and intellectual contributions to the development of my project and to my progress as a scientist. I would also like to thank Drs. Stephen Bearne and David Spafford for being on my examining committee.

Many thanks go to our collaborators at the University of Manchester, Drs. Mark Dunstan and Graeme Conn, for their contributions to the understanding of TSR. I am happy to see that our joint efforts have culminated into a beautiful X-ray crystal structure of TSR. I extend my deep appreciation to those who provided excellent technical assistance: Robyn Landers (computations), Dr. Richard Smith (mass spectrometry) and Jan Venne (NMR).

Warmest acknowledgements are due to members of the Honek laboratory, who provided an excellent network of knowledge, support and fun: Danish Khan, Dr. Christine Hand, Meijun Lu, Ignace Moya, Kadia Mullings, Cullen Myers, Dr. Nicole Sukdeo, Dr. Zhengding Su, Uthaiwan Suttisansanee, Dr. Mark Vaughan, Paula Walasek and Ronald Zahoruk. I would like to thank Dr. Elisabeth Daub in particular for her initial involvement in the construction of the TSR overexpression system. Also her friendly and wise advice about academic and non-academic matters was highly valuable. In addition, I would like to thank Grace Ng for her assistance in the TS antibiotic modifications.

I am also grateful for my friends that I have made over the years both in and outside the department; I cannot begin to express my gratitude and appreciation for their friendship: Thank you for being all the pillars, cheerleading squad and sounding boards that I have ever needed.

Finally, I would like to thank my family. The road to my graduate degree has been long and winding, and their presence helped make the completion of my graduate work possible. To my husband, Nevin: Your love, understanding and support have throughout this entire academic journey has been phenomenal. You have demonstrated rare and amazing patience. Words cannot describe how thankful I am to have you in my life. To my parents and brother: Thank you for your unconditional love - I owe you an eternal debt of thanks for your endless love and affection, your tireless efforts, and your unwavering belief in me throughout all my endeavours.

This thesis is dedicated to my loving parents,
Phat and Anh Hang,
For their love, endless support and encouragement

TABLE OF CONTENTS

LIST OF TABLES ..... **XVII**

LIST OF FIGURES ..... **XIX**

LIST OF ABBREVIATIONS ..... **XXIII**

CHAPTER 1: INTRODUCTION

1.1. *S*-ADENOSYL-L-METHIONINE **1**

1.1.1. STRUCTURE AND BIOCHEMISTRY OF *S*-ADENOSYL-L-METHIONINE (ADOMET) 1
1.1.2. ROLE OF *S*-ADENOSYL-L-METHIONINE (ADOMET) IN METHYLATION 2

1.2. *S*-ADENOSYL-L-METHIONINE-DEPENDENT METHYLTRANSFERASES **3**

1.2.1. CLASSIFICATION AND STRUCTURAL FOLDS 4
1.2.1.1. Class I: The Classical AdoMet-dependent MTase Fold *6*
1.2.1.2. Class II: B_{12}-dependent Methionine Synthase *8*
1.2.1.3. Class III: Methyltransferases Involved in Vitamin B_{12} Biosynthesis *9*
1.2.1.4. Class IV: The SpoUT MTases with a Deep Trefoil Knot *10*
1.2.1.5. Class V: The SET MTases – the Protein Lysine MTases *11*
1.2.2. CONFORMATION OF COFACTOR BINDING IN *S*-ADENOSYL-L-METHIONINE- DEPENDENT METHYLTRANSFERASES 13
1.2.3. INHIBITION OF *S*-ADENOSYL-L-METHIONINE-DEPENDENT METHYLTRANSFERASES 15

1.3. RRNA METHYLTRANSFERASES AND THEIR ROLE IN ANTIBIOTIC RESISTANCE **16**

1.3.1. ANTIBIOTICS AND ANTIBIOTIC RESISTANCE 16
1.3.2. METHYLATION AS A RESISTANCE MECHANISM: ERYTHROMYCIN RESISTANCE AS A PARADIGM 19
1.3.3. OTHER MTASES THAT CONFER ANTIBIOTIC RESISTANCE 22

1.4. THIOSTREPTON AND THIOSTREPTON RESISTANCE **23**

1.4.1. THE THIOPEPTIDE ANTIBIOTIC THIOSTREPTON 23
1.4.2. MODE OF ACTION OF THIOSTREPTON 24
1.4.3. MECHANISM OF RESISTANCE: THIOSTREPTON-RESISTANCE RRNA METHYLTRANSFERASE 27

1.5. RESEARCH OBJECTIVES **29**

CHAPTER 2: OVEREXPRESSION AND PURIFICATOIN OF *STREPTOMYCES AZUREUS* THIOSTREPTON-RESISTANCE RRNA METHYLTRANSFERASE

2.1. CLONING AND PURIFICATION OF HEXAHISTIDINE-TAGGED THIOSTREPTON RESISTANCE RRNA METHYLTRANSFERASE **32**

2.1.1. AFFINITY TAGS 33
2.1.2. REMOVAL OF AFFINITY TAGS 36
2.1.3. PURIFICATION WITH A HISTIDINE-TAGGED AFFINITY TAG 37
2.1.4. PLAN OF ACTION 39

2.2. MATERIALS AND METHODS **39**

2.2.1 REAGENTS AND MATERIALS 39

2.2.2 General Equipment 40
2.2.2.1. Cell Disruption Equipment *40*
2.2.2.2. Centrifuges *41*
2.2.2.3. Chromatographic Equipment *41*
2.2.2.4. Incubators *42*
2.2.2.5. Protein Concentration Devices *42*
2.2.2.6. Spectrophotometry *42*
2.2.2.7. Thermal Cyclers *43*
2.2.2.8. Mass Spectrometer *43*
2.2.3 General Experimental Protocols 43
2.2.3.1. Gel Electrophoresis *43*
2.2.3.2. DNA Manipulation and Cloning Methods *45*
2.2.3.3. Trichloroacetic Acid Precipitation *45*
2.2.3.4. Determination of Protein Concentration *46*
2.2.3.5. Mass Spectrometric Analysis *46*
2.2.4. Cloning of TSR into E. coli 47
2.2.5. Overexpression of TSR 50
2.2.5.1. Optimization of Overexpression of TSR in Rich Media *50*
2.2.5.2. Harvest of Induced Cells *50*
2.2.6. Purification of $(His)_6$-tagged TSR (HTSR) 51
2.2.6.1. Cell Lysis *51*
2.2.6.2. Purification of Hexahistidine-tagged TSR with IMAC *51*
2.2.7. Removal of $(His)_6$-tag from Recombinant TSR 53
2.2.7.1. Time Course on Thrombin Cleavage of Histag from TSR *53*
2.2.7.2. Thrombin Cleavage and Clean up of de-tagged TSR (TSR′) *54*
2.2.8. Further Purification of TSR′ 54
2.2.9. Gel Filtration Chromatography of TSR′ 55

2.3. RESULTS AND DISCUSSION 55

2.3.1. Expression of Recombinant Histagged-TSR in *E. coli* 55
2.3.2. Enhancing Purification Histagged-TSR in E. Coli After IMAC Purification 57
2.3.2.1. Batch Purification of TSR with Ni-NTA Superflow resin *57*
2.3.2.2. Enhancing TSR Solubility During Dialysis *59*
2.3.3. Removal of Hexahistidine tag from HTSR 64
2.3.4. Final step in TSR Purification 66
2.3.5. Gel Filtration of TSR′ 67

2.4. CONCLUSIONS AND FUTURE WORK 67

CHAPTER 3: BIOCHEMICAL CHARACTERIZATION OF *STREPTOMYCES AZUREUS* THIOSTREPTON-RESISTANCE RRNA METHYLTRANSFERASE

3.1. METHODS TO DETECT METHYL TRANSFER REACTIONS 70

3.1.1. Principles of Radiometric Filter Binding Assays 70
3.1.2. Scintillation Proximity Assay (SPA) Technology 71
3.1.3. Alternative Non-Radiometric Assay Methods for MTases 72
3.1.4. Plan of Action 74

3.2. MATERIALS AND METHODS 75

3.2.1. Reagents and Materials 75
3.2.2. General Equipment 76
3.2.2.1. Liquid Scintillation Counter *76*
3.2.2.2. Centrifuges *76*
3.2.2.3. Cell Disruption Equipment *76*

3.2.2.4. Chromatographic Equipment *76*
3.2.3 GENERAL EXPERIMENTAL PROTOCOLS 77
3.2.3.1. Minimization of RNAse Contamination *77*
3.2.3.2. Reducing Specific Activity of S-adenosyl-L-[methyl-^{3}H]-methionine *78*
3.2.4. FILTER BINDING ASSAY FOR TSR′ 78
3.2.4.1. TSR´Filter Binding Assay Refinement and Optimization *79*
3.2.4.2. Optimized TSR´Filter Binding Assay *82*
3.2.5. TOWARDS THE DEVELOPMENT OF A SCINTILLATION PROXIMITY ASSAY FOR TSR′ 83
3.2.5.1. Selection of SPA Bead Type *83*
3.2.5.2. TSR´SPA Refinement and Optimization *84*

3.3. RESULTS AND DISCUSSION 84

3.3.1. FILTER BINDING ASSAY FOR TSR′ 84
3.3.1.1. Refolding the Ribosomal RNA Substrate *85*
3.3.1.2. Enzyme Manipulations *86*
3.3.1.3. Refinment of Other Technical Assay Variables *89*
3.3.1.3. Evaluation of Kinetic Parameters of TSR´with Optimized Filter Binding Assay *94*
3.3.2. SCINTILLATION PROXIMITY ASSAY DEVELOPMENT FOR TSR′ 95
3.3.2.1. Selection of SPA Bead Type and Amount *96*
3.3.2.2. TSR´Refinement and Optimization *98*

3.4. CONCLUSIONS AND FUTURE WORK 104

CHAPTER 4: STRUCTURAL STUDIES OF THIOSTREPTON-RESISTANCE RRNA METHYLTRANSFERASE

4.1. HOMOLOGY MODELLING AS A STRATEGY TO STUDY TSR′ STRUCTURE 109

4.1.1. HOMOLOGY MODELLING: BASIC BACKGROUND AND METHODOLOGY 110
4.1.1.1. Selection of the Template Protein *111*
4.1.1.2. Target-Template Alignment *112*
4.1.1.3. Homology Model Building *112*
4.1.1.3. Evaluation of Model *113*
4.1.2. PLAN OF ACTION 114

4.2. MATERIALS AND METHODS 114

4.2.1 REAGENTS AND MATERIALS 114
4.2.2 GENERAL EQUIPMENT 115
4.2.2.1. Computational Hardware and Software *115*
4.2.2.2. Centrifuges *116*
4.2.2.3. Chromatographic Equipment *116*
4.2.2.4. Incubators *116*
4.2.2.5. Protein Concentration Devices *117*
4.2.2.6. Spectrophotometry *117*
4.2.2.7. Thermal Cyclers *117*
4.2.2.8. Mass Spectrometer *117*
4.2.3 GENERAL EXPERIMENTAL PROTOCOLS 118
4.2.3.1. Gel Electrophoresis *118*
4.2.3.2. DNA Manipulation and Cloning Methods *119*
4.2.3.3. Determination of Protein Concentration *119*
4.2.3.4. Mass Spectrometric Analysis *119*
4.2.4. HOMOLOGY MODEL DEVELOPMENT 120
4.2.4.1. Template Selection and Alignment *120*
4.2.4.2. Homology Model Building *122*

4.2.4.3. Refinement and Evaluation of Homology Models *124*
4.2.5. X-RAY CRYSTALLOGRAPHY OF TSR′ 127
4.2.5.1. Selenomethionine Incorporation into TSR *127*
4.2.5.2. Purification of SeMet TSR *128*
4.2.5.3. Sample Preparation for X-ray Crystallography *128*
4.2.5.4. Data Collection, Structure Determination and Refinement *129*
4.2.5.5. Modelling TSR-RNA Interactions *129*
4.2.6. SITE DIRECTED MUTAGENESIS 129
4.2.6.1. QuikChange *129*
4.2.6.2. SOE *131*
4.2.6.3. Expression and Purification of Mutants *133*

4.3. RESULTS AND DISCUSSION 134

4.3.1. HOMOLOGY MODEL DEVELOPMENT 134
4.3.1.1. Template Selection and Alignment *134*
4.3.1.2. Homology Model Construction *136*
4.3.1.3. Homology Model Refinement and Evaluation *139*
4.3.1.4. A Closer Examination of the Homology Models *147*
4.3.2. X-RAY CRYSTALLOGRAPHY OF TSR′ 151
4.3.2.1. Overall Structure of S. azureus TSR *151*
4.3.2.2. Structural Insights: RNA-TSR Interactions *157*
4.3.3. COMPARISON OF HOMOLOGY MODEL WITH X-RAY MODEL 162

4.4. CONCLUSIONS AND FUTURE WORK 165

CHAPTER 5: STRUCTURE-ACTIVITY STUDIES OF THIOSTREPTON

5.1. APPROACHES TO THE STUDY OF THIOSTREPTON 170

5.1.1. COMPUTATIONAL CHEMISTRY 170
5.1.1.1. Molecular Mechanics *171*
5.1.1.2. Ab initio Calculations *172*
5.1.1.3. Semi-empirical Methods *173*
5.1.2. MODIFICATION OF THIOSTREPTON 174
5.1.2.1. Development of Novel Antibiotics *174*
5.1.2.2. Modification of Nocathiacins: A Member of the Thiazole Peptide Antibiotics *176*
5.1.2.3. Semi-Synthesis of Thiostrepton Analogues *178*
5.1.3 PLAN OF ACTION 180

5.2. MATERIALS AND METHODS 181

5.2.1. REAGENTS AND MATERIALS 181
5.2.2. GENERAL EQUIPMENT 181
5.2.2.1. Computational Hardware and Software *181*
5.2.2.2. Chromatographic Equipment *182*
5.2.2.3. Mass Spectrometer *182*
5.2.2.4. Nuclear Magnetic Resonance (NMR) Spectrometer *182*
5.2.2.5. Incubators *183*
5.2.2.6. Spectrophotometry *183*
5.2.3. COMPUTATIONAL METHODS 183
5.2.3.1. Experimental TS Structure *183*
5.2.3.2. Geometry Optimizations of Thiostrepton *184*
5.2.3.3. Molecular Orbital and Ab Initio Charge Calculations *185*
5.2.3.4. Investigation into Conformational Flexibility of Thiostrepton *185*
5.2.4. MODIFICATION OF THIOSTREPTON WITH 2-MERCAPTOETHANESULFONIC ACID METHODS 186

5.2.4.1. General Procedure for the Michael Addition of 2-Mercaptoethanesulfonic acid (2-MESNA) to Thiostrepton *186*
5.2.4.2. Purification of Modified Thiostrepton (mTS-2MESNA) *187*
5.2.4.3. In vitro Susceptibility Test *189*

5.3. RESULTS AND DISCUSSION **191**

5.3.1. GEOMETRY OPTIMIZATIONS OF THIOSTREPTON 191
5.3.2. MOLECULAR ORBITAL AND AB INITIO CHARGE CALCULATIONS 195
5.3.3. CONFORMATIONAL FLEXIBILITY OF THIOSTREPTON 197
5.3.3.1. LMOD Conformational Search *197*
5.3.3.2. Stochastic Dynamics Studies *199*
5.3.4. MODIFICATION OF THIOSTREPTON 201
5.3.4.1. Reaction of Thiostrepton with 2-Mercaptoethanesulfonic Acid *201*
5.3.4.2. Purification of Thiostrepton Derivative (mTS-2MESNA) *203*
5.3.4.3. Susceptibility Testing of mTS-2MESNA *207*

5.4. CONCLUSIONS AND FUTURE WORK **211**

REFERENCES **215**

APPENDICES

APPENDIX 1: RADIOMETRIC ASSAY SUPPLEMENTARY INFORMATION

A1.1. REDUCING THE SPECIFIC ACTIVITY OF *S*-ADENOSYL-L-[METHYL-^{3}H]-METHIONINE **231**

A1.1.1. CALCULATING HOW MUCH NON-RADIOLABELLED ADOMET IS REQUIRED 231
A1.1.2. USING THE COLD ADOMET STOCK SOLUTION TO REDUCE SPECIFIC ACTIVITY 232
A.1.3. HOW MUCH ^{3}H-ADOMET*$_{REDUCED}$ TO BE ADDED TO EACH ASSAY TUBE 233
A1.1.4. CALCULATING THE CONCENTRATION OF [^{3}H]-ADOMET*$_{REDUCED}$ 233

A1.2. CONVERSION OF DISINTEGRATIONS PER MINUTE TO A MOLE QUANTITY **234**

APPENDIX 2: *S. AZUREUS* TSR PROTEIN STRUCTURE

A2.1. X-RAY DIFFRACTION DATA COLLECTION, STRUCTURE DETERMINATION AND REFINEMENT **235**

A2.2. MODELLING TSR-RNA INTERACTIONS **238**

APPENDIX 3: GEOMETRIC DISTORTIONS IN HOMOLOGY MODELS

A3.1. GEOMETRIC DISTORTIONS FOR *TSRMONOMER2* **239**

A3.2. GEOMETRIC DISTORTIONS FOR *PRIMETSR* **240**

A3.3. GEOMETRIC DISTORTIONS FOR TSRDIMER **241**

APPENDIX 4: MUTAGENESIS

A4.1. QUIKCHANGE™ SITE-DIRECTED MUTAGENESIS **243**

A4.2. SPLICING OVERLAP EXTENSION MUTAGENESIS **244**

A4.3. MASS SPECTRA OF TSR MUTANTS **245**

A4.3. PRELIMINARY CD AND DSC OF TSR MUTANTS.....248

APPENDIX 5: TS MODELLING SUPPLEMENT

A5.1. CONFORMATIONAL FLEXIBLITY OF THIOSTREPTON.....249
A5.2. ELECTRONIC STRUCTURE OF THIOSTREPTON.....250
A5.3. AM1-GEOMETRY OPTIMIZED THIOSTREPTON COORDINATES.....254

LIST OF TABLES

CHAPTER 1: INTRODUCTION

TABLE 1.1: KNOWN STRUCTURES OF ADOMET-DEPENDENT MTASES. 5
TABLE 1. 2: DIHEDRAL ANGLES OF ADOMET OR ADOHCY FOUND IN THE DIFFERENT CLASSES OF ADOMET-DEPENDENT MTASES. 13
TABLE 1. 3: COMPARISON OF *KM* VALUE FOR ADOMET AND *KI* VALUE OF ADOHCY/SAH FOR SELECTED MTASES. 15

CHAPTER 2: OVEREXPRESSION AND PURIFICATION OF *STREPTOMYCES AZUREUS* THIOSTREPTON-RESISTANCE RRNA METHYLTRANSFERASE

TABLE 2. 1: COMMON AFFINITY TAGS UTILIZED AND THEIR MATRICES. 35
TABLE 2. 2: DIFFERENT AGENTS UTILIZED TO REMOVE AFFINITY TAGS. 36
TABLE 2.3: DIFFERENT CONDITIONS SCREENED TO ENHANCE TSR SOLUBILITY DURING DIALYSIS. 52
TABLE 2.4: EFFECT OF DIFFERENT TYPES AND AMOUNTS OF KOSMOTROPES IN DIALYSIS BUFFER ON HTSR SOLUBILITY. 60
TABLE 2.5: EFFECT OF DIFFERENT TYPES OF THIOL-REDUCING AGENTS IN PURIFICATION BUFFERS ON HTSR SOLUBILITY. 61
TABLE 2.6: EFFECT OF PH AND TIME ON TSR SOLUBILITY. 61

CHAPTER 3: BIOCHEMICAL CHARACTERIZATION OF THIOSTREPTON-RESISTANCE RRNA METHYLTRANSFERASE

TABLE 3.1: DIFFERENT VARIABLES OF THE FILTER BINDING ASSAY OPTIMIZED. 79
TABLE 3.2: DIFFERENT VARIABLES OF THE SCINTILLATION PROXIMITY ASSAY OPTIMIZED. 84
TABLE 3.3: DIFFERENT COMBINATIONS OF FILTERS AND TCA PRECIPITATION CONDITIONS USED FOR OPTIMIZATION OF THE FILTER BINDING ASSAY. 91
TABLE 3. 4: KINETIC PARAMETERS FOR THE TSR′ CATALYZED METHYLATION OF 16S/23S RRNA. 94

CHAPTER 4: STRUCTURAL STUDIES OF THIOSTREPTON-RESISTANCE RRNA METHYLTRANSFERASE

TABLE 4.1: TEMPLATE STRUCTURES UTILIZED DURING COMPARATIVE MODELLING OF TSR$^{\delta}$. 135
TABLE 4. 2: LOCAL ENERGY MINIMA REACHED BY COMPARATIVE MODELS USING GROMOS96. 141
TABLE 4. 3: COMPARISON OF 3D-1D VERIFY 3D SCORE BETWEEN THE HOMOLOGY MODELS OF THE TSR MONOMER. 143
TABLE 4.4: DISTRIBUTION OF RESIDUES IN HOMOLOGY MODELS IN RAMACHANDRAN PLOTS. 145
TABLE 4.5: COMPARISON OF THE NUMBER OF GEOMETRIC DISTORTIONS IN THE MONOMERIC HOMOLOGY MODEL AS DETERMINED BY USING PROCHECK. 145
TABLE 4. 6: GLOBAL AND LOCAL RMSD BETWEEN COMPARATIVE MODELS AND THE CRYSTAL STRUCTURE BASED ON THEIR Cα ATOMS, BACKBONE, HEAVY ATOMS AND ALL ATOMS. 162
TABLE 4. 7: PROPOSED ROLES AND MUTATIONS FOR CONVERSED RESIDUES IN TSR HOMOLOGY MODELS. 164
TABLE 4. 8: LIST OF MUTANTS MADE SO FAR AND MOLECULAR WEIGHT CONFIRMATION BY MASS SPECTROMETRY. 165
TABLE 4. 9: ADDITIONAL IMPORTANT RESIDUES OF TSR IDENTIFIED BY THE CRYSTAL STRUCTURE. 165

CHAPTER 5: STRUCTURE-ACTIVITY STUDIES OF THIOSTREPTON

TABLE 5. 1: OPTIMIZATION OF MICHAEL ADDITION REACTIONS OF AMINES TO NOCATHIACIN I 178
TABLE 5. 2: CONCENTRATIONS UTILIZED FOR KIRBY-BAUER DISC DIFFUSION TEST FOR THIOSTREPTON AND ITS ANALOGUE. 190

TABLE 5. 3: CONCENTRATIONS USED FOR ANTIBACTERIAL SUSCEPTIBILITY TESTING FOR THIOSTREPTON AND ITS ANALOGUE. 191
TABLE 5. 4: THE NUMBER OF BONDS OF HIGH, MEDIUM AND LOW QUALITY BONDS CALCULATED FOR STRETCH/BEND/TORSIONAL PARAMETERS IN EACH FORCE FIELD AVAILABLE IN MACROMODEL 8.0. 191
TABLE 5. 5: SUMMARY OF REACTIONS CONDITIONS ATTEMPTED FOR THE MICHAEL ADDITION OF 2-MESNA TO TS AT ROOM TEMPERATURE. 203
TABLE 5. 6: SUMMARY OF REACTIONS CONDITIONS ATTEMPTED FOR THE MICHAEL ADDITION OF 203
TABLE 5. 7: INHIBITION ZONE DIAMETERS OF THIOSTREPTON AND ITS DERIVATIVE ON *B. SUBTILIS* AND *S. AUREUS*. 208

APPENDIX 1: RADIOMETRIC ASSAY SUPPLEMENTARY INFORMATION

TABLE A1. 1: INFORMATION ON RADIOLABELLED AND NON-RADIOLABELLED ADOMET 231

APPENDIX 2: S. AZUREUS TSR MTASE PROTEIN STRUCTURE

TABLE A2. 1: X-RAY DATA COLLECTION AND REFINEMENT STATISTICS FOR THE TSR-ADOMET COMPLEX. 237

APPENDIX 3: TS MODELLING SUPPLEMENT

TABLE A5. 1:MULLIKEN CHARGES DETERMINED BY AM1 AND B3LYP/6-31G(D), AND B3LYP/6-31G(D) CHELPG¥ ELECTROSTATIC FIT CHARGES ON THE AM1 GEOMETRY-OPTIMIZED STRUCTURE. 250
TABLE A5. 2: COORDINATES FOR THE AM1-GEOMETRY OPTIMIZED STRUCTURE OF THIOSTREPTON. 254

LIST OF FIGURES

CHAPTER 1: INTRODUCTION

FIGURE 1.1: BIOSYNTHESIS OF *S*-ADENOSYL-L-METHIONINE. 1
FIGURE 1.2: THE *S*-ADENOSYL-L-METHIONINE (ADOMET CYCLE). 3
FIGURE 1.3: CATECHOL *O*- METHYLTRANSFERASE IS A MEMBER OF THE CLASS I SUPERFAMILY RESEMBLING THE ROSSMANN PROTEINS. 6
FIGURE 1.4: THE C-TERMINAL, ADOMET BINDING DOMAIN OF METHIONINE SYNTHASE IS THE ONLY MEMBER OF THE CLASS II MTASES. 9
FIGURE 1.5: THE MONOMER OF A CLASS III MTASE: PRECORRIN-2 C^{20}- MTASE. 10
FIGURE 1.6: THE MONOMER OF A YIBK METHYLTRANSFERASE POSSESES A DEEP TREFOIL KNOT AT ITS ACTIVE SITE. 11
FIGURE 1.7: THE MONOMER OF A SET7/9 MTASE HAS A PSEUDO-KNOT IN THE C-TERMINUS. 12
FIGURE 1.8: THE STRUCTURE OF *S*-ADENOSYL-L-METHIONINE (ADOMET) AND THE DIHEDRAL ANGLES USED TO COMPARE COFACTOR BINDING IN DIFFERENT CLASSES OF MTASES. 13
FIGURE 1.9: BINDING OF COFACTOR ADOMET/ADOHCY AMONGST DIFFERENT CLASSES OF MTASE DEMONSTRATES CONFORMATIONAL FLEXIBILITY. 14
FIGURE 1. 10: NATURAL INHIBITORS OF ADOMET-DEPENDENT MTASE REACTIONS ARE STRUCTURAL ANALOGUES OF ADOMET. 16
FIGURE 1.11: THE FOUR MAJOR TARGETS OF ANTIBIOTICS AND ANTIMICROBIALS. 17
FIGURE 1.12: ANTIBIOTIC RESISTANCE MECHANISMS UTILIZED BY BACTERIA. 18
FIGURE 1.13: MACROLIDES BLOCK THE THE POLYPEPTIDE EXIT TUNNEL OF THE LARGE RIBOSOMAL UNIT. 21
FIGURE 1.14: EXAMPLES OF LINCOSAMIDES AND STREPTOGRAMIN BS. 22
FIGURE 1.15: THIOSTREPTON INHIBITS PROTEIN BIOSYNTHESIS BY BINDING TO THE GTPASE CENTRE OF THE RIBOSOME. 24
FIGURE 1. 16: SECONDARY STRUCTURE OF THE 23S RRNA IN THE GTPASE REGION. 25
FIGURE 1. 17: STEPS IN THE PEPTIDE ELONGATION CYCLE IN PROTEIN BIOSYNTHESIS. 26
FIGURE 1. 18: THIOSTREPTON BINDING TO THE L11BD. 27
FIGURE 1.19: RECOGNITION HAIRPIN ON 23S RRNA FOR TSR MTASE. 28

CHAPTER 2: OVEREXPRESSION AND PURIFICATION OF *STREPTOMYCES AZUREUS* THIOSTREPTON-RESISTANCE rRNA METHYLTRANSFERASE

FIGURE 2. 1: METHYLATION OF THE 2′-O HYDROXYL MOIETY OF A1067 OF THE 23S RRNA BY THIOSTREPTON-RESISTANCE RRNA METHYLTRANSFERASE (TSR). 31
FIGURE 2. 2: GENERAL OVERVIEW OF THE PURIFICATION OF A HISTIDINE-TAGGED PROTEIN AND ITS SUBSEQUENT REMOVAL. 38
FIGURE 2.3: *S. AZUREUS* THIOSTREPTON-RESISTANCE RRNA METHYLTRANSFERASE DNA AND PROTEIN SEQUENCE. 49
FIGURE 2.4: CLONING STRATEGY FOR THE CONSTRUCTION OF PET-28A(+)-*TSR* (PTSR10). 56
FIGURE 2.5: TIME COURSE OF EXPRESSION OF TSR IN DIFFERENT RICH MEDIA. 57
FIGURE 2.6: SDS PAGE ANALYSIS OF FRACTIONS COLLECTED DURING PURIFICATION OF HTSR USING A Ni^{2+}-NTA SUPERFLOW COLUMN. 58
FIGURE 2.7: POSITIVE ION MODE ELECTROSPRAY MASS SPECTRUM OF PURIFIED HTSR. 58
FIGURE 2. 8: IMAC PURIFICATION OF HTSR WITH HISTRAP Ni^{2+}-SEPHAROSE COLUMN. 63
FIGURE 2. 9: THE $(HIS)_6$-TAGGED TSR METHYLTRANSFERASE. 64
FIGURE 2. 10: CHROMATOGRAM SHOWING THE SEPARATION OF TSR′ FROM THROMBIN PROTEASE AND UNCLEAVED HTSR. 65
FIGURE 2. 11: POSITIVE ION MODE ELECTROSPRAY MASS SPECTRUM OF PURIFIED TSR′. 65
FIGURE 2. 12: SECTION OF ELUTION PROFILE OF ANION EXCHANGE MONO-Q CHROMATOGRAPHY OF TSR′. 66

FIGURE 2. 13: SUMMARY OF STAGES OF PURIFICATION FOR TSR. 66
FIGURE 2. 14: ELUTION PROFILE OF TSR′ IN THE ABSENCE OF THIOL. 67

CHAPTER 3: BIOCHEMICAL CHARACTERIZATION OF THIOSTREPTON-RESISTANCE rRNA METHYLTRANSFERASE

FIGURE 3.1. TRANSMETHLYATION REACTION CATALYZED BY ADOMET-DEPENDENT MTASES....69
FIGURE 3.2. FILTER BINDING ASSAY....70
FIGURE 3. 3. OVERVIEW OF SCINTILLATION PROXIMITY ASSAY....72
FIGURE 3. 4. NON-RADIOMETRIC ASSAYS DEVELOPED FOR MTASES....74
FIGURE 3. 5: SHORT 15 MINUTE TIME COURSE WHERE THE RRNA SUBSTRATE WAS DENATURED AT ELEVATED TEMPERATURES AND REFOLDED OVER TIME. 86
FIGURE 3. 6: TIME COURSE OF METHYLATION REACTIONS WITH DIFFERENT TSR′ CONCENTRATIONS. 87
FIGURE 3.7: CHROMATOGRAM SHOWING THE SEPARATION OF UT-TSR FROM THE CRUDE CELL LYSATE MIXTURE. 88
FIGURE 3.8: ELUTION PROFILE OF UT-TSR FROM THE ANION EXCHANGE MONO-Q COLUMN. 88
FIGURE 3.9: REPRESENTATIVE TIME COURSE OF UT-TSR. 89
FIGURE 3.10: SHORT TIME COURSES WITH LOWER SPECIFIC ACTIVITIES OF [^{3}H]ADOMET*. 90
FIGURE 3. 11: COMPARISON OF DIFFERENT TCA PRECIPITATION TIMES BETWEEN GF/C AND GF/B GLASS FILTERS. 92
FIGURE 3.12: TIME COURSE OF METHYLATION THAT SHOWED DRASTIC IMPROVEMENT AFTER SEVERAL ADJUSTMENTS WERE MADE. 94
FIGURE 3. 13: MICHAELIS-MENTON PLOT OF A REPRESENTATIVE SET OF KINETIC DATA FOR BOTH SUBSTRATES, ADOMET (A) AND 16S/23S RRNA (B). 95
FIGURE 3.14: FALSE SIGNAL DECTECTION IS POSSIBLE WITH SPA BEADS. 97
FIGURE 3.15: OPTIMAL SPA BEAD AMOUNTS WERE DETERMINED FOR TWO DIFFERENT TYPES OF BEADS. 98
FIGURE 3.16: EXAMPLE OF TIME COURSE DATA OBTAINED WITH POLYLYSINE YSI BEADS. 99
FIGURE 3. 17: SPA TIME COURSES WITH DIFFERING CONCENTRATIONS OF ENZYME AND RNA SUBSTRATE. 100
FIGURE 3.18: SPA TIME COURSE AT ELEVATED TEMPERATURES. 100
FIGURE 3.19: SPA TIME COURSE WITH REFOLDED RNA SUBSTRATE 101
FIGURE 3.20: DIFFERENT BLOCKING AGENTS USED FOR SPA TIME COURSE. 103

CHAPTER 4: STRUCTURAL STUDIES OF THIOSTREPTON-RESISTANCE rRNA METHYTRANSFERASE

FIGURE 4.1: DIFFERENT TYPES OF KNOTS THAT CAN BE FOUND WITH PROTEIN STRUCTURE. 107
FIGURE 4.2: CONSERVED SEQUENCE MOTIFS OBSERVED IN SPOUT MTASES. 108
FIGURE 4.3: PARTIAL SEQUENCE ALIGNMENT OF REPRESENTATIVE MEMBERS OF THE SPOUT MTASE CLASS OF ENZYMES. 109
FIGURE 4.4: FLOW CHART OF STEPS INVOLVED IN HOMOLOGY MODELLING. 110
FIGURE 4.5: MULTIPLE SEQUENCE ALIGNMENT OF TSR AND SPOU MTASES USED AS TEMPLATES FOR THE HOMOLOGY MODELLING. 136
FIGURE 4. 6: REPRESENTATIVE MONOMER STRUCTURES OF SPOUT MTASE. 137
FIGURE 4.7: DIMER STRUCTURE OF AVIRB (1X7P) IN STEREOVIEW. THE DIMER IS FORMED THROUGH INTERACTION BETWEEN THE TWO C-TERMINAL DOMAINS OF EACH PROTOMER. ORANGE AND BLUE SHOW THE DIFFERENT MONOMERS. 137
FIGURE 4.8: THE THREE INITIAL TSR HOMOLOGY MODELS GENERATED USING SWISSMODEL AND PRIME. 139
FIGURE 4.9: SUPERIMPOSITION OF TSR MODEL OVER CRYSTAL STRUCTURE TEMPLATES USED FOR HOMOLOGY MODELLING. 140
FIGURE 4.10: SUPERIMPOSITION OF TSR MODEL OVER CRYSTAL STRUCTURE TEMPLATES. 140
FIGURE 4. 11: PROSA ENERGY PLOTS 142

FIGURE 4. 12: RAMACHANDRAN PLOTS FOR THE COMPARATIVES MODELS GENERATED. 144
FIGURE 4.13: ERRAT RESULTS FOR THE THREE HOMOLOGY MODELS OF TSR. 146
FIGURE 4.14: THE DEEP TREFOIL KNOT IN THE TSR DIMER HOMOLOGY MODEL. 148
FIGURE 4.15: THE THREE SPOUT SEQUENCE MOTIFS IN TSR. 148
FIGURE 4.16: CONSERVED RESIDUES HIGHLIGHTED IN TSR MONOMER MODEL (*PRIMETSR*). 149
FIGURE 4.17: ELECTROSTATIC SURFACE POTENTIAL OF *TSRDIMER*. 150
FIGURE 4.18: TOPOLOGY AND X-RAY CRYSTAL STRUCTURE OF TSR-ADOMET COMPLEX. 153
FIGURE 4. 19: TSR HAS A DEEP TREFOIL KNOT. 154
FIGURE 4.20: THE ADOMET BINDING POCKET AND EXTENDED CONFORMATION OF ADOMET 154
FIGURE 4.21: CLASSIFICATION OF ADOMET-DEPENDENT MTASES. 156
FIGURE 4. 22: TSR CRYSTAL PACKING AND N-TERMINAL DOMAIN FLEXIBILITY. 157
FIGURE 4.23: THE ELECTROSTATIC SURFACE POTENTIAL OF THE TSR DIMER. 158
FIGURE 4. 24: THE SECONDARY STRUCTURE OF THE 58 NUCLEOTIDE L11 RRNA BINDING DOMAIN (L11BD). 158
FIGURE 4. 25: MODELLED RNA-TSR INTERACTIONS. 159
FIGURE 4.26: THE MODELLED RRNA STRUCTURE DOCKED AGAINST THE TSR DIMER. 160
FIGURE 4.27: PROPOSE BASE FLIPPING MECHANIM OF A1067. 161
FIGURE 4. 28: SUPERIMPOSITION OF THE X-RAY CRYTAL STRUCTURE OF TSR (BLUE) AND HOMOLOGY MODELS (PURPLE). 163
FIGURE 4. 29: SUPERIMPOSITION OF THE CTD BETWEEN PRIMETSR (PURPLE) AND CRYSTAL STRUCTURE (BLUE). 164

CHAPTER 5: STRUCTURE-ACTIVITY STUDIES OF THIOSTREPTON

FIGURE 5. 1: TERNARY COMPLEX OF THIOSTREPTON BOUND IN THE BINDING POCKET BETWEEN RIBOSOMAL PROTEIN L11 (RED) AND 23S RRNA (WHITE). 171
FIGURE 5. 2: SEMI-EMPIRICAL CALCULATIONS ARE A MIDDLE GROUND BETWEEN *AB INITIO* AND MOLECULAR MECHANICS. 174
FIGURE 5. 3: THE CHEMICAL STRUCTURE OF THE ANTIBIOTIC ERYTHROMYCIN (5-2) AND ITS KETOLIDE DERIVATIVE, TELITHROMYCIN (5-3). 176
FIGURE 5. 4: REACTIVE GROUPS ON THE ANTIBIOTIC THIOSTREPTON. 179
FIGURE 5. 5: LOW QUALITY TORSION ANGLES OF THIOSTREPTON FOUND IN OPLS-AA. 192
FIGURE 5. 6: A CLOSER EXAMINATION OF THE THIOSTREPTON (TS) STRUCTURE. 193
FIGURE 5. 7: RELAXED STEREOVIEW OF THIOSTREPTON STARTING CRYSTAL STRUCTURE WITH OPLS-AA ENERGY-MINIMIZED STRUCTURE *IN VACUO* AND WATER WITH HYDROGENS ELIMINATED FOR CLARITY [246]. 194
FIGURE 5. 8: RELAXED STEREOVIEW OF SUPERIMPOSED STRUCTURES OF THE THIOSTREPTON CRYSTAL STRUCTURE WITH THE AM1-MINIMIZED STRUCTURE (RMS = 0.9623) WITH HYDROGENS ELIMINATED FOR CLARITY [246]. 195
FIGURE 5. 9: OVERLAY OF THE OPLS-AA MINIMIZED THIOSTREPTON STRUCTURE *IN VACUO* WITH THE AM1-MINIMIZED STRUCTURE (RMS = 1.0433) IN RELAXED STEREO MODE WITH HYDROGENS ELIMINATED FOR CLARITY [246]. 195
FIGURE 5. 10: OVERLAY OF THE OPLS-AA MINIMIZED THIOSTREPTON STRUCTURE IN WATER WITH THE AM1-MINIMIZED STRUCTURE (RMS = 0.9904) IN RELAXED STEREO MODE WITH HYDROGENS ELIMINATED FOR CLARITY [246]. 195
FIGURE 5. 11: THE HOMO AND LUMO OF THIOSTREPTON. 196
FIGURE 5. 12: ELECTROSTATIC POTENTIALS (-2.000E^{1} [RED]-1.00E^{1} [BLUE]) MAPPED ONTO ELECTRON DENSITY (DENSITY = SCF) FOR AM1 ENERGY-MINIMIZED STRUCTURE. ISOVALUE FOR ISOSURFACE: 0.0004 ELECTRONS/AU^{3}. 197
FIGURE 5. 13: SUPERIMPOSED GLOBAL MINIMIZED ENERGY STRUCTURES CALCULATED FROM LMOD IN VACUUM (GREEN) AND WATER (CPK) AND THE STARTING THIOSTREPTON STRUCTURE (MAGENTA) [246]. 198
FIGURE 5. 14: STOCHASTIC DYNAMICS PLOT (*IN VACUO* AND WATER) OF THE DIHEDRAL ANGLE (H^{175}-C^{164}-N^{15}-H^{33}) OF THE N^{15} SECONDARY AMINE (D, FIGURE 5.5) OVER TIME (1 NS) [246]. 200
FIGURE 5. 15: STOCHASTIC DYNAMICS PLOT (*IN VACUO* AND WATER) OF THE DIHEDRAL ANGLE (C^{142}-O^{144}-C^{153}-C^{154}) OF THE INTERNAL LACTONE RING (C, FIGURE 5.5) OVER TIME (1 NS) [246]. 200

FIGURE 5. 16: STOCHASTIC DYNAMICS PLOTS (*IN VACUO* AND WATER) OF THE DISTANCE BETWEEN THE TWO MACROCYCLIC RINGS (LOOP 1 AND 2, FIGURE 5.5) BETWEEN C^2 AMD N^{155} OVER TIME (1 NS) [246].....201
FIGURE 5. 17: CHROMATOGRAM SHOWING THE SEPARATION OF MTS-2MESNA.....204
FIGURE 5. 18: SECTION OF ELUTION PROFILE OF THE PURIFICATION OF MTS-2MESNA WITH 1%/MIN GRADIENT. 205
FIGURE 5. 19: FURTHER SEPARATION WAS ACHIEVED WITH A SLOWER GRADIENT OF 0.4%/MIN. 205
FIGURE 5. 20: POSITIVE ION MODE ELECTROSPRAY MASS SPECTRUM OF MTS-2MESNA.....206
FIGURE 5. 21: COMPARISON OF PARTIAL ^{1}H NMR SPECTRUM OF THE MODIFIED TS (TOP) AND THE ORIGINAL TS (BOTTOM) IN $CDCL_3$.....207
FIGURE 5. 22: BACTERIAL GROWTH CURVES FOR *B. SUBTILIS* (A AND B) AND *S. AUREUS* (C AND D) IN THE PRESENCE OF ANTIBIOTIC IN AQUEOUS OR ORGANIC SOLVENT.....210
FIGURE 5. 23: FURTHER PURIFICATION OF MTS-2MESNA. 212

APPENDIX 2: *S. AZUREUS* TSR PROTEIN STRUCTURE

FIGURE A2. 1: X-RAY CRYSTAL STRUCTURE OF TSR-ADOMET COMPLEX IN THREE ORTHOGONAL VIEWS. 237
FIGURE A2. 2: YEAST L30E DOMAIN STRUCTURE WITH RNA BINDING. 238

APPENDIX 3: GEOMETRIC DISTORTIONS IN HOMOLOGHY MODELS

FIGURE A3. 1: GEOMETRIC DISTORTIONS FOR THE HOMOLOGY MODEL *TSRMONOMER2*.....239
FIGURE A3. 2: GEOMETRIC DISTORTIONS FOR THE HOMOLOGY MODEL *PRIMETSR*. 240
FIGURE A3. 3: GEOMETRIC DISTORTIONS FOR THE HOMOLOGY MODEL *TSRDIMER*.....241

APPENDIX 4: MUTAGENESIS

FIGURE A4. 1: OVERVIEW OF THE QUIKCHANGE™ SITE DIRECTED MUTAGENESIS METHOD. ADAPTED FROM STRATAGENE CLOSING SYSTEMS QUIKCHANGE™ SITE-DIRECTED MUTAGENESIS KIT MANUAL. 243
FIGURE A4. 2: OVERVIEW OF SPLICING OVERLAP EXTENSION SITE-MUTAGENESIS METHOD.....244
FIGURE A4. 3: POSITIVE ION MODE ELECTROSRAPY OF S246A TSR′. 245
FIGURE A4. 4: POSITIVE ION MODE ELECTROSRAPY OF R135A TSR′.....246
FIGURE A4. 5: POSITIVE ION MODE ELECTROSRAPY OF R135K TSR′.....246
FIGURE A4. 6: POSITIVE ION MODE ELECTROSRAPY OF N248A TSR′.....247
FIGURE A4. 7: POSITIVE ION MODE ELECTROSRAPY OF N248D TSR′.....247
FIGURE A4.8: CD SPECTRA OF MUTANTS S246A, R135A AND R135K COMPARED TO THE WILDTYPE TSR′.....248
FIGURE A4.9: RAW DSC DATA FOR A REPRESENTATIVE SCAN OF WILDTYPE TSR′ AND S246A. 248

APPENDIX 5: TS MODELLING SUPPLEMENT

FIGURE A5. 1: SUPERIMPOSITION OF THE 158 CONFORMATIONS DETERMINED *IN VACUO* BY LMOD CALCULATIONS. 249
FIGURE A5. 2: SUPERIMPOSITION OF THE 293 CONFORMATIONS DETERMINED IN WATER BY LMOD CALCULATIONS. 249

LIST OF ABBREVIATIONS

[^{3}H]-AdoMet*	*S*-adenosyl-L-[methyl-^{3}H] methionine
AdoHcy	*S*-adenosyl-L-homocysteine
AdoMet	*S*-adenosyl-L-methionine
ATP	adenosine triphospate
bp	base pair
BSA	bovine serum albumin
CPK	Corey, Pauling, Kultin
CTD	C-terminal domain
DNA	deoxyribonucleic acid
dNTP	deoxynucleotide triphosphate
GTPase	guanosine triphosphatase centre
EC	enzyme commission
EDTA	ethylenediamine tetraacetic acid
ESI	electrospray ionization
FB	filter binding
FPLC	fast protein liquid chromatography
HOMO	highest occupied molecular orbital
HTSR	Hexahistidine-tagged TSR
IMAC	immobilized metal ion adsorption chromatography
IPTG	isopropyl-β-thiogalactopyranoside
L11BD	L11 binding domain
LB	Luria-Bertani
LMOD	low mode
LUMO	lowest unoccupied molecular orbital
LSC	liquid scintillation counter
β-ME	β-mercaptoethanol
2-MESNA	2-mercaptoethanesulfonic acid
MTase	methyltransferase
MW	molecular weight
Ni^{2+}-NTA	nickel nitriloacetic acid
NMR	nuclear magnetic resonance
NPE	non-proximity effects
NSB	non-specific binding
OD	optical density
PCR	polymerase chain reaction
PDB	protein data bank
Pi	phosphate
PPi	pyrophosphate
PMSF	phenylmethylsulfonyl fluoride
NTD	N-terminal domain
RMSD	root mean square deviation
RNA	ribonucleic acid
rRNA	ribosomal ribonucleic acid
tRNA	transfer ribonucleic acid

SAH	*S*-adenosyl-L-homocysteine
SeMet	selenomethionine
SET	***S***uppressor of variegation 3-9 (Su(var)3-9) ***E***nhancer of zeste (E(z)) [1] and ***T***rithorax
SDS-PAGE	sodium dodecyl sulphate polyacrylamide gel electrophoresis
SOE	splicing overlap extension
SPA	scintillation proximity assay
SPoUT	***Spo***U-***T***rmD
TAE	tris-acetate-EDTA
TB	Terrific Broth
TCA	trichloroacetic acid
TS	thiostrepton
TSR′	thiosptrepton-resistance rRNA methyltransferase with hexahistidine-tag removed
TSR	thiosptrepton-resistance rRNA methyltransferase
UT-TSR	untagged thiosptrepton-resistance rRNA methyltransferase
w/v	weight per volume
YSi	yttrium silicate

CHAPTER 1: INTRODUCTION

1.1. *S*-Adenosyl-L-methionine

1.1.1. Structure and Biochemistry of S-Adenosyl-L-methionine (AdoMet)

Since its discovery in 1952 by Giulio Cantoni, *S*-adenosyl-L-methionine (AdoMet, **1-1**) has been found to be involved in a myriad of essential biological processes [2]. It is second only to adenosine triphosphate (ATP) as the most frequently utilized cofactor in biochemical reactions [3,4]. AdoMet is synthesized via a condensation reaction between the 5′-carbon of ATP and the sulphur of L-methionine, as shown in Figure 1.1. This reaction is catalyzed by AdoMet synthase (also referred to as methionine adenosyltransferase, EC 2.5.1.6) and results in the complete dephosphorylation of ATP to eventually yield one pyrophosphate (PPi) and one phosphate (Pi). Subsequently the PPi is hydrolyzed to two Pis by pyrophosphatase [4,5]. The synthesis of AdoMet is the only reaction known to date that requires the complete hydrolysis of all three phosphates from ATP, making AdoMet a very energetically costly molecule to synthesize [5].

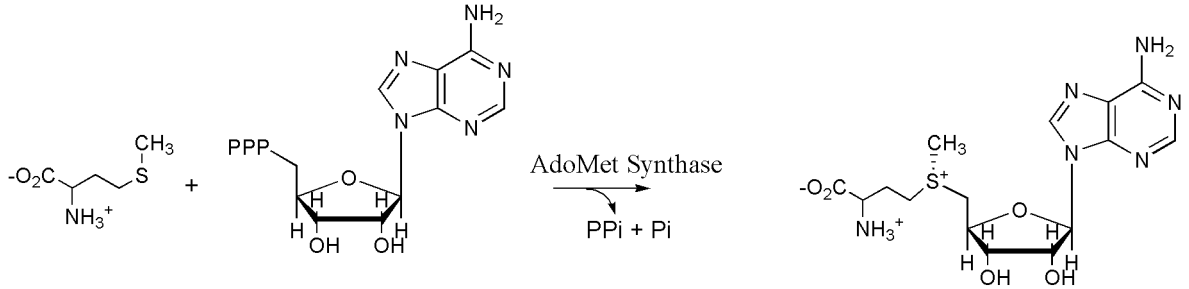

1-1

Figure 1.1: Biosynthesis of *S*-adenosyl-L-methionine.
AdoMet (AdoMet; **1-1**) is biosynthesized from methionine and ATP by AdoMet synthase.

The AdoMet molecule possesses a positively charged chiral sulfonium group bearing an *S*-configuration with a 5′-deoxyadenosine, an aminopropylcarboxylate and a methyl moiety appended to it. The three substituents (attached to the sulphur atom) all play a role as precursors or sources of chemical moieties utilized in biochemical reactions such as polyamine biosynthesis, 5′-deoxyadenosyl radical reactions, and posttranscriptional modification of tRNAs, making AdoMet an extremely versatile biological molecule [6,7]. However, out of all of the essential biological activities that it is involved in, AdoMet is best known as the universal methyl group donor in cellular alkylation processes [8].

1.1.2. Role of S-Adenosyl-L-methionine (AdoMet) in Methylation

The majority (approximately 95%) of *S*-adenosyl-L-methionine produced by cells is utilized in transmethylation reactions [9]. AdoMet can alkylate a number of nucleophiles containing oxygen, carbon, sulphur and the substrates that are methylated range in size from small molecules to macromolecules such as proteins and DNA [10]. AdoMet is the principle methyl group donor in the cell and is a few orders of magnitude more reactive to polarizable nucleophiles (N, O, and S) than another group of methyl donors, the methylated folates [3].

The powerful methylating ability of AdoMet arises from its chemical structure: the methyl group is attached to the electron-deficient sulphonium atom, which confers thermodynamic instability on the molecule (ΔG^{o}_{H2O} = -17 kcal/mol) [3,10]. This destabilization confers substantial reactivity to the methyl moiety, enabling its donation to the substrate. Thus, the presence of the cationic sulphonium centre renders AdoMet the preferred biological methyl donor.

When AdoMet transfers its methyl group, it is converted to *S*-adenosyl-L-homocysteine (SAH or AdoHcy). The methylation is catalyzed by methyltransferases.

Following this event, SAH is then hydrolysed by SAH hydrolase to yield adenosine and homocysteine. At this point, homocysteine can act as a substrate for methionine synthase, which uses a folate derivative to methylate and regenerate methionine. AdoMet can then be generated by AdoMet synthase, completing what is referred to as the AdoMet cycle (Figure 1.2) [4,6,8].

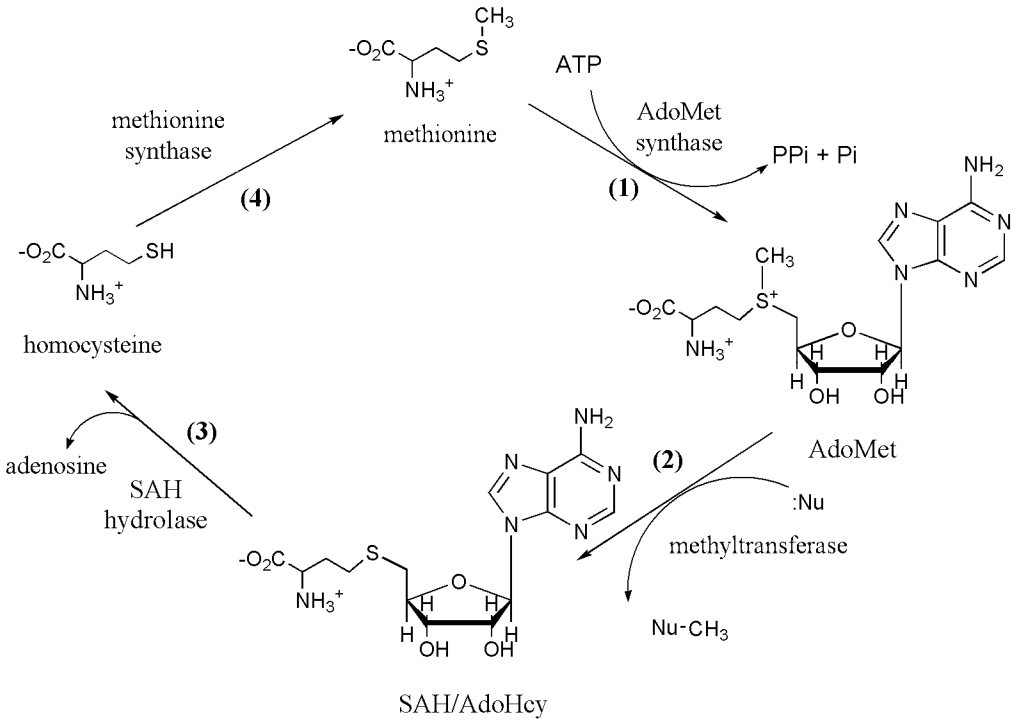

Figure 1.2: The *S*-adenosyl-L-methionine (AdoMet cycle).
(1) AdoMet is formed from the reaction of methionine and ATP catalyzed by AdoMet synthetase. **(2)** Methyl group transfer from AdoMet to a nucleophile (:Nu) by methyltransferases yield *S*-adenosylhomocysteine (SAH/AdoHcy). **(3)** SAH hydrolase catalyzes the hydrolysis of SAH to give homocysteine which is then **(4)** methylated by methionine synthase to regenerate methionine to complete the cycle.

1.2. *S*-Adenosyl-L-methionine-dependent Methyltransferases

Methyl transfer reactions involving AdoMet are catalyzed by a large group of enzymes referred to as the *S*-adenosyl-L-methionine-dependent methyltransferases (AdoMet-dependent MTases; E.C. 2.1.1.X). The by-product of all transmethylation reactions is *S*-adenosyl-L-homocysteine (SAH or AdoHcy), which functions as a natural potent inhibitor of all methyltransferase reactions [11]. The crystal structures of over 40 AdoMet-dependent

MTases modifying small molecules, proteins, DNA and RNA have been determined, and have coordinates deposited in the Protein Data Bank.

1.2.1. Classification and Structural Folds

Structural commonalities within AdoMet-dependent MTases are observed despite low levels of sequence identity [12]. It was 1993 when the very first AdoMet-dependent MTase structure was determined (*M. HhaI* DNA-MTase; PDB: 6MHT) [13]. For a number of years, all MTase structures were considered to share a common structural core which eventually led to the designation of the "AdoMet-dependent MTase fold" [12]. However, recently determined AdoMet-dependent MTase structures revealed that not all MTases conform to this canonical fold. Presently, there are five distinct AdoMet-dependent MTase superfamilies based on structure (Table 1.1).

Table 1.1: Known Structures of AdoMet-dependent MTases.

E.C. Classification	Enzyme Name	PDB code[γ]
Class I		
2.1.1.2	Guanidinoacetate *N*-MTase	1KHH
2.1.1.5	Betaine-homocysteine *S*- MTase	1LT7
2.1.1.6	Catechol *O*- MTase	1VID
2.1.1.7	Nicotinate *N*- MTase	5MHT
2.1.1.8	Histamine *N*- MTase	1JQD
2.1.1.20	Glycine *N*- MTase	1BHJ
2.1.1.28	Phenylethanolamine *N*-MTase	1HNN
2.1.1.33	tRNA (guanine-N^7-)-MTase	2FCA
2.1.1.37	DNA (cytosine-C^5-)- MTase	1HMY
2.1.1.48	rRNA (adenine-N^6-)- MTase	1QAO
2.1.1.52	rRNA (guanine-N^2-)-methyltransferase	2PJD
2.1.1.56	mRNA (guanine-N^7-)- MTase	1Z3C
2.1.1.57	mRNA (nucleoside-2'-O-)- MTase	2GA9
2.1.1.63	DNA(methylguanine-O^6):[protein]-L-cysteine *S*-MTase	1EH6
2.1.1.67	Thiopurine *S*- MTase	2BZG
2.1.1.68	Caffeate *O*- MTase	1KYW
2.1.1.72	Adenine-specific DNA- MTase	1AQI
2.1.1.77	Protein-L-isoaspartate(D-aspartate) *O*- MTase	1D15
2.1.1.79	Cyclopropane-fatty-acyl-phospholipid synthase	1KP9
2.1.1.80	Protein-glutamate *O*- MTase	1AF7
2.1.1.104	Caffeoyl-CoA *O*-MTase	1SUI
2.1.1.113	cytosine-N^4-specific DNA-MTase	1BOO
2.1.1.125	Histone-arginine I- MTase	1ORH
Class II		
2.1.1.13	Methionine synthase	1MSK
Class III		
2.1.1.107	Uroporphyrinogen-III *C*-MTase	1S4D
2.1.1.130	Precorrin-2 C^{20}- MTase	2E0K
2.1.1.133	Precorrin-4 C^{11}- MTase	1CBF
Class IV		
2.1.1.31	tRNA (guanine-N^1-)- MTase	1P9P
2.1.1.34	tRNA guanosine-2'-*O*- MTase	1V2X
2.1.1.51	rRNA (guanine-N^1-)- MTase	1P91
2.1.1.?	rRNA 2'-*O*- MTase	1GZ0
2.1.1.?	rRNA uridine-2'-*O*- MTase	1X7P
2.1.1.?	tRNA (guanosine-2'-O-) methyltransferase	1J85
2.1.1.?	rRNA 2'-O- MTase	1IPA
Class V		
2.1.1.43	Histone-lysine *N*- MTase	1O9S
2.1.1.127	[Ribulose-bisphosphate-carboxylase]-lysine *N*-MTase	1MLV

[γ]Multiple PDB structures may exist for some enzymes. Only one representative PDB was chosen for this table.

1.2.1.1. Class I: The Classical AdoMet-dependent MTase Fold

The majority of AdoMet-dependent MTases characterized to date belongs to the Class I or Classical Fold. Their structural core is reminiscent of the well-known nucleotide-binding Rossman proteins having the β/α/β/α/β arrangement [14]. These Rossmann-based MTases are comprised of a seven-stranded β-sheet surrounded by α-helices in an alternating fashion to form an open α/β/α-sandwich. The order of the strands is 3214576 with strand 7 being antiparallel to the others inserted between strands 5 and 6 (3↑2↑1↑4↑5↑7↓6↑) [12]. All Rossmann-fold like MTases possess this core fold or some related topological variant, where the C-terminal region of the enzyme contains the catalytic domain and the N-terminus constitutes the AdoMet binding region [12,15]. The structure of the small molecule MTase, catechol-*O*-MTase (E.C. 2.1.1.6) exemplifies the Class I fold and is shown in Figure 1.3 [16].

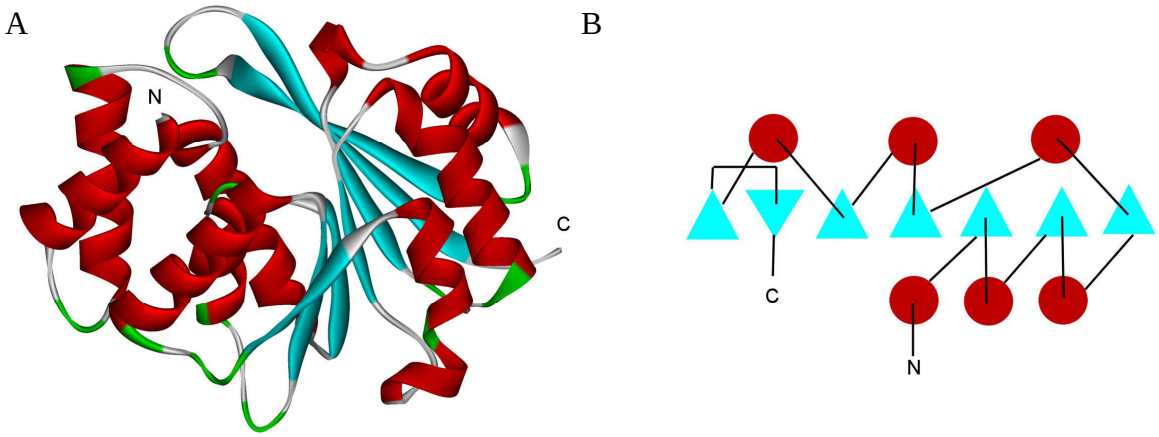

Figure 1.3: Catechol *O*- methyltransferase is a member of the Class I superfamily resembling the Rossmann fold.
(A) Crystal structure (PDB: 1VID) and **(B)** topology of catechol *O*-MTase. Red represents α-helices, cyan represents β-strands, and green represents loops.

Multiple sequence alignments by a number of groups reveal conserved regions in the AdoMet-binding domain [17-20] (Motifs I – X). Motif I is a glycine rich sequence (E/DXGXGXG) located at β1, the loop between β1 and αA and part of the N-terminal region

of αA [20] and is involved in interacting with the amino acid moiety of AdoMet [12]; the main chain NH groups of the enzyme hydrogen bond with the carboxyl group of the aminopropylcarboxylate moiety of AdoMet [20]. The glycines in Motif I are not absolutely conserved; residues with small side chains or amino acids that induce bends are suitable substitutions [18].

The loop between β2 and αB forms Motif II. The last residue of the β2 strand is a conserved acidic residue whose side chain hydrogen bonds to the ribose hydroxyls of AdoMet [20]. Furthermore, there are a high number of aromatic amino acids populating this region [17], which is believed to engage in van der Waals interactions with the adenine ring of AdoMet [20]. The conserved region of Motif III encompasses the first position of the αC helix, where a conserved acidic residue's main chain NH hydrogen bonds with the N^6-atom of adenine [20,21]. Motifs I to III occupy what has been designated as the AdoMet binding region and it is often that cocrystallization of AdoMet or the product, AdoHcy, is found to be located by the conserved residues. Furthermore, Motifs IV and V do make additional contacts with AdoMet. Motif IV is a diprolyl motif (D/N/E-PPY) and is located at the carboxyl end of strand β4 [21]. It interacts with the amino and sulfonium groups of the amino acid moiety of AdoMet [18]. Motif V (D/E-LYXXF-L/V/I) is comprised of helix αD and helps stabilize AdoMet binding [20,21].

Motif VI forms strand β5 which starts with an invariant glycine residue ends with G/P/A/S/N [21]. It makes contacts with the methionine moiety of AdoMet at the amino and sulfonium groups [18]. Motif VII is weakly conserved and has a NY in the loop region between αE and β6. It assists in the formation of the active site pocket. Motif VIII has a conserved sequence of N/QXRXR and also plays a role in the catalytic region. Motif IX

(RX_4E) is also one of the less conserved motifs and is involved in maintenance of the structural integrity of the enzyme. The C-terminus of the enzyme folds together with Motif I to help form the AdoMet binding site and is termed Motif X with YX_3GN in its sequence [19,21].

1.2.1.2. Class II: B_{12}-dependent Methionine Synthase

The one and only member of the Class II superfamily is the B_{12}-dependent methionine synthase (Met synthase; E.C. 2.1.1.13). It converts homocysteine to methionine in the AdoMet cycle (Figure 1.2) by catalyzing the transfer of a methyl group from methyltetrahydrofolate to cobal(I)amin [4,6,8,22]. The cobal(I)amin can be oxidized to the coba(II)amin species, which is inactive. Reactivation requires AdoMet to convert cobal(II)alamin to methylcobalamin [22]. The C-terminal region of the enzyme binds to AdoMet and this region is found to have a very different structure to that of the Class I Rossmann-like MTases [10].

The 38 kDa AdoMet binding domain has an overall C-shaped architecture with a β-sheet consisting of β1, β2, β5 and β8 mixed with α-helices (Figure 1.4). This core β-sheet is adjacent to a long 28-residue with α-helix (α6) and the concave face of the C-shaped domain is where the AdoMet binding region resides. The co-substrate makes the majority of its contacts with the α6-helix with the recognition sequence of R-(P/F/Y)-(A/S)-(P/F/C)-G-y-(P/G)(A/S)-X-P [22].

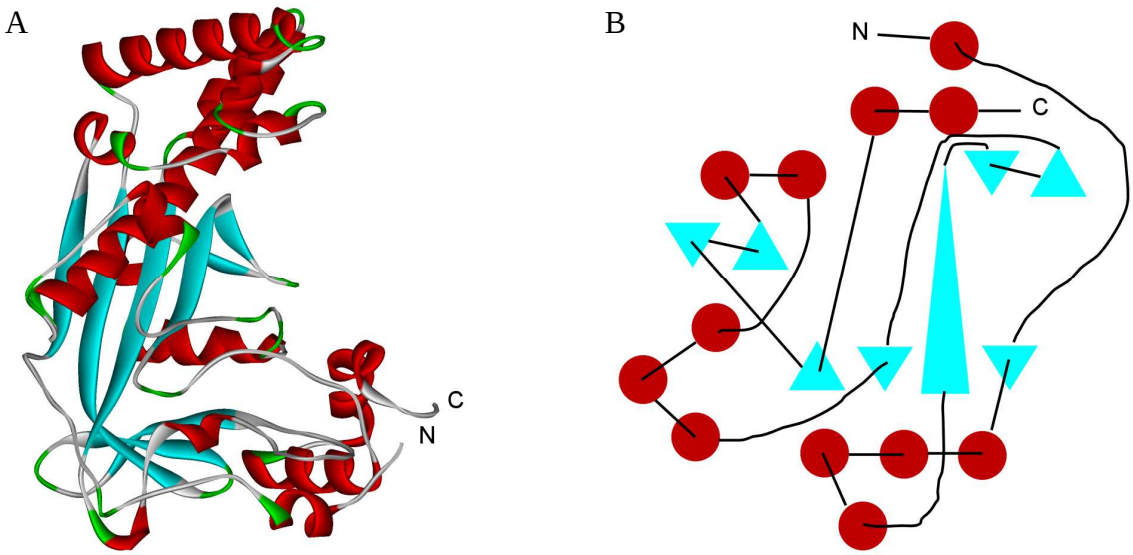

Figure 1.4: The C-terminal, AdoMet binding domain of methionine synthase is the only member of the Class II MTases.
The **(A)** Crystal structure (PDB: 1MSK) shows a general concave shape and **(B)** Topology of the C-terminal domain of Met synthase show no resemblance to the Class I MTases. Red represents α-helices, cyan represents β-strands, and green represents loops.

1.2.1.3. Class III: Methyltransferases Involved in Vitamin B_{12} Biosynthesis

Cobalamin (vitamin B_{12}) biosynthesis involves numerous steps. Biosynthesis of the corrin ring entails the transfer of six methyl groups of AdoMet by six separate, but similar MTases to the tetrapyrrole scaffold [23]. Thus far, only three members to this superfamily have been structurally characterized: SUMT, which is responsible for the methlylation of uropophyringoen III to precorrin II [24]; CbiF, which methylates C11 of the tetrapyrrole ring of Co-precorrin 4[23]; and CbiL, which methylates the C20 position of the ring [25].

The Class III MTase structure has two distinct α/β domains (Figure 1.5) and is homodimeric. The two α/β domains form a kidney-shaped molecule, and both have a five stranded β-sheet surrounded by four α-helices; however, they do not possess the same topology. In the N-terminal domain, the strand order is 3↑2↑4↑1↑5↑, while in the C-terminal domain, the order is 1↑2↑5↓3↑4↓ [23]. There is a conserved glycine rich sequence (GXGXG) at the end of the first β-strand similar to Motif I in the Classical MTases [24].

However, unlike Motif I in the Classical MTases, this glycine-rich region does not interact directly with AdoMet [10,24]. Instead, the AdoMet cofactor binding pocket for Class III MTases resides between concave region of the kidney-like structure, between the N-terminal and C-terminal domains [23-25].

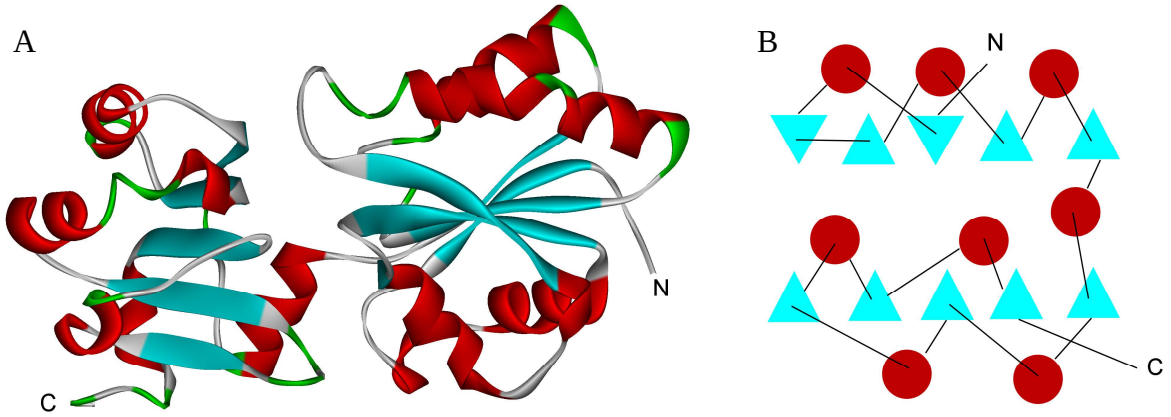

Figure 1.5: The monomer of a Class III MTase: precorrin-2 C^{20}- MTase.
(A) The crystal structure (PDB: 2E0K) shows the two distinct α/β domains **(B)** Topology diagram of precorrin-2 C^{20}- MTase. Red represents α-helices, cyan represents β-strands, and green represents loops.

1.2.1.4. Class IV: The SpoUT MTases with a Deep Trefoil Knot

In 2002, a novel chain fold with an unexpected structural feature was observed: a deep trefoil knot [26]. Subsequently, approximately ten MTases have been found to possess this unique topological feature and have been designated as the Class IV or SpoUT (***Spo***U-***T***rmD) MTases. These enzymes possess a α/β structure similar to the Class I MTases; however, they do not posses any sequence similarity [18]. SpoUT MTases contain a six stranded parallel β-sheet with the first three strands forming half of the Rossmann fold [10]. The β-strands are surrounded by seven α-helices to form a distinct α/β/α sandwich. The C-terminal backbone region is tucked back within itself to form a deep trefoil knot, and is part of the active site and is critical to enzyme activity (Figure 1.6). Additionally, all members of

this class are homodimeric structures in which the active site is situated on the subunit interface and the catalytic residues are comprised from both protomers [10,27].

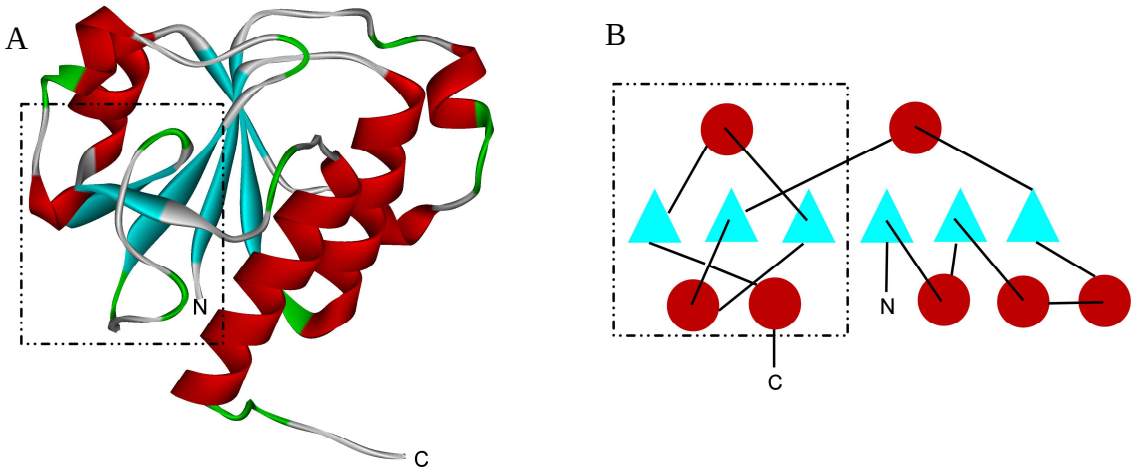

Figure 1.6: The monomer of a Yibk methyltransferase posseses a deep trefoil knot at its active site. The (A) crystal structure (PDB: IJ85) (B) Topology of YibK MTase. Red represents α-helices, cyan represents β-strands, and green represents loops. Deep trefoil knot is highlighted with dashed box.

Three sequence motifs have been identified in SpoUT MTases (Motifs I – III). Motif I is located at the N-terminus (X-N/D/E-X-G/S-X_3-R-X_5-G) [28]. The AdoMet binding motif is the second motif (Motif II: h-V/L/I/M-h-G-X-E/Y-X_2-G-V/L/I/M/P-X, where h is a hydrophobic residue) which has bulky hydrophobic residues with two glycines within; it resembles Motif I in the Classical MTases [28,29]. The last motif is Motif III and it is situated in the C-terminal region and has a sequence of V/I-X-I-P-M-X_5-S-L/M-N-X_3 [28].

1.2.1.5. Class V: The SET MTases – the Protein Lysine MTases

The SET MTases are a superfamily of MTases known to methylate lysine residues of proteins. Originally thought to only contain histone MTases, the SET MTases' namesake comes from the conserved domain found in histone modifying MTases from *Drospophila melanogaster*: ***S***uppressor of variegation 3-9 (Su(var)3-9) [30], ***E***nhancer of zeste (E(z)) [1] and ***T***rithorax [31]. The SET domain is roughly 130 amino acid residues and is rich in β-

conformation forming three small β-sheets. In the C-terminal region of the SET domain, the polypeptide backbone passes through a preceding loop to form a knot-like structure (Figure 1.7) [10,32,33]. This loop and the C-terminal region that passes through it contain two highly conserved sequence motifs containing SET domains [33]. It consists of ELXF/YDY and RFNHS/CXXPN [32,34] and forms the active site. There is an absolutely conserved tyrosine (tyr) that has been implicated in catalysis. It is proposed that the tyrosine deprotonates the amino group of the lysine substrate to promote nucleophilic attack on the AdoMet molecule [33].

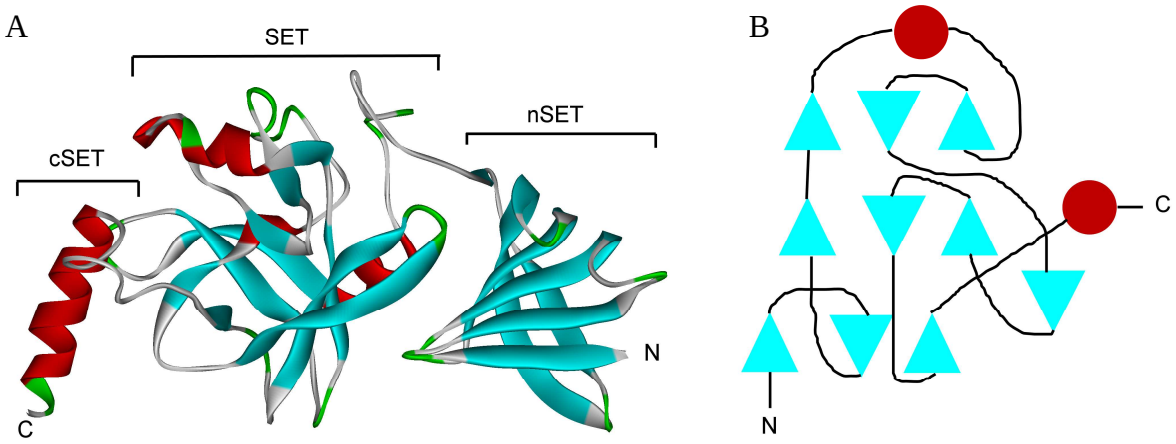

Figure 1.7: The monomer of a SET7/9 MTase has a pseudo-knot in the C-terminus. Flanking the core SET domain are the preSET (nSET) and postSET (cSET) domains that some SET MTases have. The **(A)** Crystal structure (PDB: IO9S) **(B)** Topology diagram of SET7/9 MTase. Red represents α-helices, cyan represents β-strands, and green represents loops.

Although the core of the SET domain is structurally conserved, protein lysine MTases can differ in their other domains. Some SET MTases may possess a pre-SET (nSET) or post-SET (cSET) (Figure 1.7). The preSET domain is rich in cysteines ($CXCX_5CX_4CXCX_N$-CX_3CXCX_3C where N varies depending on the SET MTase) and is involved in interacting with amino acid residues of the core SET domain to maintain structural stability. Some SET MTases may have metal ions coordinating to the structure, such as in the case of the Su(var)

family members where the cysteines in the preSET domain coordinate to Zn^{2+} to form a Zn_3Cys_9 triangular cluster [32]. Other SET MTases may possess a postSET domain that houses aromatic residues to form a hydrophobic channel by packing against the core SET domain and forming part of the active site [34].

1.2.2. Conformation of Cofactor Binding in S-Adenosyl-L-methionine-dependent Methyltransferases

Given the distinct structural folds for AdoMet-dependent MTases, it is not surprising that the binding conformations of Adomet or AdoHcy are found to vary among MTases. Four different features of the cofactor molecule can be compared when bound to different classes of MTases: 1) Sugar ring pucker, 2) dihedral angle of O4′-C1′-N9-C4, 3) dihedral angle of O4′-C4′-C5′-Sδ, and 4) dihedral angle of C4′-C5′-Sδ-Cγ (Figure 1.8, Table 1.2) [10].

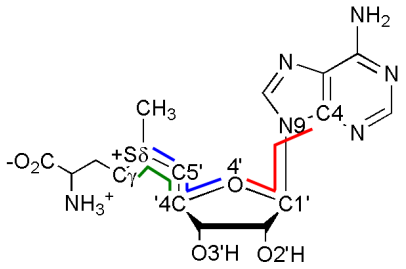

Figure 1.8: The structure of *S*-adenosyl-L-methionine (AdoMet) and the dihedral angles used to compare cofactor binding in different classes of MTases.
Red: O4′-C1′-N9′-C4; Blue: O4′-C4′-C5′-Sδ; Green: C4′-C5′-Sδ-Cγ.

Table 1. 2: Dihedral angles of AdoMet or AdoHcy found in the different classes of Adomet-dependent MTases.

Class	Ring pucker	O4′-C1′-N9-C4	O4′-C4′-C5′-Sδ	C4′-C5′-Sδ-Cγ
I	2′endo	~135° (*anti*)	~ 180°	~ 180°
II	3′endo	~180° (*anti*)	~ -90°	~ 180°
III	3′endo	~180° (*anti*)	~ -90°	~ -90°
IV	3′endo	~180° (*anti*)	~ 80°	~ -90°
V	3′endo	~180° (*anti*)	~ -90°	~ -90°

In the classical Rossmanoid MTase class, AdoMet assumes an extended conformation with a 2′-endo sugar ring pucker and this adenine in the *anti* position (dihedral angle of O4′-

C1′-N9′-C4′ is ~135°). The dihedral angle for O4′-C4′-C5′-Sδ is approximately 180°, as is the ligand dihedral angle (of C4′-C5′-Sδ-Cγ) (Figure 1.9a) [10]. For the Class II methionine synthase, the AdoMet also assumes for the most part an extended conformation, with the exception of the dihedral angle of O4′-C4′-C5′-Sδ (it is -90° instead of 180°), additionally, the conformation of the ribose sugar is 3′-endo [10]. For Class III to Class IV, one observes a more folded conformation for the cofactor; the dihedral angles of O4′-C4′-C5′-Sδ are also -90° for Class III and V and for Class IV 80°, however for the ligand dihedral angle (C4′-C5′-Sδ-Cγ), Class III – V all have a tightly folded conformation (Figure 1.9) [23,35].

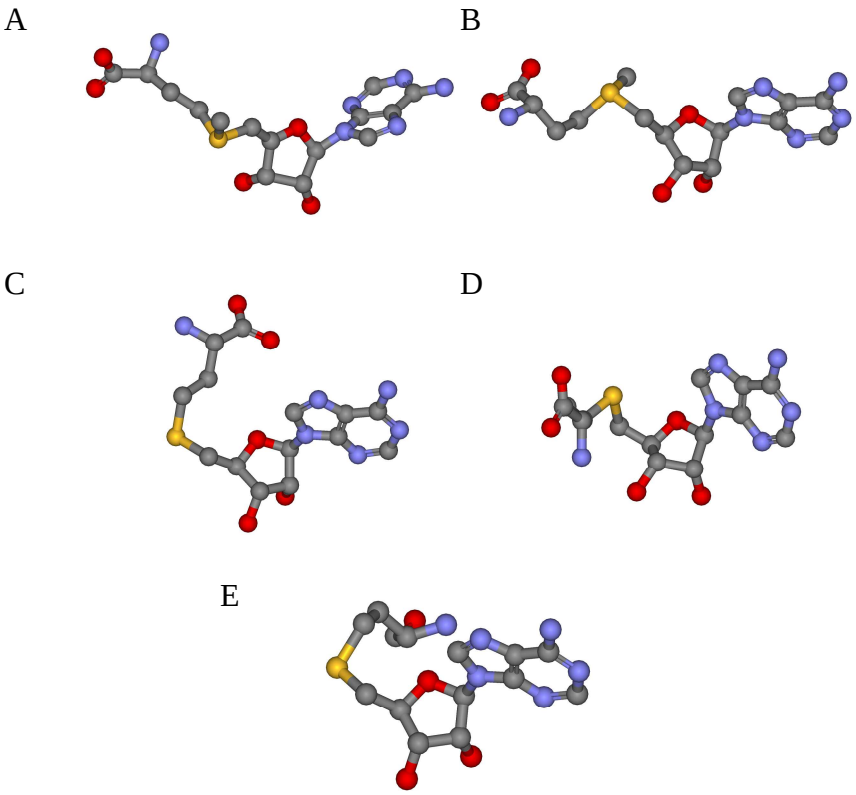

Figure 1.9: Binding of cofactor AdoMet/AdoHcy amongst different classes of MTase demonstrates conformational specificity.
(A) Class I, Classical MTase (1VID) **(B)** Class II (1MSK) **(C)** Class III (1CBF) **(D)** Class IV, SpoUT MTase (1MXI) and **(E)** Class V, SET MTase (IO9S).

1.2.3. Inhibition of S-Adenosyl-L-methionine-dependent Methyltransferases

AdoHcy/SAH (**1-2**) is the transmethylation product arising from AdoMet-dependent methyl transfer reactions and is one of the most effective competitive inhibitors of this reaction (Figure 1.2) [11]. The *Ki* value for AdoHcy/SAH is often less than the *Km* value of AdoMet (Table 1.3), suggesting that the active sites of AdoMet-dependent MTases have similar or higher affinities for the demethylated product. Consequently, syntheses of structural analogues of AdoHcy/SAH and AdoMet as novel inhibitors of AdoMet-dependent MTases have been of considerable interest. Most notably, in an elegant series of structure-activity studies, Borchardt and coworkers designed potential inhibitors of AdoMet-dependent MTases by systematically modifying the structure of AdoHcy/SAH and AdoMet; modifications were done on the amino acid [36-38], base [37,39]and ribose sugar [37,40,41] moieties.

Table 1. 3: Comparison of *Km* value for AdoMet and *Ki* value of AdoHcy/SAH for selected MTases.

MTase	***Km* (AdoMet)**	***Ki* (AdoHcy/SAH)** $\times 10^{-6}$ **M**	**Reference**
Protein carboxy-*O*-MTase	3.2	0.64	[42]
Catechol-*O*-MTase	14	4.4	[11]
Phenylethanolamine *N*-MTase	10	1.4	[11]
Acetylserotonin MTase	14	2.1	[11]
tRNA (adenine) MTase	3	0.11	[43]
Protein-L-isoaspartyl MTase	2	0.08	[44]
Glycine *N*-MTase	100	35	[45]
DNA MTase (Dnmt3a)	0.52	0.163	[46]
Histamine MTase	6	5	[47]

A naturally occurring AdoHcy analogue is the antifungal antibiotic sinefungin (A9145), which was first isolated by Hamill and Hoehn from *Streptomyces griscolus* [48]. In lieu of the thiomethyl moiety in AdoMet, sinefungin possesses an amino group ($-CH^{+}NH_3$) (**1-3**). It is believed that the analogue may be recognized as AdoMet-like structures but with the inability to donate a methyl group to an incoming nucleophile. Sinefungin and its related

compound A9145C (**1-4**) have been reported to be very potent inhibitors of methyl transfer reactions with *Ki* values in the nanomolar range compared to the *Ki* of AdoHcy/SAH (Table 1.3) about making sinefungin-based target design very attractive [49-52] (Figure 1.10).

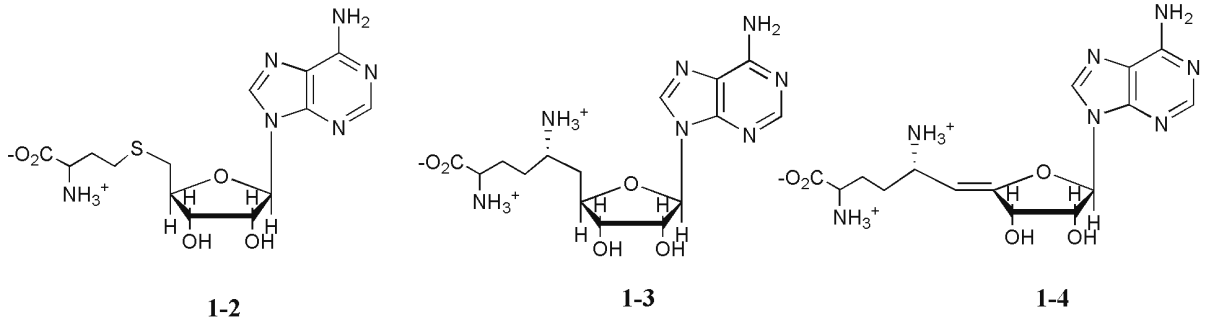

Figure 1. 10: Natural inhibitors of AdoMet-dependent MTase reactions are structural analogues of AdoMet.

1.3. rRNA Methyltransferases and Their Role in Antibiotic Resistance

1.3.1. Antibiotics and Antibiotic Resistance

Antibiotics can be considered one of the greatest discoveries of the twentieth century. Between 1940 and 1960, major strides and successes were made in the development of antibiotics in the clinical setting; it was during this time that penicillin, streptomycin, tetracycline, chlormaphenicol, erythromycin, cephalosporin and vancomycin were introduced. As a result this time period is often heralded as the "golden" era of antibiotics [53,54]. It was thought that the battle against infectious diseases had come to an end and victory was declared for humankind [55]. However, with the appearance of antibiotics, antimicrobial resistance soon followed, and has remained a concern for the health and medical community [56].

There are four main mechanisms of action of antibiotics/antimicrobials, involving the inhibition of: 1) cell wall biosynthesis, 2) protein biosynthesis, 3) DNA/RNA biosynthesis and, 4) certain metabolic pathways (Figure 1.11). Antimicrobials that interfere with cell wall

biosynthesis compromise the structural integrity of the rigid peptidoglycan cell wall such that the cell undergoes osmolysis. These antimicrobials include the penicillins, vancomycin and cephalosporins [57]. Prevention of protein biosynthesis is another common mode of action. Tetracyclines, macrolides and aminoglycosides, all bind to the large 50S or small 30S ribosomal unit and stop protein synthesis at different stages. This can eventually lead to cell death. Interference of nucleic acid biosynthesis, whereby the antimicrobial inhibits essential enzymes involved in DNA (i.e. fluoroquinolines) or RNA replication (i.e. rimfampin) is also effective. Lastly, inhibition of folate biosynthesis (i.e. sulfonamides) or other essential metabolic pathways will lead to the eventual demise of the cell and is often targeted by antimicrobials [54,57-59].

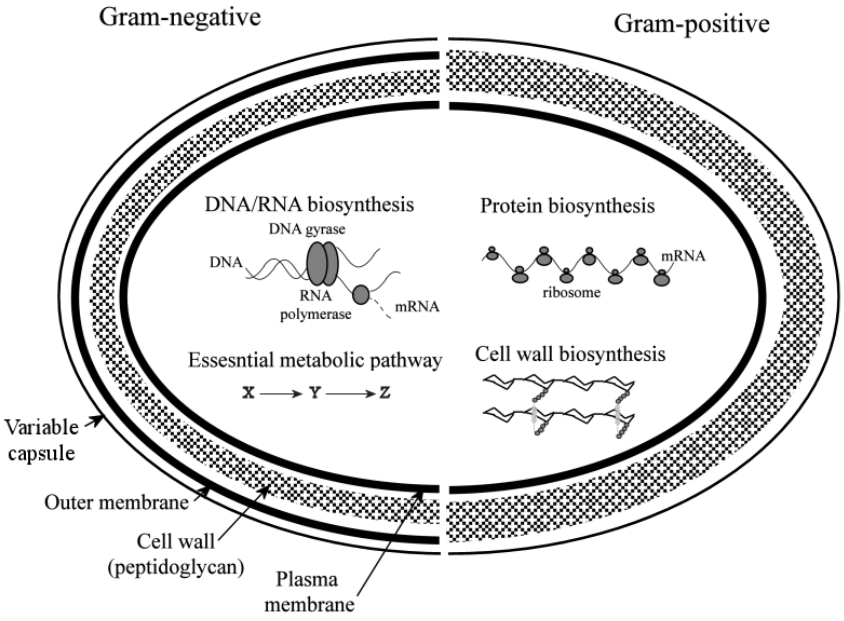

Figure 1.11: The four major targets of antibiotics and antimicrobials.
1) DNA/RNA biosynthesis 2) Protein biosynthesis 3) Cell wall biosynthesis and 4) Major metabolic pathways

With the increased use of antibiotics and antimicrobials, bacteria have evolved a number of strategies to circumvent their action. Resistance can appear between months and years after the first introduction of an antimicrobial into a clinical setting [60]. The

significant mechanisms that bacteria employ to achieve resistance are: 1) reduction of antibiotic accumulation, 2) enzymatic degradation or modification of the antibacterial, and 3) modification of the target site (Figure 1.12) [61]. In order for an antibacterial to be effective, it must be able to reach its target site within the cell. Intrinsic resistance is possible for Gram-negative bacterial species whose outer membrane acts as a barrier to antimicrobials. Likewise, cell permeability can be reduced by mutations resulting in a decrease in expression or activity of small channels within the lipid bilayer. Alternatively, increasing the expulsion of antibiotics across the membrane by the action of efflux pumps will reduce the antibiotic's intracellular concentration [54,58,61-63].

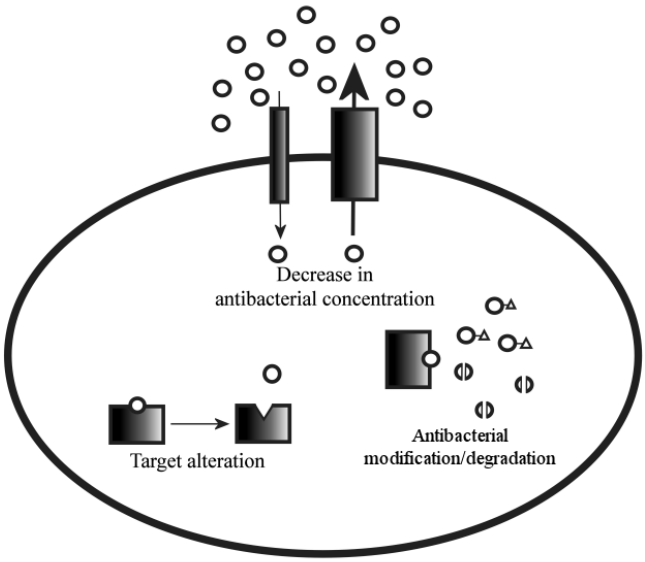

Figure 1.12: Antibiotic resistance mechanisms utilized by bacteria.
1) Decreasing the internal concentration of the antibiotic 2) modification of the target site 3) modification of the antibacterial

Modification or hydrolysis of the antibiotic is a common mechanism of resistance employed by bacteria. β-Lactamases are a classic example of this type of resistance mechanism. These enzymes degrade penicillin by hydrolyzing the β-lactam ring of the antibiotic rendering it ineffective. Likewise, altering the target site prevents the antibiotic

from binding and exerting its action. This is the case for DNA gyrase and topoisomerase, which are targets for fluoroquinolone antibacterials [54,58,61-63].

1.3.2. Methylation as a Resistance Mechanism: Erythromycin Resistance as a Paradigm

The order Actinomycetes (in particular *Streptomyces* genus) has long been recognized as a prolific producer of antibiotics [64]. Any antibiotic-producing bacteria must find a way to avoid the toxicity of its own product (discussed briefly in the *Section 1.3.1*). One common molecular mechanism utilized to confer resistance to autogenous antibiotics is methylation (target alteration). Many antibiotic producers have genes that encode for AdoMet-dependent ribosomal RNA (rRNA) MTases that methylate ribosomes at specific sites. Methylation either on the 23S rRNA in the 50S subunit or the 16S rRNA in the 30S subunit blocks the antibiotic from binding so that it can no longer exert its action [65]. Resistance to the antibiotic erythromycin exemplifies this type of resistance mechanism, and will be a focus of this section.

Erythromycin is a member of the macrolide class of antibiotics whose structural features are defined by a large macrocylic lactone ring (12-16 carbons) substituted with one or more sugar moieties [66,67]. Erythromycin A was first isolated from *Saccharopolyspora erythraea* (formerly known as *Streptomyces erythreus*) and is a 14-membered macrocylic lactone with two substituted sugars: β-D-desoamine in the C-5 position and α-L-cladinose in the C-3 position (**1-5**). Erythromycin is a commonly administered antibiotic and is active primarily against Gram-positive bacteria and some Gram-negative species [68,69].

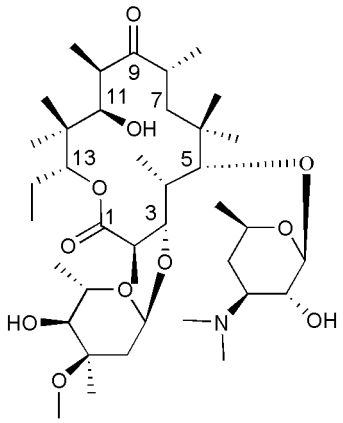

1-5

Macrolide antibiotics such as erythromycin are inhibitors of protein synthesis in prokaryotes by binding to the 50S subunit of the ribosome at the peptidyl transferase centre. The antibiotic prevents the growth of the nascent protein chain after two or three residues have been synthesized and causes premature dissociation of the peptidy-tRNA from the ribosome [70,71]. The binding site for erythromycin and other macrolides resides in domains II and V of the 23s rRNA [72]. In the completely folded 50S ribosomal subunit, hairpin 35 of domain II and the petidyl transferase loop of domain V are folded into close proximity to each other [73,74] (Figure 1.13).

Footprinting studies have shown that erythromycin interacts with adenine 2058 (A2058, *E. coli* numbering) and adenine 2059 (A2059) of domain V and adenine 705 (A705) of domain II (Figure 1.13) [72,74,75]. Ribosomal protein L22 interacts with all six domains of the 23S rRNA. It forms the majority of the polypeptide exit channel, and the narrowest constriction of this channel is comprised of L22 and L4 [73,76]. Upon binding of erythromycin or other macrolides into the binding pocket, the polypeptide exit tunnel is blocked, effectively stopping polypeptide elongation (Figure 1.13) [77,78].

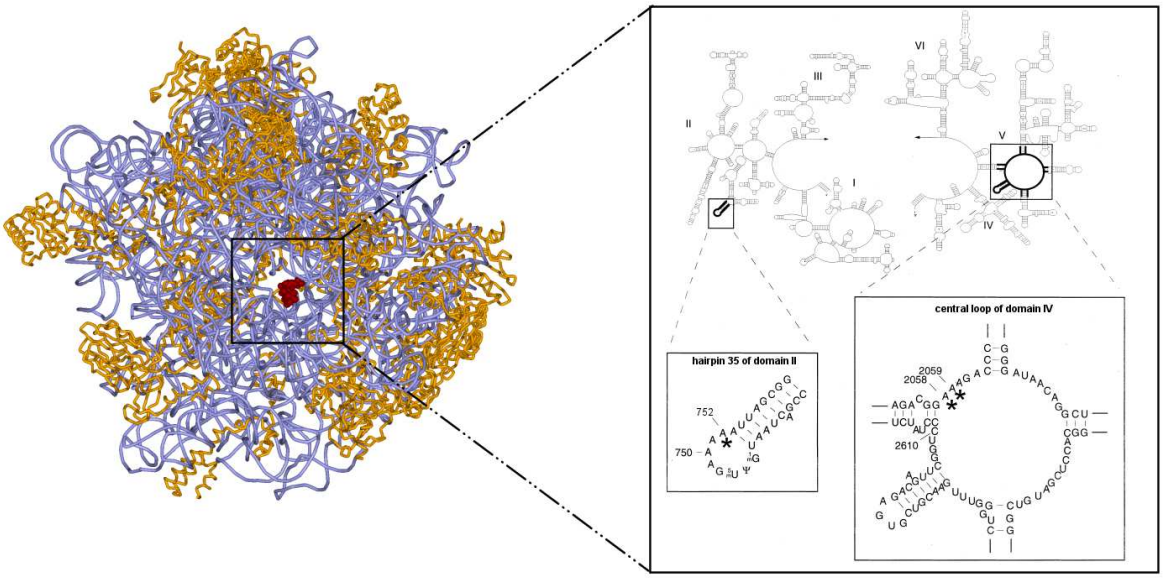

Figure 1.13: Macrolides block the the polypeptide exit tunnel of the large ribosomal unit. Erythromycin (red) blocking the entrance to stop the progression of polypeptide growth (PDB: 1YI2). Six domains comprise the 23S rRNA in the large 50S subunit of the ribosome and is shown on the right hand side. Ribosomal proteins are shown in yellow and RNA in blue. Hairpin 35 of domain II and the peptidyl transferase loop make the binding region of erythromycin. Foot binding studies show that the antibiotic interacts with A752 of hairpin 35 and A0258 and A2059 of central loop of domain V (Adpated from [74]).

Resistance to erythromycin can be achieved by mono- or di-methylation of the exocyclic amino group of a single adenine group (A2058) on domain IV carried out by erythromycin resistance methyltransferase [79-81]. Conversion of the adenine residue to N^6, N^6-dimethyladenine (or N^6-methyladenine) reduces the binding affinity of erythromycin through disruption of hydrogen bonding interactions between the macrolide and the nucleotide, and consequently impedes erythromycin's action. Furthermore, the presence of the additional methyl groups introduced by Erm MTase obstruct the interaction of erythromycin with binding to its cognate target [78-81]. Methylation renders resistance not only to macrolides, but provides cross-resistance to several structurally dissimilar antibiotics such as the lincosamides and streptogramin B (Figure 1.14). This resistance is collectively referred to as MLS_B, or Macrolide-Lincosamide-Streptogramin B resistance [82].

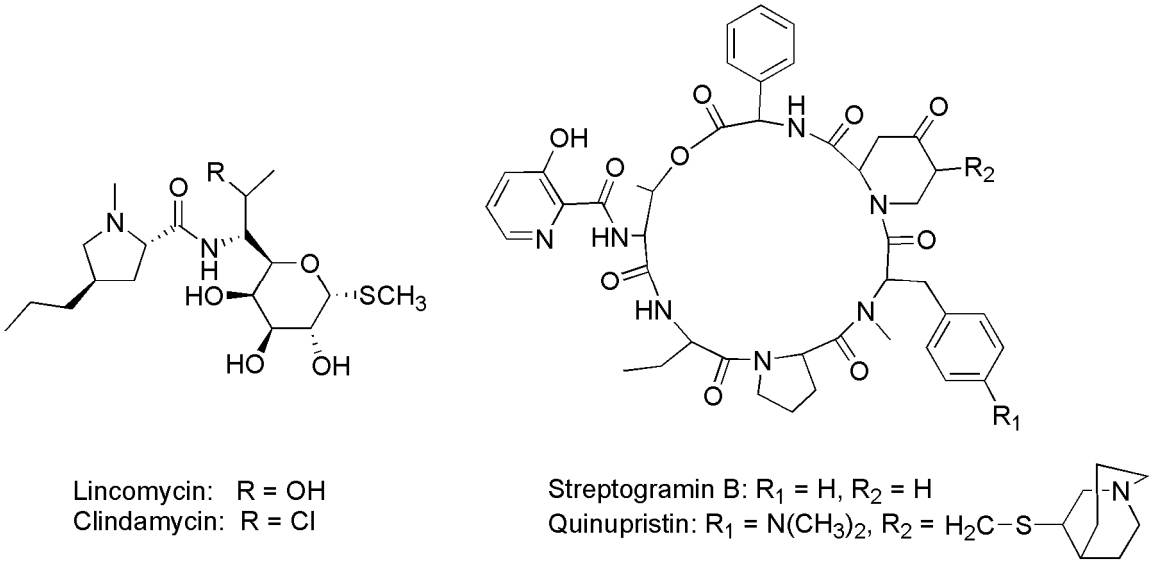

Figure 1.14: Examples of lincosamides and streptogramin Bs.
Resistance to macrolides confers resistance two these two families of antibiotics despite structural dissimilarity.

1.3.3. Other MTases that Confer Antibiotic Resistance

There are a number of other MTases that are known to confer antibiotic resistance. Methylation is an emerging resistance mechanism for clinically relevant aminoglycosides such as kanamycin and gentamycin [83]. Methylation of A1408 of the istamycin producer, *Streptomyces tenjimarienus* bestows resistance to kanamycin and apramycin, while methylation of G1405 of *Micromonospora purpurea* mediates resistance to kanamycin and gentamicin [84]. AviRb from *Streptomyces viridochromogenes Tü57* methylates U2479 of 23S rRNA and gives rise to resistance to avilamycin A, an antibiotic commonly used as a growth promoter in animal feed [85]. Resistance to chloramphenicol, florfenical and clindamycin can be achieved by methylation of A2503 in *Staphylococcus sciuri* [86]. Therefore, methylation by AdoMet-dependent MTases plays a significant role in antibiotic resistance mechanisms. The focus of this thesis is on the peptide antibiotic thiostrepton and the MTase that confers resistance to it, thiostrepton-resistance rRNA MTase (TSR) in the antibiotic producing organism *Streptomyces azureus*.

1.4. Thiostrepton and Thiostrepton Resistance

1.4.1. The Thiopeptide Antibiotic Thiostrepton

Thiostrepton (TS; $C_{72}H_{85}N_{19}O_{18}S_5$, mw = 1665 g/mol; **1-6**) is a member of a family of multicyclic peptide antibiotics known as the thiopeptide antibiotics. These antibiotics all share common structural features such as thiazole groups, dehydro amino acid residues scattered throughout the peptide backbone scaffold and a piperidine or dehydropiperidine serving as linchpin between two or three macrocylic domains [87].

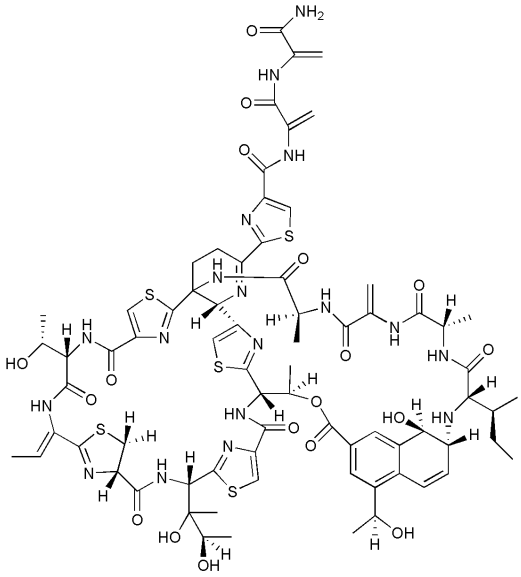

1-6

TS was originally isolated from *Streptomyces azureus* [88,89] and later found in *Streptomyces hawaiiensis* [90] and *Streptomycyes laurentii* [91]. It is effective against Gram-positive bacteria. Gram-negative species are intrinsically resistant due to the impermeability of the outer membrane to TS [92]. TS also exhibits activity against *Plasmodium falciparum*, the major organism responsible for human malaria [93].

1.4.2. Mode of Action of Thiostrepton

All members of the thiopeptide antibiotics not only possess a similar structure, but they also share a similar mechanism of action. TS inhibits protein biosynthesis by binding to the 50S ribosomal subunit at the GTPase centre. This centre is comprised mainly of ribosomal protein L11 complexed with a region of the 23S rRNA termed the L11 Binding Domain (L11BD). Thiostrepton binds between the cleft that is formed between the rRNA and the N-terminal domain of L11 [94-97] (Figure 1.15).

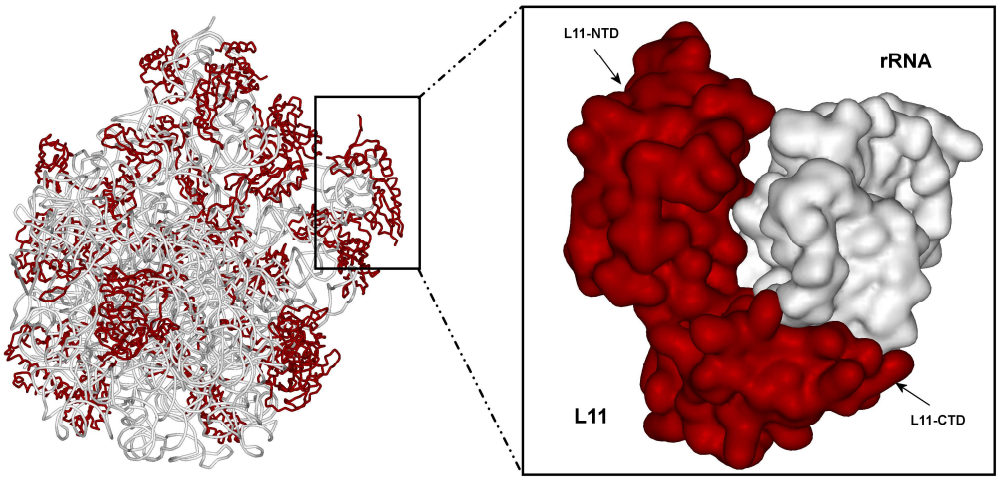

Figure 1.15: Thiostrepton inhibits protein biosynthesis by binding to the GTPase centre of the ribosome. The GTPase centre is comprised of 23S rRNA (white) and Protein L11 (red) (PDB: 3CF5 and 1OLN).

The L11BD is a well conserved 58 nucleotide sequence (nt 1051 to 1108) that forms a hairpin structure to which TS binds very tightly ($K_D = 10^{-7}$M) [98] (Figure 1.16). However, binding affinity of TS in the presence of protein L11 is several orders of magnitude greater [98,99]. Ribosomal protein L11 has two distinct domains tethered by two conserved proline residues. The C-terminal domain (CTD) is responsible for anchoring the protein to the ribosome and binds to the L11BD, making extensive contacts with the rRNA backbone. Conversely, the proline rich N-terminal domain (NTD) makes limited contacts to the rRNA [100,101].

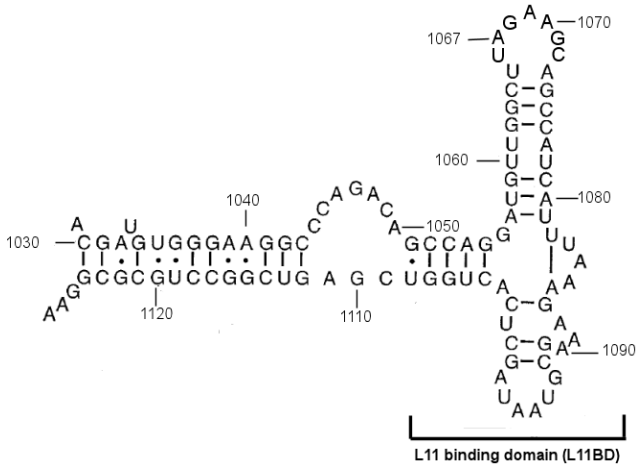

Figure 1. 16: Secondary structure of the 23S rRNA in the GTPase region.
Nucleotides 1051-1108 (*E. coli* numbering) comprise the L11 Binding Domain (L11BD) which binds to the C-terminal domain of protein L11.

The NTD undergoes a sequence of conformational changes during the elongation step of protein biosynthesis that facilitate the essential GTP hydrolysis reactions [102]. Figure 1.17 shows a general overview of the elongation cycle during protein chain growth. The process begins with Elongation Factor-Tu (EF-Tu) complexed with GTP delivering the aminoacyl-tRNA to the ribosomal aminoacyl site (A site) (Step 1). Upon binding, GTP is hydrolyzed, with the concomitant transfer of the growing peptide chain on the peptidyl-tRNA to the aminoacyl-tRNA that just arrived (Step 2). Translocation of the aminoacyl-tRNA from the A site to the Peptidyl site (P site) is mediated by the binding and hydrolysis of the Elongation Factor-G (EF-G) • GTP complex. The deacylated tRNA now leaves through the exit site (E site) and the cycle repeats (not shown in figure) [103]. It has been postulated that the flexible L11-NTD region functions as a molecular switch, playing a significant role in the release of EF-Tu and EF-G [104,105].

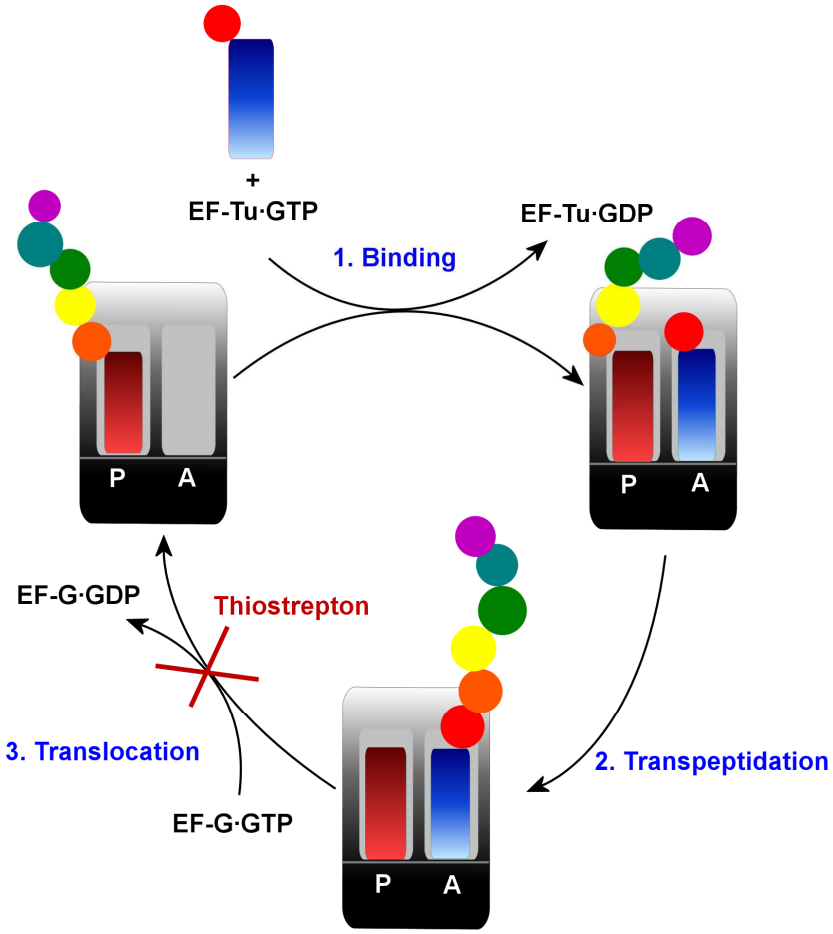

Figure 1. 17: Steps in the peptide elongation cycle in protein biosynthesis.
See text for a brief description of protein biosynthesis. The antibiotic thiostrepton inhibits the hydrolysis of the GTP in the EF-G•GTP•ribosome complex thus halting the process.

The binary complex (L11 and rRNA) is the functional state to which elongation factors are able to bind freely and reversibly, however, with the antibiotic present, EF-G binding is prevented. When TS binds, the L11-NTD rotates and the domain moves closer to the rRNA (Figure 1.18). This binding imposes conformational rigidity to the NTD to the same degree as the CTD [106]. Therefore, the presence of TS locks this "molecular switch" in the "off position" [107], and as a consequence, protein biosynthesis is stopped prematurely at the translocation step [106-108].

A second molecular switch, which has also been proposed to be turned off upon binding of TS involves ribosomal protein L7. Ribosomal protein L7 is important in the release (but not the hydrolysis) of phosphate (Pi) [109]. In the presence of TS, a conformational change within the L11-NTD interrupts the otherwise stable interaction between protein L11 and the C-terminal domain L7. This interaction permits the L7-CTD to interact with EF-G such that the GTP-binding pocket of EF-G allows for Pi to be released [107]. Therefore, the binding of TS turns off two molecular switches by initiating an interdomain and intradomain change of protein L11.

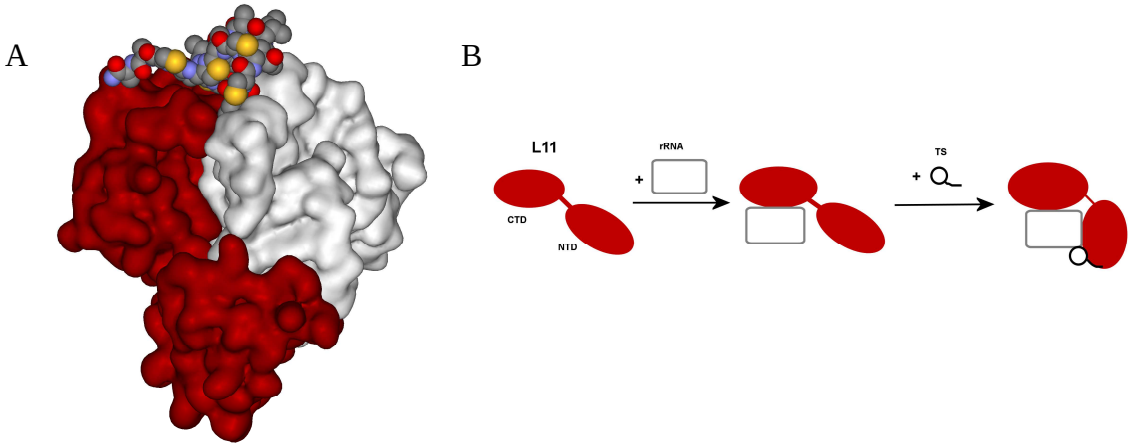

Figure 1. 18: Thiostrepton binding to the L11BD.
(A) Structure of thiostrepton (TS) bound to the rRNA (white) and Protein L11 (red) (PDB: 2JQ7). **(B)** The relative orientation of the C-terminal domain (CTD) and the N-terminal domain (NTD) of Protein L11 changes upon 23S rRNA binding. The NTD is brought closer to the rRNA when TS binds (Adapted from [106]).

1.4.3. Mechanism of Resistance: Thiostrepton-resistance rRNA Methyltransferase

Streptomyces species are quite sensitive to TS; however, the TS-producer, *S. azureus* is unaffected by the production of its own antibiotic. For example, *Streptomyces coelicolor* did not grow on nutrient plates containing 1 μg/mL of TS while *S. azureus* growth remained resilient at high concentrations (50 μg/mL) [110]. *S. azureus* encodes a gene that confers resistance by preventing TS from binding at the 23S rRNA target site. The gene product is a

RNA-pentose MTase, thiostrepton-resistance rRNA MTase (TSR), which, methylates a specific adenosine (A1067, *E. coli* numbering) at the 2-*O*′-hydroxyl group to give 2′-*O*-methyladenosine. The introduction of a methyl group precludes binding of thiostrepton, thereby rendering the ribosome resistant to the antibiotic [94,111,112].

TSR is produced within *S. azureus* and can only methylate protein-free 23S rRNA and has no effect on intact ribosomes. Methylation is only observed *in vitro* when salt treated (LiCl) are stripped to their "core particles". However when the "split" proteins are added back to reconstitute ribosomes, methylation did not occur. This suggests that *in vivo*, TSR must act early during transcription and prior to the assembly of the 50S subunit [111]. Through a series of mutagenesis experiments, elements on the L11BD essential for TSR recognition and enzyme methylation have been determined. TSR enzyme activity requires U1061, U1057 and the sequence of U1066-A1067-G1068-A1069-A1070, which contains the methylation target itself. The majority of residues on the hairpin encompassing residues 1051-1108 on the L11BD is also required for recognition (Figure 1.19) [113].

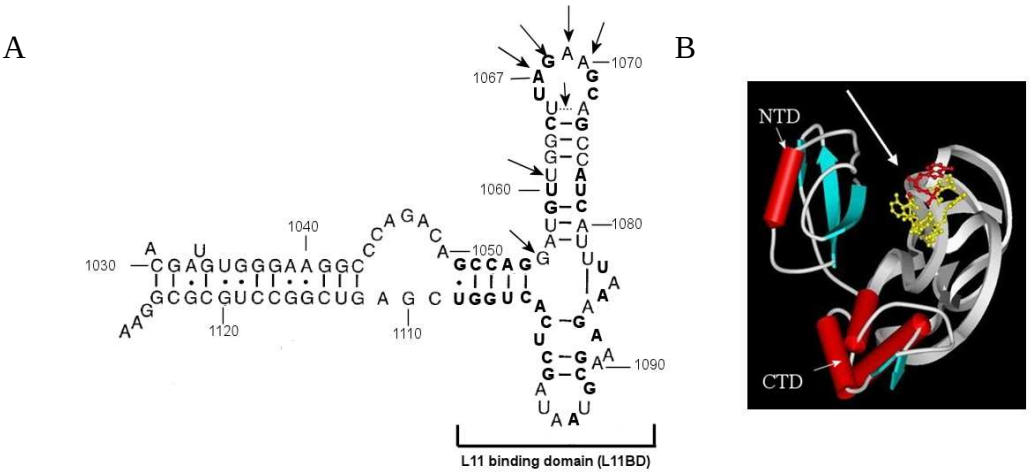

Figure 1.19: Recognition hairpin on 23S rRNA for TSR MTase.
(A) Secondary structure of the *E. coli* 23S rRNA GTPase centre at the L11 binding domain. Arrows point to nucleotide bases that are essential for the enzyme activity of thiostrepton-resistance rRNA methyltransferase (TSR), and bold residues are residues required for recognition. **(B)** Complex of protein L11 (red cylinders and blue arrows) and 23S rRNA fragment (grey ribbon). Yellow residues are bases important for the recognition by TSR. The arrow points to the site of methylation, A1067 shown in red (PDB: 1OLN).

1.5. Research Objectives

The widespread use of antibiotics has been accompanied by the appearance of antibiotic resistance in bacteria. The strategies by which antibiotic-producing bacteria maintain resistance to their endogenous drug's action have been subjected to in depth investigation. This doctoral thesis explores the structure and function of TSR, with the intent of better understanding antibiotic-ribosome interactions. We overexpressed, isolated and characterized TSR, and this research is described in *Chapter 2* and *Chapter 3*. The structure of the enzyme was approached, initially by *in silico* means (homology modelling) and later through X-ray crystallography by our collaborators. Towards the end of completion of this thesis research, a successful X-ray crystal structure was acquired by our collaborators, in the laboratory of Dr. Graeme Conn; *Chapter 4* focuses on a detailed analysis of the structure of TSR.

In addition to studying the enzyme, we also endeavoured to study the cognate antibiotic, TS (*Chapter 5*). We performed molecular mechanics, semi-empirical and *ab initio* studies to further understand the structural and electronic properties of this antibiotic. In conjunction with this study, we began an investigation on single site chemical modifications of thiostrepton to attempt to improve its solubility while maintaining its antimicrobial activity.

CHAPTER 2: OVEREXPRESSION AND PURIFICATION OF *STREPTOMYCYES AZUREUS* THIOSTREPTON-RESISTANCE rRNA METHYLTRANSFERASE

It has been known for a number of years that resistance to the peptide antibiotic, thiostrepton (TS), can be achieved through methylation of the ribosomal RNA (rRNA) at the guanosine triphosphatase region [97,98]. The thiostrepton producer, *Streptomyces azureus*, possesses a gene (*tsr*) that encodes for a 23s rRNA methyltransferase which catalyzes the methylation of the 2′-hydroxyl group of adenosine 1067 (A1067, *E. coli* numbering) (Figure 2.1).

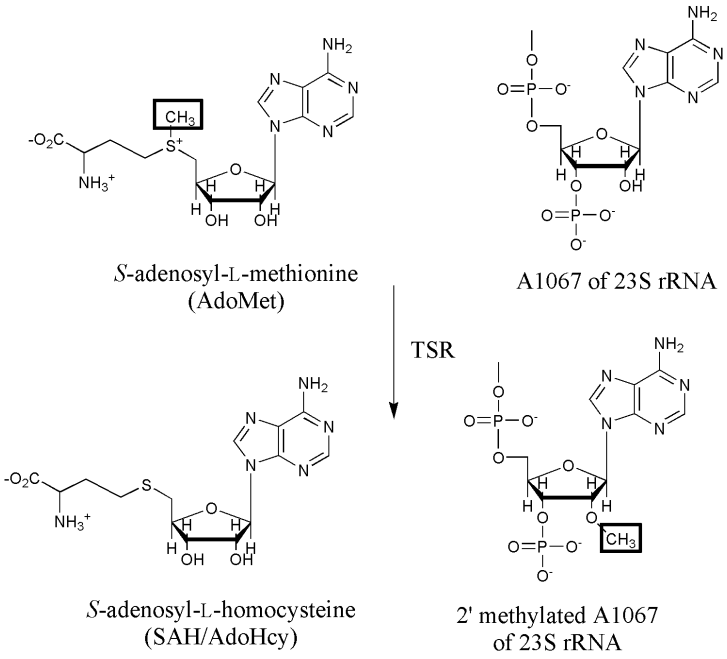

Figure 2. 1: Methylation of the 2′O hydroxyl moiety of A1067 of the 23S rRNA by thiostrepton-resistance rRNA methyltransferase (TSR).

This enzyme, thiostrepton-resistance rRNA methyltransferase (TSR; EC 2.1.1.66), utilizes the methylating agent *S*-adenosyl-L-methionine (AdoMet) and modifies the 23S rRNA such that it prevents TS from binding between the hairpin region containing A1067

and the ribosomal protein L11; as a result, protein translocation can continue without interruption [94,97,110-112].

TSR is composed of 269 amino acid residues with a molecular mass of 28901 Da, and initial isolation and characterization of this enzyme was performed by Thompson and Cundliffe [114] and Bechthold and Floss [113] in 1981 and 1994 respectively. Although the function of TSR has been briefly studied and documented in the literature, its structure was not available until recently [113,114]. Interestingly, through sequence analyses, TSR is found to possess certain conserved sequence elements possessed by members of the newly identified SpoUT (Class IV) methyltransferase superfamily [29,115]. Therefore, it is very likely that TSR possesses the unique topological feature observed in this superfamily: a deep trefoil knot in its active site region. Proteinaceous knots are observed in nature and are quite rare: less than one percent of all protein structures deposited in the Protein Databank contain knots [116]. Therefore, TSR not only presents an attractive enzyme for which to study protein-RNA interactions and antibiotic resistance mechanisms, but its putative knot presents a fascinating aspect to protein structure-function relationships worthy of investigation.

2.1. Cloning and Purification of Hexahistidine-tagged Thiostrepton Resistance rRNA Methyltransferase

Previous work in the Honek laboratory resulted in the cloning of the *S. azureus* TSR gene (a generous gift from Dr. Gerry Wright, McMaster University) into a pET-22b expression vector and then introduced into *E. coli* BL21 (λDE3)/pLys. Purification of the enzyme was done by conventional chromatographic means: anion exchange, hydrophobic interaction, hydroxyapatite chromatography followed by a second anion exchange column. Although this purification of TSR yielded enzyme of substantial purity, unfortunately it was

still not sufficiently pure for X-ray crystallography and at each purification step, a substantial amount of protein was lost, giving a very low overall yield. Since the determination of the X-ray crystal structure of TSR would require large amounts of highly purified enzyme, efforts to find an alternative, and more efficient method of purification were directed to the use of fusion tags.

2.1.1. Affinity Tags

A fusion or affinity tag can be defined as an exogeneous amino acid sequence with a high affinity for a specific ligand (biological or chemical) [117]. These fusion tags can be classified as protein tags (small globular proteins) or peptide tags (less than 25 amino acid residues), and have become highly efficient tools for protein isolation [118]. Affinity tags can be introduced at the N- or C-terminal of the target protein, and they exploit the selective and specific interaction and recognition of the fusion protein to a complementary ligand immobilized on the stationary matrix. Fusion tags enable the purification of different proteins with different biochemical properties using a common procedure [117,119].

Advantages of using affinity tags over conventional techniques are that they not only facilitate facile purification of their fusion partner (one step purification), but they can also increase overall purification yield [120], increase solubility [121], enhance proper protein folding [122] and prevent proteolysis [123]. On the otherhand, the presence of a fusion tag may lead to negative effects on the protein such as change in protein conformation [124], lower yields [125], and compromised enzyme activity [126]. It is imperative to choose an affinity tag that does not affect the structure or function of their fusion partner.

There are a number of different affinity tags available, all of which follow a similar protocol with slight changes in buffer conditions [127] (Table 2.1). A comprehensive review

of these affinity tags is beyond the scope of this thesis, but the topic has been reviewed extensively elsewhere in the literature [117,118,127,128].

Table 2. 1: Common Affinity Tags Utilized and their Matrices.
(Adapted from [127])

Affinity Tag	**Size (aa)**	**Sequence**	**Matrix**
Poly-His	2-10 *(5)*	HHHHHH	Ni^{2+}-NTA, Co^{2+}-CMA* (Talon®)
Poly-Arg	5-6 *(6)*	RRRRR	Cation exchange resin
FLAG	8	DYKDDDDK	Anti-FLAG monoclonal antibody
Strep-tag II	8	WSHPQFEK	Strep-Tactin (modified streptavidin)
c-myc	11	EQKLISEEDL	Monoclonal antibody
S-tag	15	KETAAAKFERQHMDS	S-fragment of RNase A
HAT (natural his affinity tag)	19	KDHLIHNVHKEFHAHAHNK	Co^{2+}-CMA (Talon®)
Calmodulin-binding peptide	26	KRRWKKNFIAVSAANRFKKISSSGAL	Calmodulin
Cellulose-binding domain	27-189	Domains	Cellulose
SBP	38	MDEKTTGWRGGHVVEGLAGELEQLRARLEHHPQGQREP	Streptavidin
Chitin-binding domain	51	TNPGVSAWQVNTAYTAGQLVTYNGKTYKCLQPHTSLAG WEPSNVPALWWQLQ	Chitin
Glutathionine S-transferase	211	Protein	Gluthathione
Maltose-binding protein	396	Protein	Cross-linked amylose

*CMA = caroxylmethylaspartate

2.1.2. Removal of Affinity Tags

The presence of an affinity tag may not alter the biological activity of a protein, and thus the removal of the affinity tag may not be necessary. Nonetheless, the presence of a fusion tag could potentially alter the protein in an unpredictable manner and it is usually preferable that the tag be removable [117]. Affinity tags are typically removed enzymatically [127], although treatment with harsh chemicals such as cyanogen bromide is an alternative method [129] (Table 2.2). Enzymatic cleavage is preferred over chemical methods because they are more specific and are performed under mild conditions, whereas with chemical cleavage can lead to modification of side chains and protein denaturation [117].

Table 2. 2: Different Agents Utilized to Remove Affinity Tags. (Adapted from: [118])

Cleavage Agent	Cleavage Specificity
Chemical Treatment (harsh)	
Cyanogen bromide	X-M-↓-Xaa
Hydroxylamine	Asn-↓-Gly
Formic Acid	Asp-↓-Pro
Acetic Acid	Asp-↓-Pro
Enzymatic Treatment (mild)	
Endopeptidases	
Thrombin	Arg-Gly-Pro-Arg-↓-Xaa
Trypsin	Arg/Lys-↓-Xaa
Factor Xa	Ile-Glu-Gly-Arg-↓-Xaa
Subtilisin	Ala-Ala-His-Tyr-↓-Xaa
Enterokinase	Ala-Ala-Ala-Ala-Lys-↓-Xaa
Exopeptidases	
Carboxypeptidase A	Poly His-↓-Xaa
Carboxypeptidase B	Ply Arg-PolyLys-↓-Xaa
Aminopeptidase I	Glu-Ala-Glu-↓-Xaa
Dipeptidylaminopeptidase	Xaa-Tyr-↓-Xaa (not Pro)

Xaa = unspecified amino acid

A protease specific cleavage sequence is introduced between the fusion tag and the fusion partner [130]. Cleavage can be performed with either endoproteases such as thrombin and trypsin or exopeptidases such as carboxypeptidase A or aminoeptidase I. Depending on

the protease, cleavage of the tag can be “clean” or leave a few amino acid residues extra on the protein [118]. Overall protein yield may decrease if there is unexpected cleavage or incomplete cleavage, thus optimization of cleavage conditions is required. Furthermore, after removal of the tag, the “detagged” protein must be isolated from the protease and the affinity tag [117,118,127].

2.1.3. Purification with a Histidine Affinity Tag

The most widely utilized affinity tag is the poly-histidine tag that is comprised of a stretch of histidine residues of varying numbers. His-tags are relatively small and work under both native and denaturing conditions. Its affinity resin is relatively inexpensive and elution conditions are mild. All these advantages make the histidine affinity tag a very attractive fusion tag to use on an enzyme system [128]. The general purification protocol of his-tagged-proteins involves immobilized metal ion adsorption chromatography (IMAC) [131]. The crude cell lysate containing all of its endogenous proteins is passed through a column containing immobilized transition metal ions such as nickel, cobalt or zinc on an adsorbant (typically nitrilotriacetic acid). The histidine imidazole effectively chelates the metal ions allowing for the his-tagged-protein to be retained on the column. The target protein is eluted by washing the column with increasing concentrations of imidazole which displaces the polyhistidine-tagged protein from the column [127] (Figure 2.2). IMAC is a very efficient method of protein purification, although it is not recommended for metalloproteins [117].

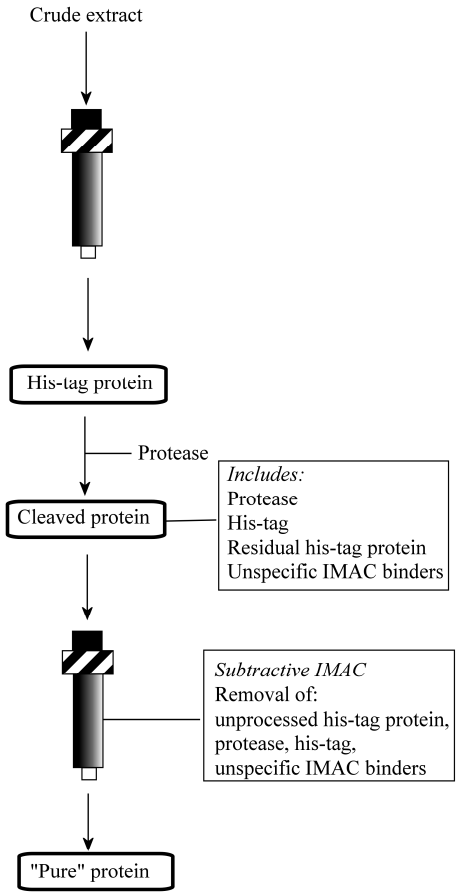

Figure 2. 2: General overview of the purification of a histidine-tagged protein and its subsequent removal. Adapted from [117].

The strength of binding of the affinity handle to the matrix is determined by the number of histidine residues present. However, at any given time, only two histidine residues in the sequence can coordinate to one metal ion. Therefore, the more histidine residues present, the higher the likelihood that two will be in a favourable orientation to coordinate with the immobilized metal. The most commonly employed histidine-tag is the hexahistidine-tag [118].

2.1.4. Plan of Action

With the above considerations of fusion tags in mind, we endeavoured to overexpress and purify TSR with a hexahistidine-tagged appended to its N-terminus. While the hexahistidine-tagged TSR was expressed as a soluble protein, throughout the purification process, large amounts of protein precipitated, making TSR a very difficult enzyme to handle. A number of different screening conditions were examined and eventually, it was found that removal of the tag and addition of certain buffer additives yielded enough soluble protein for biochemical and structural studies. This chapter describes the experiments involved in the overexpression and isolation of TSR.

2.2. Materials and Methods

2.2.1 Reagents and Materials

The following reagents and materials were obtained from the following companies:

BDH (VWR) (Mississauga, ON): citric acid, 38% formaldehyde, sodium acetate

Bioshop (Burlington, ON): agarose, bacto-tryptone, chloramphenicol, imidazole, isopropyl-β-thiogalactopyranoside (IPTG), kanamycin, trichloracetic acid, Tris (hydroxymethyl) aminomethane hydrochloride (Tris-HCl), and Tris (hydroxymethyl) aminomethane hydroxide (Tris-OH), phenylmethylsulfonyl fluoride (PMSF), yeast extract

EMD Pharmaceuticals (Durham, NC): acetone, 14.8 M ammonium hydroxide, ethylenediamine tetraacetic acid (EDTA), glacial acetic acid, glycerol, methanol, sodium dodecyl sulphate (SDS), sodium chloride, sodium hydroxide

GE Healthcare (formerly Amersham Biosciences) (Uppsala Sweden): thrombin protease, Phastgels, Phastgel buffer strips

Qiagen (Mississauga, ON): nickel (II) nitrolotriacetic (Ni-NTA) super flow resin

New England Biolabs: 100 bp DNA ladder, *Nde*I, *Bam*HI

Sigma Chemical Company (St. Louis, MO): β-mercaptoethanol, bovine serum albumin, bromophenol blue, Coomassie Brilliant Blue G-250, ethidium bromide, nickel (II) sulphate,

2.2.2 General Equipment

2.2.2.1. Cell Disruption Equipment

Lysates of cells for purification were obtained from sonication of resuspended cells with a Sonicator™ cell disruptor model W225 from Heat Systems-Ultrasonics, Inc (Plainview, NY), converter model #2 with a standard tapered mircrotip at an output control setting at 5.

2.2.2.2. Centrifuges

Microvolume centrifugation was carried out using the Biofuge A microcentrifuge (Heraeus Sepatech GmbH, Germany). For large volume samples (>20 mL), centrifugation was done on a Beckman Avanti® J-25I centrifuge (Mississauga, ON) or on the Beckman Coulter Avanti® JE centrifuge (Fullerton, CA, USA). For protein concentration with starting volumes between 1 – 2.5 mL, Vivascience Vivaspin concentrators were used at a speed of 5000 rpm on the VWR Clinical 100 Microcentrifuge.

2.2.2.3. Chromatographic Equipment

All columns utilized in the purification process (HisTrap™ HP, HiTrap Benzamidine FF and MonoQ) were acquired from GE Healthcare (formerly Amersham Biosciences, Uppsala, Sweden). Purification of TSR was either performed on a Fast peptide and protein liquid chromatography (FPLC®) machine or a high performance liquid chromatography apparatus (HPLC). FPLC was performed on a Pharmacia Biotech (now GE Healthcare, Uppsala, Sweden) system comprising of: LCC-500 chromatography controller, two P-500 pums, MV-7 motor valve and Empower Pro (Build 1154) software. HPLC was carried out on a Waters HPLC system (Milford, MA, USA) consisting of the following components: Waters 600S controller, Waters 626 pump, Waters 2996 Photodiode Array Detector, in addition to Waters Empower 2 software, Build 2154. All aqueous buffers were filtered through a 0.2 μm membrane filter (Pall Life Sciences, East Hills, NY). Before injection, all samples were filtered through a syringe filter: 0.2 μm polyethersulfone membrane (VWR International, Mississauga, ON). All buffers were degassed prior to use.

2.2.2.4. Incubators

Growth of liquid bacterial cultures employed either a Series 25 controlled environment incubator shaker (New Brunswick Scientific Co., Inc., Edison, NJ) or Innova™ 4330 refrigerated incubator shaker (New Brunswick Scientific) both shaking ~ 200 rpm. For standing or plated bacterial cultures, growth was done in a Precision® gravity convection incubator from Precision Scientific, Inc (Chicago, IL).

2.2.2.5. Protein Concentration Devices

Concentration of purified protein was accomplished using Amicon Centricon® YM 10 (Millipore, Bedford, MA) centrifugal concentrators, VivaScience Vivaspins (Stonehouse, UK) with a molecular weight cut off of 10 000 Da, or Nanosep® Centrifugal devices with 10K molecular weight cutoff (PALL, East Hills, NY)

2.2.2.6. Spectrophotometry

Protein quantitation assays using the Bradford Assay method were performed using one of the following instruments: Varian Cary 3 UV-Visible Spectrophotomter (Mississauga, ON) spectrophotometer with the CaryWinUV Advanced Reads Application Software 3.00 (182); Ultrospec 2100 pro UV/Visible spectrophotometer (GE Healthcare, Uppsala, Swedan); Molecular Devices Spectramax® Plus 384 (Union City, CA, USA), SoftmaxPro v. 501 Software.

2.2.2.7. Thermal Cyclers

All polymerase chain reactionss were performed on a Techne® (Princeton, NJ, USA) Techgene cycler or Applied Biosystems GeneAmp® PCR System 2700 v. 2.04 machine (Foster City, CA, USA).

2.2.2.8. Mass Spectrometer

The nano-electrospray mass spectrometer used was a Micromass Q-TOF Ultima™ Global and supplied by the Waterloo Chemical Analysis Facility, University of Waterloo.

2.2.3 General Experimental Protocols

2.2.3.1. Gel Electrophoresis

DNA Electrophoresis

Agarose gel electrophoresis was used to separate plasmid DNA and DNA fragments based on size for further manipulations. Agarose gels consisted of 0.8-1.5% (w/v) molecular biology grade agarose and 1× TAE (Tris-acetate-EDTA buffer; 40 mM Tris base, 20 mM glacial acetic acid, 1 mM EDTA) and were prepared in the following manner: 0.8 g of agarose was added to 100 mL of 1× TAE and dissolved with heat via microwaving for approximately two minutes. The agarose was allowed to cool to approximately 50 °C prior to adding 4 μL of ethidium bromide (0.5 μg/mL) for visualization. The agarose-ethidium bromide mixture (~20 mL) was then poured into a plastic chamber and allowed to cool. DNA samples to be separated were mixed 1:5 volume of 6× loading buffer (10 mM Tris-HCl, pH 7.5, 50 mM EDTA, 10% glycerol, 0.25% Bromophenol Blue). All samples were run in

parallel with a 100 bp DNA ladder in TAE buffer at approximately 80 V. Bands were visualized under short UV-light for photographs and long UV-light for band excision.

Protein Electrophoresis

Standard sodium dodecyl sulphate polyacrylamide-gel electrophoresis (SDS-PAGE) was utlized to separate proteins based on their molecular weights. All protein samples were denatured, linearized and were made negatively charged by boiling for 5-10 min after mixing with loading buffer (150 mM Tris-OH, 2% SDS, 1% β-mercaptoethanol, 10% glycerol, 0.1 Bromophenol blue pH 8.0) at a 1:1 ratio. Separation of proteins employed the semi-automated Pharmacia PhastSystem^{TM} electrophoresis system with precast gels and buffer strips. Gradient gels (10-15%) were used for separation unless stated otherwise.

Coomassie Staining

Development of gels involved three steps: 1) staining with 0.1% Coomassie brilliant blue R, 30% methanol and 10% acetic acid 2) destaining with 30% methanol, 10% acetic acid and 3) preserving with 5% glycerol and 10% acetic acid.

Silver Staining

The silver staining protocol was adapted from Wray and coworkers [132] and involved four solutions. *Solution A:* 0.8 g $AgNO_3$ was dissolved in 4 mL of ddH_2O. *Solution B:* 10.5 mL of 0.35% NaOH mixed with 0.7 mL of 14.8 M NH_4OH. *Solution C:* Solution A was added dropwise into Solution B with constant stirring. A small amount of precipitate will appear and then dissolve before adding the next drop. When all of Solution A is added to

Solution B OR if the precipitate does not dissolve, the total volume is increased to 100 mL with ddH_2O. Solution C must be prepared fresh and used within 5 min. *Solution D:* 1.25 mL of 1% citric acid was mixed with 125 µL 38% formaldehyde and increased to a volume of 250 mL with ddH_2O. This solution must also be freshly prepared.

After protein separation has been performed, the gel was soaked in 50% reagent grade MeOH for at least 1 hour. During this time, Solution C was prepared and used to stain the gel with constant agitation. The gel was then washed in ddH_2O for 5 min before putting into the developer solution, Solution D. Development of the staining is stopped when bands appear and then the gel is washed immediately with ddH_2O and placed in 50% MeOH or 45% MeOH/CH_3COOH to stop the reaction.

2.2.3.2. DNA Manipulation and Cloning Methods

Standard bacterial and DNA cloning was performed following the standard molecular protocols outlined by Sambrook *et al*. [133].

2.2.3.3. Trichloroacetic Acid Precipitation

Protein samples recovered at low concentrations were precipitated using trichloroacetic acid (TCA) and resolved using SDS-PAGE. TCA was added to a protein sample (~100 to 300 µL) to a final concentration of 10% and placed on ice for 15-30 min. The sample was centrifuged at 4 °C at 13000 ×*g* for 15 min. The supernatant was removed and discarded and the precipitated pellet was washed and resuspended with 300 µL of ice cold acetone and respun for 5 min. The acetone was removed and discarded and the final pellet was allowed to air dry thoroughly for a minimum of 15 min. The pellet was then

resuspended in SDS loading buffer with vigorous vortexing, and boiled for 5 -10 min prior to loading onto the SDS-PAGE gel.

2.2.3.4. Determination of Protein Concentration

Protein concentration was measured based on the Bradford method [134]. The Bradford assay dye reagent was prepared by dissolving 100 mg Coomassie Brilliant Blue G-250 with 50 mL 95% ethanol. Then 100 mL of 85% (w/v) phosphoric acid was added to the solution, which was then diluted to 0.5 L with ddH_2O. Bovine serum albumin (BSA) was used as standard protein and prepared in the same buffer solution as the protein of interest and were used to calculate the correlation factor between protein concentration and absorbance at 595 nm.

2.2.3.5. Mass Spectrometric Analysis

Preparation of Protein Samples for Mass Spectrometry

Verification of protein molecular weight was performed using mass spectrometry. All protein samples were prepared by exchanging sample buffer with Milli-Q water three times using Nanosep® centrifugal devices with 10 kDa molecular weight cutoff. Alternatively, if protein precipitation occured and was problematic, removal of buffer salts was achieved by applying protein sample onto a 1 mL Sephadex G25 gel filtration column with Milli-Q water as the eluant. An additional step was occasionally required where the salts of the eluted samples were removed using a Nanosep® centrifugal device.

Electrospray Mass Spectrometry of Protein Samples

The samples, now in Milli-Q water were diluted in a solution containing 1:1 acetonitrile:water with 0.2% formic acid in a ratio of 1:1 before injecting into the mass spectrometer. Mass spectrometry was carried out with electrospray ionization (ESI) in positive ion mode. Molecular masses were obtained using the MaxEnt algorithm using the MassLynx program.

2.2.4. Cloning of TSR into E. coli

The primers used for cloning *tsr* open reading frame (ORF) were as follows and were obtained from MOBIX Central Facility (DNA Synthesis Laboratory, The Institute for Molecular Biology and Biotechnology, McMaster University, Hamilton, ON):

5′ CCA GAA TTC CAT ATG ACT **GAG TTG GAC ACC ATC GCA AAT CCG** 3′
5′ C CCA AAG CTT *GGA TCC* **TTA TCG GTT GGC CGC GAG ATT CCT GTC GAT CC** 3′

In both primers, the bold highlighted segments are homologous to part of the ORF encoding TSR. The underlined and italicized residues indicate *NdeI* and *Bam*HI restriction endonuclease sites, respectively. The *tsr* gene was a generous gift from Dr. Gerry Wright (McMaster University, Hamilton, ON) originally from PIJ702 and now in pUC-19 and given the name pUC-TSR. The *tsr* ORF was amplified using the polymerase chain reaction (PCR). Both the gel purified PCR product and the pET28b vector were digested with the above restriction enzymes and gel purified. The purified products were then ligated using T4 DNA ligase. The ligation product was transformed into chemically competent *E. coli* DH5α cells, and then plated on kanamycin-containing Luria-bertaini (LB ; per liter: 10 g tryptone, 5 g yeast extract, 10 g NaCl pH 7.0) agar (LB broth plus 1.5% agar). Plasmid was isolated from the colonies and again digested with *Bam*HI and *Nde*I restriction enzymes to confirm correct

size of *tsr* insert. The pET-28b-TSR vector, simply designated as pTSR10 was transformed into *E. coli* BL21 (λDE3) pLys. An expression test was performed and a band corresponding to the hexahistidine-tagged TSR was observed at ~30 kDa as observed on the SDS-PAGE gel. This work was completed by Graeme Couture and Dr. Elisabeth Daub.

A)

```
      3       9      15      21      27      33      39
      |       |       |       |       |       |       |
  1 ATG ACT GAG TTG GAC ACC ATC GCA AAT CCG TCC GAT CCC GCG
 43 GTG CAG CGG ATC ATC GAT GTC ACC AAG CCG TCG CGA TCC AAC
 85 ATA AAG ACA ACG TTG ATC GAG GAC GTC GAG CCC CTC ATG CAC
127 AGC ATC GCG GCC GGG GTG GAG TTC ATC GAG GTC TAC GGC AGC
169 GAC AGC AGT CCT TTT CCA TCT GAG TTG CTG GAT CTG TGC GGG
211 CGG CAG AAC ATA CCG GTC CGC CTC ATC GAC TCC TCG ATC GTC
253 AAC CAG TTG TTC AAG GGG GAG CGG AAG GCC AAG ACA TTC GGC
295 ATC GCC CGC GTC CCT CGC CCG GCC AGG TTC GGC GAT ATC GCG
337 AGC CGG CGT GGG GAC GTC GTC GTT CTC GAC GGG GTG AAG ATC
379 GTC GGG AAC ATC GGC GCG ATA GTA CGC ACG TCG CTC GCG CTC
421 GGA GCG TCG GGG ATC ATC CTG GTC GAC AGT GAC ATC ACC AGC
463 ATC GCG GAC CGG CGT CTC CAA AGG GCC AGC CGA GGT TAC GTC
505 TTC TCC CTT CCC GTC GTT CTC TCC GGT CGC GAG GAG GCC ATC
547 GCC TTC ATT CGG GAC AGC GGT ATG CAG CTG ATG ACG CTC AAG
589 GCG GAT GGC GAC ATT TCC GTG AAG GAA CTC GGG GAC AAT CCG
631 GAT CGG CTG GCC TTG CTG TTC GGC AGC GAA AAG GGT GGG CCT
673 TCC GAC CTG TTC GAG GAG GCG TCT TCC GCC TCG GTT TCC ATC
715 CCC ATG ATG AGC CAG ACC GAG TCT CTC AAC GTT TCC GTT TCC
757 CTC GGA ATC GCG CTG CAC GAG AGG ATC GAC AGG AAT CTC GCG
799 GCC AAC CGA TAA
```

Total number of bases: 810
DNA sequence composition: A: 155; C: 249; G: 248; T: 158

B)

```
           10         20         30         40         50
            |          |          |          |          |
  1 MTELDTIANP SDPAVQRIID VTKPSRSNIK TTLIEDVEPL MHSIAAGVEF
 51 IEVYGSDSSP FPSELLDLCG RQNIPVRLID SSIVNQLFKG ERKAKTFGIA
101 RVPRPARFGD IASRRGDVVV LDGVKIVGNI GAIVRTSLAL GASGIILVDS
151 DITSIADRRL QRASRGYVFS LPVVLSGREE AIAFIRDSGM QLMTLKADGD
201 ISVKELGDNP DRLALLFGSE KGGPSDLFEE ASSASVSIPM MSQTESLNVS
251 VSLGIALHER IDRNLAANR
```

Number of residues: 269
Molecular weight (MW): 28901 Da

Amino acid composition:

22	A	1	C	2	H	6	M	10	T
21	R	6	Q	25	I	9	F	0	W
9	N	15	E	26	L	13	P	2	Y
20	D	21	G	9	K	30	S	22	V

Figure 2.3: *S. azureus* thiostrepton-resistance rRNA methyltransferase DNA and protein sequence. **(A)** DNA sequence and **(B)** corresponding protein sequence. Standard one letter codes for amino acids have been used.

2.2.5. Overexpression of TSR

2.2.5.1. Optimization of Overexpression of TSR in Rich Media

A small starter culture in TB broth (per litre: 12 g tryptone, 24 g yeast extract, 4 mL glycerol in 900 mL ddH_2O plus 100 mL of 0.17 M KH_2PO_4 and 0.72 M K_2HPO_4, pH 7.0) and NZCYM media (per litre: 10 g NZ amine, 5 g NaCl, 5 g yeast extract, 1 g casamino acids, 2 g $MgSO_4$-7H_2O, pH 7.0) supplemented with kanamycin (30 μg/mL) and chloramphenicol (34 μg/mL) was inoculated from frozen stock and grown over night at 37 °C. The cultures were diluted 100 times in their respective medias and grown at 37°C with constant agitation (~200 rpm) until both sets of cells reached a mid-log phase (A_{600} = 0.5-0.8) optical density of 0.6. Isopropyl-β-thiogalactopyranoside (IPTG) was then added to the media to a final concentration of 1 mM to initiate TSR overexpression. The cells were grown for 24 h with 1 mL samples removed at various time points, then harvested by centrifugation (5 min at 13 000 ×*g*) and frozen at -80 °C.

To ascertain if TSR expressed as a soluble protein, at the end of the time course, 2 mL of the sample was taken out and subjected to three rounds of sonication (10 second pulses). The sample was separated by centrifugation (5 min at 13 000 ×*g*) and the supernatant and pellet were analyzed on SDS-PAGE along with the time-dependent sample pellets that were previously collected.

2.2.5.2. Harvest of Induced Cells

Following a large volume induction, in a large Beckman JA-15 rotor, cells were harvested by centrifugation at 6000 ×*g* for 15 min at 4 °C. Cells were washed twice with a

minimal volume of 20 mM Tris buffer pH 7.0 and re-centrifuged. Pelleted cells were frozen with liquid nitrogen and stored at -80 °C for future use.

2.2.6. Purification of $(His)_6$-tagged TSR (HTSR)

2.2.6.1. Cell Lysis

TSR was overexpressed in *E. coli* BL21 (λDE3)/pLysS strain as described above. To obtain crude cell lysate for purification of enzyme, the steps were as follows: Frozen cells were resuspended in HisBind Buffer (Buffer A: 50 mM Tris buffer pH 8.0, 20 mM imidazole, 500 mM KCl, 10% glycerol; 2-5 mL/g frozen cells) and thawed on ice in the presence of 1 mM of phenylmethylsulfonyl fluoride (PMSF) and 1 mg/mL lysozyme for ~30 minutes. The suspension was then sonicated on ice for 10-12 cycles with 10 s pulses separated with one min pauses. If the lysate is very viscous, 5 μg/mL DNase was added to it, followed by incubation (15 min). The cell lysate (soluble fraction) was collected by centrifugation at 20000 rpm (48 300 ×*g*) with a JA-25.50 rotor for 20 min at 4 °C. The supernatant was then filtered through a 0.2 μm filter prior to further remove any particulate cell debris.

2.2.6.2. Purification of Hexahistidine-tagged TSR with IMAC

Batch Purification with Nickel(II)-nitrilotriacetic (Ni-NTA) Superflow resin

Prior to the addition of clarified cell lysate, the nickel(II)-nitrolotriacetic (Ni-NTA) superflow resin (binding capacity of ~8 mg/mL) was washed at least three times with HisBind buffer (Buffer A: 50 mM Tris buffer pH 8.0, 20 mM imidazole, 250 mM KCl). The Ni-NTA resin slurry was combined with the cleared cell lysate and mixed gently on a rotary

shaker at 4°C for one hour. The lysate-resin slurry was then loaded into a 10 mL BioRad Econo®-Column. The buffer level was drained to just about the resin bed and three to five column volumes of the HisBind buffer were applied. TSR elution was achieved by applying HisElution buffer (Buffer B: 50 mM Tris buffer pH 8.0, **x** mM imidazole, 250 mM KCl; where **x** is 20 mM, 40 mM, 100 mM, 250 mM) in a stepwise fashion with increasing concentrations of imidazole. Fractions of 2 mL volume were collected and 50 - 100 μL of each fraction was analyzed on SDS-PAGE. Fractions of highest purity were then pooled and dialysed against two 1-L changes of 50 mM Tris buffer pH 7.5 at 4°C using SPECTRA/POR® dialysis tubing with a molecular weight cutoff of 12 000 – 14 000 Da. The protein concentration was estimated by the Bradford assay using BSA as a standard.

Optimization of Protein Solubility During Dialysis

Optimization of buffer conditions for enhanced solubility during the second dialysis step was achieved by screening different additives. Table 2.3 summarizes the different conditions that were tested and utilized for optimization.

Table 2.3: Different Conditions Screened to Enhance TSR Solubility During Dialysis.

Additive/Condition	**Amount/Concentration**
glycerol	0%, 10%, 15%, 20% (v/v)
β-mercaptoethanol	0 mM, 10 mM
dithiothreitol	0 mM, 1 mM
NaCl	0 mM, 75 mM, 150 mM, 500 mM
KCl	0 mM, 75 mM, 150 mM, 500 mM
pH	7.0, 7.5, 8.0
time*	3, 5, 8 h
Histrap™ HP column	Not applicable
EDTA$^{\gamma}$	2.5 mM

*Time indicating the length of the first dialysis exchange

$^{\gamma}$EDTA: ethylenediaminetetraacetic acid

Equal amounts of protein for different sets of conditions were used for dialysis with two buffer changes. The amount of precipitation (if any) was quantified by pipetting the

white protein from the dialysis bag and centrifuging at 13000 ×*g* for 10 min. The supernatant was pipetted off or decanted and the white pellet was prepared for SDS-PAGE analysis to confirm that it contained TSR. The soluble fraction of the sample was quantitated by means of Bradford assay and compared.

Optimized Purification with Histrap^{TM} HP Ni^{2+}-Sepharose column

The recombinant $(His)_6$-TSR (HTSR) was purified by IMAC on a HisTrap^{TM} HP Ni^{2+} column. A 1 mL HisTrap^{TM} HP was equilibrated with 5 column volumes of Binding/Wash Buffer (Buffer A: 50 mM Tris buffer pH 8.0, 20 mM imidazole, 500 mM KCl, 10% glycerol). The clarified cell lysate was loaded onto the column at a 0.5 mL/min flow rate. The column was washed extensively with buffer A until baseline absorbance at 280 nm to remove non-binding proteins. The hexahistidine-tagged TSR was eluted with Elution Buffer (Buffer B: 50 mM Tris buffer pH 8.0, 500 mM imidazole, 500 mM KCl, 10% glycerol). EDTA (2 mM) was added immediately to fractions containing TSR. To remove the imidizole, the eluted enzyme solution was dialyzed sequentially against 50 mM Tris buffer pH 7.5, 500 mM KCl, 10% glycerol at 4 °C using SPECTRA/POR® dialysis tubing with a molecular weight cutoff of 12 000 – 14 000 Da. The protein concentration was estimated by the Bradford assay using BSA as a standard.

2.2.7. Removal of $(His)_6$-tag from Recombinant TSR

2.2.7.1. Time Course on Thrombin Cleavage of Histag from TSR

To 100 µL of HTSR (~1 mg/mL) was added $CaCl_2$ to 2.5 mM. After, 5 µL was taken out and set aside as a mock digestion (negative control). To the remainder of the HTSR

sample, 1 μL of thrombin protease (1 U/μL) was added, since according to manufacturer's instructions, 1 unit of thrombin protease should cleave 100 μg of protein to give the corresponding cleaved TSR (TSR′). The mixture was allowed to incubate at ambient temperature and at the following time points (t = 0.5 h, 1 h, 2 h, 4 h, 12 h, 24 h), 5 μL of the sample was taken out and frozen in at -20 °C with SDS-PAGE loading dye. At the end of the time course, all samples were analyzed with SDS-PAGE.

2.2.7.2. Thrombin Cleavage and Clean up of de-tagged TSR (TSR′)

Removal of the His-tag was achieved by treatment with of thrombin protease (1U/μL) at 4 °C while gently shaking for 16-18 h in thrombin cleavage buffer (50 mM Tris buffer pH 7.5, 500 mM KCl, 10% glycerol, 2.5 mM $CaCl_2$). One unit of thrombin protease was used to cleave 100 μg of protein to give the corresponding cleaved TSR (TSR′). The thrombin protease, along with any residual uncleaved HTSR was removed with the application of the cleavage mixture onto a HiTrap Benzamdine FF Affinity column and HisTrap™ HP in tandem. TSR′ was initially collected as the flowthrough at a rate of 0.5 mL/min in Buffer A (50 mM Tris buffer pH 7.5, 500 mM KCl, 10% glycerol) and the HTSR eluted with Buffer B (50 mM Tris buffer pH 7.5, 1M KCl, 10% glycerol) at 0.5 mL/min. Lastly the thrombin protease was eluted with Thrombin elution buffer (Buffer C: 50 mM glycine pH 3.0). The cleaved TSR sample was dialyzed against 50 mM Tris buffer pH 7.5 with 10% glycerol.

2.2.8. Further Purification of TSR′

In order to achieve higher purity, anion exchange chromatography was subsequently performed using a MonoQ column. The column was initially washed to zero baseline

absorbance at 280 nm and then TSR′ was eluted with an increasing linear gradient of KCl at 1%/min from Buffer A (50 mM Tris pH 7.5, 10% glycerol) to Buffer B (50 mM Tris buffer pH 7.5, 1 M KCl, 10% glycerol) between 26-32% KCl. This purification was followed by dialysis against 50 mM Tris buffer pH 7.0, 75 mM KCl, 10 % glycerol and the protein stored at -80 °C for future use.

2.2.9. Gel Filtration Chromatography of TSR′

Superdex-75 (10/300) is a gel filtration column with a bed volume of 24 mL and was calibrated used BioRad gel filtration standard consisting of protein aggregates (unspecified molecular weight), thyroglobulin (670 kDa), bovine gamma globulin (158 kDa), chicken ovalbumin (44 kDa), equine myoglobin (17 kDa) and vitamin B12 (1.35 kDa) in 50 mM Tris pH 7.5, 150 mM KCl and 10% glycerol. In addition, carbonic anhydrase (29 kDa) and bovine serum albumin (66 kDa) standards from Sigma were employed in the calibration process. Sample volumes of 100 μL of 1.0 mg/mL were filtered with a 0.2 μm GHP membrane filter, loaded onto the column and eluted at a rate of 0.5 mL/min in a buffer consisting of 50 mM Tris pH 7.5, 150 mM KCl and 10% glycerol. To test the effects of thiol-reducing agents, to the buffers were added β-mercaptoethanol or dithiothreitol to a final concentration of 10 mM and 1 mM respectively.

2.3. Results and Discussion

2.3.1. Expression of Recombinant His-tagged-TSR in E. coli

In earlier work in the Honek laboratory, *tsr* was overexpressed successfully without a fusion tag; however, attempts at producing high levels of crystallographically pure protein

achieved only limited success. Taking this into consideration, the hexahistidine fusion vector pET28b(+) and the protease deficient BL21 (λDE3) strain harbouring pLys were chosen as the expression system. The *tsr* ORF was successfully subcloned from pUC-TSR to pET28b(+) to give pTSR10 (Figure 2.4).

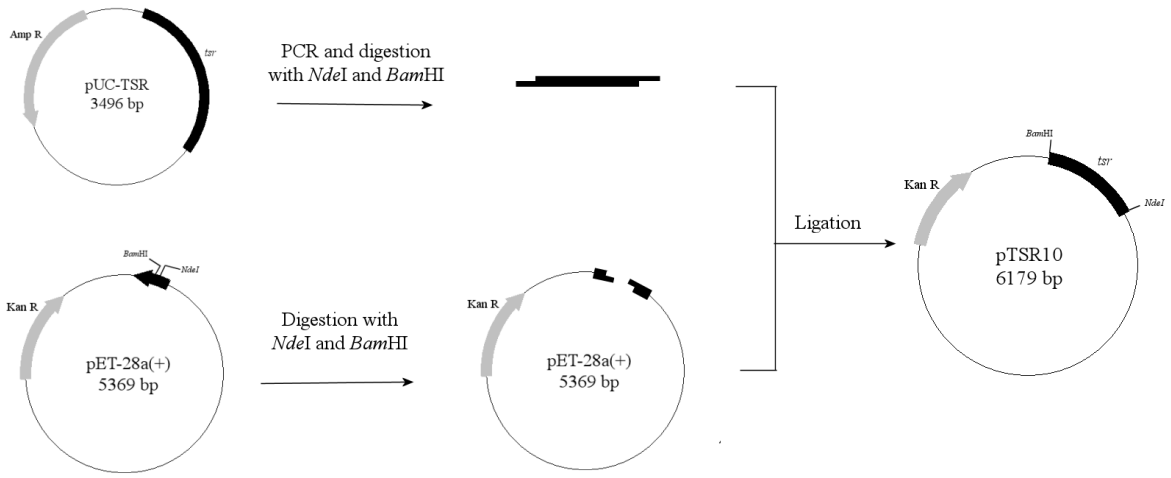

Figure 2.4: Cloning strategy for the construction of pET-28A(+)-*tsr* (pTSR10).
Amp R, ampicillin resistance marker. Kan R, kanamycin resistance marker.

Time course expression tests were performed with different types of rich media. Optimal expression occurred four hours after induction for NZCYM and between four and six hours for TB with comparable amounts of protein. Since the induction time for TB was slightly more flexible than for NZCYM and the induction time was shorter than the observed 8 h with LB, all subsequent cell growth procedures were performed with TB medium with a four hour induction with 1 mM IPTG for overexpression (Figure 2.5). Although its sequence was determined by protein solubility prediction algorithms to more likely to be expressed (74%) as insoluble inclusion bodies [135], it was observed from SDS-PAGE analysis that TSR was expressed as a soluble protein. However, its solubility during subsequent manipulation was observed to be easily compromised.

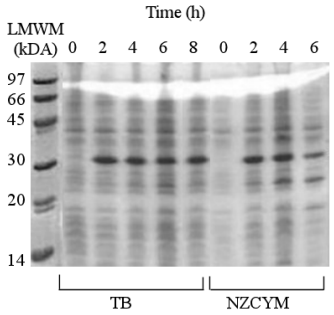

Figure 2.5: Time course of expression of TSR in different rich media.
Proteins were visualized with Coomassie staining on the 20% SDS PAGE gel. LMWM = low molecular weight marker.

2.3.2. Enhancing Purification of His-tagged-TSR in E. Coli After IMAC Purification

2.3.2.1. Batch Purification of TSR with Ni-NTA Superflow resin

Initial purification of hexahistidine-tagged TSR was achieved through batch purification of the enzyme with a gravity Ni^{2+}-affinity column. *E. coli* cells containing the overexpressed TSR were disrupted by lysozyme treatment and sonication and the clarified cell lysate incubated with the Ni^{2+}-NTA resin for one hour. The lysate-resin mixture was loaded onto a column and the unbound proteins were washed off and TSR was eluted off with increasing amounts of imidazole in the buffer. After this process, the purity of fractions was examined by SDS-PAGE (Figure 2.6).

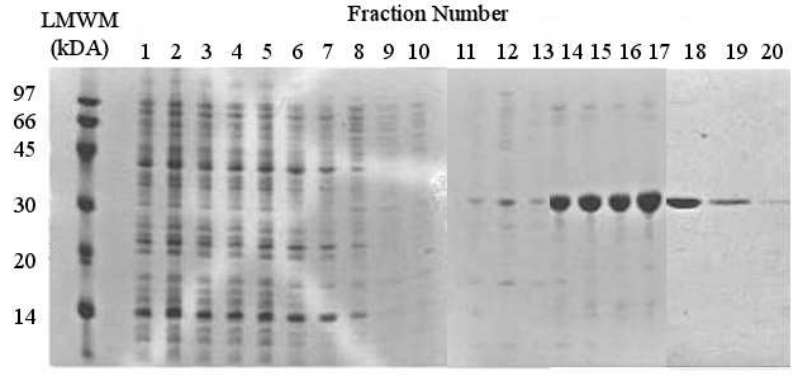

Figure 2.6: SDS PAGE analysis of fractions collected during purification of HTSR using a Ni^{2+}-NTA Superflow column.
LMW = low molecular weight marker. Fractions 14-20 show a prominent band at ~31 kDa indicative of HTSR.

A prominent TSR band at approximately 31 kDa with minor amounts of contaminating proteins was observed. Electrospray mass spectrometry confirmed this finding (Figure 2.7). Fractions containing TSR were pooled and dialysed. However, during dialysis, unwanted precipitation of TSR was observed resulting in a substantial decrease in protein yield.

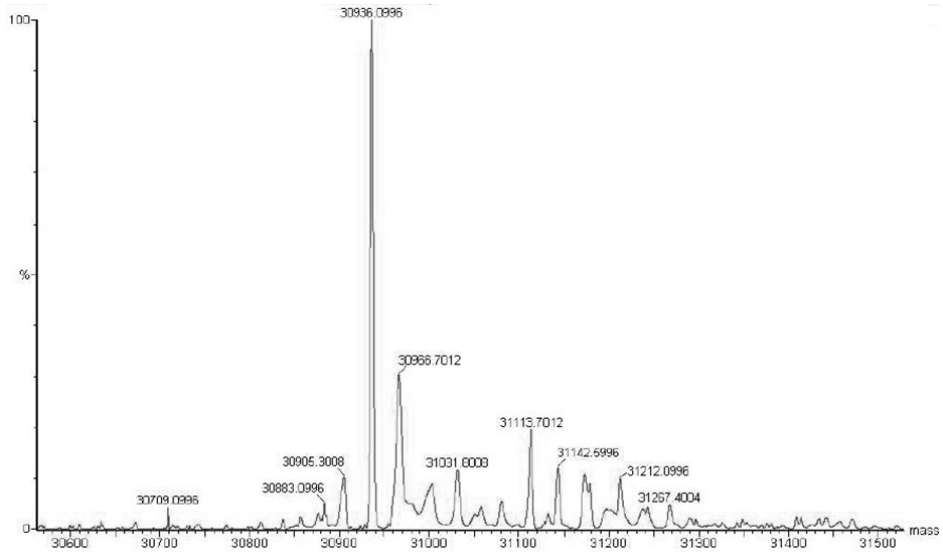

Figure 2.7: Positive ion mode electrospray mass spectrum of purified HTSR.
The expected molecular weight 31064 Da .The major peak indicates a monomeric molecular weight of 30936 Da after denaturation with the N-terminal methionine cleaved off.

2.3.2.2. Enhancing TSR Solubility During Dialysis

Prevention of precipitation and aggregation is desirable during the overexpression and isolation of a target protein. Protein can often accumulate into insoluble inactive aggregates known as inclusion bodies and can often be refolded into soluble active proteins [136,137]. Oftentimes however, the protein may be successfully expressed as soluble protein, but still have difficulty remaining soluble as in the case of TSR. Protein solubility is influenced by many different factors such as temperature, pH, salt type or concentrations [138]. Protein stability and solubility can be increased by use of buffer additives that can destabilize protein-protein interactions or stabilize intramolecular protein interactions.

It was observed that dialysis of HTSR after the first step of purification resulted in undesirable precipitation. Protein was dialysed against two 1 L changes of 50 mM Tris buffer pH 7.5 at 4°C, and precipitation only occurred after the second change of dialysis buffer. The following discusses the approaches that were undertaken to reduce or circumvent protein precipitation during the purification process.

Effect of Kosmotropes

Kosmotropes (“order makers”) is a term used to describe solutes that stabilize the native state of proteins. Kosmotropes increase ordering of water thereby enhancing the hydrophobic effect, which plays a significant role in protein solubility [139]. Both non-ionic and ionic kosmotropes were added to the buffer to increase HTSR stability.

Glycerol is a non-ionic kosmotrope whose protein stabilizing influence is widely recognized. Glycerol and other non-ionic kosmotropes are highly soluble molecules, and hydrogen bond with water, thereby enhancing the hydrogen bonding network that exist

between the ordered water molecules [139,140]. Therefore, three different concentrations of glycerol were used in buffers involving the purification and dialysis (10%, 15%, 20% v/v). The amount of enzyme recovered was compared to that of not having glycerol present using the Bradford assay. Increasing amounts of glycerol did not appear to affect the amount of enzyme recovered significantly (Table 2.4).

Table 2.4: Effect of Different Types and Amounts of Kosmotropes in Dialysis Buffer on HTSR Solubility.

Kosmotrope	Amount of Kosmotrope	% Recovery
glycerol	0% (v/v)	30 ± 10
	10% (v/v)	40 ± 5
	15% (v/v)	40 ± 5
	20% (v/v)	40 ± 5
KCl	0 mM	30 ± 10
	75 mM	30 ± 5
	150 mM	60 ± 5
	500 mM	60 ± 5
NaCl	0 mM	30 ± 10
	75 mM	30 ± 5
	150 mM	60 ± 5
	500 mM	60 ± 5

Ionic strength and ionic composition have been found to be factors that influence protein solubility. Here the influence of two different types of weak ionic kosmotropes (KCl and NaCl) was investigated. Salts can bind to the protein, providing a shielding effect for unpaired side chains that otherwise may facilitate protein-protein interactions that may lead to aggregation [138]. Furthermore, since TSR is a nucleic acid binding protein, it may require a higher concentration of salts for stabilization [141].

At concentrations above 150 mM KCl or NaCl, there was an increased yield in soluble TSR. It was therefore concluded that buffers used during dialysis should have a minimum concentration of 150 mM KCl. While the addition of kosmotropes did improve protein solubility, other additives were tried to further reduce protein aggregation.

Effect of Thiol-Reducing Agents

In the TSR sequence, there is one cysteine residue. Limited solubility of the enzyme may be due to unwanted intermolecular disulfide bond formation which may interfere with the proper folding or produce aggregates. Purification buffers were treated with reducing agents β-mercaptoethanol and dithiothreitol at 10 mM and 1 mM concentrations, respectively to break any putative disulfide bonds and promote the dissociation of aggregates. It was found that the presence of either agent did not improve its solubility (Table 2.5).

Table 2.5: Effect of Different Types of Thiol-reducing agents in Purification Buffers on HTSR Solubility.

Thiol-reducing agent	Concentration (mM)	% Recovery
β-mercaptoethanol	0	30 ± 10
	10	30 ± 10
dithiothreitol	0	30 ± 10
	1	30 ± 10

Effect of pH and Time

The pH optimum of TSR was published to be between a narrow range of 6.5 to 8.0 with the optimum being at 7.5 [114] with a calculated pI of 6.14. We sought to adjust the pH to see if there was a correlation to the amount of enzyme that precipitated. Dialyses at pH 7.0, 7.5 and 8.0 were carried out and the yield was found to be unaffected by pH (Table 2.6).

Table 2.6: Effect of pH and Time on TSR Solubility.

Condition	pH or Time	% Recovery
pH	7.0	30 ± 10
	7.5	30 ± 10
	8.0	30 ± 10
Time	3 h	30 ± 10
	5 h	30 ± 10
	8 h	30 ± 10

Precipitation of HTSR occurred only after the latter part of dialysis, that is, after the first dialysis buffer change. A relationship between the length of the first dialysis time and

precipitation was considered. Dialysis times of 3, 5 and 8 h were tried and found that precipitation occurred to the same extent regardless of the length of time of the previous dialysis step (Table 2.6). Therefore, it appears that only when the imidazole concentration within the TSR sample (carried over from the purification) is significantly lowered, that the protein preicipation occurs.

Effect of Ni^{2+} Leakage Reduction

The role of possible Ni^{2+} leakage playing a part in protein aggregation was taken into consideration. Ni^{2+} from the binding matrix of the affinity column could potentially be found in the eluted protein sample. Ni^{2+} leakage was suspected because precipitation only occurred after the first dialysis buffer change. There are two histidines in one monomer of TSR, in addition to the six histidines that the N-terminal region, and Ni^{2+}-induced oligomerization by forming histidine- Ni^{2+}-histidine interactions is a possibility. We turned to the Histrap Ni^{2+}-sepharose column developed by GE Healthcare (formerly Amersham Biosciences) that claims to have negligible Ni^{2+} leakage. Use of the Histrap column provided a more facile method of purifying HTSR on a HPLC or FPLC machine with monitoring at 280 nm compared to the gravity Ni^{2+}-NTA column. The protein was eluted in one step with elution buffer containing 500 mM imidazole and the sample subjected dialysis with the buffer additives that were determined previously to aid HTSR solubility (i.e. at least 10% glycerol and 150 mM KCl) (Figure 2.8).

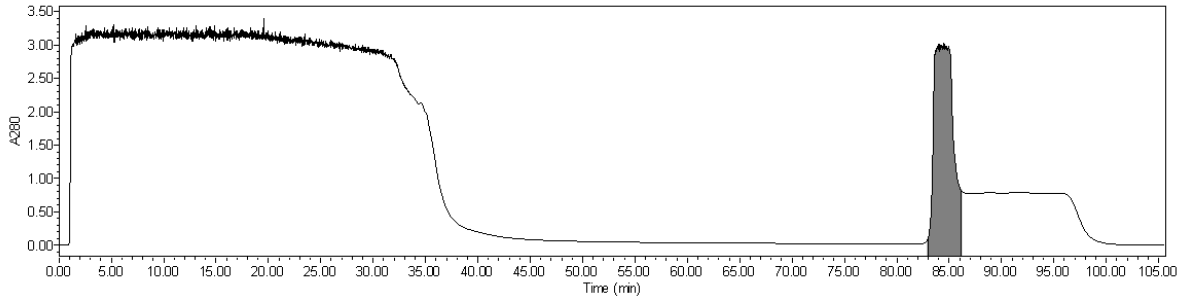

Figure 2. 8: IMAC purification of HTSR with Histrap Ni^{2+}-sepharose column.
The absorbance was monitored at 280 nm and the column was washed until the baseline absorbance was attained. At 83 min, the protein was eluted with elution buffer containing 500 mM imidazole. The area under the first major broad peak corresponds to the flow through containing proteins that did not bind to the column. The area under the second major peak, shaded grey, corresponds to the column fractions that were pooled for subsequent steps of purification. After HTSR was eluted, column was washed with wash buffer back down to baseline absorbance value.

This use of the Histrap column gave a more streamlined purification and for the majority of the time, the protein was recovered fully after dialysis. However, protein precipitation still occurred on occasion. From this we tentatively concluded that Ni^{2+} leakage was minimized significantly by the new column, but not fully. Treatment of protein precipitation when it did occur with 2.5 mM EDTA was found to be successful in resolubilizing the protein. Similar results were obtained by Sprules and coworkers who observed Ni^{2+}-induced oligomerization of their protein tagged with 10 histidines [142]. We also believe that precipitation only occurred after the second dialysis buffer change since the free imidazole was no longer present to chelate to any free Ni^{2+} ions. Therefore, fractions of HTSR that are collected from the optimized IMAC purification were immediately treated with 2.5 mM EDTA and then dialyzed. This method allowed for reliable and successful recovery of HTSR after dialysis.

2.3.3. Removal of the Hexahistidine tag from HTSR

The $(His)_6$-tag was fused at the N-terminal region of TSR with an engineered thrombin protease cleavage site (Figure 2.9). Although a hexahistidine tag is small and in most cases does not interfere with enzyme activity, removal of the tag is often desired for structural analysis such as X-ray crystallography. Removal of the tag from HTSR leaves only two residues (glycine and serine) at the N-terminus.

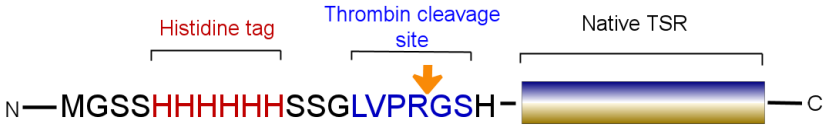

Figure 2. 9: The $(His)_6$-tagged TSR methyltransferase.
The affinity-labelled protein will have an additional 20 amino acid residues (redbox), which includes the six histidines that make up the tag on its N-terminal end. In addition, a thrombin cleavage site was engineered into the tag to allow for future removal of the histidine-tag. Cleavage will result between an arginine and glycine as indicated by the orange arrow.

From a small scale cleavage time course, optimal cleavage was determined by have occurred after 12 h. Initial attempts at large scale removal of the tag resulted in significant loss of protein through precipitation (over 50%). Re-addition of EDTA did not resolubilize the protein and therefore, aggregation due to any residual Ni^{2+} ions left over from dialysis was no longer the cause of aggregation. However, it was found that that increasing the salt concentration from 150 mM KCl to 500 mM KCl decreased the precipitation significantly, although it did not eliminate it entirely.

Following the fusion tag cleavage, the mixture was loaded onto a HiTrap Benzamidine Affinity column and HisTrap HP in tandem. The first column is designed to bind to serine proteases such as thrombin and the second column was present to remove any residual HTSR that remained. The cleaved protein (TSR′) was present in the flow through and was collected for the next stage of purification (Figure 2.10). The electrospray mass

spectrum was in agreement with the expected molecular weight of this cleaved protein (Figure 2.11).

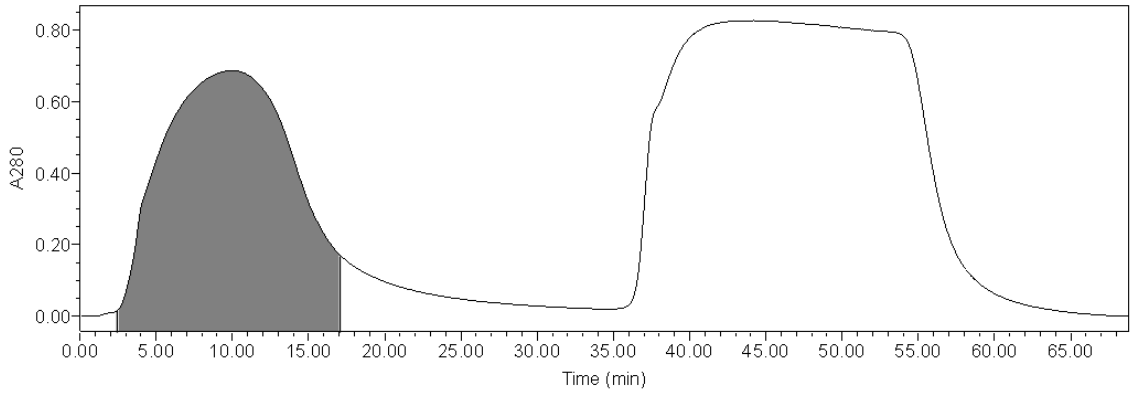

Figure 2. 10: Chromatogram showing the separation of TSR′ from thrombin protease and uncleaved HTSR. TSR′ did not bind to either column (HiTrap Benzamidine Affinity column and HisTrap HP which were attached in series). The area under the first major peak corresponds to the flow through containing TSR′. At 35 min, buffer containing 500 mM imidazole and 1 M KCl was used to elute any remaining protein on the two columns. At 50 min, columns were washed with wash buffer back down to baseline absorbance.

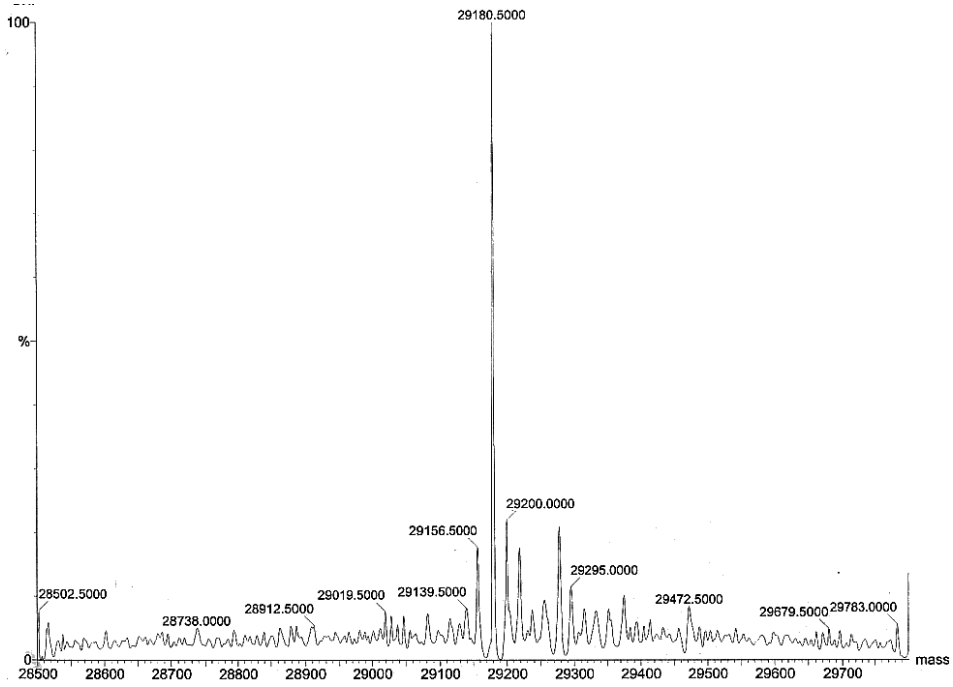

Figure 2. 11: Positive ion mode electrospray mass spectrum of purified TSR′.
The expected molecular weight 29182 Da .The major peak indicates a monomeric molecular weight of 29180 Da after denaturation showing successful removal of the tag.

2.3.4. Final step in TSR Purification

A final polishing step consisting of anion exchange chromatography was then performed after the thrombin cleavage clean-up. During this purification step, TSR′ fractions were identified over the range of KCl concentration of 260 mM – 320 mM (26-32%) (Figure 2.12). The eluted protein was then collected and stored for future biochemical and biophysical studies (Figure 2.13).

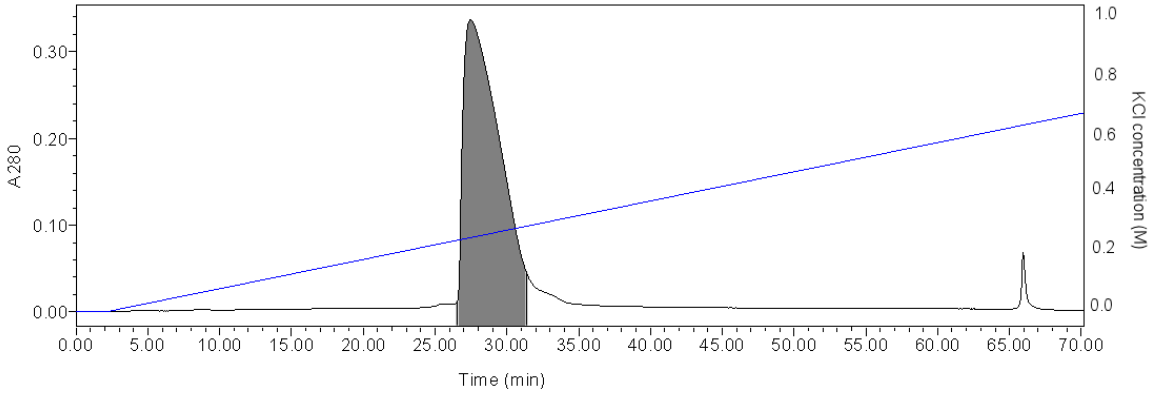

Figure 2. 12: Section of elution profile of anion exchange Mono-Q chromatography of TSR′. Protein was loaded onto the column and eluted with a 1% per minute gradient from 0 to 1 M KCl.

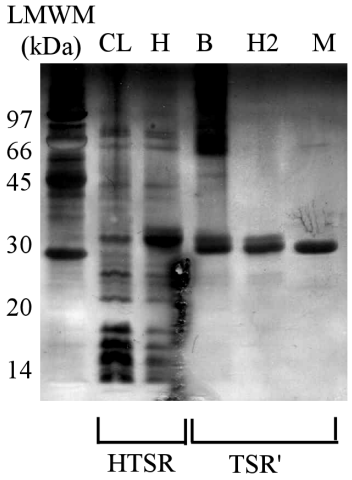

Figure 2. 13: Summary of stages of purification for TSR.
Samples were subjected to SDS-PAGE on a 20% homogeneous gel with silver staining. LMWM = Low Molecular Weight Marker. CL = cell lysate, H = Histrap, B = Benzamidine column, H2 = Second Histrap column, M = MonoQ anion exchange column.

2.3.5. Gel Filtration of TSR′

The oligomeric state of the protein was examined with gel filtration studies. Samples were loaded onto a gel filtration column with and without thiol-reducing agents. In both cases, the molecular weight calculated was found to be approximately ~52 kDa, which is close to twice the monomeric molecular weight of 29 kDa (Figure 2.14). This indicates that the native structure of TSR is dimeric and that the dimer structure is not formed with disulfide linkages between the two protomers.

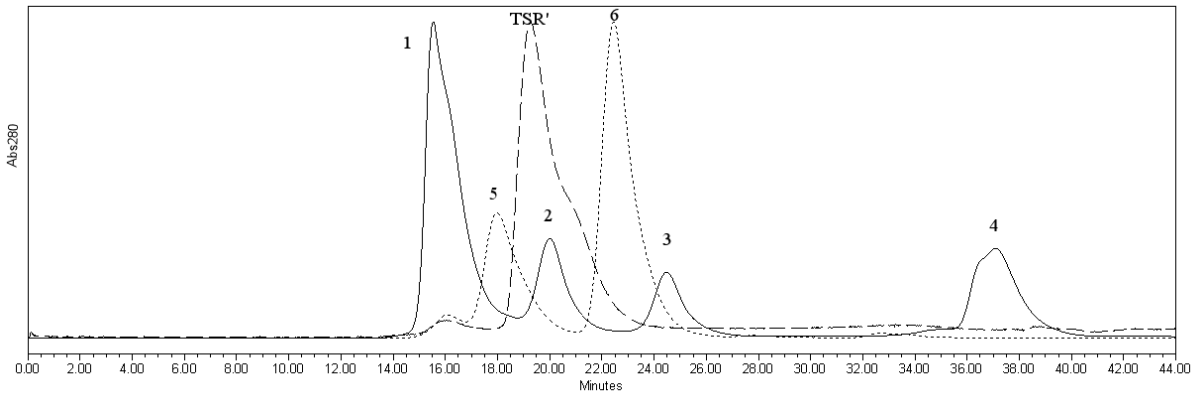

Figure 2. 14: Elution profile of TSR′ in the absence of thiol.
A similar elution profile was observed. Solid and dotted lines are peaks from BioRad and Sigma gel filtration standards, respectively. Dashed lines is the elution profile for TSR′. 1: thyrogobulin, 670Kda and bovine gamma globulin, 158 kDa; 2: chicken ovalbumin, 44 kDa; 3: equine myoglobin, 17 kDa; 4: Vitamin B12, 1.35 kDa; 5: bovine serum albumin, 66 kDa; 6: carbonic anhydrase, 29 kDa.

2.4. Conclusions and Future Work

The *tsr* gene product has been overexproduced at high levels in *E. coli* as an N-terminal hexahistidine fusion protein and purified by IMAC. The majority of the protein was purified in a one-step procedure using a Ni^{2+}-affinity column. After elution with a high concentration of imidazole and dialysed, it was found that the protein, although expressed as a soluble protein, was prone to aggregation. Difficulty in handling the enzyme remained a challenge throughout the initial stages of purification. It appears that TSR is not the only

member of the SpoUT MTase superfamily to be unstable. The avilamycin-resistance MTase (AviRb) has been reported to be unstable at ionic strengths below 0.3 M at concentrations above 0.5 mg/mL [143]. As a consequence, all purification buffers and crystallization buffers for AviRB had a minimum concentration of 500 mM NaCl.

An extensive screening of different conditions to reduce or eliminate precipitation was undertaken. A combination of buffer additives such as glycerol and salt (at least 150 mM KCl or NaCl) was found to reduce the amount of precipitation significantly. In conjunction with these buffer co-solutes, reducing the amount of Ni^{2+} leakage from IMAC purification with a different column and the addition of the metal chelator, EDTA, eliminated precipitation entirely. Therefore, one must remember that although IMAC provides a facile and quick method of purification, auto-aggregation facilitated by Ni^{2+} ion leakage from the column should be taken into consideration.

Enzymatic removal of the fusion tag was successful with the use of thrombin protease. However, solubility of the enzyme once again was an issue. Increasing the salt concentration from 150 mM KCl to 500 mM helped to improve solubility, but did not eliminate all precipitation issues. A final enrichment step with anion exchange chromatography gave enzyme of substantial purity. Gel filtration chromatography was performed on the cleaved enzyme in the presence and absence of thiol-reducing agents. It was found that the native structure of TSR is dimeric and that the dimer is not formed with disulfide bonds between the two monomers. The established and optimized purification detailed herein should enable the availability of the purified and cleaved TSR for further study on the structural and biochemical level. The final purification yield was 8 – 12 mg/L culture.

CHAPTER 3: BIOCHEMICAL CHARACTERIZATION OF THIOSTREPTON-RESISTANCE rRNA METHYLTRANSFERASE

S-adenosyl-L-methionine (AdoMet) plays a central role in biological transmethylation reactions. The class of enzymes that catalyze these methyl transfer reactions are called the AdoMet-dependent MTases. These enzymes transfer the methyl group of AdoMet to a target molecule (Figure 3.1). A wide selection of molecules can serve as substrates for these enzymes and they can vary in size from small organic molecules such as catechol to large macromolecules such as lipids, protein and nucleic acids [3,6,8,9].

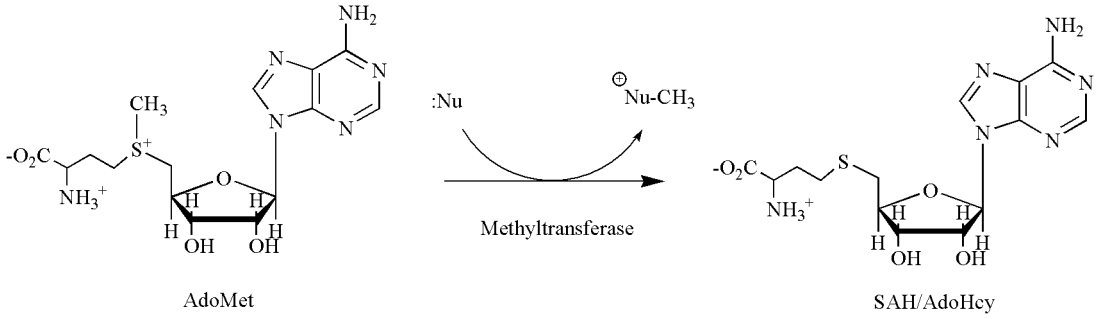

Figure 3.1. Transmethlyation reaction catalyzed by AdoMet-dependent MTases.

The methylation by-product, SAH/AdoHcy is a potent feedback inhibitor [11], but cannot be differentiated from AdoMet by ultraviolet spectroscopy. As a result, standard MTase assays that are used to detect methyl transfer activity typically involve the measurement of the incorporation of a radiolabelled methyl group into the substrate. MTase enzymes generally have low turnover numbers and radiometric methods are sufficiently sensitive for detection [144,145].

3.1. Methods to Detect Methyl Transfer Reactions

3.1.1. Principles of Radiometric Filter Binding Assays

Radiometric techniques have been utilized with much success since their introduction in the 1950s for a wide number of applications i.e. enzyme kinetics. The filter binding (FB) assay has been used effectively and extensively to determine methyl transfer activity. Radiometric FB assays are based on the conversion of a radioactive substrate to a radioactive product that can be rendered insoluble and thus quantified by filtration [145]. In standard radioactive MTase assays, the AdoMet substrate is labelled on the methyl group with ^{3}H or ^{14}C and is transferred to the substrate molecule via the MTase enzyme. The transmethylation reaction is stopped after a certain time period by the addition of an organic solvent such as ethanol or trichloroacetic acid, which also results in the precipitation of the substrate. Radioactive macromolecules are isolated by filtration for quantitation of methyl transfer [145,146]. Residual water is removed by drying in air or with heat and the samples can be analyzed by liquid scintillation counting methods (Figure 3.2).

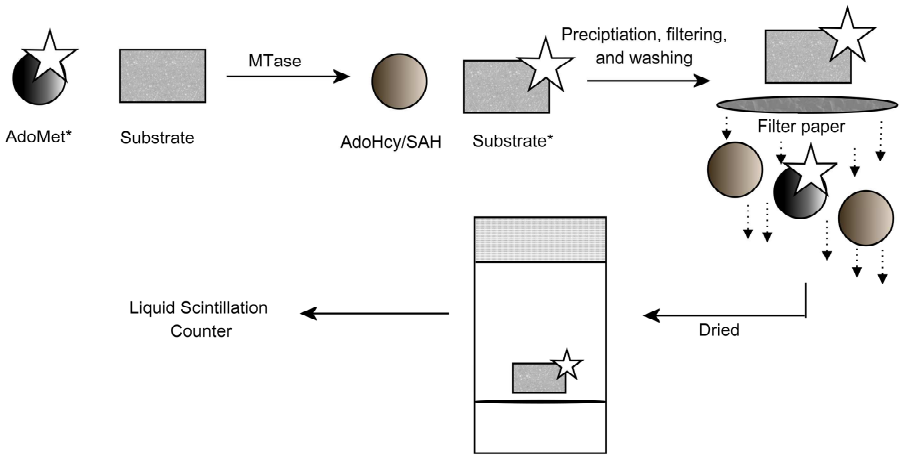

Figure 3.2. Filter Binding Assay.
The two substrates are incubated together in the presence of a methyltransferase to facilitate methyl transfer. The reaction is stopped by the addition of organic solvent and the radiolabelled product is isolated via filtration. The filter paper is dried and sample is processed for measurement with a scintillation device.

Although radioenzymatic assays are sensitive and simple, most assays of this type require the separation of labelled substrate (product) from the other assay components. This separation step in the FB assay can be laborious, tedious and time consuming when there are large numbers of samples to process. Additionally the assay can be difficult to adapt to high throughput processing. Accumulation of AdoHcy/SAH can result in product inhibition, contributing to errors in kinetic parameter determination [11]. Recently, efforts have been directed towards developing alternative assaying methods to circumvent these limitations.

3.1.2. Scintillation Proximity Assay (SPA) Technology

Scintillation proximity technology was pioneered in 1979 by Hart and Greenwald [147], and has recently become a very attractive alternative method for studies involving radioactivity. Its advantage is that it eliminates the need to filter or centrifuge a large number of samples.

With conventional FB assays, after separation of the product from the starting materials, the filter paper is placed in scintillation cocktail in a vial. The energy released by the radioisotope (i.e. β-particle from tritium) stimulates the scintillant in the cocktail and then converts the energy to light such that the signal is amplified and made readily detectable by the liquid scintillation counter. In scintillation proximity assays (SPA), the scintillant molecule is embedded in a microsphere (bead).

The basis of the SPA technology is that not only the microspheric beads contains a scintillant, but also the surface of the beads are derivatized with molecules that bind to specific radiolabelled molecules. For weak β-emitters such as tritium (^{3}H), the isotope has to be close to the scintillant to produce light (within ~1.5 μm). This makes tritium an ideal

isotope to use for SPA, since only radiolabelled molecules bound to the SPA bead are sufficiently close to the scintillant to induce emission of light. Radioligand molecules that are not bound to the bead will have their radioisotopic energy dissipated in the medium so that they do not contribute to the measurable quantity of signal (Figure 3.3). As such, the SPA technology does not require any transfer, washing and separation steps that are involved in radiometric assays, thereby minimizing any errors that may occur from inconsistencies in these other procedures.

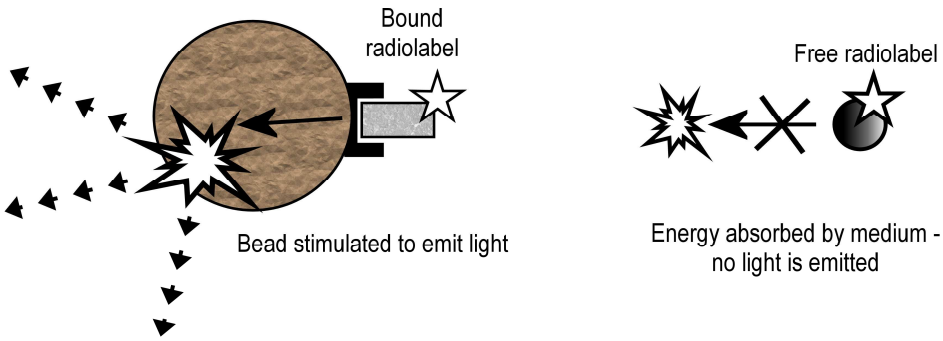

Figure 3. 3. Overview of scintillation proximity assay.
Radiolabelled molecules that are bound (close proximity) to the bead stimulate the embedded scintillant to emit light. Free, unbound radioligands are not close enough to stimulate light emission.

3.1.3. Alternative Non-Radiometric Assay Methods for MTases

A number of alternative MTase assay techniques have been developed that do not use radioactive material. These methodologies include spectrophotometric [148,149], fluorescence [150,151] and immunoassay techniques [152,153]. Most commonly, these assays measure the quantity of transmethylation product, AdoHcy/SAH. In the colorimetric assay developed by Hendricks *et. al*. [149], the AdoHcy/SAH product is converted by hydrolysis by SAH nucleosidase to give adenine and *S*-ribosylhomocysteine. *S*-Ribosylhomocysteinase (LuxS) is then used to cleave the *S*-ribosylhomocysteine to yield

homocysteine. The thiol-containing homocysteine can be measured using Ellman's reagent (5,5'-dithio-bis(2-nitrobenzoic acid, DTNB) by quantitating the absorbance of 2-nitro-5-mercaptobenzoic acid at 412 nm (Figure 3.4A). In a similar approach, an enzyme-coupled fluorescent technique used by Collazo and co-workers [150] uses SAH hydrolase to generate adenosine and homocysteine in the presence of adenosine deaminase which converts adenosine to inosine. The homocysteine is then conjugated to a thiol-sensitive fluorophore, ThioGlo^{R} 1 (Ex = 384_{max} nm; Em_{max} = 513 nm) (Figure 3.4B). Alternatively, AdoHcy/SAH product can be quantified by immunological methods where an anti-SAH antibody solution is used and subsequently a horseradish peroxidase (HRP)-conjugated rabbit anti-mouse antibody is applied; the addition of the HRP substrate (3,3,5,5-tetramethylbenzidine; TMB) produces a yellow colour upon acidification and can be quantified at 450 nm (Figure 3.4C) [152]. This assay format is a competitive immunoassay in which the the SAH from the sample and the SAH that is immobilized on a solid surface competes for the anti-SAH antibody. Therefore, the signal that is detected is inversely proportional to the concentration of SAH in the sample.

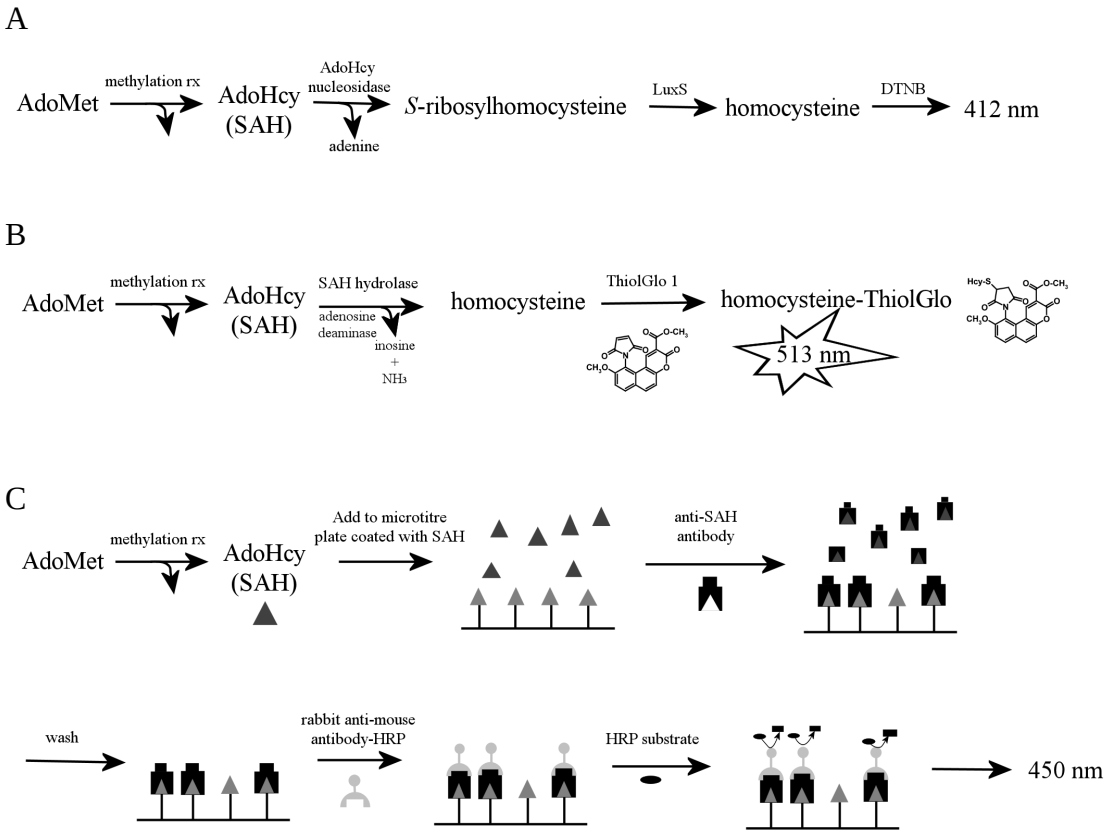

Figure 3. 4. Non-radiometric assays developed for MTases.
(A) Spectrophotometric **(B)** Fluorescence **(C)** Competitive immunoassay (HRP = horse radish peroxidase). See text for details.

3.1.4. Plan of Action

In the previous chapter (*Chapter 2*), the overexpression and purification of a hexahistidine-tagged TSR were described and discussed. This chapter describes the biochemical characterization of this purified cleaved TSR′ by means of the traditional FB assay. Although the FB assay has been the assay of choice over the years for measuring methyltransferase kinetics, it is time consuming, laborious and not suited for high throughput applications. This chapter also documents the preliminary development of a sensitive and efficient radiometric SPA method to more conveniently assay TSR′.

3.2. Materials and Methods

3.2.1. Reagents and Materials

The following reagents and materials were obtained from the following companies:

Amersham Biosciences (formerly Pharmacia Biotech) (Uppsala Sweden): *S*-adenosyl-L-[methyl-^{3}H] methionine (^{3}H-AdoMet*; 60-80 Ci/mmol), RNA YSi Binding SPA beads (uncoated), Polylysine YSi Binding SPA beads

Bioshop (Burlington, ON): ammonium chloride, *N*-2-hydroxyethylpiperazine *N*′– 2-ethanesulphonic acid (HEPES), magnesium chloride hexahydrate

EMD Pharmaceuticals (Durham, NC): glycerol, potassium hydroxide, trichloroacetic acid, RNase inhibitor

MP Biochemicals (Solon, OH): Cytoscint ES^{TM} liquid scintillation fluid

Roche Diagnostics (Laval, QC): 16S/23S ribosomal RNA (*E. coli* MRE600)

Sigma Chemical Company (St. Louis, MO): β-mercaptoethanol, *S*-adenosyl-L-methionine *p*-toluenesulfonate salt (from yeast ≥80%), diethylpyrocarbonate (DEPC)

UltiDent Scientific (St. Laurent, QC): low binding pipette tips

VWR (Mississauga, ON): Whatman GF/B and GF/C glass filters, siliconized eppendorf tubes

3.2.2. General Equipment

3.2.2.1. Liquid Scintillation Counter

All radiometric readings were carried out on a Beckman LS 5000TD (Fullerton, CA) or a Beckman LS 6500 TD (Fullterton, CA) liquid scintillation counter.

3.2.2.2. Centrifuges

Small volume centrifugation was carried out using the Biofuge A microcentrifuge (Heraeus Sepatech GmbH, Germany).

3.2.2.3. Cell Disruption Equipment

Lysis of cells for purification were obtained from sonication of resuspended cells with a Sonicator™ cell disruptor model W225 from Heat Systems-Ultrasonics, Inc (Plainview, NY), converter model #2 with a standard tapered mircrotip at an output control setting at 5.

3.2.2.4. Chromatographic Equipment

The Unosphere-Q anion exchange column was acquired from BioRad (Mississauga, ON) and the MonoQ column was obtained from Amersham Biosciences (formerly Pharmacia, Uppsala, Sweden). Purification of UT-TSR was performed on a high performance liquid chromatography apparatus (HPLC). FPLC was performed on a Pharmacia Biotech (now Amersham Biosciences, Uppsala, Sweden) system comprising of: LCC-500 chromatography controller, two P-500 pumps, MV-7 motor valve and Empower

Pro (Build 1154) software. HPLC was carried out on a Waters HPLC system (Milford, MA, USA) consisting of the following components: Waters 600S controller, Waters 626 pump, Waters 2996 Photodiode Array Detector, in addition to Waters Empower 2 software (Build 2154). All aqueous buffers were filtered through a 0.2 μm membrane filter (Pall Life Sciences, East Hills, NY). Before injection all samples were filtered through a syringe filter: 0.2 μm polyethersulfone membrane (VWR International, Mississauga, ON). All buffers were degassed prior to use.

3.2.3 General Experimental Protocols

3.2.3.1. Minimization of RNAse Contamination

A number of precautions were taken to minimize RNAse contamination, as TSR′ requires an RNA substrate. Fresh gloves were worn at all times. All preparation areas were wiped with RNase AWAY^{TM}. Spatulas, glassware etc. were wrapped in aluminum foil and placed in a 160 °C oven for a minimum of four hours prior to use, and all plastic-ware utilized was certified RNase free by their respective manufacturers. All buffers were made from RNase-free Milli-Q water (MQW). RNase-free MQW was prepared in the following manner: 0.1% v/v diethylpyrocarbonate (DEPC) was added to MQW and allowed to stir for one hour in 37 °C or overnight at ambient temperature. The DEPC treated MQW was then autoclaved to remove residual DEPC from the solution [154,155]. In assay mixtures, 1 U of RNase inhibitor was added.

3.2.3.2. Reducing The Specific Activity of *S*-adenosyl-L-[methyl-^{3}H]-methionine

The specific activity of the commercially available substrate i.e. *S*-adenosyl-L-[methyl-^{3}H]-methionine (^{3}H-AdoMet*) is often reduced for storage and assay conditions. The specific activity of a radiochemical is defined as the amount of radioactivity per unit amount of substance i.e. Ci/mmol. Reduction of specific activity can be accomplished with the addition of non-radiolabelled ("cold") compound; that is, while the absolute amount of radioactivity remains the same, the total amount of substance increases giving a smaller value for specific activity. The amount of unlabelled compound to add can be calculated with the following formula [156]:

$$W = Ma \times \left[\frac{1}{A'} - \frac{1}{A} \right]$$

Where W = weight (in mg) of unlabelled "cold" compound to be added (mg)
M = molecular weight of radiolabelled compound (g/mol)
a = total activity (GBQ, mCi) in sample
A = molar specific activity (GBq/mmol, mCi/mmol of compound as supplied)
A′ = molar specific activity (GBq/mmol, mCi/mmol) of the desired diluted compound

Typically the mass (in mg) of the cold AdoMet to be added to the "hot" sample is ~0.477 mg (achieved through addition of a stock solution at a concentration of 5 μg/μL or 10 μg/μL in 50 mM HEPES pH 7.5, 7.5 mM $MgCl_2$, 73.5 mM NH_4Cl, 3 mM β-mercaptoethanol, 10% glycerol) to give a specific activity of 500 mCi/mmol and the solution is aliquotted and stored at -20 °C. Please refer to appendices for detailed sample calculations.

3.2.4. Filter Binding Assay for TSR´

The MTase activity of the purified enzyme was analyzed *in vitro* by measuring the amount of ^{3}H-methyl (from [^{3}H]-AdoMet*) incorporated into the substrate rRNA. Kinetic

data for TSR have been previously published in the literature [113,114,157]. However, reproducibility with initial kinetic assays performed was not acheived with our experimental set-up when the literature protocol was followed. Multiple aspects of the assay preparation were refined to allow for reliable and accurate determination of TSR′ kinetic parameters. In addition, low-binding pipette tips and siliconized Eppendorf tubes were introduced in the assay to permit maximum retention of sample that may otherwise be lost through handling and manipulation.

3.2.4.1. TSR′ Filter Binding Assay Refinement and Optimization

A series of time courses and kinetic assays were performed under varying conditions. Table 3.1 shows different aspects of the assay procedure that were altered.

Table 3.1: Different Variables of the Filter Binding Assay Optimized.

Assay Variable	Manipulation
RNA	Refolding vs. no refolding (used as is from manufacturer)
Enzyme	TSR′ vs. untagged TSR enzyme (UT-TSR)
	Enzyme concentrations (20 nM, 40 nM, 80 nM, 100 nM and 160 nM)
AdoMet	Different specific activities (500 mCi/mmol, 250 mCi/mmol, 125 mCi/mmol)
Sample Handing	Filter binding paper (GF/B vs. GF/C)
	TCA precipitation time (0, 15 min , 30 min , 45 min, 1 h, 2 h)
	Volume of TCA used to washed sample (10 mL, 20 mL, 30 mL)
	Volume of TCA used to quench methylation reaction (0.5 mL, 1.5 mL)
	Concentration of TCA (5% w/v, 10% w/v)
	Liquid scintillation cocktail addition

All time-dependent measurements of enzymatic activity were performed in the following manner using the previously published methodologies [113,114,157] as a template: the 16S/23S rRNA was thawed over a period of one hour on ice prior to assay use. Incubation of 1 μM of 16S/23S rRNA, 8 pmol TSR′ in Assay buffer (50 mM HEPES pH 7.5, 7.5 mM $MgCl_2$, 73.5 mM NH_4Cl, 3 mM β-mercaptoethanol, 10% glycerol) was performed for 15 min at 25 °C. The methylation reaction (total volume 100 μL) was initiated by the

addition of 2.5 μCi of [^{3}H]-AdoMet* (with a specific activity of 500 mCi/mmol; final concentration: 1.7 mM). The methylation reaction was carried out at 25 °C for the allocated time period and quenched with 500 μL of ice-cold 5% TCA (w/v) solution. The quenched reaction mixture was kept at 0 °C on ice for one hour and the precipitated rRNA product was filtered through glass filters and washed with 10 mL of ice-cold TCA solution. The filter paper was allowed to dry overnight before addition of 10 mL of Cytoscint™ liquid scintillation cocktail. For all trial kinetic assays, the rRNA substrate concentration was varied from 0 nM to ~340 nM and the [^{3}H]-AdoMet* was kept at 2.5 μCi.

Modifications of this standard procedure were made to manipulate the variable required for assay optimization as outlined in Table 3.1:

Refolding the Ribosomal RNA Substrate

The 16S/23S rRNA was thawed on ice for one hour. The rRNA was unfolded at 65 °C for 15 min and allowed to cool to room temperature for a minimum of one hour prior to addition to the reaction mixture. Alternatively, the rRNA was unfolded at 65 °C for 30 min and allowed to refold over 1.5 h. Also, the rRNA was unfolded at 85 °C for 30 min and allowed to cool to ambient temperature over 1.5 h.

Enzyme Manipulation

Different concentrations of TSR′ were used in the development of the assay (20 nM, 40 nM, 80 nM, 100 nM and 160 nM). In addition, the untagged version of the enzyme (UT-TSR) was over-expressed and purified for semi-quantitative methylation analysis. The gene encoding *tsr* (pUC-TSR) in *E. coli* DH5α was obtained from Dr. Gerry Wright of McMaster University (Hamilton, ON). A starter culture inoculated from frozen stock was grown at 37

°C in TB broth (per litre: 12 g tryptone, 24 g yeast extract, 4 mL glycerol in 900 mL ddH_2O plus 100 mL of 0.17 M KH_2PO_4 and 0.72 M K_2HPO_4, pH 7.0) supplemented with chloramphenicol (34 μg/mL). Large scale growth was then initiated with a 100-fold dilution in media and grown at 37 °C with constant agitation (~200 rpm). The expression of the UT-TSR was induced at mid-log phase (A_{600} = 0.5-0.8) with 1 mM isopropyl-β-thiogalactopyranoside (IPTG). The cells were grown for four hours and harvested by centrifugation (5 min at 13 000 ×*g*) and frozen at -80 °C.

The cell pellets were resuspended in lysis/loading buffer (50 mM Tris pH 7.5, 10% glycerol) with 1 mM phenylmethylsulfonyl fluoride (PMSF) and thawed on ice. The cell suspension was then sonicated on ice for 10-12 cycles with 10 s pulses separated with one minute pauses. The soluble cell fraction was collected by centrifugation at 48 300 ×*g* (20000 rpm) with a JA-25.50 rotor for 20 min at 4 °C. Further removal of any remaining particular cell debris was achieved through filtering through a 0.2 μm filter.

The cell lysate was loaded onto the anion exchange column (UnoSphere). The column was washed to baseline absorbance at 280 nm. A linear gradient of KCl at 1%/min from Buffer A (50 mM Tris pH 7.5, 10% glycerol) to Buffer B (50 mM Tris buffer pH 7.5, 1 M KCl, 10% glycerol) was used and UT-TSR eluted between 7% - 23% KCl, but only fractions containing 15-18% were collected for the following step in the purification. KCl salt was dialysed away from the protein before the second stage of purification. A second anion exchange column (MonoQ) was used with the same gradient and the enzyme eluted gradually over 20% - 40% KCl. The fractions containing 28-31% salt were collected and dialyzed against 50 mM Tris buffer pH 7.0, 75 mM KCl and the purified protein was then stored at -80 °C for future use.

3.2.4.2. Optimized TSR′ Filter Binding Assay

The methylation assays were performed with the minor modifications that were used in the previous experiments. Methylation reaction mixtures contained **X** μM of 16S/23S rRNA (where **X** = 0 nM to ~340 nM), 4 pmol TSR′ (40 nM) in Assay buffer (50 mM HEPES pH 7.5, 7.5mM $MgCl_2$, 73.5 mM NH_4Cl, 3 mM β-mercaptoethanol, 10% glycerol) and were incubated for ~15 min in a 25 °C water bath. Methylation was initiated by the addition of of 2.5 μCi of [^{3}H]-AdoMet* (500 mCi/mmol); the pipette tip was washed with the methylation reaction by 10 cycles of aspiration and expellation of the tube contents. The reaction tube was also flicked gently 30 times before placing back into the water bath.

The reaction was performed at 25 °C and quenched at the desired time point by adding 1.5 mL of ice-cold 10% TCA (w/v) solution. The quenched reaction mixture was kept at 0 °C on ice for one hour and the precipitated rRNA product was filtered through a GF/C glass fibre filter paper (2.5 mL) and washed with 10 mL of ice-cold 10% w/v TCA solution. The filter paper was allowed to dry overnight before addition of 10 mL of Cytoscint™ liquid scintillation cocktail. After addition of the cocktail, the vial was vortexed vigorously for one minute and allowed to stand for a minimum of 10 min prior to placing in a liquid scintillation counter.

To obtain kinetic constants for rRNA, the [^{3}H]-AdoMet* concentration was kept at 1.7 mM (2.5 μCi; 500 mCi/mmol) and initial velocities were measured at varying concentrations of 16S/23S rRNA from 0 nM to ~340 nM. To obtain kinetic values for AdoMet, the RNA concentration was kept at 0.241 μM.

3.2.5. Towards the Development of a Scintillation Proximity Assay for TSR′

3.2.5.1. Selection of SPA Bead Type

Two different types of beads were evaluated: polylysine coated yttrium silicate (YSi) SPA beads and RNA binding YSi SPA beads. Polylysine beads were supplied as a lyophilized powder and were reconstituted in the Assay Quench buffer (167 mM sodium citrate pH 2) at a concentration of 20 mg/mL. The RNA binding beads were provided in a suspension of water (100 mg/mL) from the manufacturers, and were transferred into assay quench buffer. This was achieved by allowing the beads to settle to the bottom of an eppendorf tube and pipetting off the water and then adding the same volume of assay quench buffer. This was done for a minimum of four times over the time period (minimum of four to five hours) as the beads were quite easily suspended. The working concentration of the RNA binding beads was also at 20 mg/mL. Different concentrations of bead-quench suspension were made from the 20 mg/mL stock (0, 0.25, 0.5, 1, 1.5. 2, 2.5, 3 mg/assay).

The methylation reaction was set up in a similar manner to that of the FB assays described earlier. After the thawing of the 16S/23S rRNA on ice over one hour, the RNA substrate was incubated with 4 pmol of TSR′ in Assay Buffer buffer (50 mM HEPES pH 7.5, 7.5 mM $MgCl_2$, 73.5 mM NH_4Cl, 3 mM β-mercaptoethanol, 10% glycerol) for 15 min at 25 °C. Upon addition of 2.5 μCi of [^{3}H]-AdoMet* (specific activity of 500 mCi/mmol), the methylation reaction was initiated (total volume 100 μL) at 25 °C and allowed to proceed for 15 minutes before quenching with the bead-assay quench buffer to make a final total volume of 350 μL (250 μL quench solution + 100 μL assay volume). The bead-assay quench mixture was constantly agitated to prevent beads from settling to the bottom. This was achieved with constant light vortexing. The beads were allowed to settle for two hours or longer, and then

samples were counted with a liquid scintillation counter. A control experiment was performed in an identical fashion with rRNA substrate present, but no enzyme as a negative control.

It was found that polylysine YSi beads gave more reproducible data than the RNA binding beads. Therefore, for the rest of the assay development, polylysine YSi beads were used at 2 mg/assay.

3.2.5.2. TSR′ SPA Refinement and Optimization

A series of time course experiments were performed under varying conditions with the same procedure as described in the previous section (*Section 3.2.4.1*). Table 3.2 shows different aspects of the assay procedure that were investigated:

Table 3.2: Different Variables of the Scintillation Proximity Assay Optimized.

Assay Variable	Manipulation
RNA	Lower [rRNA] (50 nM) Refolded rRNA
Enzyme	Enzyme concentrations (20 nM, 40 nM, 8 μM, 16 μM)
Temperature	37 °C incubation with beads
Non-specific binding	Different blocking agents were evaluated: KCl, Tween-20, Triton-X100 and BSA

3.3. Results and Discussion

3.3.1. Filter Binding Assay for TSR′

Kinetic parameters of TSR′ were available in previously published literature [113,114,157] and were used as the starting estimates for concentration ranges for the enzyme and substrates in our assays. Optimization and evaluation of the assay procedure was required as reproducibility was not possible in our hands and large errors were incurred with the initial biochemical characterization of TSR′. Efforts were made to minimize error with

the introduction of low-binding pipette tips and siliconized Eppendorf tubes to the assay set-up. Other assay variables were manipulated and refined through many replicates of data sets to give a reliable and accurate determination of TSR′ parameters.

3.3.1.1. Refolding the Ribosomal RNA Substrate

Proper secondary and tertiary structure is important to the biological role of RNA [158]. The 16S/23S rRNA substrate acquired from the manufacturer was used without any manipulation for assays. On occasion, it was found that quality of the RNA from the supplier was found to be quite heterogeneous (which led to erroneous results for some replicates of kinetic data), the possibility of having to refold the rRNA substrate to a biologically functional conformation was explored. In assays performed by Bechthold and Floss [113], the RNA substrate was heated to 65 °C for 15 min and then cooled to room temperature for a period of 30-60 min. The rRNA substrate that was utilized for our assay purposes was unfolded at 65 °C for two different time periods: 15 min and 30 min and then permitted to cool to ambient temperature between one to one and a half hours. In addition, a higher temperature was utilized to perform the unfolding (85 °C) and refolded over 1.5 h (Figure 3.5).

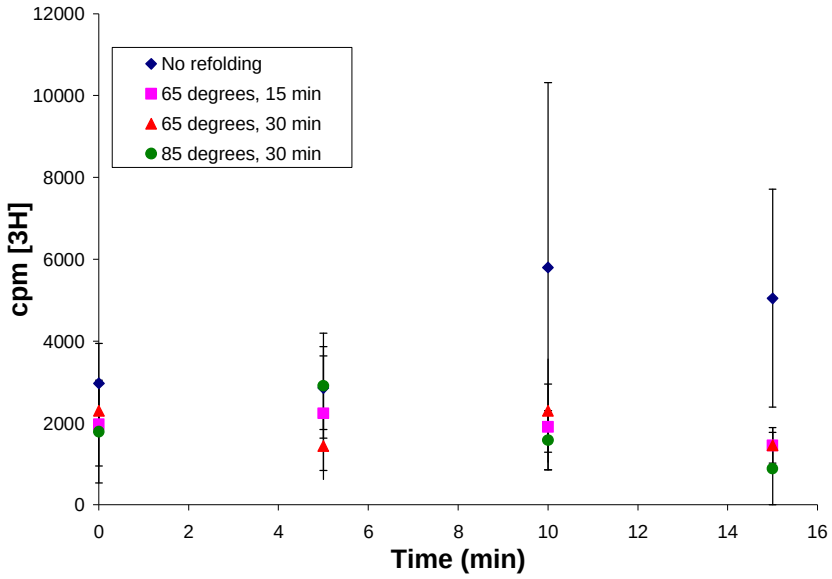

Figure 3. 5: Short 15 min time course where the rRNA substrate was denatured at elevated temperatures and refolded over time.

It was observed that in all three cases that methylation activity was completely eliminated (reduced counts) compared to the RNA substrate that was not denatured and refolded. The rRNA substrate utilized by Bechthold and Floss was a significantly smaller fragment (nucleotides 1029-1122) compared to our 16S/23S rRNA substrate. As a consequence, the heating and refolding with the same conditions and conditions of a longer time frame and/or elevated temperatures most likely did not permit the RNA to fold back to its correct secondary structure resulting in a non functional RNA substrate. Therefore, for all remaining modifications of the enzyme assay, the 16S/23S rRNA was used without unfolding and refolding.

3.3.1.2. Enzyme Manipulations

The effects of enzyme concentration on the methylation reaction were probed. One would expect a direct proportionality of the concentration of the MTase to the initial rate of methylation reaction. The error observed and the replication of three sets of data did not

make this relationship obvious indicating that another, yet to be identified variable was responsible for most of the observed experimental variations (Figure 3.6). Further assay optimization was pursued with the wild type, untagged enzyme (UT-TSR) as the histagged-TSR, which was subsequently cleaved in the latter stages of the purification (see *Chapter 2*), had proven difficult to handle. The presence of a fusion tag could potentially alter protein conformation [117,124], and this effect could potentially be irreversible even though the tag was proteolytically removed. Therefore, the untagged enzyme was isolated and purified and methylation activity of this enzyme was compared to the cleaved histagged TSR′.

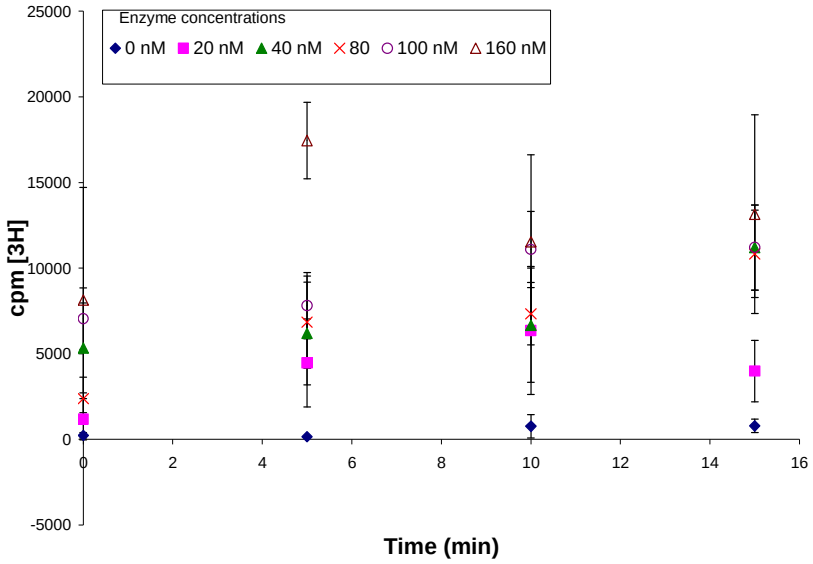

Figure 3. 6: Time course of methylation reactions with different TSR′ concentrations.
Data obtained from this experiment indicated that other aspects of the assay remained to be optimized.

The growth and induction conditions for pUC-TSR/BL21 cells were identical to that for recombinant protein production from pTSR10/BL21. After cell breakage, the crude lysate was subjected to anion exchange chromatography using an UnoSphere-Q column and fractions were identified between 7% - 20% KCl by SDS-PAGE (Figure 3.7). Fractions containing 15-18% KCl were pooled and further processed using a MonoQ anion exchange column. During this final step of purification, UT-TSR fractions were identified over the

range of KCl concentration of 20% - 40% (Figure 3.8). The fractions that contained the 28-31% salt were selected based on the protein's purity for future biochemical analysis. These fractions were dialyzed against 50 mM Tris buffer pH 7.0 containing 75 mM KCl and 10% glycerol and stored at -80 °C.

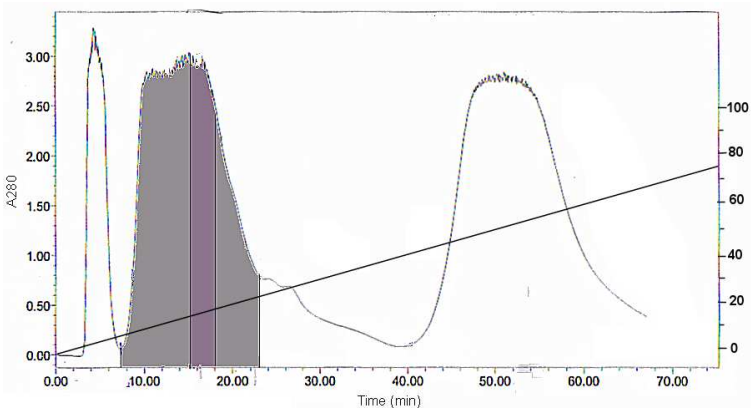

Figure 3.7: Chromatogram showing the separation of UT-TSR from the crude cell lysate mixture. Fractions eluted from the anion exchanger (Unosphere-Q) between 7-23% KCl (1%/min; shaded in light grey). Fractions containing 15-18% KCl (shaded in dark grey) were pooled together and carried to the next step of the purification.

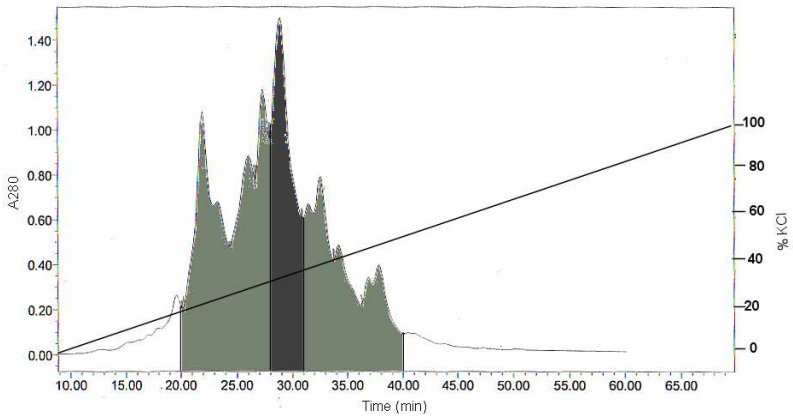

Figure 3.8: Elution profile of UT-TSR from the anion exchange Mono-Q column. Protein was loaded onto the column and eluted with a 1% per minute KCl gradient. UT-TSR was detected in fractions between 20% to 40% KCl (light grey). Only fractions containing 28-31% salt (dark grey) were collected and stored for experimental purposes.

Time courses performed on the freshly purified UT-TSR also had no consistent pattern (Figure 3.9), suggesting that His-tag cleavage of the NTA-purified enzyme did not affect activity as previously thought. It is apparent from all the data collected thus far that

methylation activity of both the TSR′ and UT-TSR was not likely compromised by the purification process, and indicated that other technical aspects of the assay required refinement and optimization. The following section discusses the assay variables that were altered to eventually obtain reliable and consistent data.

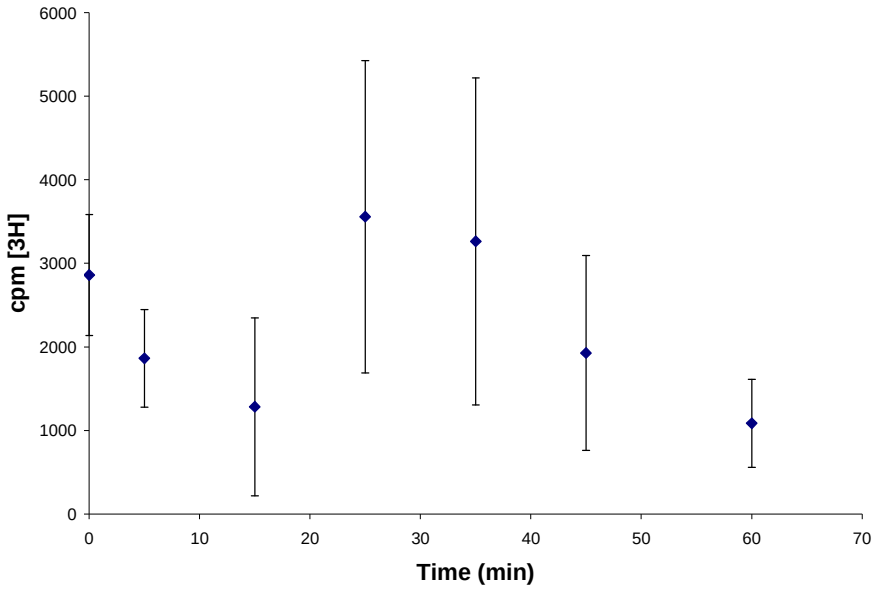

Figure 3.9: Representative time course of UT-TSR.
Results show the same inconsistency as previously time courses obtained with TSR′ indicating that the cause of the erratic data is not likely due to any detrimental effects of the presence of a hexahistidine tag.

3.3.1.3. Refinment of Other Technical Assay Variables

*Specific Activities of [^{3}H]-AdoMet**

The specific activity of radiolabelled compounds refers to the total amount of radioactivity per unit mass [156]. A compound with a specific activity of 1 Ci/mmol yields 3.7×10^{10} disintegrations per second per millimole of compound. All commercial tritiated AdoMet acquired in our study has a high specific activity (~60-90 Ci/mmol) and is diluted with excess unlabelled AdoMet to reduce the specific activity to 500 mCi/mmol for storage and assay use.

It is recommended that radiolabelled compounds be stored at lower specific activities to slow down the rate of decomposition of the compound, which can otherwise affect the results of studies. Therefore, storage of [^{3}H]-AdoMet* at lower specific activities was compared to the original 500 mCi/mmol (Figure 3.10). Overall results show that samples with lower specific activity still yielded inconsistent data. Therefore, the specific activity of 500 mCi/mmol for storage and assay purposes remained unaltered.

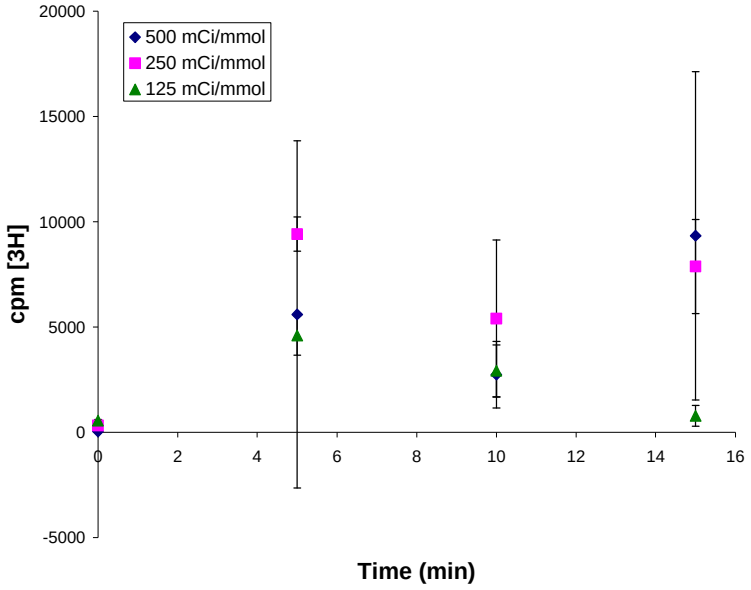

Figure 3.10: Short time courses with lower specific activities of [^{3}H]AdoMet*.
Lower specific activities were used for both storage and assay purposes and were found to have no improvement on the acquired data.

Filter Paper and TCA Conditions

The type of filter paper and different trichloroacetic acid (TCA) precipitation conditions were varied in combination with each other. Table 3.3 shows the combinations that were studied:

Table 3.3: Different Combinations of Filters and TCA Precipitation Conditions Used for Optimization of the Filter Binding Assay.

Combination	Glass Filter	TCA condition
1	GF/B	Precipitation time (0, 15 min , 30 min , 45 min, 1 h, 2 h) Higher TCA concentration (10% w/v)
2	GF/C	Precipitation time (0, 15 min , 30 min , 45 min, 1 h, 2 h) Higher TCA concentration (10% w/v)
3	GF/C	TCA Quench solution volume (0.5 mL, 1.5 mL) Higher TCA concentration (10% w/v)
4	GF/C	Washing volume (10 mL, 20 mL, 30 mL) Higher TCA concentration (10% w/v)

The filter paper that was chosen for the assays was Whatman GF/B glass microfiber filter paper. Whatman GF/B filter papers were initially chosen over the standard Whatman GF/C filters for their ability to collect precipitated macromolecules such as protein and nucleic acids. The length of time required for the precipitation of the tritiated rRNA was investigated to ascertain if the length of the time allowed for substrate precipitation influenced the measurements. Since small volumes/amounts were utilized in the assay, errors during handling of assay components during the separation and counting, such as a small amount of rRNA not being precipitated, could have translated into a significant variation of radioactive counts.

A comparison of both filter papers was performed in combination with variation in the length of time used for precipitation. This enzymatic reaction was performed over a fixed duration (15 min) and it was observed that after 15 min with 10% TCA on ice, there did not appear to be a significant difference in counts between that and longer precipitation times (Figure 3.11).

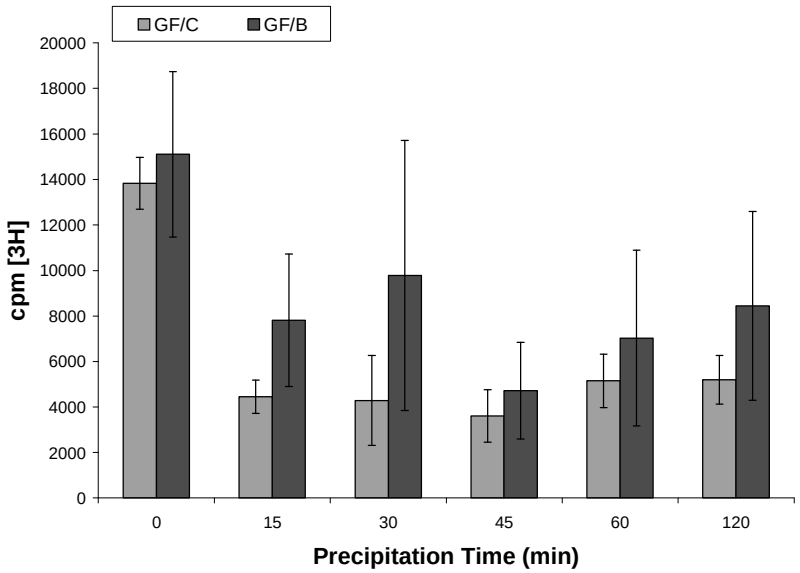

Figure 3. 11: Comparison of different TCA precipitation times between GF/C and GF/B glass filters.

The GF/C filter paper is significantly thinner than its GF/B counterpart permitting faster processing time during the washing process. The vacuum used for filtration assays had to be adjusted to allow rapid filtering but not to tear the membranes. It appeared that better overall washing occurred with the thinner filter membrane, and it was observed that the error was reduced for the GF/C filtered samples when compared to the use of GF/B filters. Therefore, the filter paper used for our vacuum system in all subsequent studies was the standard and thinner GF/C glass fibre filter paper in conjunction with the higher concentration of 10% w/v TCA.

A time course study was then performed using the thinner GF/C filters, in conjunction with a larger TCA quench buffer volume. In lieu of stopping the enzyme reaction with 0.5 mL of 10% w/v TCA, 1.5 mL was used instead. The GF/C filter paper was better suited for our vacuum system significantly less error between replicates. Additionally, the larger quench volume most likely provided a quicker termination of enzyme methylation reaction

by dilution effects along with the drastic pH change provided by the acid. However, it was evident that further optimization of the assay was required.

Since the error in the time courses was manifested not only between replicates, but also between time points, it was assumed that excess [^{3}H]AdoMet* was not being thoroughly removed from the filter paper during the washing process in spite of changing to a thinner glass filter paper. It is imperative that filters be washed sufficiently to remove as much unbound radiolabelled AdoMet to maximize the specific binding signal detection. Larger volumes (two and three times) of TCA used for washing the filter paper were used. It was found that 10 mL of 10% w/v TCA used for washing was sufficient and larger volumes did not aid reduce error, but only contributed to the time required to perform the assay.

Liquid Scintillation Cocktail Addition

The last step prior to the counting of replicates is the addition of the LSC cocktail to the filter paper (dried overnight). Surprisingly, it was found that after the addition of the LSC cocktail, vigorous mixing of the LSC vial with the vortex apparatus for one minute and letting the vial sit for 10 min allowed for more consistent and reliable data. Prior to this, the LSC cocktail was simply added and the vial inverted three times before putting in the liquid scintillation counter to obtain counts. Therefore, sufficient incubation time was required to allow the embedded radiocompound within the filter paper to become accessible to the liquid scintillation counter for maximum signal and reduced variability (Figure 3.12).

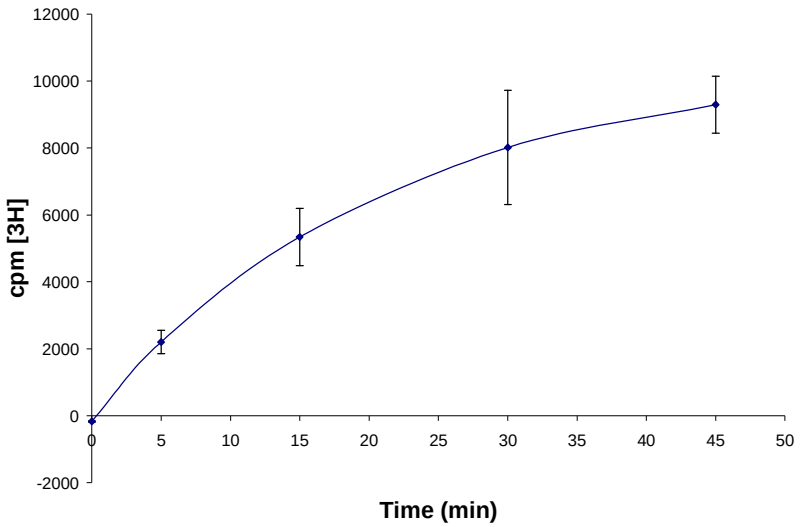

Figure 3.12: Time course of methylation that showed drastic improvement after several adjustments were made described in the text.
The last adjustment made was the LSC incubation time that eliminated error between time samples.

3.3.1.3. Evaluation of Kinetic Parameters of TSR′ with Optimized Filter Binding Assay

With the optimized FB assay, these slight adjustments and improvements have yielded an assay procedure that generates reproducible replicates of kinetic data. The kinetic parameters for TSR′ obtained in this study are shown in the Table 3.4:

Table 3. 4: Kinetic parameters for the TSR′ catalyzed methylation of 16S/23S rRNA.

	***K*m (μM)**	***V*max (μmol/min/mg) ($\times 10^{-2}$)**	***k*cat (s^{-1}) ($\times 10^{-2}$)**	***k*cat/Km ($M^{-1}s^{-1}$) ($\times 10^{-4}$)**
AdoMet*	40 ± 5	1.0 ± 0.1	N/A	N/A
16S/23 S rRNA*	0.7 ± 0.3	2.3 ± 0.4	2.3 ± 0.2	3.8 ± 0.2
AdoMet[Ψ]	100	N/A	N/A	N/A
58-mer hairpin rRNA[Ψ]	2.0 ± 0. 5	5.4 ± 0.5	2.6 ± 0.2	1.6
AdoMet[Ψ]	100	N/A	N/A	N/A
23 S rRNA[Ψ]	2.0 ± 0.5	4.3 ± 0.9	2.0 ± 0.5	1.2

[Ψ]As reported by Bechthold and Floss [113]
* To obtain kinetic parameters for rRNA, the AdoMet concentration was kept at 1.7 mM and rRNA concentrations were varied from 0 nM to 340 nM. To obtain kinetic parameters for AdoMet, the RNA concentration was kept at 0.241 μM and the AdoMet concentration was varied from 0 mM to 0.255 mM.

Kinetic data obtained for TSR′ converges with the values reported by Bechthold and Floss [113]. The magnitude of the Km and Vmax values are comparable to previous studies for the AdoMet and rRNA substrate, although the slight differences did result in a

corresponding two to three time difference in the catalytic efficiency (kcat/Km) of the enzymes. Figures 3.13 show the Michaelis-Menten plot of a representative set of kinetic data:

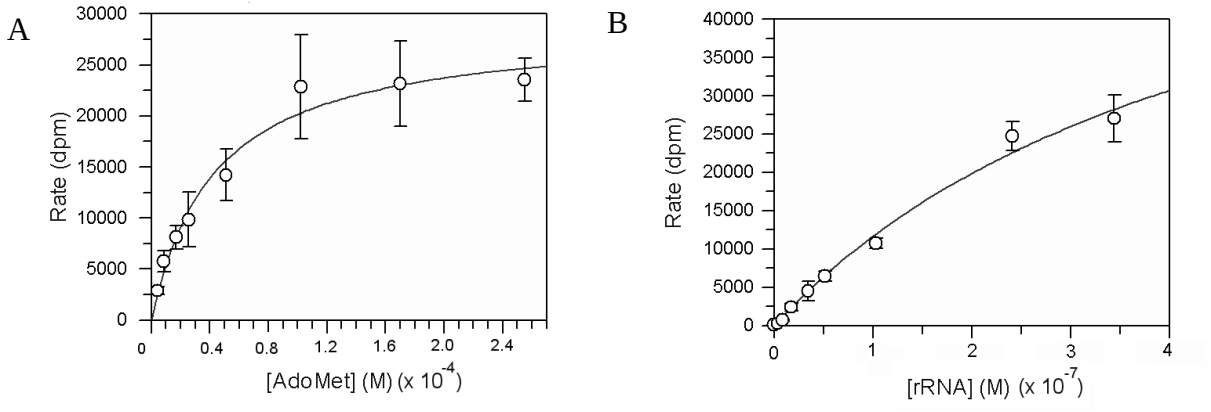

Figure 3. 13: Michaelis-Menten plot of a representative set of kinetic data for both substrates, Adomet **(A)** and 16S/23s rRNA **(B)**.

3.3.2. Scintillation Proximity Assay Development for TSR′

Throughout the entire assay refinement process for the filter binding method, it was noted that the conventional filter binding (FB) assay was time and labour intensive. Alternative methods were sought and the Scintillation Proximity Assay appeared to be well suited for our assay purposes. SPA is an approach that does not involve post-reaction handling steps that could contribute to experimental error in our current system. Efforts towards the development of a SPA method for TSR′ were pursued concomitantly during the FB assay optimization.

We selected a solution phase signal increase assay format. In solid phase SPA, the substrates are immobilized on the SPA bead and are somewhat compartmentalized from the enzyme, which could affect the parameters of the Michaelis-Menten kinetics. Signal increase assays are also recommended for monitoring enzyme activity, where the labelled product, in this case the 16S/23S rRNA, is coupled or bound to the SPA bead. Therefore, the increase in the signal detected is proportional to the activity of the methyltransferase.

3.3.2.1. Selection of SPA Bead Type and Amount

Various types of SPA beads are available commercially, which differ in their matrix composition (polyvinyltoluene or yttrium silicate) and in the "capture molecule" coupled to the surface of the bead. Two types of beads were chosen for evaluation: polylysine and uncoated yttrium silicate (YSi) beads. The positively charged polylysine (polylys) residues derivatized on the surface of the bead can form ionic interactions with negatively charged molecular species such as nucleic acids [159], while uncoated YSi beads (also known as RNA-binding beads) have been demonstrated to interact with phosphate groups in small molecules such as ATP, oligonucleotides and larger biomolecules such as RNA and DNA [159].

Initial development of the SPA method involved optimizing bead concentration; other reaction conditions were adapted from the FB assay. Incubation times for methylation were 15 min and the reaction was terminated with quench buffer in the presence of SPA beads. The bead content utilized ranged from 0 to 3 mg of SPA YSi bead per assay reaction. We sought to obtain a signal and minimize background caused by non-specific binding (NSB) and/or close proximity effects (CPE) (Figure 3.14). NSB can be be overcome by use of blocking agents so that free radiolabel is prevented from adhering to the bead surface. CPE can be a result of a high concentration of radiolabel and or a high concentration of SPA beads. Although the radiolabel is not bound to the bead, it is in close enough to elicit a signal.

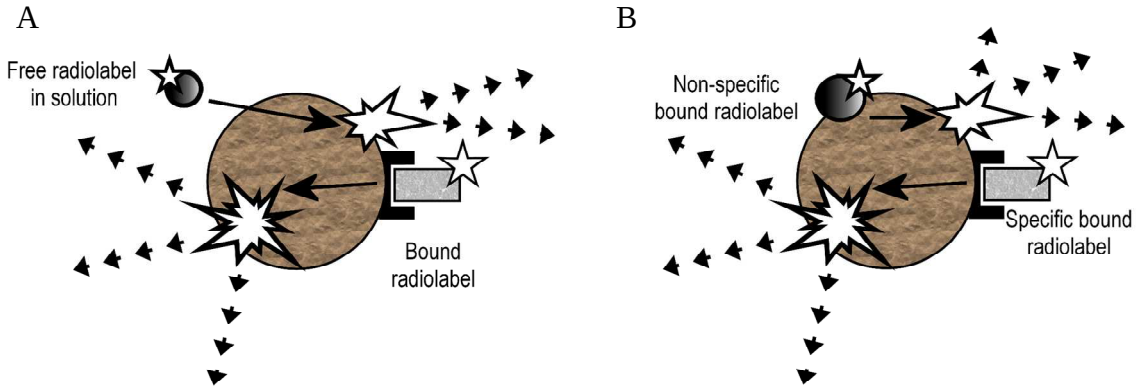

Figure 3.14: False signal dectection is possible with SPA beads.
Close proximity (A) and Non-specific binding (B) effects can contribute to higher signal readings than expected.

For both polylys and RNA binding beads, both the signal and the NSB/false positive effects increased with increasing amount of beads (Figure 3.15). For polylys Ysi beads saturation of binding was reached between 2 to 2.5 mg/assay as the signal to noise ratio decreased at higher amounts of beads. Therefore, for maximal sensitivity and minimal background noise, assays should be executed at 2 mg/assay using polylys YSi beads (Figure 3.15A). With the naked RNA binding beads, 2 mg/assay was also required for optimal assaying conditions; however, the error over the entire range of SPA bead amounts was large (Figure 3.15B). Errors are most likely incurred during the buffer change process; the RNA binding beads are supplied in water and must be changed over to the assay buffer. However, beads are likely to be lost during the bead washing process and changeover process. Furthermore, preparation of the RNA binding beads in the assay buffer required a minimum of four to five hours with the washing and bead settling process. With the polylys beads being supplied as a lyopholized powder, stock preparations were facile and less time consuming. Therefore, all SPA assays were performed with polylys beads at 2mg/assay amounts.

A

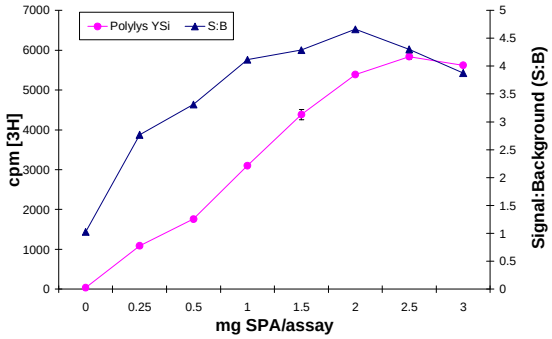

B

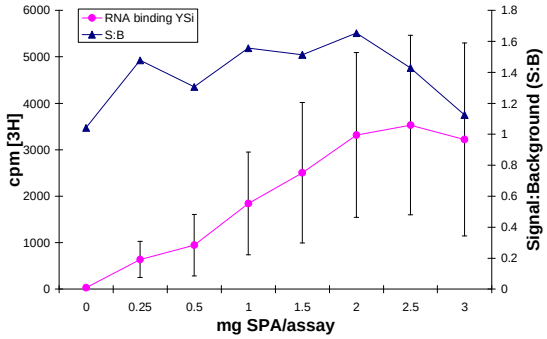

Figure 3.15: Optimal SPA bead amounts were determined for two different types of beads. **(A)** Polylysine YSi beads and **(B)** RNA binding Ysi beads. Both types of beads at 2mg/assay reaction were found to give the largest signal with least amount of background. It was observed that polylysine beads were easier to handle and gave less error than the naked beads.

3.3.2.2. TSR′ Refinement and Optimization

Following the optimization of the bead amount for the SPA platform, a time course analysis of the TSR′ methyltransferase SPA enzyme assay was performed. Although CPE and NSB effects were taken into consideration from the previous bead amount study, it was observed over a collection of time course data that methylation did not increase over time (Figure 3.16). In a similar approach in the refinement of the FB assay, a number of assay variables were addressed such as different enzyme and RNA concentrations, incubation of the beads at an elevated temperature, refolding the RNA substrate and further minimizing any possible CPE and NSB effects.

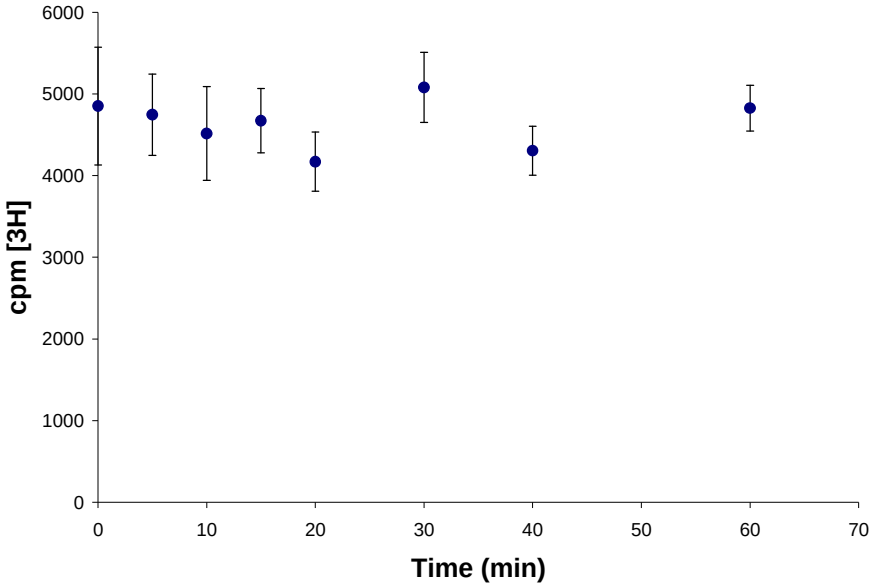

Figure 3.16: Example of time course data obtained with Polylysine YSi beads.
Methylation did not increase over time indicating that further adjustments are needed to be made.

Enzyme and rRNA Concentrations Varied

Enzyme concentrations half of and 200- and 400-times the original enzyme concentration were used. The data did not show an increase in methylation over time and remained the same with very little error between replicates (Figure 3.17). However, what was observed was that the signal produced correlated to the amount of enzyme present, indicating that enzyme methylation activity was not compromised. Furthermore, a quick comparison to the FB method lent further support that the enzyme remained active and functional and not an artefact of inactive dead enzyme. Likewise, a reduction in the rRNA substrate from 1 μM to 50 nM concentration yielded similar results (Figure 3.17).

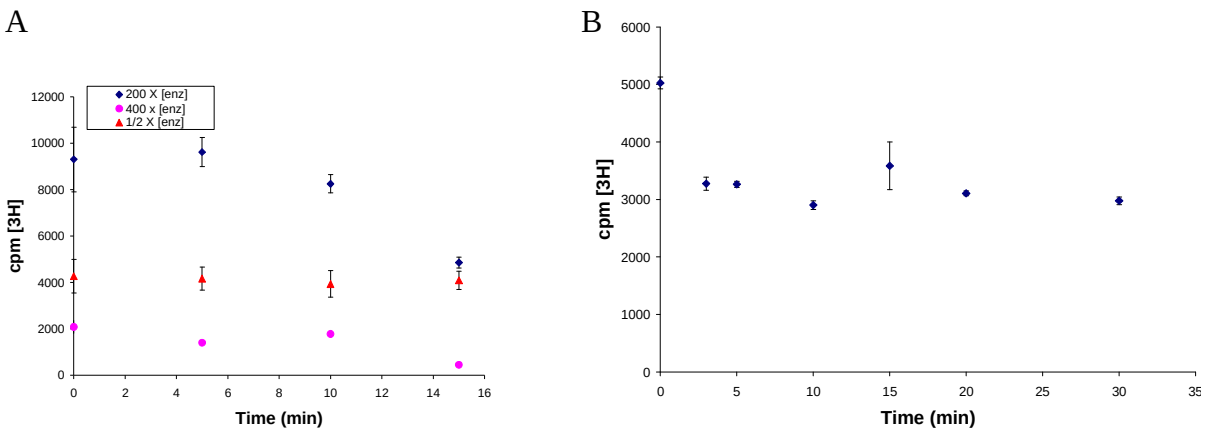

Figure 3. 17: SPA time courses with differing concentrations of enzyme and RNA substrate.
Varied concentrations of TSR′ **(A)** and RNA **(B)** were attempted. Methylation remains unchanged over time. [enz] = 40 nM.

Elevated Temperature Effects

The methylation reaction was also carried out at an elevated temperature of 37 °C. The ice cold bead-quench solution was added and also further incubated at 37 °C in which the SPA beads were allowed to settle at that temperature. Incubation of beads at a higher temperature did not increase the effectiveness of labelled product binding to the bead, but appeared to reduce it (Figure 3.18).

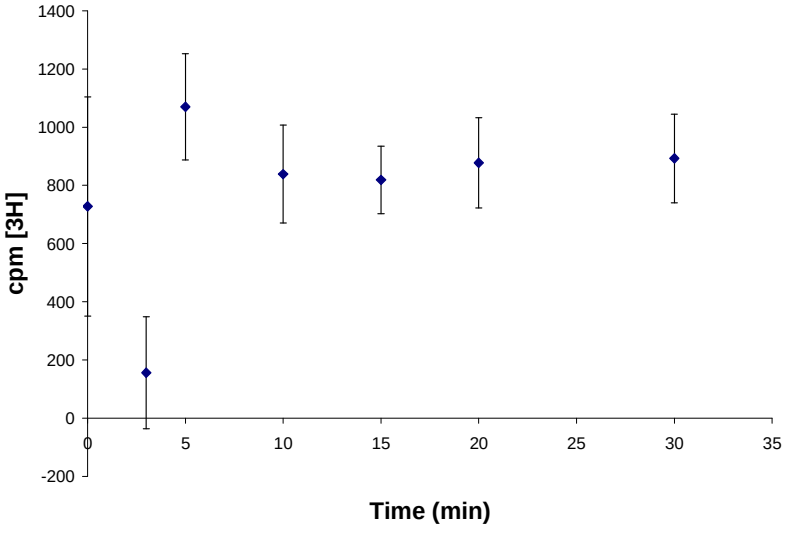

Figure 3.18: SPA time course at elevated temperatures.
At higher temperatures, methylation across time did not change and appeared to be compromised.

Refolding the rRNA Substrate

In a similar fashion to the FB assay, the 16S/23 rRNA was thawed over a time period of one hour and followed by unfolding at a temperature 65 °C for 15 min. The RNA was permitted to cool to ambient temperature for a minimum of one hour. Under the same conditions for the FB assay, the methylation activity was completely eliminated. It was assumed that the RNA was either not unfolded efficiently or refolded corrected to its native structure. However, the data acquired for the SPA method were rather ambiguous, and it was not clear that methylation activity was compromised (Figure 3.19). One would expect similar results to the FB assay and therefore, it is more than likely that NSB and/or false positive effects were giving a false signal.

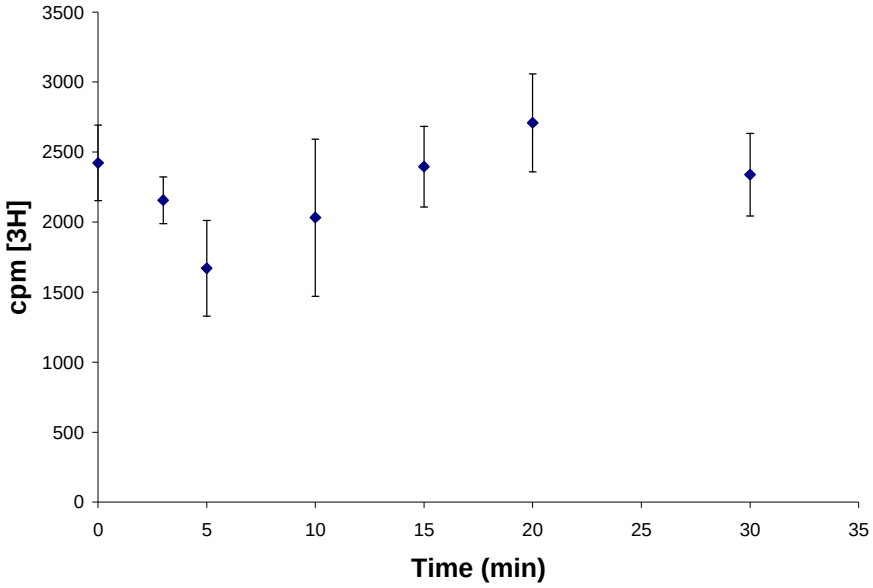

Figure 3.19: SPA time course with refolded RNA substrate.

Non-Specific Binding Effects

Results from the RNA refolding experiments suggest that either NSB or false positive signal effects are playing a role in the linear counts seen across time. Non-specific capture of the radiolabelled co-substrate on exposed areas of the SPA bead may result in the apparent

signal detected at a time point of zero minutes. NSB effects can be overcome with the addition of “blocking agents” in the bead-quench buffer solution. Different blocking agents were used in the formulation of the new quench buffer. Varied concentration of KCl, detergents such as TWEEN-20 and Triton X-100 and BSA were employed (Figure 3.20). The addition of salt and detergents did not alter results; a linear trend of counts was observed. With increasing amounts of BSA, we observe a significant decrease in counts; at extremely high concentration of BSA (1 mg/mL), the protein did not only reduce non-specific binding, but circumvented specific binding as well. Most publications show an addition of 0.1% BSA to reduce NSB, however at that concentration, we did not observe a significant difference.

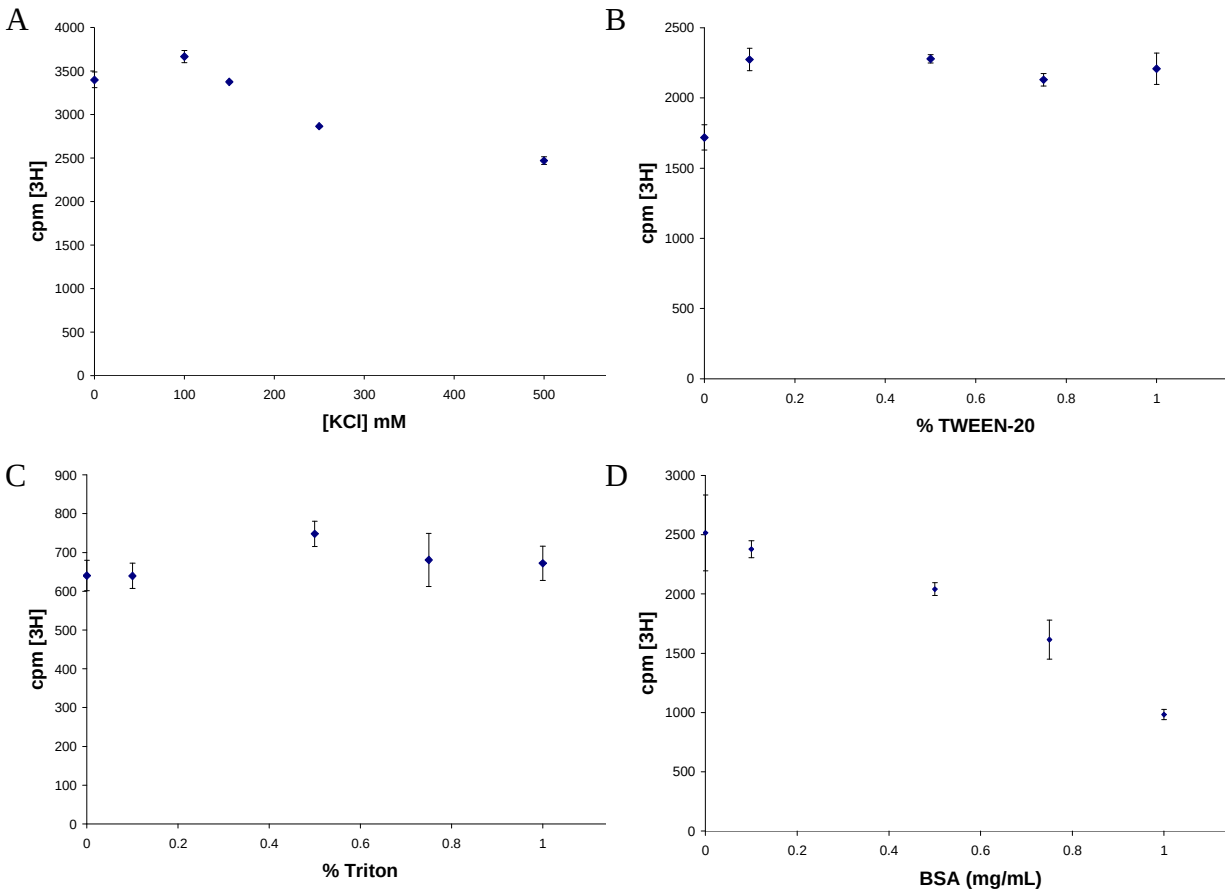

Figure 3.20: **Different blocking agents used for SPA time course.**
Various blocking agents were attempted to reduce any non-specific binding that may be occurring. **(A)** Ionic strength variation with KCl **(B)** Tween-20 **(C)** Triton X-100 and **(D)** varying BSA concentrations.

Further Optimization Required

Further investigation of the interaction and properties of the SPA media is required. NSB effects do not appear to play a significant role in measurements in all the time courses studied. Other false positive effects needs to be addressed, where free [^{3}H]AdoMet* may not have physically adhered to the bead, but is in close enough distance to elicit a signal (close proximity effects). This can be overcome by adding more quench buffer and substantially diluting the assay volume prior to counting in the liquid scintillation counter. For the time

being, the FB method provides some detectable index of enzyme activity until the SPA method is fully optimized.

3.4. Conclusions and Future Work

In the early stages of research, the traditional filter binding assay was problematic to implement. Although shown to be previously executed in earlier published works, conditions were not optimal for our enzyme and experimental set up. Errors typically incurred with a radiometric FB assays involve loss of product associated with handling of small masses and dilute solutions, unwanted nuclease activity (if working with DNA or RNA) and quenching effects (in particular with low energy of tritium β-particles) [145]. It was observed quality of our data was found to be more sensitive to technical factors of the assay such as the type of filter paper used, volume of TCA quench solution and adequate mixing of filtered material with scintillation fluid. When these refinements of the protocol were carried out, the result was that appropriate data sets were attainable for the determination of kinetic parameters. While carrying out the FB assay, alternative and more streamlined methods of assay for TSR′ were investigated. The scintillation proximity assay (SPA) method is a procedure that has become increasingly popular for its facile handling over the FB method. Efforts towards establishing an SPA protocol for TSR′ were undertaken. An optimal bead amount was established for assay use and adjustments involving enzyme and RNA concentrations, temperature and blocking agents were carried out. Further work is needed to investigate the proper signal detection such as deciphering the role that NPEs may play. In summary, the FB assay has been successfully optimized for our enzyme system while SPA experiments are

still undergoing optimization. The comparison of kinetic data to the FB assay will be performed at a later date to validate the SPA methodology.

CHAPTER 4: STRUCTURAL STUDIES OF THIOSTREPTON-RESISTANCE rRNA METHYLTRANSFERASE

Knots in proteins are a relatively rare occurrence in nature; less than one per cent of protein structures deposited in the Protein Data Bank have knots identified within their structure [116]. There are different types of knots of varying complexities found in proteins such as the simple trefoil knot (3_1 knot) and the figure-of-eight knot (4_1 knot), which have three crossings and four crossings respectively (Figure 4.1) [160,161]. More recently, the enzyme ubiquitin hydrolase has been shown to have the most complex knot structure yet [162], a knot that possesses five crossings. Knots with five crossings can adopt two different topologies: the doughnut form (5_1 knot) and the less symmetrical pretzel form (5_2 knot) (Figure 4.1) [160,161]. The majority of knots that have been observed have the simple trefoil knot (also known as the three-foil) [163].

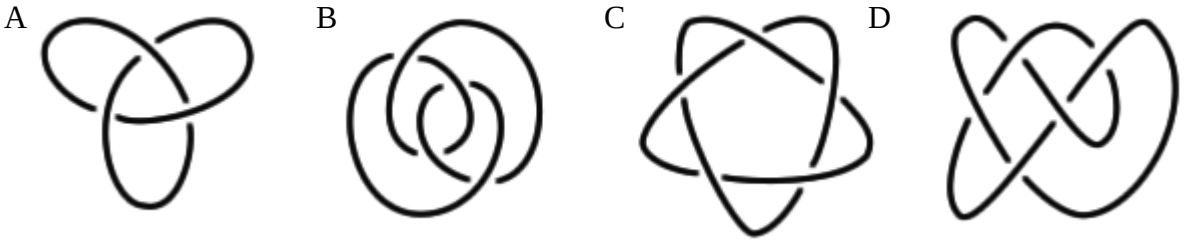

Figure 4.1: Different types of knots that can be found with protein structure.
(A) trefoil knot with three crossings (mathematically denoted as 3_1); **(B)** figure-of-eight knot with four crossings (mathematically denoted as 4_1); **(C)** a five crossing knot with symmetry, known as the doughnut knot (mathematically denoted as 5_1) **(D)** a non symmetric five crossing knot, the pretzel knot (mathematically denoted as 5_2). Adapted from [161].

Most prevalent in the α/β knot superfamily [164] are some *S*-adenosyl-L-methionine (AdoMet) –dependent RNA methyltransferases (MTase) that were found to have a carboxy-terminal domain that houses a deep trefoil knot structure responsible for catalysis [27]. These MTases are denoted as the SpoUT (***Spo***U-***T***rmD) class of MTases (Class IV), whose double

name comes from the amalgamation of two MTase families that were previously thought to be unrelated (the SpoU and TrmD families) [29]. As previously discussed in *Chapter 1*, all MTases in this class function as homodimers, and the C-terminal knot binds to AdoMet. The active site is formed by residues from both monomers, suggesting that dimerization is essential for catalytic activity [27].

The overall sequence similarity is weak among SpoUT MTases relative to their structural conservation [27]. Nonetheless, they do possess sequence motifs that are conserved between members (*Chapter 1*) (Figure 4.2) [27,115,165]. Based on amino acid sequence alignment analysis of several RNA ribose 2′-*O*-MTases [29], it was observed that TSR′ is a member of the SpoUT MTases (Figure 4.3).

Motif I: X-N/D/E-X-G/S-X_3-R-X_5-G
Motif II: h-V/L/I/M-h-G-X-E/Y-X_2-G-V/L/I/M/P-X
Motif III: V/I-X-I-P-M-X_5-S-L/M-N-X_3

Figure 4.2: Conserved sequence motifs observed in SpoUT MTases. Hydrophobic residues are represented as h and X is any amino acid residue.

SpoU family

	Motif I			Motif II		Motif III		
	35	37	41	124		143	150	152
tRNA (Gm18) MTase	|	|	|	|		|	|	|
T. thermophilus HB8 TrmH	-----H	**N**	L **S**	AIL **R**	T-----	**VLFG**	A **E**	KW **G**	VSE-----	K **IP**	MLGMVQ **S**	L **NV**	---
E. coli TrmH	-----H	**N**	V **S**	AII **R**	T-----	**VLMG**	Q **E**	KT **G**	ITQ-----	V **IP**	MIGMVQ **S**	L **NV**	---
A. aeolicus TrmH	-----H	**N**	F **S**	AIV **R**	T-----	**LVVG**	N **E**	LQ **G**	VSP-----	V **IP**	MYGMAQ **S**	L **NV**	---
23S rRNA (Gm2251) MTase													
E.coli RmlB	-----H	**N**	L **G**	AC **L**	R **S**	-----	**LVXG**	A **E**	GE **G**	XRR-----	S **IP**	XAGSVS **S**	L **NV**	---
23S rRNA (Am1068) MTase														
S. azureus TSR	-----G	**N**	I **G**	AIV **R**	T-----	**LLFG**	S **E**	KG **G**	PSD-----	S **IP**	MMGQTE **S**	L **NV**	---
Function unknown protein														
T. thermophilus HB8 RrmA	-----G	**N**	L **G**	AVL **R**	S-----	**IAVG**	P **E**	HE **G**	LRA-----	R **IP**	MQGQAD **S**	L **NV**	---
H. influenzae YibK	-----Q	**N**	T **G**	NII **R**	L-----	**LMFG**	P **E**	TR **G**	IPM-----	R **IP**	MTANSR **S**	M **NV**	---

TrmD family

tRNA (m1G37) MTase													
E. coli TrmD	-----T	**D**	Y **G**	VTG **R**	A-----	**LVCG**	R **Y**	-E **G**	IDE-----	S **IG**	DYVL-S **GG**	**EL**	---
S. typhimurium TrmD	-----T	**D**	Y **G**	VTG **H**	A-----	**LVCG**	R **Y**	-E **G**	VDE-----	S **IG**	DYVL-S **GG**	**EL**	---
H. influenzae TrmD	-----T	**E**	F **G**	VTG **R**	A-----	**LVCG**	R **Y**	-E **G**	IDE-----	S **IG**	DYVL-T **GG**	**EL**	---
A. aeolicus TrmD	-----S	**E**	Y **G**	IVK **Q**	A-----	**IICG**	R **Y**	-E **G**	VDE-----	S **LG**	DFIL-S **GG**	**EI**	---

Figure 4.3: Partial sequence alignment of representative members of the SpoUT MTase class of enzymes. The three conserved sequence motifs are shown and bold amino acid residues show conserved residues. Adapted from [115].

4.1. Homology Modelling as a Strategy to Study TSR′ Structure

Information obtained from a three-dimensional structure of a protein or enzyme, in conjunction with biochemical experiments, offers essential insight into its molecular function. Traditionally, a detailed atomic structure is obtained by means of X-ray crystallography or nuclear magnetic resonance (NMR) methods [166]. X-ray crystallography requires that the protein be of high purity at a high concentration in order to form well ordered crystals for diffraction. Unfortunately, because of these requirements, not all proteins are amenable to this method. NMR is only applicable for proteins of a soluble nature and small molecular weight, although this limit has been raised to 35 kDa [167]. While both techniques have proven to be effective, they both require a substantial amount of time and labour [168] and remain unavailable for use with certain proteins [169]. The rate at which

protein structures are elucidated by these two methods still remains a limitation as the number of protein sequences available is high relative to the number of protein structures available [170]. Fortunately, the development of homology modelling has permitted computational protein prediction methods to help alleviate some of the demand for solving structures teo gain structural insights on proteins [168,171].

4.1.1. Homology Modelling: Basic Background and Methodology

Homology modelling, also referred to as comparative modelling, is a computational method that predicts the three-dimensional structure of a protein using only its sequence, and the known structures of proteins, whose amino acid sequences display a high degree of similarity [172]. The basic assumption of this method is that evolutionarily related proteins should have similar structure and sequence [168].

There are four general steps in comparative modelling: 1) identification of homologous proteins that can be used as template based on sequence of interest (target) 2) alignment of target sequence with selected template structures 3) building a model for the target based on the information obtained from target-template alignment 4) evaluations of the model. This process is repeated until a satisfactory model is obtained (Figure 4.4) [171-173].

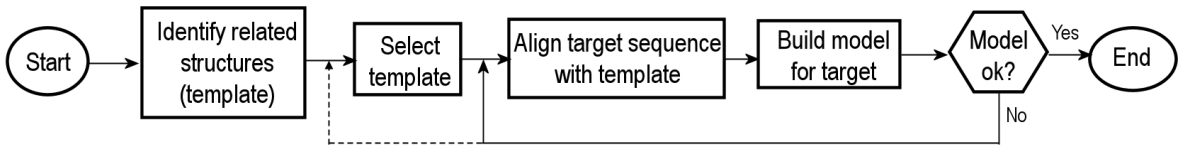

Figure 4.4: Flow chart of steps involved in homology modelling.
Adapted from [172].

4.1.1.1. Selection of the Template Protein

The initial step is to identify at least one template protein structure related to the target sequence. This can be accomplished by performing a sequence similarity search in a database using the target sequence as the search query. Many of these databases are publicly available through websites [172]. There are three general approaches in searching for homologues.

The first is the most simple and most popular method [174]. Pairwise sequence comparisons with every known protein structure in a database (i.e. The Protein Data Bank [175]) are made and sequence identity, similarity and E-values are calculated [168,172]. Programs such as BLAST [176,177] and FASTA [177] are typically used [168,172].

The second method is based on a series of multiple sequence alignments performed to expand the number of potential templates that can be used [172] and works well with homologues with less than 30% identity [171]. The homologues that are found are then used to construct a profile sequence to be used as a search query again to obtain new homologues. Subsequently, a new profile is then generated and the process is carried out in an iterative fashion until no more new homologues are found [171,172,174]. From the final profile, a sequence can then be used to search against the structure database. PSI-BLAST [178] is a program that is used often and is capable of seeking out distant evolutionarily related proteins compared to BLAST [171,172,174].

The third technique is called protein threading, where the target sequence is threaded through a library of 3D folds. This is a pairwise comparison of the target sequence to a protein structure and alignment of each sequence-structure pair is optimized and scored to see if the sequence can adopt that particular fold [172,174]. This method is applicable when

the above two methods (sequence and profile based) mentioned are unable to identify any homologues for the target sequence [172].

4.1.1.2. Target-Template Alignment

The accuracy of homology models is directly influenced by how similar the target is to the template sequence. Generally speaking, a high sequence identity (50% or higher) can generate a fairly accurate model with a 1 Å root mean square deviation (RMSD) between their backbones, whereas proteins with sequence identities of 30%-50% have a RMSD of 2-3 Å with 80% of the structure being conserved [179]. Protein sequences with sequence identities between 20-30% fall in the "twilight zone" region [180] where structural conservation of proteins can be as low as 55% [179]. Anything determined to be lower than 20% in sequence identity is likely to give inaccurate and unreliable results. Therefore, not only in homology modelling where selection of a proper template is essential, the alignment of the template to the target is just as important.

For sequences with high identity, errors with alignment between the target and the template are rare. However, error greatly increases as one moves towards the twilight zone, as the number of gaps and local regions of residue dissimilarity increase in size and number. It is imperative at this stage of modelling that an accurate alignment be obtained.

4.1.1.3. Homology Model Building

Following the template-target alignment step is the actual construction of the 3D model. There are a number of ways to construct the model and will be briefly introduced in this section. However for further details, an excellent review written by Martí-Renom *et al*. is recommended [172]. The first method is the rigid-body assembly method, in which the

homology model is constructed from the average of C_α positions of structurally conserved regions (SCR) from a collection of template structures (the framework). Loops and side chains can be obtained from the aligned structures or scanning databases for segments of variable amino acids that can "connect" the SCRs [172,181]. Alternatively, a model can be generated by using segments of amino acid residues (usually seven) and using the atomic positions of conserved atoms (usually C_α atoms) from template structures as guiding positions. Therefore, the model is made in segments, using structures or segments of template proteins that can obtained by a protein structure database of all known proteins or by conformational searching [172,181]. Lastly, a homology model can be generated by using the restraints from the starting templates. The basis of this method is the concept that any restraints or constraints of the template in terms of bond lengths, bond angles, dihedral angles etc. will be similar in the target protein. Therefore, these spatial restraints are used as a guideline for geometry and optimization minimization techniques [172,181].

4.1.1.3. Evaluation of Model

The accuracy of the 3D homology model obtained must be assessed. The errors accumulated in the model are directly related to the sequence similarity shared by the target and template. Therefore, verification of model quality should be undertaken. The first thing to be verified is whether the model has the correct fold. It will only have the right fold if the correct template was used and the alignment was acceptably correct. Once this is confirmed, other details of the structure can be looked at such as the stereochemistry, spatial distribution of small charged groups, main chain hydrogen bonding etc using free online programs such as PROCHECK [182] and VERIFY3D [183].

4.1.2. Plan of Action

Comparative analysis of TSR′ suggested it to be a SpoUT enzyme with a deep trefoil knot in the C-terminal region [27,29,115,165]. However, the actual structure of this enzyme remained elusive and had yet to be elucidated. In the absence of any reported crystal structure, prediction of the structure of the enzyme was pursued by computational means. Homology models of TSR′ have been developed by our lab both for the monomer and the dimer. At the same time, efforts along with our collaborators resulted in an X-ray crystal structure of TSR in the absence and presence of AdoMet.

4.2. Materials and Methods

4.2.1 Reagents and Materials

The following reagents and materials were obtained from the following companies:

Amersham Biosciences (formerly Pharmacia Biotech) (Uppsala Sweden): thrombin protease, Phastgels, Phastgel buffer strips

Bioshop (Burlington, ON): agarose, bacto-tryptone, chloramphenicol, imidazole, isopropyl-β-thiogalactopyranoside (IPTG), kanamycin, trichloracetic acid, Tris (hydroxymethyl) aminomethane hydrochloride (Tris-HCl), and Tris (hydroxymethyl) aminomethane hydroxide (Tris-OH), phenylmethylsulfonyl fluoride (PMSF), yeast extract

EMD Pharmaceuticals (Durham, NC): acetone, ethylenediamine tetraacetic acid (EDTA), glacial acetic acid, glycerol, methanol, sodium dodecyl sulphate (SDS), sodium chloride, sodium hydroxide

New England Biolabs: 100 bp DNA ladder, *Nde*I, *Bam*HI

Sigma Chemical Company (St. Louis, MO):

β-Mercaptoethanol, bovine serum albumin, Bromophenol Blue, Coomassie Brilliant Blue G-250, ethidium bromide, nickel (II) sulphate,

4.2.2 General Equipment

4.2.2.1. Computational Hardware and Software

Calculations of the homology model of the monomeric TSR′ was executed on a Silicon Graphics Inc. (SGI, Mountain View, CA) O_2 workstation or the University of Waterloo's multi-CPU SGI Origin 3800 system called Flexor. Hardware specifications for Violin (Honek lab SGI O_2): IRIX 3.5X operating system, MIPS R10000 processor chip, MIPS R10010 floating point chip, 195 MHz IP32 Processor, 750 MB RAM. Hardware specifications for Flexor: 64-bit IRIX 6.5.27f operating system and is a collection of forty 400 MHz MIPS R12000 CPUS and twelve 500 MHz MIPS R14000 CPUs with 52 GB of RAM.

Homology modelling of the monomer and the dimer was pursued with Swiss-Model (http://swissmodel.expasy.org), an automated protein homology server [170,184,185] using the visual client and tool DeepView – Swiss-Pdb Viewer (http://spdbv.vital-it.ch/) [184]. In addition, comparative modelling software used was Prime Suite 1.2 (Schrödinger Inc, Portland, OR) using the graphical interface Maestro (Schrödinger Inc, Portland, OR) for the TSR monomer.

4.2.2.2. Centrifuges

Microvolume centrifugation (< 1.5 mL) was carried out using the Biofuge A microcentrifuge (Heraeus Sepatech GmbH, Germany). For large volume samples (>20 mL), centrifugation was done on a Beckman Avanti® J-25I centrifuge (Mississauga, ON) or on the Beckman Coulter Avanti® JE centrifuge (Fullerton, CA, USA).

4.2.2.3. Chromatographic Equipment

The following columns utilized in the purification process were acquired from Amersham Biosciences (formerly Pharmacia, Uppsala, Sweden): HisTrap™ HP, HiTrap Benzamidine FF and MonoQ. Protein purification of SeMet incorporated TSR and TSR′ was performed on a high performance liquid chromatography apparatus (HPLC) on a Waters HPLC system (Milford, MA, USA). The HPLC was comprised of: Waters 600S controller, Waters 626 pump, Waters 2996 Photodiode Array Detector, in addition to Waters Empower 2 software, Build 2154. All aqueous buffers were filtered through a 0.2 μm membrane filter (Pall Life Sciences, East Hills, NY). Before injection all samples were filtered through a syringe filter: 0.2 μm polyethersulfone membrane (VWR International, Mississauga, ON). All buffers were degassed prior to use.

4.2.2.4. Incubators

For standing or plated bacterial cultures, growth was done in a Precision® gravity convection incubator from Precision Scientific, Inc (Chicago, IL). Liquid bacterial culture growth used a a Series 25 controlled environment incubator shaker (New Brunswick Scientific Co., Inc., Edison, NJ) or Innova™ 4330 refrigerated incubator shaker (New Brunswick Scientific) both shaking ~ 200 rpm.

4.2.2.5. Protein Concentration Devices

Concentration of purified protein was accomplished using VivaScience Vivaspins (Stonehouse, UK) with a molecular weight cut off of 10 000 Da, or Nanosep® Centrifugal devices with 10 kDa molecular weight cutoff (PALL, East Hills, NY)

4.2.2.6. Spectrophotometry

The following instruments were used to quantitate protein concentration by the Bradford Assay method [134]: Varian Cary 3 UV-Visible Spectrophotomter (Mississauga, ON) spectrophotometer with the CaryWinUV Advanced Reads Application Software 3.00 (182); Ultrospec 2100 pro UV/Visible spectrophotometer (Amersham Biosciences, Uppsala, Swedan); Molecular Devices Spectramax® Plus 384 (Union City, CA, USA), SoftmaxPro v. 501 Software.

4.2.2.7. Thermal Cyclers

All PCR was performed on a Techne® (Princeton, NJ, USA) Techgene cycler or Applied Biosystems GeneAmp® PCR System 2700 v. 2.04 machine (Foster City, CA, USA).

4.2.2.8. Mass Spectrometer

Mass spectrometric analyses were performed at the Waterloo Chemical Analysis Facility (University of Waterloo) with a Micromass Q-TOF Ultima™ Global mass spectrometer.

4.2.3 General Experimental Protocols

4.2.3.1. Gel Electrophoresis

DNA Electrophoresis

Separation of plasmid DNA and DNA fragments were accomplished using agarose gel electrophoresis. Agarose gels consisted of 0.8-1.5% (w/v) molecular biology grade agarose and 1× TAE (Tris-acetate-EDTA buffer; 40 mM Tris base, 20 mM glacial acetic acid, 1 mM EDTA). Gels were prepared by adding 0.8 g of agarose to 100 mL of 1 × TAE and dissolved with heat (microwaving for approximately two minutes). The visualization agent, ethidium bromide (4 μL, 0.5 μg/mL) was added to the molten agarose (~50°C) before pouring into plastic chamber and allowed to cool. DNA samples to be run on the gel were mixed 1:5 volume of 6× loading buffer (10 mM Tris-HCl, pH 7.5, 50 mM EDTA, 10% glycerol, 0.25% Bromophenol Blue). All samples were run in parallel with a 100 bp DNA ladder in TAE buffer at approximately 80 V. Bands were visualized under short UV-light for photographs and long UV-light for band excision.

Protein Electrophoresis

Standard sodium dodecyl sulphate polyacrylamide-gel electrophoresis (SDS-PAGE) was utilized to separate and visualize proteins based on their molecular weights. Separation of proteins employed the semi-automated Pharmacia PhastSystem^{TM} electrophoresis system with precast gels and buffer strips. Gradient gels (10-15%) were used for separation unless stated otherwise. All protein samples were denatured, linearized and were made negatively charged by boiling for 5-10 min after mixing with loading buffer (150 mM Tris-OH, 2%

SDS, 1% β-mercaptoethanol, 10% glycerol, 0.1 bromophenol blue pH 8.0) at a 1:1 ratio prior to separation.

Coomassie Staining

Development of gels involved three steps: 1) Staining with 0.1% Coomassie brilliant blue R, 30% methanol and 10% acetic acid 2) Destaining with 30% methanol, 10% acetic acid and 3) Preserving with 5% glycerol and 10% acetic acid.

4.2.3.2. DNA Manipulation and Cloning Methods

Standard bacterial and DNA cloning was performed following the standard molecular protocols outlined by Sambrook *et al*. [133].

4.2.3.3. Determination of Protein Concentration

Protein concentrations of sample were measured based on the Bradford method [134]. The Bradford assay dye reagent was prepared by dissolving 100 mg Coomassie Brilliant Blue G-250 in 50 mL 95% ethanol. Then 100 mL of 85% (w/v) phosphoric acid was added to the solution, which was then diluted to 0.5 L with ddH_2O. Bovine serum albumin (BSA) was used as standard protein and prepared in the same buffer solution as the protein of interest. These solutions were used to determine a standard curve relating protein concentration to absorbance at 595 nm.

4.2.3.4. Mass Spectrometric Analysis

Preparation of Protein Samples for Mass Spectrometry

Verification of protein molecular weight was performed by analysis of data from mass spectrometry. Buffer salts were removed from protein samples by exchanging protein

into MQW using Nanosep® centrifugal devices with 10 kDa molecular weight cutoff. If protein precipition occurs during this exchange, protein was exchanging using a 1 mL Sephadex G25 gel filtration column with MQW as the mobile phase. An additional step was occasionally required where the eluted protein sample was put through the Nanosep® centrifugal device to remove any remaining salts.

Electrospray Mass Spectrometry of Protein Samples

All samples (in MQW) were diluted with a solution of 1:1 acetonitrile:water containing 0.2% formic acid in a ratio of 1:1. Mass spectrometry was carried out with electrospray ionization (ESI) in positive ion mode. Molecular mass was obtained using the MaxEnt algorithm using the MassLynx program.

4.2.4. Homology Model Development

All four steps involved in homology model construction: template identification, alignment, model building and evaluation [171-173] were be carried out from end to end using the homology server SwissModel (http://swissmodel.expasy.org) [170,184,185], or software suite Prime 1.2 (Schrödinger Inc, Portland, OR). Steps that involved third-party programs will be indicated.

4.2.4.1. Template Selection and Alignment

Swiss-Model Homology Server:

For the Swiss-Model homology server, third party programs were accessed for the template selection and alignment process and this is detailed in the text below.

The *Streptomyces azureus* TSR protein sequence (accession number: P18466) was used initially as a search query for the non-redundant (nr) database using the BLASTp

algorithm (http://blast.ncbi.nlm.nih.gov/Blast.cgi) [176] with default parameters. After the identification of conserved domains, the same query was performed against the PDB database to obtain a set of homologues whose structure was available as a modelling template. The same search process was repeated using PSI-BLAST [178]. The crystal structures of RrmA (I1PA) [26], RlmB (1GZ0) [165] and AviRb (1X7P) [143] were selected to be used for multi-template modelling processes whereas, only RrmA (I1PA) was selected for single sequence template comparative modelling. For dimeric comparative modelling, the AviRb (1X7P) was used as the template based on results from monomeric modelling.

The multiple sequence alignment (MSA) was generated using online programs such as CLUSTALW (http://www.ebi.ac.uk/Tools/clustalw2/index.html) [186] and MultiAlin (http://bioinfo.genotoul.fr/multalin/multalin.html) [187] with default parameters. The MSA was analyzed manually and is determined that manual re-adjustment was not necessary based on conserved sequence motifs observed to be present in SpoUT MTases [29,115].

Prime Protein Structure Prediction 1.2

The TSR sequence FASTA file was imported into the workspace and submitted as a query for the homologue search. The BLAST algorithm [176,177] was used to search the non-redundant PDB database and a list of homologues was generated, in addition to the sequence alignment. Homologues with available structural coordinates were indicated and a search of the protein family based on the primary sequence of TSR was also carried out and the protein was identified as a SpoU methyltransferase. The top two homologues (1IPA and 1GZ0) were in agreement with the template selection process done for the Swiss-Model projects. However 1X7P did not appear on the list so its sequence and PDB file were

imported into the workspace as a modelling template. The three structures were then structurally aligned by Prime before continuing on to the alignment process.

A secondary structure prediction was performed for the TSR query prior to the alignment procedure. Prime performs sequence alignments based on both sequence and secondary structural information. The alignment was compared with the multiple sequence alignment (MSA) obtained previously with Multalin [187] and adjustments were made.

4.2.4.2. Homology Model Building

SwissModel – TSR Monomer and Dimer Building

TSR Monomer Construction

Initially a DeepView project was made and loaded with the raw TSR sequence (target). Prior to loading the three PDB structures of the templates (1IPA, 1GZ0 and 1X7P), all structures were edited to ensure that they were in the monomeric form using Accelyrs DS Visualizer. The template structures were initially structurally aligned based on their Cα backbone using the "Magic Fit" function which provides a preliminary structural alignment, following by a crude "threading" of the raw TSR sequence onto the aligned structures. During this process a MSA was also generated in which it was manually edited so that it was in agreement with the Multalin [187] alignment obtained in the previous template identification step. Afterwards, a second superimposition was performed using the "Fit Molecules" function using absolutely conserved residues as part of this structural alignment. Care was taken to avoid placing gaps in secondary structural elements. Side chains that formed clashes in the alignment were reduced and corrected by substitution with a different amino acid rotamer when possible. The project file was then submitted to the Swiss-Model server for model construction.

TSR Dimer Construction

A single structure, PDB: 1X7P, was selected as the template sequence for which the dimer model was to be based on. Manipulation of the PDB structure was required in DeepView before modelling submission for the dimer. The two chains, 1X7PA and 1X7PB, comprised the homodimer, however it was observed that within the B-chain (1X7PB) a number of segments were missing from the structure, making it unacceptable for homology modelling by Swiss Model. Therefore, a new dimer template had to be generated using two A Chains.

The crystal structure of 1X7P was loaded into DeepView and the protomer that had the complete structure (Chain A) was saved as its own layer and designated IX7PA. Afterwards, it was saved a second time as a different layer with the label IX7PB, for use as the second protomer. The two chains on separate layers were structurally aligned with each of the monomers of the original template dimer (1X7P) in order to maintain proper protomer orientation. This was merged as a new dimer structure with two complete intact protomers, and was called 1X7Pspecial and was used for dimeric comparative modelling.

In order to construct the dimer, two separate monomer models must be generated first. The protomer model for the dimer was generated in the same fashion as the TSR monomer discussed above. The two monomer models were merged together by aligning to the 1X7Pspecial template, making it the merged dimer target query structure.

A different DeepView project was started with the TSR dimer target and the 1X7Pspecial dimer crystal structure was now loaded. The sequence of steps that followed were similar to that of monomer homology performed previously with DeepView and SwissModel, with the exception that the sequence was twice as long since there were two

protomers. A crude “Magic Fit” alignment was followed by a reiterative “Magic fit” and subsequently an alignment done by Deepview and then visually inspected. All gaps were carefully looked over and amino acid residue clashes were minimized with a rotamer library. The project file was then submitted to the Swiss-Model server for model construction. During this time, side chains, loop building and energy minimization was performed along with building of the backbone structure.

Prime Protein Structure Prediction 1.2 – TSR Monomer Building

The build process of Prime follows the sequence alignment step. Regions of the template sequences were selected that were to be used for the model development. Regions that were chosen were the conserved amino acids and then submitted to Prime for model construction.

4.2.4.3. Refinement and Evaluation of Homology Models

SwissModel – TSR Monomer and Dimer Evaluation

Monomer Evaluation

Model quality evaluation was performed automatically by the server during model construction by programs such as ANOLEA [188]. Nonetheless, the pdb structure that was given from the Swiss-Model server was submitted to the ProFunc Server [189,190] to confirm that the overall structural fold of the model was correct. Following this, the the PDB structure of the monomeric TSR was visually inspected using DeepView. Using the B-factor colouring option, segments of the model that were found to deviate greatly from the template structures were highlighted. Most noticeably, a high B-factor loop (highlighted by red) encompassing residues Phe61-Asn73 was found to deviate from the α-helices observed in the

template crystal structures. Therefore, a new loop was built using Pro60 and Ile74 as the anchoring residues and a scan of structures loop structure library was performed and the helix chosen that most fitted the template structures. This structure was energy minimized after the loop was built. This momomeric structure was given the name: *TSRMonomer1*.

Further inspection of the amino acid sequence indicated that the loop comprising residues Glu49-Ser56 more than likely should be a β-strand based on the original templates. Using Val48 and Asp57 as anchors, a new β-strand was built that most fit the template structures and afterwards energy minimized. Afterwards, any side chain clashes formed by the introduction of the β-strand were selected and substituted with a different amino acid rotamer when possible. After this change, it was decided that the model quality was acceptable and required no readjustment to the sequence alignment to obtain another model. This monomeric structure was given the name: *TSRMonomer2*.

Third party programs were used to further assess the monomeric model. However, the structure was first energy minimized using GROMOS96 [191] available through DeepView. Structures were minimized by method of steep descent with the number of cycles that permitted convergence to 0.05 KJ/mol. The structure coordinates of the model were submitted to the Structure Analysis and Verification Server (SAVES, http://nihserver.mbi.ucla.edu/SAVES/). Verification of the structure was performed by the programs within the server: VERIFY 3D [183], PROCHECK [182] and ERRAT [192].

Dimer Evaluation

A similar approached was used for the dimer. The first round of modelling was the formation of a model of each of the protomers. During evaluation of the two separate protomers, all secondary structures were present and none needed to be modelled in. Side

chain clashes were minimized with the substitution of the rotamers available in a library on DeepView. The dimer was then modelled using the two comparative protomer models combined. No major adjustments were made to the dimer and this structure was given the name: *TSRDimer*. The model was energy minimized by GROMOS96 [191] and then further evaluated by the Structure Analysis and Verification Server (SAVES, http://nihserver.mbi.ucla.edu/SAVES/). Verification of the structure was performed by VERIFY 3D [183], PROCHECK [182] and ERRAT [192].

Prime Protein Structure Prediction 1.2 – TSR Monomer Evaluation

The structure that was generated in the previous Build Structure step of Prime can be optionally further refined by the user with the available Refine feature of the program. Loops can be refined, side chain conformation can be adjusted and the structure can be energy minimized. The loop refinement task was chosen and a list of loops present for TSR were all selected to be refined. When multiple loops were selected to be refined in series, it resulted in an error. Therefore, individual loops were selected to alleviate computational demands; however, the task still could not be completed. Therefore, the structure was imported into the DeepView Interface for analysis, after doing the overall fold analysis with ProFunc [189,190]. The α-helix and β-strand that had to be modified in the Swiss-Model structures was did not require adjustment in the Prime model. Visual inspection of the loop and gap regions of the model revealed that no additional changes needed to be made. This structure was given the name: *PrimeTSRMonomer*. The Prime structure was also energy minimized with GROMOS96 [191] available in Deepview. Third party programs were used to further assess the monomeric model. An overall quality check of the enzyme models were verified using ProSa (Protein structure analysis, https://prosa.services.came.sbg.ac.at) [193], to

highlight any potential errors in the structure. After this, an in depth evaluation was performed with the Structure Analysis and Verification Server (SAVES, http://nihserver.mbi.ucla.edu/SAVES/). Verification of the structure was performed by PROCHECK [182], VERIFY 3D [183] and ERRAT [192].

4.2.5. X-ray Crystallography of TSR′

The X-ray crystallographic work on TSR′ was performed in collaboration with Drs. Mark Dunstan and Graeme Conn (University of Manchester). General details are found within this chapter while detailed experimental procedures and data tables are included within the appendices.

4.2.5.1. Selenomethionine Incorporation into TSR

The plasmid containing the DNA encoding the *S. azureus* hexahistidine-tagged TSR (pTSR10), was transformed into an *E. coli* B834pLysS (DE3) auxotrophic cell line. During the development of an efficient means of incorporating selenomethionine (SeMet) into the protein structure, different incorporation times (0, 2, 4, 6, 8, 12, 16, 24 h) and concentrations (0.3 mM and 2 mM) were investigated.

A small starter culture of Luria-Bertaini (LB; per liter: 10 g tryptone, 5 g yeast extract, 10 g NaCl pH 7.0) supplemented with kanamycin (15 μg/mL) and chloramphenicol (17 μg/mL) was inoculated from frozen stock and grown overnight at 37 °C. The culture was then diluted 100-fold with $M9^{+}$ (M9; per liter: 12.8 g $Na_2HPO_4{\cdot}7H_2O$, 3 g KH_2PO_4, 0.5 g NaCl, 1 g NH_4Cl, pH 7.2; M9+; M9 media and 2 mL 1 M $MgSO_4$, 1 mL 100 mM $CaCl_2$, 10 mL 40% glucose, 1mL 100mM L-Met). The cells were grown with constant agitation (~200 rpm) at 37 °C until mid-log phase (A_{600} = 0.5-0.8) optical density of 0.6 was reached.

The cells were centrifuged at 4 °C for 15 min (6000 ×*g*) and the supernatant was decanted. The minimal medium M9 was used to resuspend the cells and the sample centrifuged a second time for 15 min at 6000 ×*g* to eliminate residual methionine present. The supernatant was removed once again and half the original cell culture volume was resuspended in $M9^{+}$ media. Cells were permitted to grow for an additional half hour prior to the addition of 1 mM isopropyl-β-thiogalactopyranoside (IPTG) and SeMet (final concentration of 0.3 mM and 2 mM respectively). The cells were grown for 24 h with 1 mL samples removed at various time point for analysis, then harvested by centrifugation (5 min at 13 000 ×*g*) and frozen at -80°C for SDS-PAGE analysis.

4.2.5.2. Purification of SeMet TSR

The purification of SeMet-incorporated TSR is as described for the hexahistidine-tagged TSR (*Chapter 2, Sections 2.2.6-2.2.8*). The complete replacement of all six methionine residues was confirmed by mass spectrometry. Yield: 5-10 mg/L of culture.

4.2.5.3. Sample Preparation for X-ray Crystallography

Both the TSR′ and SeMet-TSR were purified and purity checked by analysis with SDS-PAGE and silver-staining (*Chapter 2, Section 2.2.3.1*). The purified protein was dialyzed against 50 mM Tris buffer pH 7.0 containing 75 mM KCl, 10 mM β-mercaptoethanol and 10% glycerol. The protein was concentrated using Vivascience Vivaspins (MWCO 10 kDa). During the protein concentration process, protein was found to precipitate as the concentration increased. All precipitated protein was filtered and the concentration was determined by Bradford analysis using BSA as a standard.

4.2.5.4. Data Collection, Structure Determination and Refinement

Diffraction data was collected on beamline ID23-1 at the European Synchrotron Radiation Facility (ESRF) and the data processed with X-ray Detector Software (XDS) [194]. Using the CCP4 program MOLREP [195,196], the protein structure was solved with molecular replacement (MR) using the SpoUT MTase RrmA (1IPA; 27% identity) C-terminal domain to improve the starting model. For further details please refer to the appendices.

4.2.5.5. Modelling TSR-RNA Interactions

Modelling of TSR and RNA interactions was performed by our collaborators. Details of their experiments can be found in the appendices. The figures in the appendices were prepared by Drs. Graeme Couture and Mark Dunstan.

4.2.6. Site Directed Mutagenesis

Point mutations of TSR were performed. If the Quikchange method did not yield the desired mutant after multiple attempts and primer re-design, the splicing overlap extension method was employed. Please refer to the appendices for a detailed description of these two methods. The primers designed for the mutagenesis were synthesized at Invitrogen Canada (Burlington, ON). Sequencing confirmation was performed by the DNA Sequence Facility at the Department of Biology at the University of Waterloo.

4.2.6.1. QuikChange

The following primers were made for the following mutants, and were homologous to the DNA encoding TSR containing the site of target change underlined:

N248A (AAC → GCC)

5′ G ATG AGC CAG ACC GAG TCT CTC *GCC* GTT TCC GTT TCC CTC GGA ATC G 3′
5′ C TAC TCG GTC TGG CTC AGA GAG *CGG* CAA AGG CAA AGG GAG CCT TAG C 3′

N248D (AAC → GAC)

5′ G ATG AGC CAG ACC GAG TCT CTC *GAC* GTT TCC GTT TCC CTC GGA ATC G 3′
5′ C TAC TCG GTC TGG CTC AGA GAG *CTG* CAA AGG CAA AGG GAG CCT TAG C 3′

For all Quikchange mutants, the following PCR conditions (50 μL) were performed:

- 250 ng of *S. azureus* pTSR10 DNA added as template
- Forward and reverse primers (above) added to a final concentration of
- dNTPs added at a final concentration of 0.2 mM each
- 5 μL of 10× Pwo buffer
- Four different $MgSO_4$ concentrations were attempted (0.5 mM, 1 mM, 1.5 mM and 2 mM)

The thermal cycle profile is as follows:

- Initial denaturation at 95 °C for 5 min
- "Hot start" holding temperature of 85 °C during the addition of polymerase (0.5 μL Pwo)
- 16 cycles of:
    - Denaturation at 95 °C for 30 s
    - Annealing 60 °C for 6 min
    - Extension 72 °C for 45s
- Final extension time of 72 °C for 10 min
- Hold at 4 °C until reaction was retrieved for the following step.

The PCR reaction mixture was then incubated with DpnI at 37 °C for one hour to degrade the methylated wild-type DNA. The plasmid containing the mutated *tsr* ORF, pTSR10, was introduced into *E. coli* DH5α competent cells by $CaCl_2$ transfomation. This cell line is deficient in restriction enzymes to degrade non-methylated DNA. Colonies that grew were selected for kanamycin resistance and grown in a small culture (3mL) and DNA isolated for sequencing for confirmation of successful mutagenesis. Once confirmed, the isolated DNA

was transformed into *E. coli* BL21pLysS ($CaCl_2$ heat shock) for future protein production and isolation.

4.2.6.2. Splicing Overlap Extension (SOE) Method

The following sets of primers were used for the following mutants, and were homologous to the DNA encoding TSR containing the site of target change underlined:

S246A (TCT → GCG)

```
T7 forward: 5' TAA TAC GAC TCA CTA TAG GG 3' (a)
T7 reverse: 3' ATT ATG CTG AGT GAT ATC CC 5' (d)

             5′ CG CAG ACC GAG GCG CTC AAC GTT TCC GTT TCC CTC 3′ (c)
3′ GGG TAC TAC TGC GTC TGG CTC CGC GAG TTG C 3′ (b)
```

R135A (CGC → GCG)

```
T7 forward: 5' TAA TAC GAC TCA CTA TAG GG 3' (a)
T7 reverse: 3' ATT ATG CTG AGT GAT ATC CC 5' (d)

                 5′ CG ATA GTA GCG ACG TCG CTC GCG CTC GGA GCG 3′ (c)
3′ CCC TTG TAG CCG CGC TAT CAT CGC TGC AGC GAG C 3′ (b)
```

R135K (CGC → AAA)

```
T7 forward: 5' TAA TAC GAC TCA CTA TAG GG 3' (a)
T7 reverse: 3' ATT ATG CTG AGT GAT ATC CC 5' (d)

                 5′ CG ATA GTA AAA ACG TCG CTC GCG CTC GGA GCG 3′ (c)
3′ CCC TTG TAG CCG CGC TAT CAT TTT TGC AGC GAG C 3′ (d)
```

To generate the mutant, a total of three PCR steps were performed with the following set of primer combinations:

- **PCR I:** Primers (A) and (B)
- **PCR II:** Primer (C) and (D)
- **PCR III:** Primers (A) and (D)

PCR I and PCR II conditions (50 μL) were performed:

- 5 ng – 20 ng of *S. azureus* pTSR10 DNA added as template
- Primers A and B (or Primers C and D for PCR II) was added to a final concentration of 0.03 μM - 0.06
- dNTPs added at a final concentration of 0.2 mM each
- 5 μL of 10× Pwo buffer (with 20 mM $MgSO_4$ present)
- 5-10% DMSO

The thermal cycle profile is as follows:

- Initial denaturation at 95 °C for 5 min
- "Hot start" holding temperature of 85 °C during the addition of polymerase (0.5 μL Pwo)
- 10 cycles of:
    - Denaturation at 95 °C for 30 s
    - Annealing 60 °C for 60 s
    - Extension 72 °C for 45s
- 15 cycles of:
    - Denaturation at 95 °C for 30s
    - Annealing 60 °C for 60s
    - Extension 72 °C for 45 s (extension time increased by 5 s for each cycle)
- Final extension time of 72 °C for 10 min
- Hold at 4 °C until reaction was retrieved for the following step.

The PCR reaction mixture was digested with *Bam*HI and *Nde*I and the fragments were isolated and separated with a 1.5-1.8% agarose gel with ethidium bromide. The fragments were visualized under UV light. The fragment of the correct size was identified and gel purified using a Qiagen miniprep column. The amplification product was stored at -20 °C for future use.

PCR III conditions (50 μL) were performed:

- PCR product from PCRI and PCR II added as template
- Primers A and D was added to a final concentration of 0.03 μM - 0.06
- dNTPs added at a final concentration of 0.2 mM each
- 5 μL of 10× Pwo buffer (with 20 mM $MgSO_4$ present)
- 5-10% DMSO

The thermal cycle profile is as follows:

- Initial denaturation at 95 °C for 5 min
- "Hot start" holding temperature of 85 °C during the addition of polymerase (0.5 μL Pwo)
- 10 cycles of:
    - Denaturation at 95 °C for 30 s
    - Annealing 60 °C for 60 s
    - Extension 72 °C for 45s
- 15 cycles of:
    - Denaturation at 95 °C for 30s
    - Annealing 60 °C for 60s
    - Extension 72 °C for 45 s (extension time increased by 5 s for each cycle)
- Final extension time of 72 °C for 10 min
- Hold at 4 °C until reaction was retrieved for the following step.

The PCR reaction mixture was digested with restriction enzymes *Bam*HI and *Nde*I and the fragments were isolated and separated with a 1.5-1.8% agarose gel with ethidium bromide. The fragments were visualized under UV light. The fragment of the correct size was identified and gel purified using a Qiagen miniprep column. The amplification product was stored at -20 °C for future use.

The pET28b vector was also digested with *Bam*HI and *Nde*I and a ligation of the full length product with mutation (from PCR III) was inserted with the use of T4 ligase at 16 °C overnight. The subcloned fragment was then transformed into *E. coli* BL21pLysS for protein production and isolation.

4.2.6.3. Expression and Purification of Mutants

The expression and purification of the mutants were performed in the same manner as the wildtype TSR described in *Chapter 2*.

4.3. Results and Discussion

4.3.1. Homology Model Development

It is known, based on sequence analysis, that TSR is an RNA MTase that belongs to the novel SpoUT MTase class [27,29,115,165]. However, no detailed structural information about the enzyme by means of an X-ray crystal or NMR structure was available. We have used a computational approach to determine the structure of TSR to circumvent the lack of a high resolution structure. Comparative modelling approaches permitted the prediction of the 3-dimensional structure of a protein based on its primary sequence.

4.3.1.1. Template Selection and Alignment

Templates for a homology model for *S. azureus* TSR were identified based on results from BLASTp [176] and PSI-BLAST analysis [178]. It was revealed that TSR contains a SpoU MT fold and while nine structures were reported by the algorithm, the list was reduced to the top three scoring structures for monomer modelling and to one for dimer modelling (Table 4.1). All other structures were deemed unsuitable for either of the following reasons: 1) the structure was not an MTase 2) the MTase was not a SpoUT member 3) the E-value, an indicator of whether the alignment occurred by chance, was too high. For dimer modelling, only RlmB (1GZ0) and AviRb (1X7P) had dimer structures available. Since both RlmB (1GZ0) and AviRb (1X7P) had comparable E-value and crystal structure resolution, AviRb (1X7P) was chosen since AviRb has a higher sequence identity (31%) and is an MTase that confers resistance to an antibiotic.

Table 4.1: Template structures utilized during comparative modelling of TSR[δ].

Name	PDB	Source	% identity	% similarity	E-value	Resolution (Å)	Reference
RrmA[ϕ]	I1PA	*Thermus theromophilus*	24	46	6×10^{-13}	2.4	[26]
RlmB[*]	1GZ0	*Escherichia coli*	26	50	5×10^{-7}	2.5	[165]
AviRb[γ]	1X7P	*Streptomyces viridochromogenes*	31	50	7×10^{-7}	2.55	[143]

[δ]All three PDB structures were used for monomer modelling. For dimer modelling only AviRb (1X7P) was selected.
[ϕ]RrmA is a hypothetical SpoU MTase
[*]RlmA is a SpoU MTase that methylates G2251 of the 23S rRNA that is essential for maturation of the large ribosomal unit
[γ]AviRb is a SpoU MTase that methylates U2479 and provides resistance to the oligosaccharide antibiotic avilamycin

The multiple sequence alignment was performed by two different programs (CLUSTALW [186] and MULTALIN [187]), both of which gave an identical alignment (Figure 4.5).

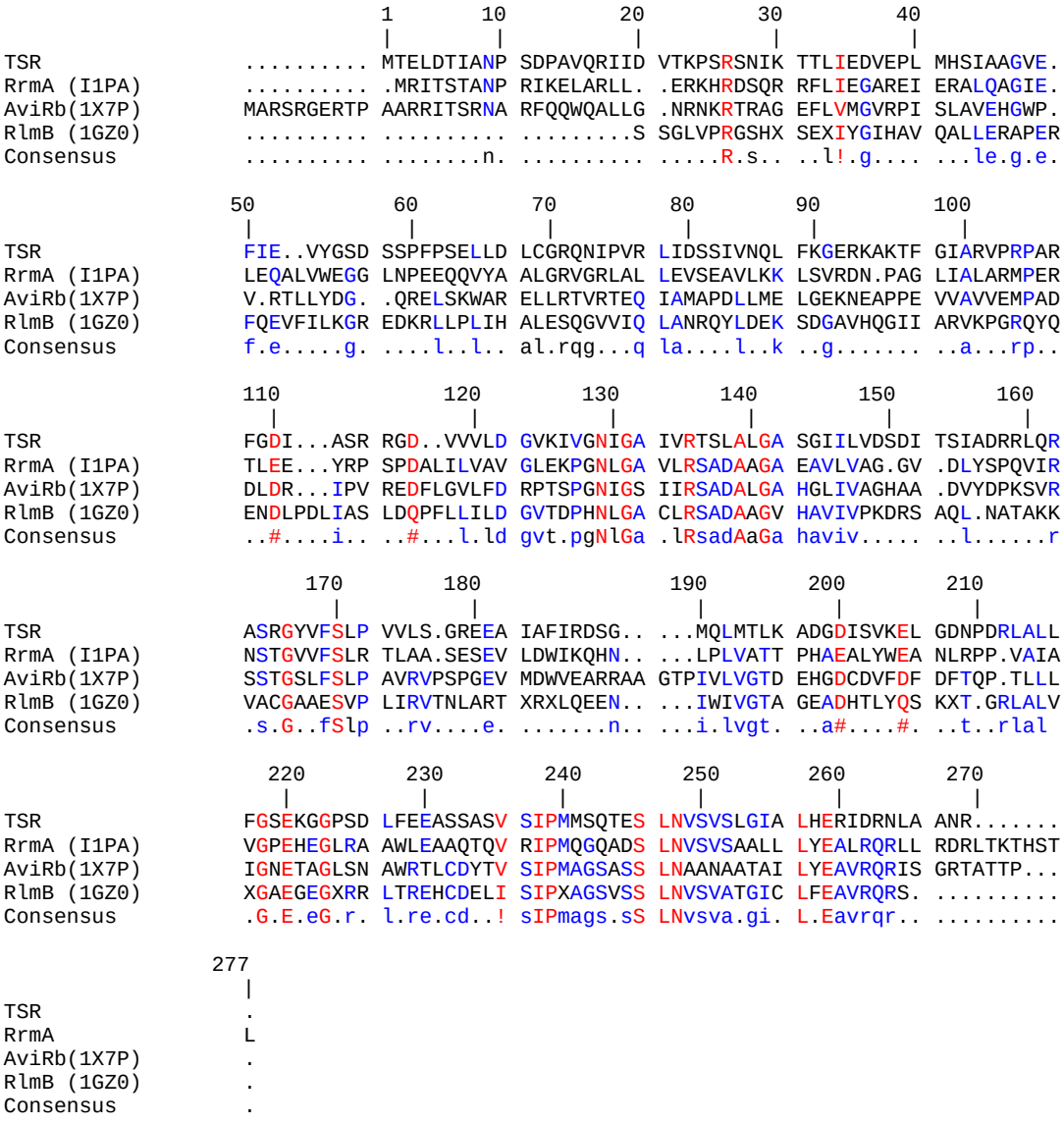

Figure 4.5: Multiple sequence alignment of TSR and SpoU MTases used as templates for the homology modelling.
Residue numbering is based on the TSR sequence. Red and blue residues indicate identical and similar residues, respectively. The symbol "!" indicate residues can the residue I or V and the symbol "#" indicate it can be N, D, Q or E.

4.3.1.2. Homology Model Construction

All SpoUT monomers (with the exception of TrmH [197]) have two distinct domains, the N-terminal recognition domain and the catalytic Rossman-like C-terminal domain that

has an unique deep trefoil knot [10]. Both domains are tethered together by a flexible liner giving the monomeric form an overall dumbbell shape. Figure 4.6 shows the structures of the three template MTases that were used in this homology study. In addition, SpoUT MTases are only functional as homodimers, in which dimerization occurs between the C-terminal domains (Figure 4.7). The active site is formed by residues of both protomers [27,28].

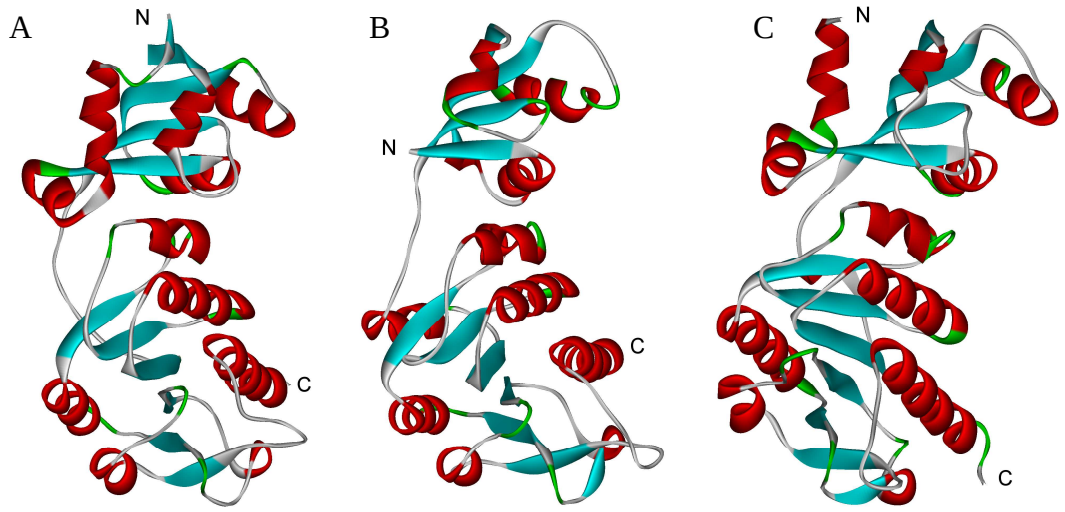

Figure 4. 6: Representative monomer structures of SpoUT MTase.
These three structures were used as a homology template in the generation of the monomeric TSR. **(A)** RrmA (I1PA) **(B)** RlmB (1GZ0) **(C)** AviRb (1X7P). Red represents α-helices, cyan represents β-strands and green represents loops.

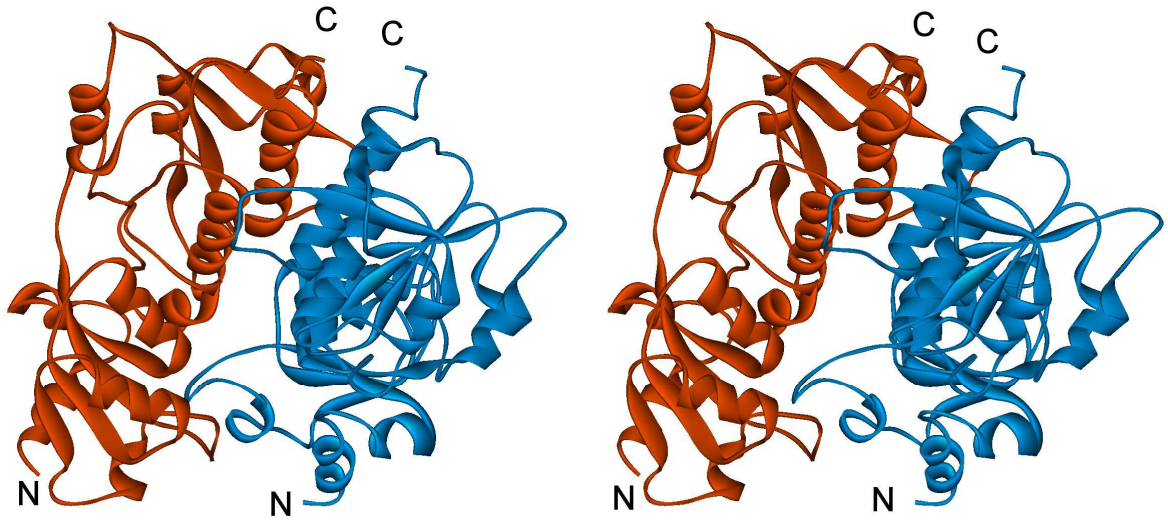

Figure 4.7: Dimer structure of AviRb (1X7P) in stereoview. The dimer is formed through interaction between the two C-terminal domains of each protomer. Orange and blue show the different monomers.

The three dimensional structure of the target monomeric TSR protein was modelled using the Swiss-Model Homology server program [170,184,185]. An alternative model was generated using Prime Protein Prediction Suite (Schrödinger Inc, Portland, OR). These monomeric structures were generated based on the multiple sequence alignment (with RrmA, RlmB and AviRb sequences) generated in the previous step. A structural alignment of all the crystal structure templates and a rough threading of the TSR sequence onto the structures were carried out prior to submission to the homology modelling server.

The TSR dimer comparative model was constructed only using the Swiss-Model Server, as the Prime Prediction Suite is unable to model oligomeric proteins. A single template approach was implemented and the crystal structure of AviRb (1X7P) was chosen. While RrmA (1IPA) (Table 4.1) gave the best score to use as the model scaffold, there was no available crystal structure available for the dimer. The avilamycin-resistance rRNA MTase (AviRB) was chosen over RlmB (1GZ0), since it possessed a higher sequence identity (31% vs. 26%).

In order to generate the dimer, the model for each of the protomers must be generated first. The protomer model was based on the Chain A of AviRb was performed. The protomer model generated was evaluated and no major manual changes were made to the structure. The two models were then combined and a rough structural alignment was performed with the AviRb dimer before modelling the dimer.

The initial three preliminary homology models of TSR (two monomers and one dimer) based on the aforementioned templates gave rise to structures that closely resembled typical Class IV (SpoUT) fold according to visual inspection. The overall structural fold was evaluated and confirmed by ProFunc [189,190], an online server

(http://www.ebi.ac.uk/thornton-srv/databases/ProFunc/) that predicts the possible function of a protein based only on its 3-dimenstional structure. ProFunc identified protein structures with matching folds belonging to SpoUT MTases, thereby indicating that the TSR homology models have the overall correct fold (Figure 4.8). The following section details the modification, refinement and evaluation of the quality of these models.

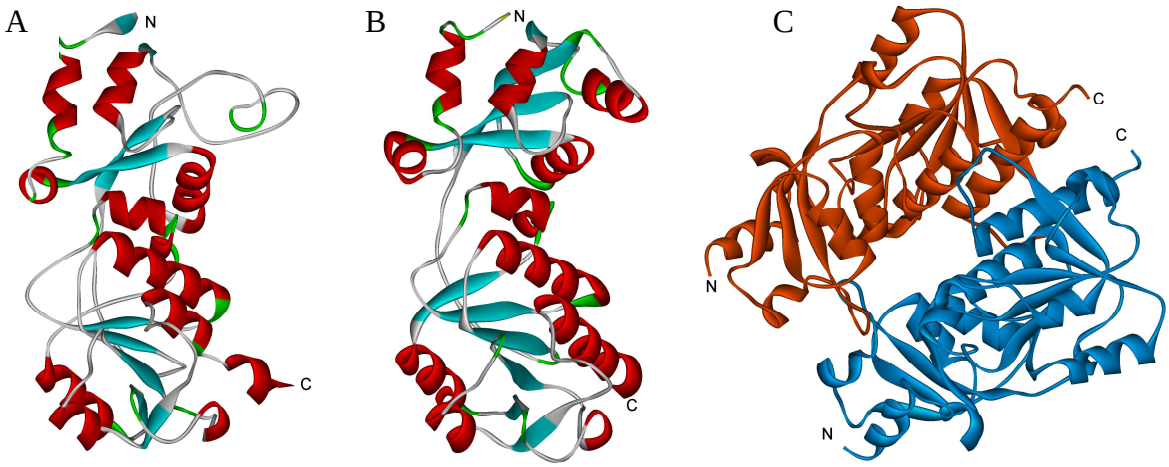

Figure 4.8: The three initial TSR homology models generated using SwissModel and Prime. **(A)** Swiss-Model monomer **(B)** Prime monomer **(C)** Swiss-Model dimer. Red represents α-helices, cyan represents β-strands and green represents loops. Orange and blue show the different protomers within the dimer.

4.3.1.3. Homology Model Refinement and Evaluation

Homology Model Refinement

Swiss-Model Monomer

Visual inspection of the TSR monomer made with the Swiss-Model homology software revealed that there were two segments of the model that were found to deviate from the templates. Section Phe61-Asn73 of TSR was modelled to be a loop, whereas the corresponding areas on the templates were found to be α-helical (Figure 4.9a). A new loop was built using the Scan Loop feature available in Deepview, where a library of loops from solved crystal structures of other proteins is proposed based on the loop identities and similarities. After the new α-helix was added (Figure 4.9b), it was energy minimized and the

structure was checked for any additional residue clashes and fixed if possible. There were no additional residue classes and this structure was called *TSRMonomer1*.

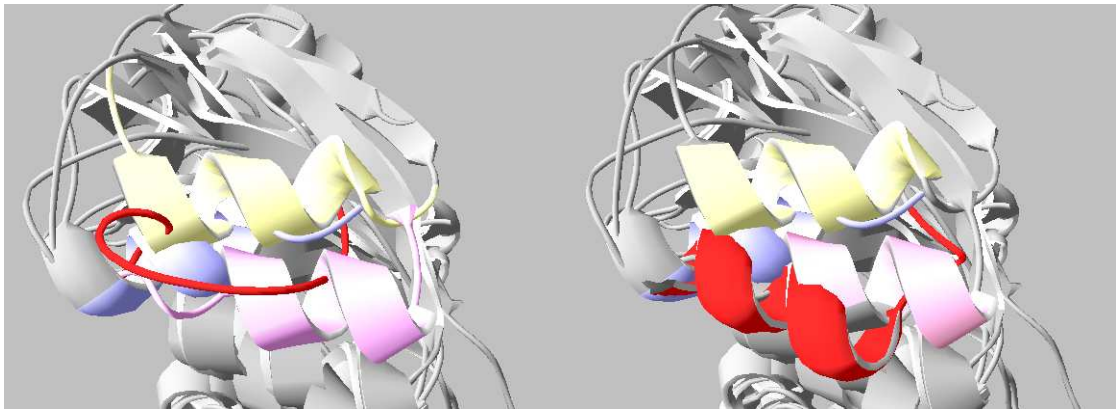

Figure 4.9: Superimposition of TSR model over crystal structure templates used for homology modelling. The residues between Phe61-Asn73 were changed from a loop (**A**, red) to an α-helix (**B**, red) to match the template secondary structure (Blue: 1IPA; Pink: 1GZ0; 1X7P: Yellow).

Further adjustments were made to the structure. Residues Glu49-Ser56 were changed into a β-strand using the scan library approach. The β-strand was energy-minimized and this model was designated as *TSRMonomer2* (Figure 4.10).

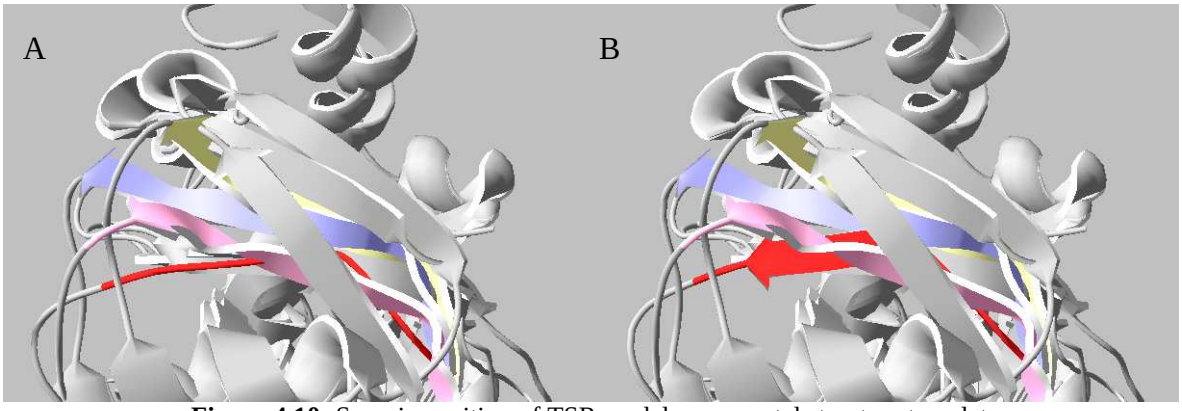

Figure 4.10: Superimposition of TSR model over crystal structure templates. The residues between Glu49-Ser56 were changed from a loop (A, red) to an β-strand (B, red) to match the template secondary structure (Blue: 1IPA; Pink: 1GZ0; 1X7P: Yellow).

Prime Monomer

The protein prediction suite, Prime 1.2, was also used to create the TSR model using the three same templates as a starting scaffold. During the building of the structure, the program not only takes into consideration the atomic positions of template(s), but also

solvent, ligands (if any), force fields (i.e. OPLS2000-AA), etc. Areas that are dissimilar to the template(s), such as loops and certain side chains can be refined by either building the loops by *ab initio* methods or re-calculating side chain conformations [169]. The Prime model that was constructed did not undergo any loop or side chain refinement due to computation limitations of our system. Therefore, the default loops generated for the structure were kept and the structure was imported to DeepView to correct side chains that were forming clashes with other atoms within the protein. No further adjustments to the structure were made afterwards. This structure was called *PrimeTSR*.

TSR Dimer

The protomers of the dimer model were evaluated by visual inspection and no changes were made before proceeding with the final stages of dimer generation. With the dimer generated, side chain clashes were relieved using the rotamer library containing more favourable side chain conformations and was evaluated as is. This model was called *TSRDimer*.

Homology Model Evaluation

Prior to further model evaluation, all models were refined with an energy minimization computation with GROMOS96 force field *in vacuo* [191] that was implemented by the DeepView software program. The local energy minima of all the models were compared and shown in Table 4.2.

Table 4. 2: Local energy minima reached by comparative models using GROMOS96.

	Local Minimum (kJ/mol)	**No. of cycles of steepest descent***
TSRMonomer2	-12295.252	1374
PrimeTSR	-13675.838	773
TSRDimer	-25695.434	567

*Number of cycles /steps until energy reached a convergence of 0.05 kJ/mol

ProSa (Protein Structure Analysis) was used in the initial assessment of the overall model quality. A database with a compilation of potentials of mean force from known structures is used as a statistical analysis tool [198]. A Z-score is a measure of the total energy of the structure with respect to energy distributions from random conformations. If the Z-score is not within the range of scores given by native proteins, then the model is considered to be of poor quality and possesses errors. A plot of residue energies is also given. Positive values indicate areas of the structure that may contain errors [193]. The Z-scores obtained by the homology models were as follows: -6.8 for *TSRMonomer2*, -6.98 for *PrimeTSR* and -6.75 for *TSRdimer*. All these values were in the range of native conformations and the residue energies are mostly negative (Figure 4.11), demonstrating that overall, the models are of good quality. Further detailed evaluation of the structures is discussed below.

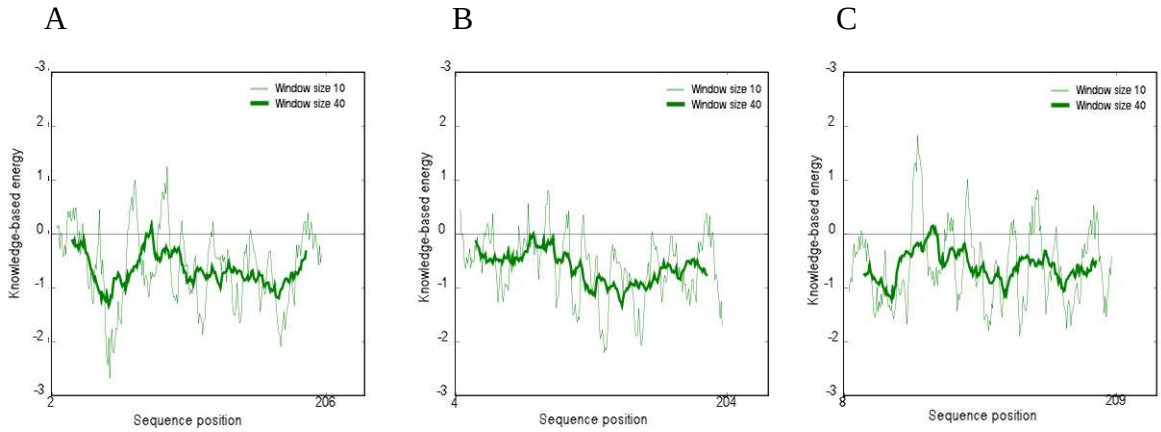

Figure 4. 11: ProSa energy plots
(A) *TSRMonomer2* **(B)** *PrimeTSR* **(C)** *TSRDimer*.

VERIFY 3D is a program that analyzes the compatibility of the protein model with its amino acid sequence. Each position within the atomic structure of the protein is characterized by the statistical preference of an amino acid residue for a certain environment (termed the 3D-1D score). The environment comprises three parameters: area of residue that is buried,

area that is covered by polar atoms (O and N) and local secondary structure. For each residue, the scores of a sliding 21-residue window (-10 to +10) are added and plotted, and for the most part should stay above 0.2 [183].

All models were assessed by VERIFY3D on the 3D-1D profile, and it was found that all of them had good compatibility between their amino acid residues and the local 3D structure (Table 4.3). Changes made to the initial TSR Swiss Model structure showed a marked improvement (57% to 64%), while the Prime model had a higher score of 72%, and the TSR dimer had the best score out of all the structures with 86%.

Table 4. 3: Comparison of 3D-1D VERIFY 3D score between the homology models of the TSR monomer.

Model	% 3D-1D score > 0.2	Low Scoring Amino Acid Regions
Initial TSR Monomer	57.36	Phe50-Lys95 (loop and α4) Arg101-Gly109 (part of β2) Ile145-Arg159 (β4-part of α6)
TSRMonomer2	64.15	Leu65-Lys95 (part of α4 and α5) Gly144-Arg158 (β2 and α4)
PrimeTSR	72.5	Val53-Gln72 (β2 - α4)
TSRDimer	86.31	Phe61-Ser82 (α4-α5)

PROCHECK is a suite of programs that is used to check the stereochemical quality of protein structures [182]. Ramachandran plots were generated and the distribution of amino acid residues based on their torsion angles (ψ and ϕ) [199] provided an insight into the torsional quality of the structure (Figure 4.12). All residues are limited to certain conformations within the protein structure, and therefore certain regions of the Ramachandran plot. There are core favoured regions, additionally favoured regions and generously allowed regions.

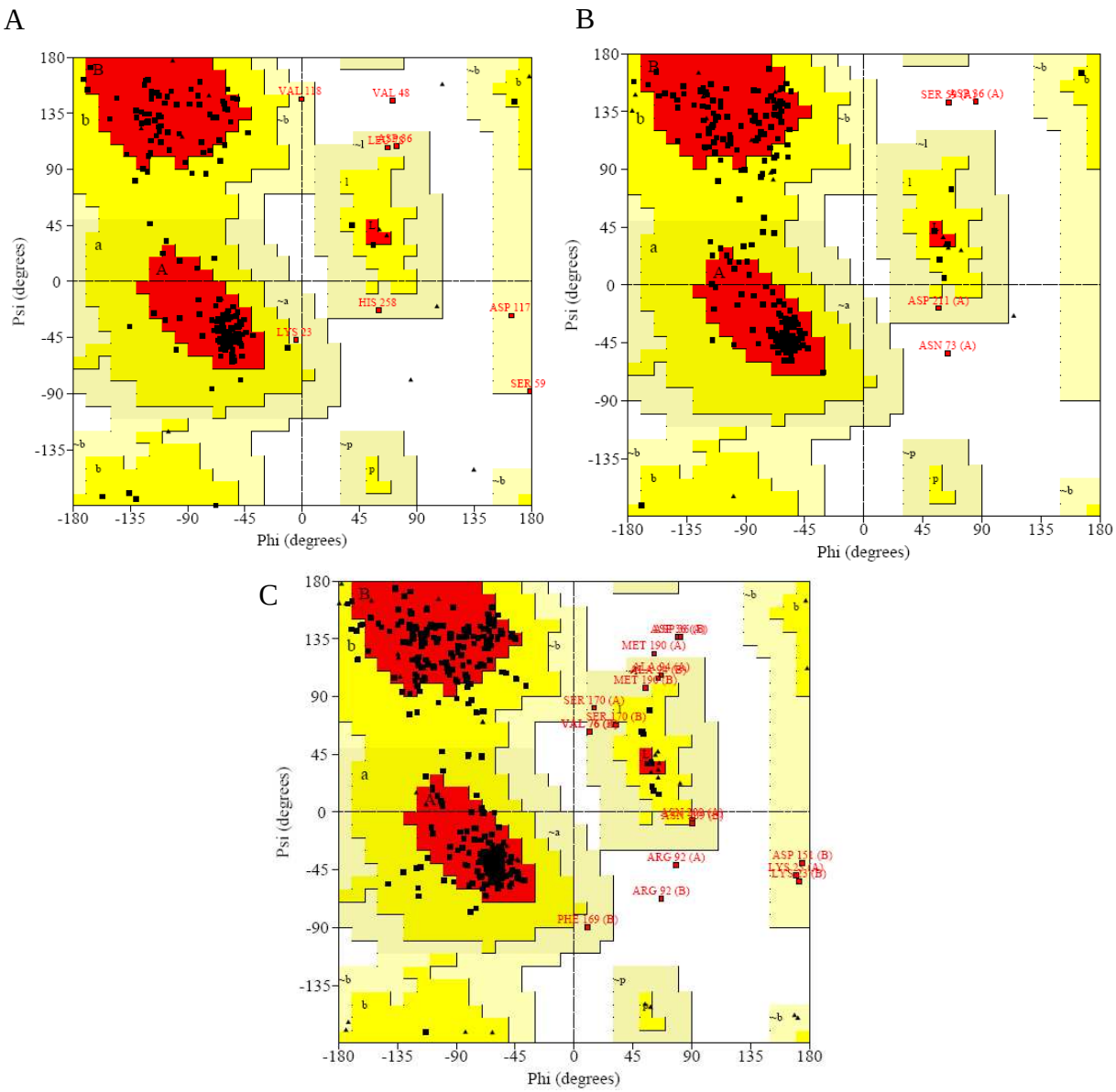

Figure 4. 12: Ramachandran plots for the comparatives models generated. (A) *TSRMonomer2* (B) *PrimeTSR* (C) *TSRDimer*. The red regions are core favoured regions; yellow are additionally favoured regions and light beige are generously allowed regions. Each residue is represented by a square and glycine and prolines are represented by triangles.

For a structure to be considered favourable, 80-90% of its residues should be found in the favoured regions, with the majority remaining in the additionally allowed region, and

very little in the generously allowed region [200]. All of the models generated were all comparable and considered to be of reasonably good quality.

Table 4.4: Distribution of Residues in Homology Models in Ramachandran plots.

	% in Region		
	TSRMonomer2	***PrimeTSR***	***TSRDimer***
Core favourable	83.8	87.2	82.3
Additionally allowed	11.9	11.1	13.4
Generously allowed	3.8	0.4	3.1
Disallowed	0.5	1.3	1.2

A further investigation into the stereochemical nature of the models was undertaken where all bond angles and lengths and planar group geometric distortions were taken into consideration. Distortions with respect to main chain bond lengths and angles were minimal, however there were more planar group distortions across all three models (Table 4.5). Please refer to the appendices for specific distortions.

Table 4.5: Comparison of the Number of Geometric Distortions in the Monomeric Homology Model as Determined by Using ProCheck.

	Geometric Distortion		
	Bond lengths*	**Bond angles***	**Planar groups**
TSRMonomer2	0	0	14
PrimeTSR	1	0	12
TSRDimer	7	0	34

*main chain

Pairwise interactions between non-bonding atoms in the protein structure (CC, CN, CO, NN, NO and OO) were statistically evaluated by the program ERRAT [192] (Figure 4.13). In general, carbon, nitrogen and oxygen atoms are distributed throughout a protein structure non-randomly due to different energetic and geometric constraints. Errors in models often will give a more randomized distribution. ERRAT analyzes the non-covalent interactions and compares them with statistical distributions from a database of known proteins. Results from the ERRAT analysis show that the monomeric models had a high overall quality factor. Both models (*TSRMonder2* and *PrimeTSR*) differed in low quality

areas and namely localized in the N-terminal region, which is to be expected since the NTD is more variable across SpoUT MTases. However, the dimer structure had almost a 10% lower quality factor with low quality areas not only in the NTD, but in the CTD as well. We believe that a multiple template for that domain may improve the quality of non-bonded interactions.

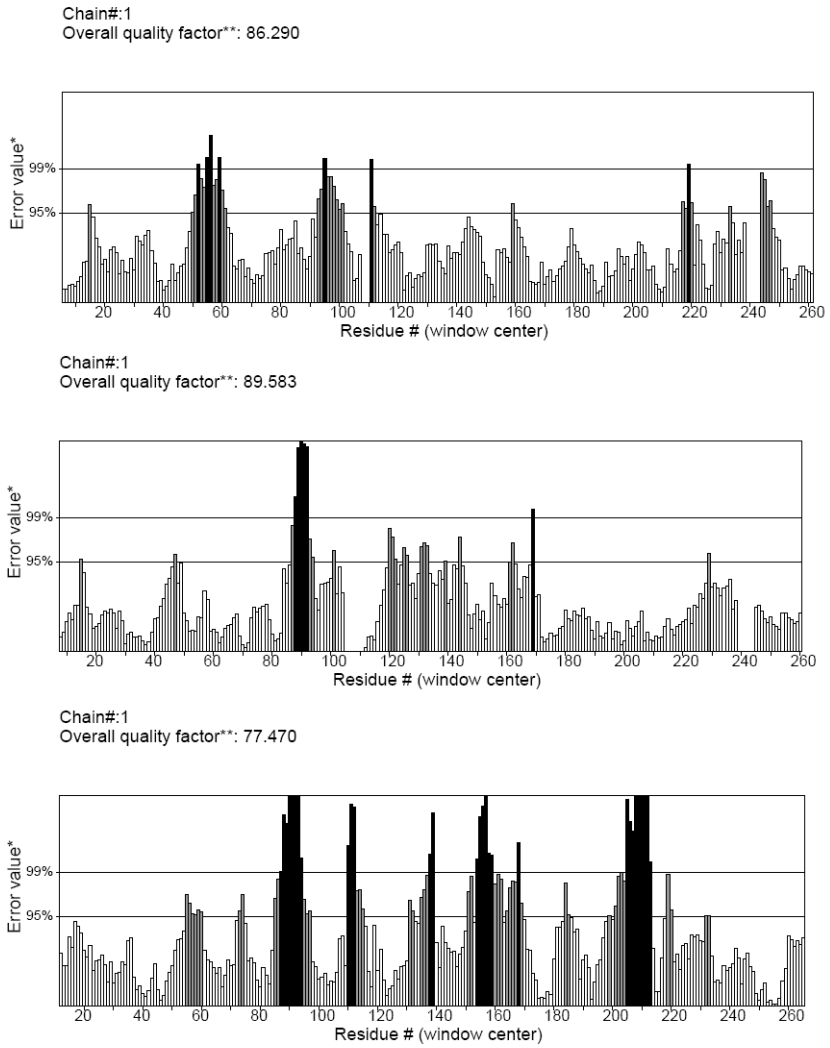

Figure 4.13: ERRAT results for the three homology models of TSR.
(A) *TSRMonomer2* **(B)** *PrimeTSRmonomer* **(C)** *TSRdimer*. *Lines drawn at 95% and 99% error value show regions in which structure of the model show poor quality. **Overall quality factor is based on the percentage of the protein which has error values below the 95% rejection limit.

4.3.1.4. A Closer Examination of the Homology Models

The quality of a homology model depends on the degree of sequence identity. Models that have a sequence identity to their starting template above 40% have 90% of their C_α atoms within 1 Å of their correct positions [171]. For models that have a sequence identity between 30%-40%, only 80% of the C_α atoms are placed within 3.5 Å of their real positions [171]. Anything lower than 30% sequence identity, only 50% the backbone atoms are within an RMSD of 3.5 Å [172].

For TSR, we could not obtain a highly accurate comparative model due to the low sequence identity (24%-31%, Table 4.1). Nonetheless, a lower resolution TSR structure for both the monomer and the dimer was computationally generated and appeared to be quite reasonable. The monomer was constructed using two different programs, and the two models were found to be in good agreement with 1.5 Å RMSD between the C_α backbone.

Based on the three models, TSR has the typical topology of SpoUT MTases, possessing two distinct domains, each having a central β-sheet surrounded by α-helices. The N-terminal domain (residues 1-106) is connected to the catalytic C-terminal domain containing the deep trefoil knot that has been implicated in the binding of AdoMet. The knot is formed by a stretch of approximately 45 residues beginning with Glu220 to Ile238 threading through an opening formed by residues Leu192 to Ser219 (Figure 4.14).

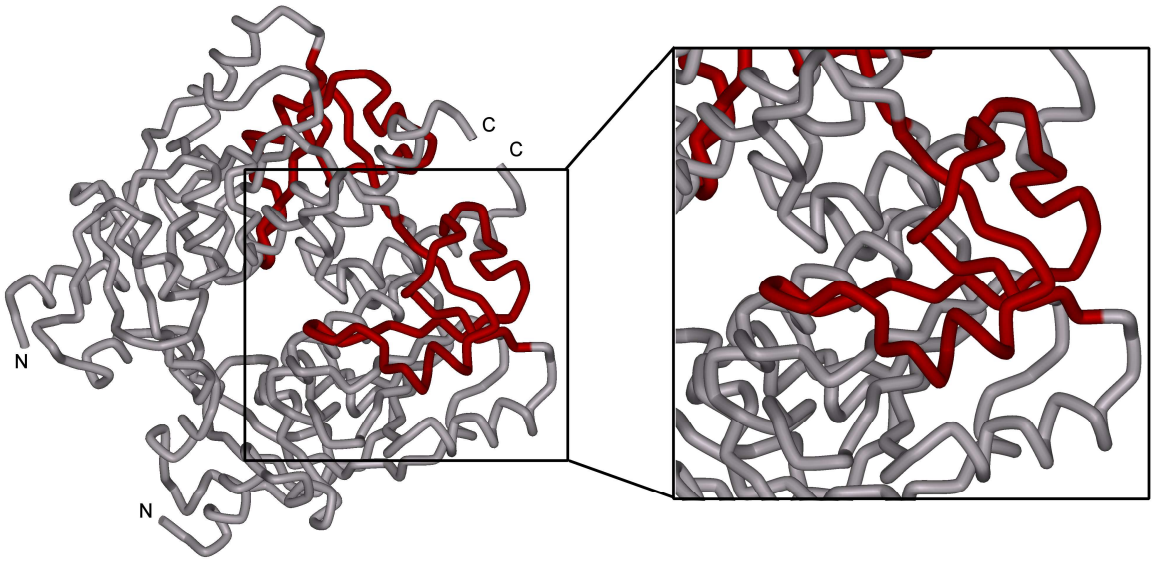

Figure 4.14: The deep trefoil knot in the TSR dimer homology model.
The trefoil knots are highlight in red.

The CTD of the homology TSR forms the dimer interface with the inner face of helices α6 and α11 of both protomers, and contains or is in close proximity to highly conserved SpoUT residues. These highly conserved amino acid residues from the three motifs (Figure 4.2 and Figure 4.15) were highlighted (Figure 4.16) and an hypothetical role was assigned to each residue as to its involvement with respect to AdoMet binding, catalysis or rRNA recognition.

TSR Motif I: ^{128}G-**N**-I-G-A-I-V-**R**-T-S-L-A-L-**G**^{141}
TSR Motif II: ^{215}L-L-F-**G**-S-**E**-K-G-**G**-P-S^{225}
TSR Motif III: ^{236}V-S-**I**-**P**-**M**-M-S-Q-T-E-**S**-L-**N**-V-S-V^{251}

Figure 4.15: The three SpoUT sequence motifs in TSR.
Absolutely conserved residues are indicated in bold.

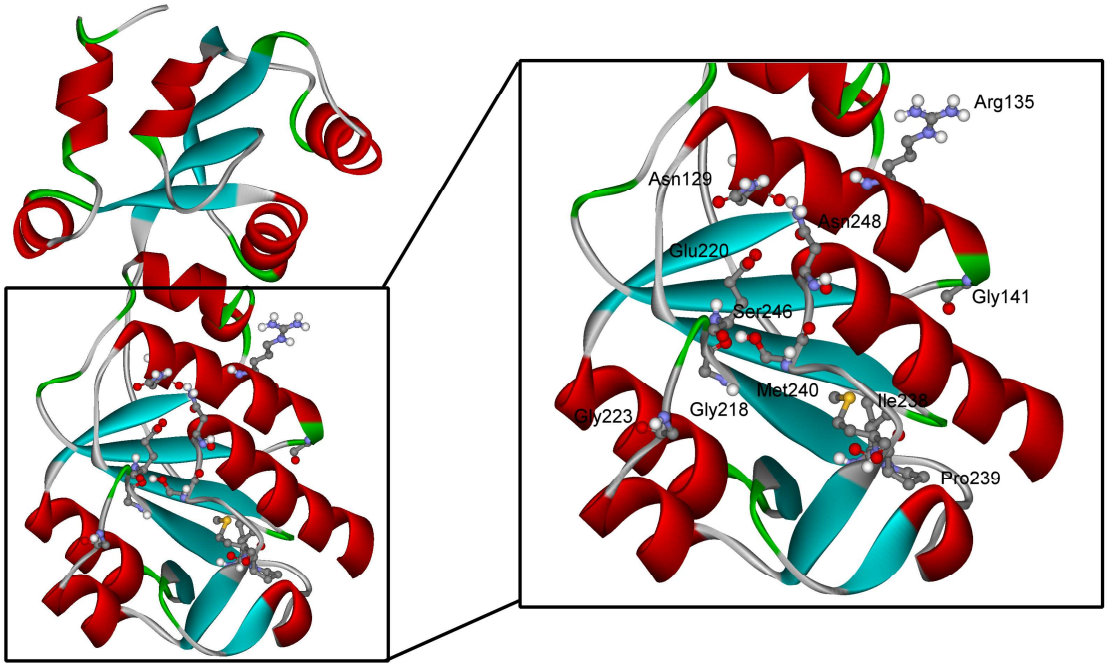

Figure 4.16: Conserved residues highlighted in TSR monomer model (*PrimeTSR*).

These role assignments were based on other biochemical studies performed on other SpoUT MTases. Various roles for residues in Motif I have been suggested. For example, it has been suggested that Arg135 could either fix the attacking ribose sugar of A1067 at the 2′OH group [143] or the Arg135 from the other protomer acts as a general base and depronates the 2′OH of the ribose of A1067, resulting in a subsequent nucleophilic attack of the methyl group of AdoMet [115]. It should be noted that although Arg residues are typically protonated at physiological pHs, and thus are unlikely to act as a general base, they have been suggested to take on the role of a catalytic base in certain cases [201,202]. Asn129 in the motif, could be involved in cofactor binding [26,143,197], while no role as yet been assignmed to Gly141.

Residues of Motif II are situated along the protein knot. Glu220 could potentially serve as a catalytic base [143]; alternatively it could maintain the structural integrity of the knot and the AdoMet binding site [143,197]. The residues in Motif 3 have also been

implicated in playing a role in the recognition of AdoMet. The hydrophobic residues in this motif (Ile238, Pro239 and Met240) form a hydrophobic pocket in which the adenine moiety can bind [26,165,197]. Ser246 and Asn248 could also play a role in the stabilization the adenine ring or the positioning of methionine moiety to prime the substrate for methyl group transfer [165].

A limited amount of information about the RNA substrate binding to the enzyme is gained from these homology models. The electrostatic potential surface of the dimer model was examined using the Accelyrs DS Visualizer, and it was shown that the TSR dimer possesses a large positive area in the cleft formed by both NTDs (Figure 4.17). This suggests that the negatively charged RNA can position itself along this surface such that the methylation can occur. No other areas on the dimer exhibited a large positive charge indicating that area is most likely the sole binding area of the RNA substrate. Therefore, one would only expect to see one RNA substrate per dimeric TSR [143].

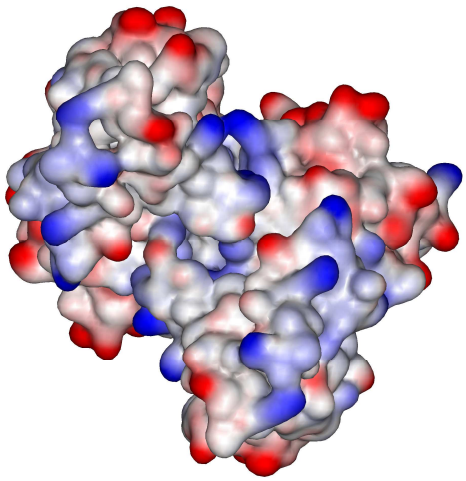

Figure 4.17: Electrostatic surface potential of *TSRDimer*.
Blue shows areas of positive charge and red shows areas of negative charge. A large area of positive charge is found between the two N-terminal domains of TSR and is the potential binding site of the RNA substrate. Electrostatic potential surface was generated using Accelyrs DS Visualizer v2.01.7347.

4.3.2. X-ray Crystallography of TSR′

4.3.2.1. Overall Structure of *S. azureus* TSR

The X-ray crystal structure of TSR was obtained, after our work on the homology model was completed, in a collaborative investigation with Drs. Graeme Couture and Mark Dunstan of the University of Manchester. At the time of writing this thesis, a manuscript detailing the work described in this section was submitted for review.

The TSR structure elucidated was found to contain features conserved by Class IV MTases such as the Rossman-like fold in the C-terminal catalytic domain and the proteinaceous knot. While sequence analyses [29] proposed that TSR is a SPoUT MTase member, the solved crystal structure has now definitively confirmed its membership. The TSR crystal structure with AdoMet bound was determined at 2.45 Å resolution, and was achieved by incorporating selenomethionine and the structure solved by molecular replacement.

TSR is a homodimer with 2 × 269 amino acid residues and a molecular mass of 2 × 28901 Da, and was expressed in *E. coli* with a hexahistine tag that was cleaved with thrombin after the first stage of purification. The purified TSR was confirmed to be a dimer with gel filtration chromatography (*Chapter 2*). In the crystal structure, it is revealed that extensive interaction between two α-helices (α6 and α11) on the inner face of the protein and the loop formed by residues 238 to 245 of the protein knot form the dimer. Dimerization buries approximately 30% of the total surface (~3500 Å) and involves many hydrophobic and ionic interactions between the two protomers. Leu247 and Val251 engages in reciprocal hydrophobic interactions with Thr136′ and Leu140′ of the other subunit, while His258 interacts with G259′ reciprocally forms salt bridges. Both His258 and His258′ are close to

the dimeric interface and flank Glu259 and Glu259′. This ionic interaction is further enhanced by salt bridges formed by Lys204 and Lys204′.

Similar to the proposed homology model for the monomer, TSR has two distinct structural domains: the N-terminal domain (NTD) formed by amino acids 1 to 102 and the C-terminal domain (CTD) is formed by residues 108 to 269. The two domains both consist of a central β-sheet that is surrounded by α-helices, and are connected by a flexible linker (residues 101-118) that starts at the fourth β-strand (β4) and ends with a short α-helix (α5), giving the enzyme monomer and elongated dumbbell shape.

The C-terminal Catalytic Domain

The carboxy domain is the catalytic SpoUT domain with the deep trefoil knot. The seven stranded β-sheet is flanked between three α-helices on the outer surface and four α-helices in the inner dimer surface, forming the open α/β/α sandwich common in Class IV MTases (Figure 4.18).

A

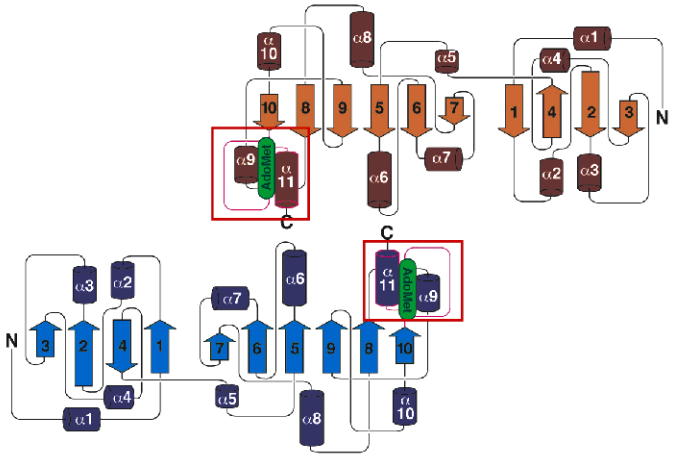

B

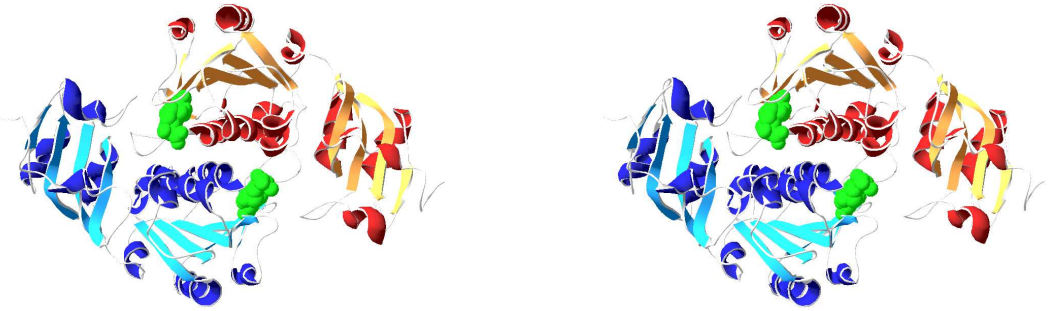

Figure 4.18: Topology and X-ray crystal structure of TSR-AdoMet complex.
(A) Protein secondary structure topology diagram. Cylinders are α-helices and arrows are β-strands. One monomer is coloured blue and the other is coloured red. The red box highlights residues that constitute the protein knot. Figure courtesy or Drs. Mark Dunstan and Graeme Conn **(B)** Stereoview of TSR dimer with bound AdoMet (green).

The X-ray crystal structure of TSR was acquired with two AdoMet molecules bound to the dimer at the carboxy domain at the deep trefoil knot that is characteristic of the Class IV MTases. The knot is formed by threading residues 237-269 through amino acids 195-203, which contains Motif 3 of SpoUT MTases [28,29] (Figure 4.19).

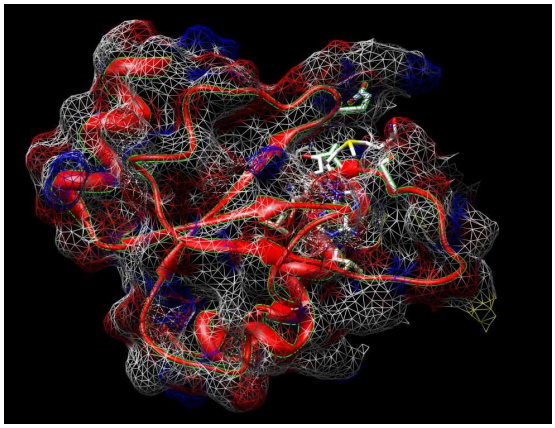

Figure 4. 19: TSR has a deep trefoil knot.
The enzyme is shown in mesh with the knot highlighted, while the Adomet bound is shown as stick.

This motif (IPM-X_4-SLN) on the knot plays a pivotal role in the binding of AdoMet, forming a deep hydrophobic pocket in which the adenosine moiety of AdoMet can be positioned. AdoMet forms contacts with residues coming from both protomers, with the majority of interactions coming from one of the monomers suggesting that only one of the two monomers is catalytic. The N1 and N6 of the adenosine moiety ring hydrogen bonds with the main chain amino and carbonyl, respectively, of Ile238 (Figure 4.19) while Leu195 and Gly218 participates in hydrogen bonding interactions with the 2′-OH and 3′-OH of the ribose sugar, respectively.

A B

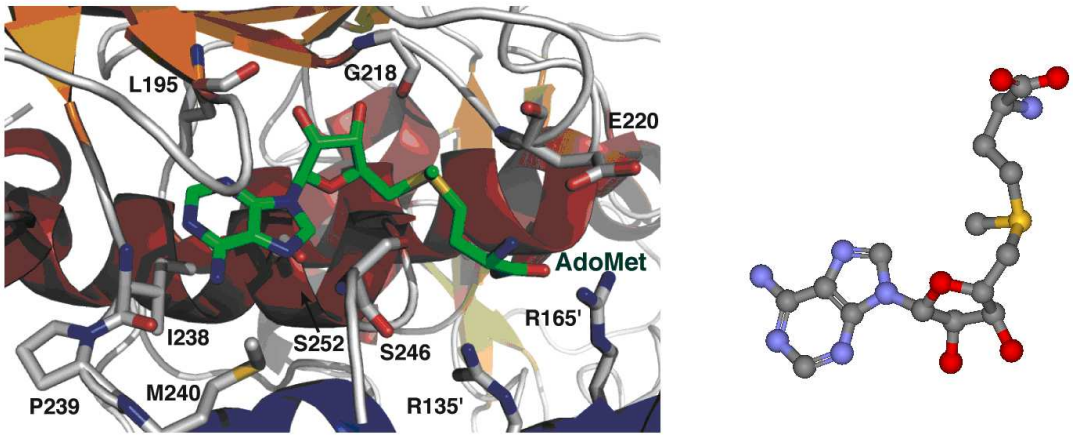

Figure 4.20: The AdoMet binding pocket and extended conformation of AdoMet
(A) Binding pocket with key TSR amino acid residues are indicated. Figure courtesy of Drs. Mark Dunstan and Graeme Conn. **(B)** AdoMet is bound in an extended conformation. See text for more description.

The TSR crystal structure also reveals an interesting aspect of the TSR-AdoMet complex. While most SpoUT MTases bind AdoMet in a tightly folded conformation [10,35], the AdoMet bound to TSR was in an extended conformation that is typically observed in Class I and Class II MTases [10] with dihedral angles of 151° and 152° for O4′-C4′-C5′-Sδ and C4′-C5′-Sδ-Cγ, respectively. This conformation is stabilized with electrostatic interactions between the methionine group of AdoMet that is positioned against Glu220 and Ser246 with Val249 situated below, and the highly conserved Arg135′ and non-conserved Arg165′ of the adjacent monomer (Figure 4.20). Residues of the equivalent position to Arg165′ in other SpoUT MTases are observed to be non-basic, suggesting that the presence of this basic residue may play a role in the unique AdoMet binding conformation of TSR (Figure 4.20).

The N-terminal Recognition Domain

Class IV MTases can be subdivided into the SpoU and TrmD families. The SpoU family can be further subdivided based on the presence of domains in addition to the catalytic domain: 1) single domain (i.e. not additional domain, just the catalytic domain is present), or additional N-terminal domains that resemble ribosomal proteins 2) L30 and 3) L5 [143] (Figure 4.21).

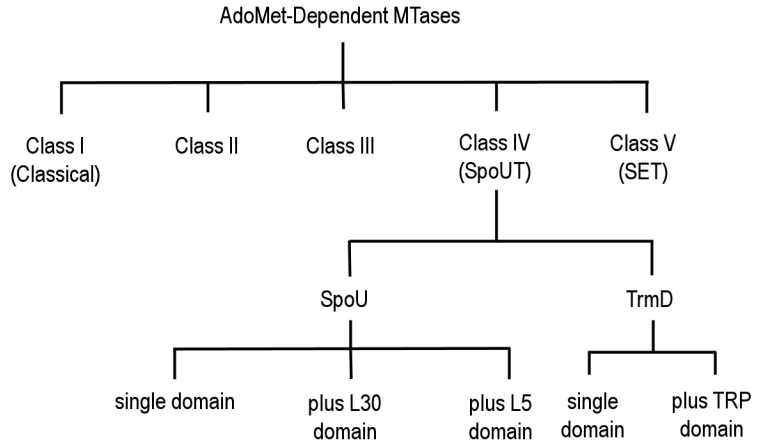

Figure 4.21: Classification of AdoMet-dependent MTases.
TSR belongs to the SpoU family that contains a L30-like domain. Figure adapted from [143].

The NTD of TSR consists of a central four stranded β-sheet core that is flanked by two pairs α-helices on each side. The pairs of α-helices are positioned perpendicular relative to each other and in the β-sheet there is a topological switch with the fourth β-strand to give the arrangement of β3↑β2↑β4↓β1↑ (Figure 4.18). While the sequence of NTDs of SpoUT MTases are not conserved, a structure-based search using the DALI algorithm [203] revealed that the TSR NTD resembles yeast ribosomal proteins L30e and L7e, the eukaryotic release factor (eRF) 1, and two related SpoU MTases, AviRb [143] and RlmB [165] that also contain the "L30-like" NTDs.

Its structural relationship with ribosomal proteins suggests that the NTD of TSR guides the enzyme to the appropriate region of the RNA. This domain is tethered to the CTD with a flexible linker (residues 101-118). Based on the limited crystal packing contacts made by the NTD (Figure 4.22) and the poorly defined electron density map of the NTD for one of the monomers, there is reason to believe that there may be domain movement or rotation that play a significant role in rRNA target recognition and binding. The inherent flexibility of this domain is corroborated by the higher crystallographic B-factors observed for the NTDs

relative to the CTDs. It is very likely that one rRNA region binds in between the cleft formed by the two NTDs and domain re-orientation occurs to accommodate the target.

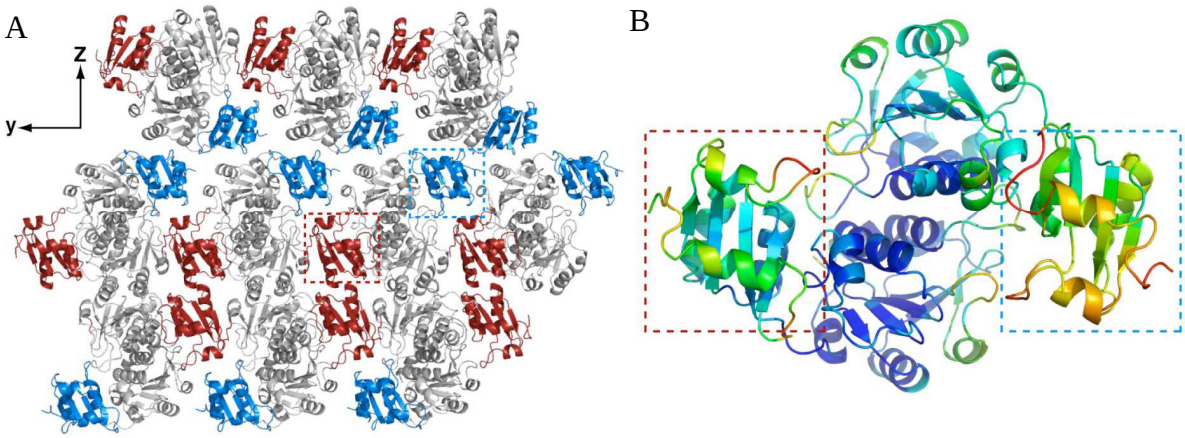

Figure 4. 22: TSR crystal packing and N-terminal domain flexibility.
(A) Crystal packing of TSR dimers with CTD shown in grey and the NTDs in red and blue. (B) TSR dimer coloured by main chain B-factors. The TSR NTDs are boxed with colours corresponding to those in (A). Figure courtesy of Drs. Mark Dunstan and Graeme Conn.

4.3.2.2. Structural Insights: RNA-TSR Interactions

The crystal structure was solved in the absence of the RNA substrate. Therefore, an *in silico* approach to studying the RNA-protein interactions was pursued. Prior to modelling in the rRNA, the electrostatic potential of the dimer surface was examined. Similar to what was observed in the homology model (Figure 4.17), a large strip of positive residues were found between the cleft formed by the NTDs of the two monomers (Figure 4.23). On the reverse side, there is a large preponderance of negative charges across the centre, therefore precluding any binding of RNA. Thus, a rigid body docking was performed with the 58 nucleotide (nt) L11 binding domain (L11BD) (Figure 4.24) that contains the A1067 methylation target, and was oriented to face the positive electrostatic potential surface of the dimer.

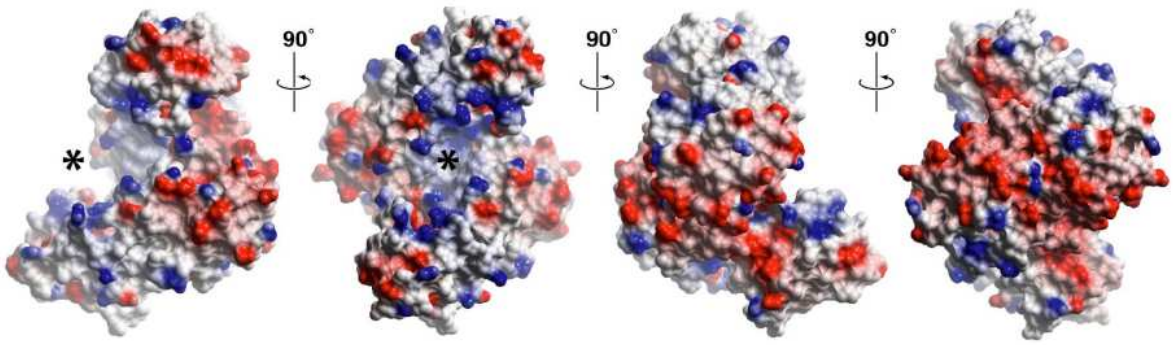

Figure 4.23: The electrostatic surface potential of the TSR dimer.
The TSR dimer structure is shown in four orthogonal views rotated around the z-axis with the electrostatic surface potential indicated in red (negative) and blue (positive). The asterisk (*) represents where RNA can be bound to the large positive area of the dimer. Figure courtesy of Drs. Mark Dunstan and Graeme Conn.

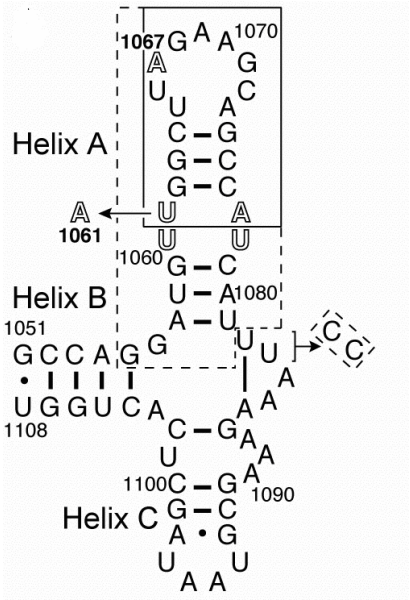

Figure 4. 24: The secondary structure of the 58 nucleotide L11 rRNA binding domain (L11BD).
The TSR target methylation site (A1067) is located on the apex of the hairpin in Helix A. The mutation from U1061 to A is shown to significantly decrease methylation activity.

The backbone of the modelled RNA L11BD Helix A lies predominantly along the surface TSR. The A1067 methylation target loop is situated deep within the cleft formed by the dimeric CTDs (Figure 4.25). Only a single strand of RNA can be accommodated in this cleft. Its binding orientation delineates one monomer to be catalytic, that is the bound AdoMet co-factor bound to it will donate the methyl group, and the other to be non-catalytic. All residues in the later group is denoted with a prime symbol throughout this body of text.

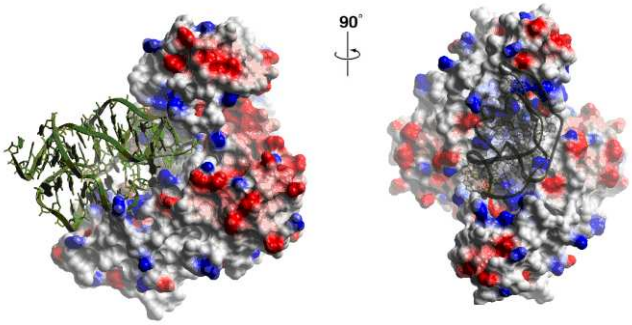

Figure 4. 25: Modelled RNA-TSR Interactions.
Orthogonal views of the 58 nucleotide L11 binding domain RNA docked to the TSR dimer. The enzyme is shown with an electrostatic surface potential where red is negative and blue is positive. Figure courtesy of Drs. Mark Dunstan and Graeme Conn.

The NTDs of each TSR monomer are oriented such that they embrace the RNA strand and recognizes the two distinct structural features of the RNA: the target loop and the internal bulge in Helix A (Figure 4.24). The RNA target loop is located next to the non-catalytic NTD of one TSR monomer, opposite to the modelled active site, while the catalytic TSR's NTD contacts the internal bulge loop in the centre of Helix A. No other contacts with the other regions of the RNA substrate are predicted (i.e. Helix B and C), indicating that the recognition of the 58-nt domain is very likely to be based solely on the sequence and unique structure of Helix A.

A large cluster of basic residues is observed on the surface of TSR in both amino and carboxy domains. These residues include Arg17, Lys23, Arg26 and Lys89 from the NTD and residues Arg158, Arg159 and possibly Arg162 from the CTD. The non-catalytic TSR molecule is implicated to play a role in the recognition of the A1067 target loop, with Lys89′ and Arg92′ of the NTD and the Lys125′, Arg158′, Arg159′ and Lys221′ of the CTD. An exposed Phe88 is positioned near the open RNA minor groove. As TSR is a SpoU MTase with L30-like domain, examining the equivalent residue in the yeast L30e-mRNA, may offer insight to the potential interactions that TSR may engage in. In the X-ray and NMR structures of the yeast translation autoregulatory complex, stacking interactions were

observed between the equivalent Phe85 and the first unpaired nucleotide (G56) in the internal loop [204,205] (see appendices). Mutation of this amino acid residue caused a 20-fold reduction in binding. The Phe88 of TSR is not exposed on the surface of the protein and is hidden within a hydrophobic pocket. In order to engage in stacking interactions with the RNA substrate, it must rotate towards the RNA upon binding (Figure 4.26). Additional interactions were predicted between residues 152 to 157 of a loop of the catalytic TSR monomer and U1061. This base, along with A1070 of Helix A, is turned outwards such that they engage in stacking interactions. Mutation of either base dramatically reduces enzyme activity, suggesting that TSR recognizes this tertiary structure element of the RNA [113].

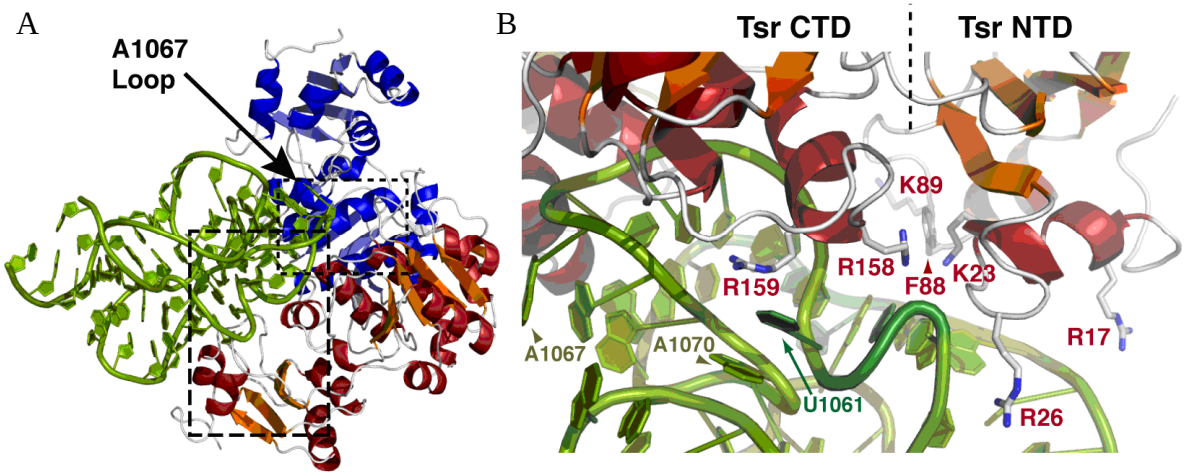

Figure 4.26: The modelled rRNA structure docked against the TSR dimer.
(A) Overview structure of RNA binding **(B)** Internal loops of Helix A of L11BD and target site A1067. Figure courtesy of Drs. Mark Dunstan and Graeme Conn.

The CTD of the catalytic TSR monomer is shown to interact with the loop containing the A1067 target site; specifically, residues Gly128, Arg162 and Arg158 are implicated in interacting with the RNA backbone and possibly recognizing base edges of U1066, G1068 and A1069. The methylation target, A1067, situated at the top of the L11BD Helix A (Figure 4.24), has its base and ribose moiety moiety exposed on the surface for possible interactions. Docking of the RNA reveals that the 2′-OH of A1067 is ~10 Å away from the sulphur atom

of AdoMet, which places the methyl group at too great of a distance for any possible methyl group transfer.

Thus, in order to position the 2′-OH of A1067 at an optimal distance for methylation, a base-flipping mechanism is proposed. Base flipping mechanisms are often used by DNA MTases [206,207]. A base flip occurance would place the 2′-OH group at a distance of 5 Å from the sulphur atom which is a closer distance for methyl group transfer. In addition, if the sugar ring pucker undergoes an inversion to C2′-endo, the 2′-OH group would be brought into even closer proximity to the sulphur atom of AdoMet. Sugar pucker changes have been observed within the 58-mer L11BD substrate itself [100,105].

Furthermore, upon flipping, A1067 will be in close proximity to many of the amino acid residues that have been implicated in having an important role in RNA and AdoMet binding in other SpoUT MTases. For example, the conserved residue Asn129 is within hydrogen bonding distance of the A1067 base edge, suggesting that perhaps this residue has a role in base recognition or positioning the target for methylation (Figure 4.27).

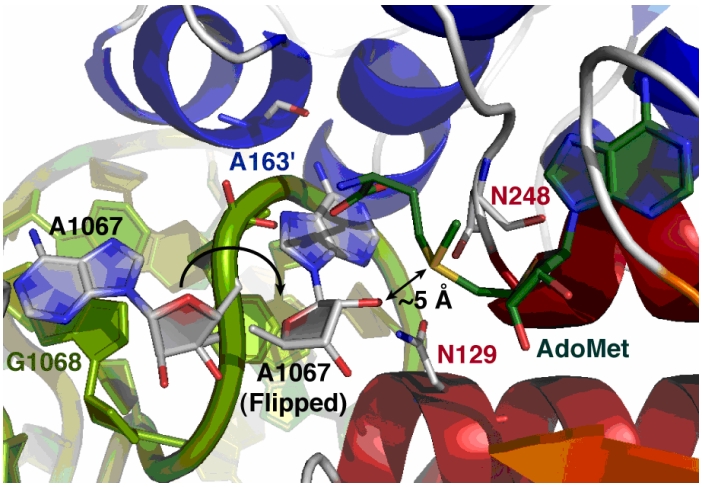

Figure 4.27: Propose base flipping mechanim of A1067.
Upon flipping, the 2′ OH is closer to the sulphur atom of AdoMet, permitting the transfer of its methyl group. Figure courtesy of Drs. Mark Dunstan and Graeme Conn.

4.3.3. Comparison of Homology Model with X-ray Model

During the earlier stages of the project, the absence of an experimentally determined protein structure, a homology model was developed and is described above. It is generally accepted that the accuracy of a homology model is proportional to the degree of the sequence identity between the target and the template [172]. With the X-ray crystal structure now obtained by our collaborators, it become possible to assess the quality of the comparative model.

A preliminary assessment of the crystallographic model and the homology models demonstrated very similar tertiary structure. The same secondary structure elements and fold were conserved between the structures as was the strip of positive residues is found between the two monomers that implicated for RNA binding. To assess model accuracy, the RMSD values between the superimposed comparative model and the X-ray crystal structure based on the Cα carbons, the backbone, heavy atoms and all atoms were calculated (Table 4.6).

Table 4. 6: Global and Local RMSD between comparative models and the crystal structure based on their Cα atoms, backbone and all atoms.

Comparison	**Homology Model**	**RMSD (Å)**		
		Cα atoms	**Backbone atoms**	**All atoms**
Global	*TSRMonomer2*	7.75	7.69	8.23
	PrimeTSR	7.89	7.84	8.51
	TSRdimer	10	9.94	10.5
Local CTD	*TSRMonomer2*	1.20	1.20	2.19
	PrimeTSR	1.06	1.06	2.07
	TSRdimer	1.18	1.22	2.17
Local NTD	*TSRMonomer2*	6.15	6.02	6.84
	PrimeTSR	5.04	4.94	5.71
	TSRdimer	6.65	6.64	7.40

*The local comparison of the comparative model to the crystal structure based on the C-terminal domain or the N-terminal domain.

Upon comparison of the crystallographic model to both the SwissModel and Prime homology models, it was observed that all RMSD values were similar, with values between

7.5Å to 10 Å. The large values indicate that the models are of lower resolution. Given that the sequence identity with the templates was between 24-31%, this was to be expected. RMSD values for the dimeric form were much higher and can be a result from using only a single template, unlike the for the monomer model. Visual inspection of the superimposed structure reveals that the high RMSD values stem largely from the differences of the N-terminal domain between the models and the crystal structure (Figure 4.28).

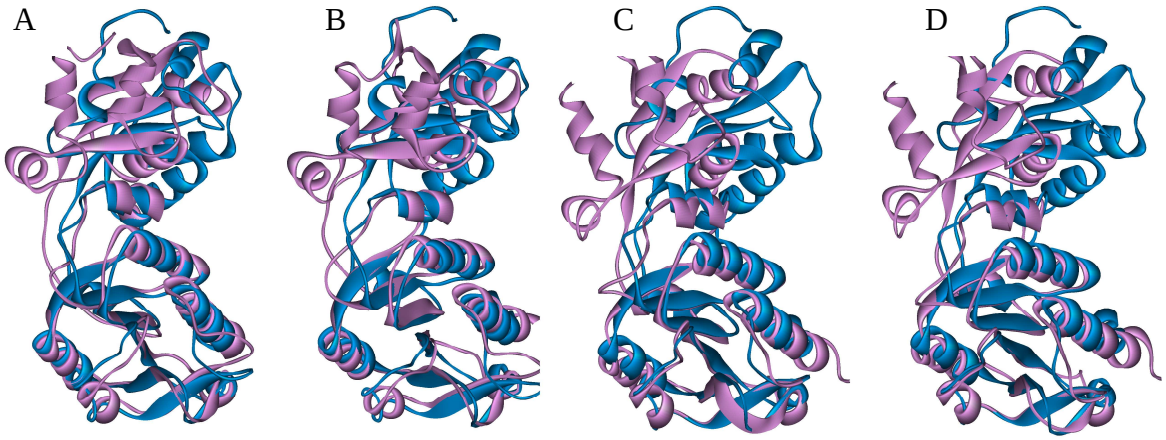

Figure 4. 28: Superimposition of the X-ray crytal structure of TSR (blue) and homology models (purple). **(A)** *TSRMonomer2* **(B)** *PrimeTSR* **(C)** *TSRdimer Chain A* **(D)** *TSRdimer Chain B.* Structural features superimposed very well for the CTD, while the NTD was found to vary greatly from the crystal structure.

While the significant deviation of the NTDs give an overall poor model quality and high RMSD values ranging between 5 to 7 Å, the agreement of secondary structural elements localized on the C-terminal domain was found to be extremely good (Figure 4.28); RMSD values were between 1 to 2 Å (Table 4.6, Figure 4.29). This is to be expected as the CTD is the domain that contains all the conserved structural features of the SpoUT MTases, while the evolutionary divergence is observed for the N-terminal recognition domain, permitting a range of different substrates. Therefore, choosing alternative SpoUT MTases as templates or using changing the sequence alignment will more than likely not give a significant

improvement in the quality of the amino domain. The reliability of the homology model is only good for the C-terminal region.

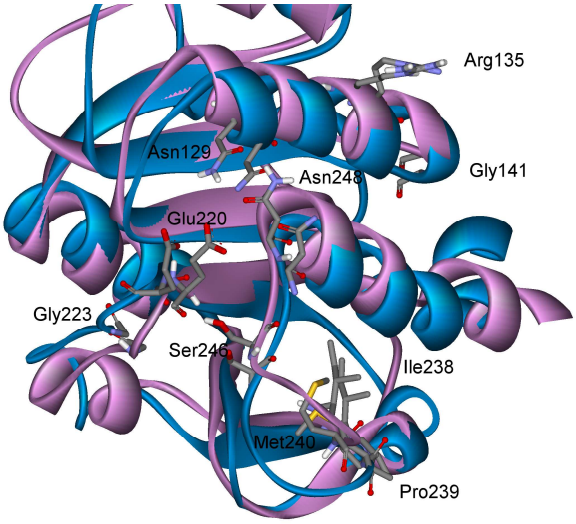

Figure 4. 29: Superimposition of the CTD between *PrimeTSR* (purple) and crystal structure (blue). Residues shown are conserved binding/active site of the enzyme.

After the development of the homology model, a series of conserved amino acid residues important for catalysis were selected as a guide for mutagenesis experiments (Figure 4.16). The homology model did not have AdoMet docked into its active sight, making it difficult to speculate on the roles of various residues. However, based on other published studies, the potential roles of residues were assigned and summarized below in Table 4.7.

Table 4. 7: Proposed roles and mutations for conversed residues in TSR homology models.

Motif	Residues	Proposed role	Mutants
Motif I	Asn129	Cofactor binding	N129A, N129D
	Arg′135	Nucleophilic base or positioning of 2′ OH of A1067	R135A*, R135K*
	Gly141	No defined role assigned	N/A
Motif II	Glu220	Catalytic base or maintaining knot integrity	E220A, E220Q
	Gly218, Gly223	No defined role assigned	N/A
Motif III	Ile238-Pro239-Met240	Forms hydrophobic pocket for adenine of A1067	ΔI238-M240
	Ser246	Adenine stabilization or positioning of methyl group	S246A*
	Asn248	Adenine stabilization or positioning of methyl group	N248A*, N248D*

*mutants that have been made thus far, currently biochemcally characterized and shown to have no activity

These residues were discussed earlier in *Section 4.3.1.4*. Prior to obtaining the crystallographic model, mutagenesis was carried out. The following mutants have been made

successfully: S246A, R135A, R135K, N248A, N238D. The mutations have been confirmed by DNA sequencing and by mass spectrometry (Table 4.9). Preliminary CD and DSC on some of the mutants have shown that the single base change did not produce any determinal effects to the protein structure (appendices). Biochemical characterization of these mutants is ongoing in our laboratory.

Table 4. 8: List of mutants made so far and molecular weight confirmation by mass spectrometry.

Mutant	MW* Expected (Da)	MW* Obtained by MS (Da)
S246A	29166	29166
R135A	29095	29097
R135K	29152	29154
N248A	29137	29139
N248D	29182	29183

*MW = molecular weight; for mass spectra, please refer to appendices

The high resolution TSR structure and the RNA docking experiment gave light to what additional residues may be involved in AdoMet binding and catalysis. Table 4.9 summarizes these roles and details can be found discussed earlier in *Section 4.3.2*. This crystal-structure based identification of important residues in TSR must be confirmed by biochemical means with quantitative measures in the form of methylation assays.

Table 4. 9: Additional important residues of TSR identified by the crystal structure.

Residues	Proposed Role	Mutants
Gly128, Arg158, Arg 162	Interacts with backbone of RNA (U1066, U1068 and A1069)	ΔG128, ΔR158, ΔR162
Ala163′	Hydrogen bonding with A1067	ΔAla163
Phe88	Stacking interactions with A1067	F88A
Leu185, Gly218	Hydrogen bonding with 2′OH and 3′OH of A1067	ΔL185, ΔGly218
Ile238-Pro239-Met240	Forms hydrophobic pocket for adenine of A1067	ΔIle238-Met240

4.4. Conclusions and Future Work

Comparative analysis of the TSR sequence suggested that it can be classified as a SpoUT MTase. Using the computational techniques of protein homology modelling, a 3D structure of TSR for both the monomeric and dimeric forms was produced. The TSR model

was generated using two different homology modeling software programs and either employed multiple (monomer structure) or single crystal (dimer) structures of other SpoUT MTases as a template; validation of the homology models was performed using various programs and mutagenesis efforts were begun.

Towards the end of this project, the crystal structure of TSR with AdoMet bound was solved by our collaborators. This solved structure has definitively confirmed that TSR is an SpoUT MTase with a deep trefoil knot. RNA docking studies by our colleagues helped us gain insight into the protein-RNA interactions that may take place during binding of the rRNA substrate. A base-flipping mechanism, common to DNA MTases, was proposed for the methyl group transfer to A1067.

A comparison of the homology models with that of the crystal structure showed suboptimal modelling for the overall structure. The homology models and the crystal structure were superimposed and RMSD values were calculated for the Cα atoms, backbone, heavy atoms and all atoms and all were found to be high. These high values can be attributed to the deviation of the N-terminal domains, which is quite apparent during visual inspection. The C-terminal domain was agreed nicely and gave very low RMSD values, indicating that the C-terminal domain of SpoUT MTases are highly conserved and the more variable N-terminal is for recognition of different substrates.

Biochemical confirmation is needed to substantiate the roles that have been implicated for certain residues. Some mutagenesis work was begun and methylation assays have been initiated for the mutants that have been made. Thus far, no activity has been detected for the mutants using the same range of substrate concentrations that was used for the wildtype enzyme. These mutations have eliminated all methylation activity. Further

biochemical experiments such as equilibrium dialysis and isothermal titration calorimetry are ongoing.

CHAPTER 5: STRUCTURE-ACTIVITY STUDIES OF THIOSTREPTON

Thiostrepton (TS) (**5-1**) ($C_{72}H_{85}N_{19}O_{18}S_5$, mw = 1665 Da) is a paradigm for the class of multicyclic thiazole-containing antibiotics. This family of antibiotics has been reported to exhibit potent antimicrobial activity against Gram-positive bacteria through a common mechanism: inhibition of bacterial protein synthesis [87]. The most thoroughly studied member, TS, interacts with a region of the 23S rRNA and ribosomal protein L11 of the large 50S ribosomal unit termed the guanosine triphosphatase (GTPase) centre [94-97]. Tight binding of this drug within this vicinity imposes conformational constraints on protein L11, resulting in an abolishment of GTP hydrolysis reactions involved in the protein elongation cycle [106]. TS also exhibits activity against *Plasmodium falciparum*, the major causative agent of malaria; it preferentially binds to the malarial plastid GTPase domain at nucleotides surrounding A1067 (*E. coli* numbering) [93]

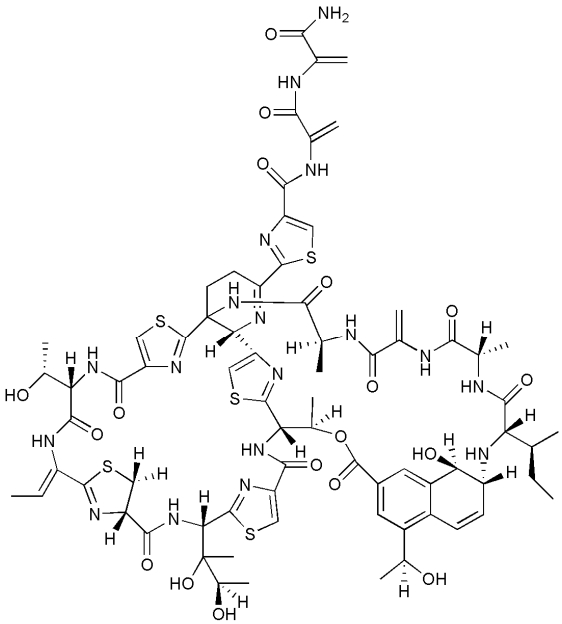

5-1

Much interest has been focused on the biochemistry and chemistry of TS, culminating in the recent and impressive total synthesis of the antibiotic, allowing for the preparation of analogues to probe structure-activity relationships [208,209]. Multidrug resistance is a critical problem and the development of either new targets or increasing the efficiency of known antibiotics is essential.

5.1. Approaches to the Study of Thiostrepton

5.1.1. Computational Chemistry

The crystal structure of TS was first reported in 1970, although the structural coordinates were never released [210]. However, the recent release into the public domain of an X-ray structure based on sulphur anomalous dispersion techniques has provided the coordinates for the heavy atoms in TS [211]. This information has since been utilized in docking experiments against the TS-RNA-L11 target complex [157]. The crystal structures of other cyclic thiazole peptides such as nosiheptide [212,213] and GE2270A [214] have also been determined. Recently, a high resolution NMR structure of the TS-RNA-L11 complex was published [106], and at the time this thesis was being written, the X-ray crystallographic structures of TS, nosiheptide and micrococcin bound to the large ribosomal unit of *Deinococcus radiodurans* were solved at a resolution between 3.3 – 3.7 Å [107] (Figure 5.1).

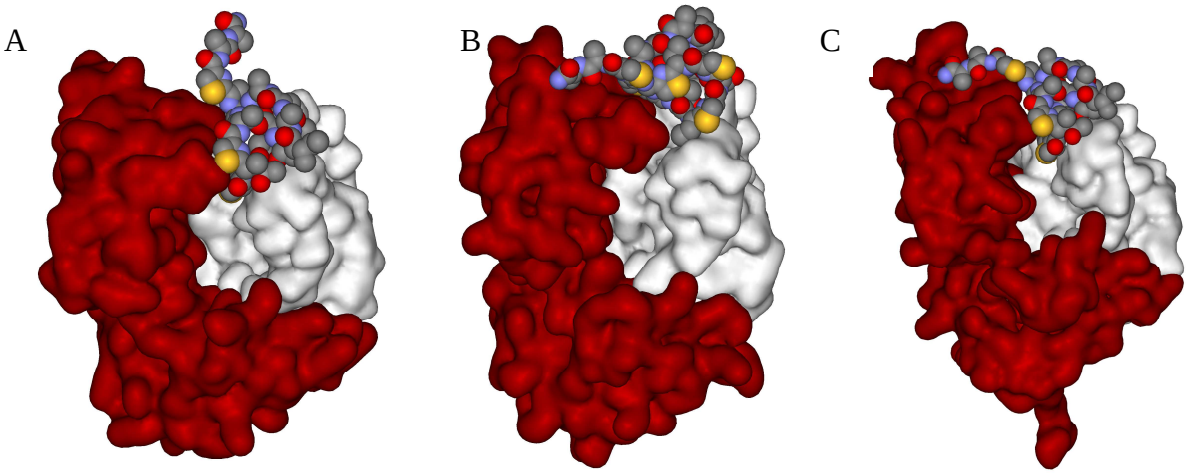

Figure 5. 1: Ternary complex of thiostrepton bound in the binding pocket between ribosomal protein L11 (red) and 23s rRNA (white).
(A) Docking model PDB: 1OLN [157] **(B)** NMR structure PDB: 2JQ7 [106] **(C)** X-ray crystal PDB: 3CF5 [107].

Nevertheless, it is well known that crystal packing forces can play important roles in the overall structures determined by X-ray diffraction methods. In addition, the ability of a molecule to sample different conformations makes it imperative to study the structure of an antibiotic by a variety of techniques [215]. Computational chemistry is a technique that can lead to insight into the conformation profile of a molecule. There are a number of general approaches to molecular modelling. Three types will be briefly introduced in this chapter: molecular mechanics [216], *ab initio* calculations [154] and semi-empirical methods [217].

5.1.1.1. Molecular Mechanics

Molecular mechanics calculations are based on classical mechanics [216,218]. The behaviour of the molecule can be derived through application of traditional mechanics where each atom in a molecular structure is considered to be a sphere of specific mass connected to other atoms by springs (representing chemical bonds). The potential energy (steric energy) of a molecule is the sum of all energy terms, including bond stretching, bond angle bending, dihedral angle rotation, and non-bonding interactions such as hydrogen bonding, electrostatic

and van der Waals interactions and is the basis of a *force field* [218,219]. A force field can be defined as a collection of these energy terms and parameters utilized to calculate the overall energetics of a particular molecule. Force fields are developed for different molecules ranging from small organic molecules to large biomolecules such as proteins, and are derived from *ab initio* calculations and experimental data [220]. One of the great strengths of using molecular mechanics techniques is that it is one of the fastest computational methods, and thus can be applied to quite large molecular systems. Unfortunately, its greatest limitation comes from its accuracy as it is based on selecting a force field with parameters appropriate for the system of interest. In addition, since molecular mechanics calculations do not involve electronic properties, one cannot obtain information on the chemical reactivity of the molecule [216].

5.1.1.2. Ab initio Calculations

Ab initio computations on the other hand are based on quantum chemistry first principles and use minimal experimental parameters and approximations [218]. All calculations are done purely mathematically based on Schrödinger's equation to calculate the behaviour and probable positions of electrons in a system (the *wavefunction*) [218,221]. This approach, by far is the most consistent and accurate for a varied range of molecular systems; starting with only the molecular structure and a small number of constants, chemical properties and reactivity of the molecule can be calculated. However, this method is computationally "expensive", that is, it places a considerable amount of demand on computer resources and time. Therefore, many *ab initio* calculations have been confined to smaller, simpler molecules of no more than 50 - 100 atoms (depending on computing power available) [218,220].

5.1.1.3. Semi-empirical Methods

Semi-empirical methods are often considered as the middle ground between *ab initio* and molecular mechanics calculations; it is based on quantum chemistry similar to that of *ab initio* methods, but, like molecular mechanics, is not restricted by molecular size [222]. Semi-empirical methods address the issue of size and time limitations encountered by *ab initio* methods by introducing approximations and simplifying the mathematics based on experimental parameters [217,222]. Although not as accurate as *ab initio* calculations, semi-empirical computations permit users to study the behaviour of larger molecules relatively quickly [222].

Not only are semi-empirical methods considered as an intermediate between *ab initio* and molecular mechanics in terms of speed, but they are also useful for range of applications [222,223]. *Ab initio* methods can be widely used to calculate a large range of properties of a molecule, and require little, if any, additional experimental data; however, they can only be used for smaller molecules [218]. On the other hand, where molecular mechanics makes up for the size and speed problem, it is restricted in its generality. These methods are confined by these parameters of the force fields chosen for a particular system [216]. If a parameter and/or a suitable force field is not well suited for a system, meaningful calculations cannot be performed. Semi-empirical calculations are very versatile in that they have a large range of applicability for large molecules (Figure 5.2) [222].

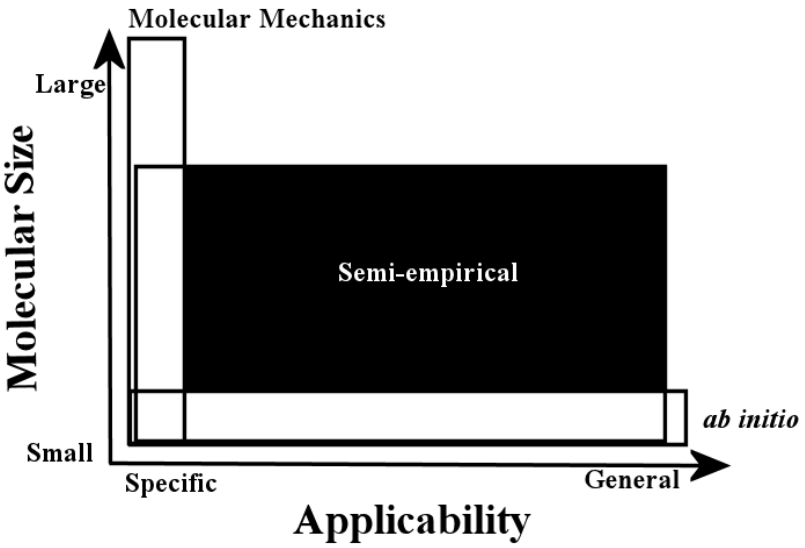

Figure 5. 2: Semi-empirical calculations are a middle ground between *ab initio* and molecular mechanics. *Ab initio* methods are most general, having the largest range of applicability, however, are restricted to small molecular size. Molecular mechanics are more specific, but can be used to calculate properties of larger sized molecules. The region in black shows calculation ranges covered by semi-empirical methods. Figure adapted from [222].

5.1.2. Modification of Thiostrepton

Thiostrepton was first isolated in 1955 and was found to exhibit extremely high antibacterial activity against Gram-positive organisms. It was also found to be effective against microorganisms resistant to penicillin and erythromycin [88]. It showed great promise; however, its low water solubility and poor bioavailability has restricted its use to topical application in veterinary practices (i.e. Panalog®) [224]. We embarked on developing TS analogues with improved aqueous solubility through chemical modification of the antibiotic, without compromising its biological activity.

5.1.2.1. Development of Novel Antibiotics

With the emergence of antibiotic resistance, the need for developing new antimicrobials is ever so pressing. In the past few decades, there has been very limited success in the development of novel classes of antimicrobials. Current strategies involve

efforts towards improving existing antimicrobial agents [225]. A prime example is the introduction of the ketolides. Erythromycin is a macrolide antibiotic that was introduced into clinical practice in the early 1950s for use against the Gram-positive *Staphylococcus aureus* when penicillin resistance was first observed to be problematic [75]. Similar to TS, erythromycin acts by binding to the 23s rRNA of the large bacterial ribosomal unit and prevents the growing polypeptide chain from leaving the peptide exit tunnel (see *Chapter 1, section 1.3.2* for more detail) [70,71].

One of the major limitations of erythromycin is that it is labile to acidic conditions, making it unstable in the acidic gastrointestinal tract [226]. A number of semi-synthetic derivatives of erythromycin A derivatives that are acid stable were made (azithromycin, clarithromycin, dirithromycin and roxithromycin). These semi-synthetic derivatives were effective only for a short period of time before resistant strains began to appear [75]. As a result, the ketolide class of antibiotics was developed. Ketolide antibiotics have the same structural core as erythromycin A (**5-2**), however a keto group replaces the 3-L-cladinose moiety. Although the cladinose group has been implicated as the part of the pharmacophore of erythromycin, modifications throughout the structure readily compensate for the absence of the group [75]. For example, telithromycin (HMR 3647) (**5-3**) has an additional carbamate group between the C11 and C12 of the lactone ring. It was found that telithromycin has high *in vitro* activity against a wide spectrum of Gram-positives species; it was also shown that it was effective against strains of *Streptococcus pneumoniae* that were erythromycin-resistant [227].

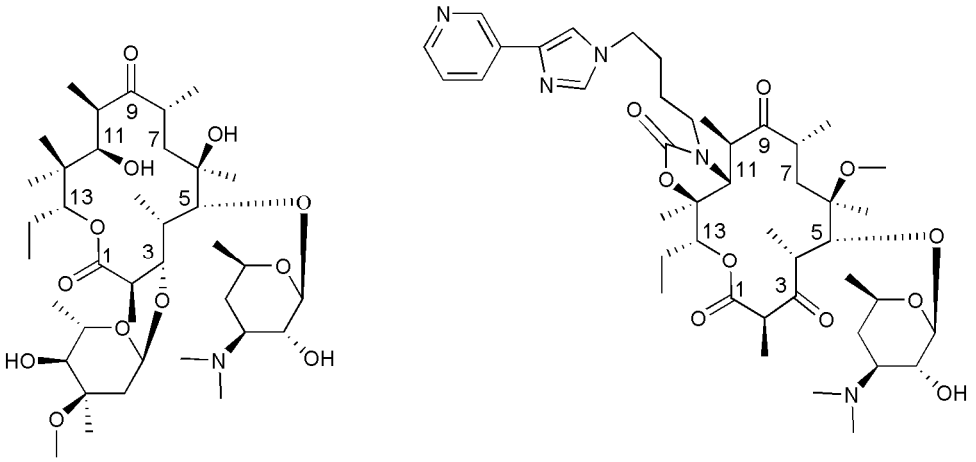

5-2 5-3

Figure 5. 3: The chemical structure of the antibiotic erythromycin (**5-2**) and its ketolide derivative, telithromycin (**5-3**).
The ketolides replaces the sugar moiety at the 3 position of the lactone ring with a keto group.

5.1.2.2. Modification of Nocathiacins: A Member of the Thiazole Peptide Antibiotics

The nocathiacins are the latest members of the thiazoyl peptide family of antibiotics. They were isolated from the fermentation broths of *Nocardia* sp [228,229]. They are tricyclic molecules and are the only members of the thiopeptide antibiotics to contain an indole group within their framework. They display potent activity against Gram-positive bacteria. Like TS, the nocathiacins bind to the large ribosomal subunit at the 23S rRNA and protein L11 to stall protein translation [230].

Nocathiacin I (**5-4**) has a slightly better solubility profile at lower pHs than other thiopeptide antibiotics; however, its solubility still remains inadequate for intravenous administration [231]. A research group at Bristol-Myers Squibb successfully prepared semi-synthetic nocathiacin I derivatives with improved aqueous solubility relative to the parent compound while retaining its biological activity [231-237]. One successful strategy employed in that study was the conjugation of the dehydroalanine side chain to water-solubilizing or charged groups.

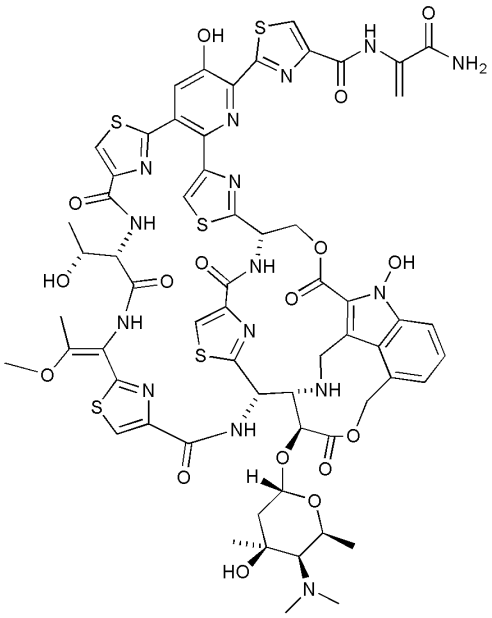

5-4

Nocathiacins are soluble in methanol and initial efforts toward the optimization of the Michael addition of methylamine to the dehydroalanine tail were carried out at room temperature for one hour, and resulted in multiple side products. Although Michael additions are typically performed in organic solvents, recent attention has been directed to the use of water as the solvent of choice in organic synthesis [238]. It was reported that modifications performed in water gave the desired product in good yields with minimal side products. Even more surprising, it was observed by the authors that reaction at -20°C gave the highest yield and purity product in the shortest reaction time (Table 5.1). It was concluded that the low temperature (-20°C) played a role in limiting the number of side products formed [231,233]. Efficient conjugation was observed under the same conditions with various thiols. The biological activity of these nocathiacin analogues were tested and found to be similar to the parent antibiotic both *in vivo* and *in vitro* assays [236].

Table 5. 1: Optimization of Michael Addition Reactions of Amines to Nocathiacin I. Adapted from [231].

Amine/equiv	Solvent	T (°C)	Time (h)	% Yield	% unreacted Nocathiacin I
$MeNH_2$/25	MeOH	22	3	Low*	N/A
$MeNH_2$/10	MeOH	22	7	Low*	N/A
$MeNH_2$/10	H_2O	22	1	70	5
Me_2NH_2/10	H_2O	22	1	76	N/A
Morpholine/10	H_2O	22	24	50	14
Morpholine/10	H_2O	5	24	70	14
Morpholine/10	H_2O	-20	5.5	90	3
Morpholine/10	1:4 MeOH/H_2O	-20	120	70	27

*multiple products were observed

5.1.2.3. Semi-Synthesis of Thiostrepton Analogues

The biological activity of TS and other thiopeptide antibiotics is attractive, since their mode of action is unique and different from other clinically available antibiotics. Therefore, an approach similar to the modification of the nocathiacins can be undertaken, where the drug can undergo chemical transformation such that improved solubility might be achieved. There are a number of sites on the TS molecule that can undergo chemical modification: three dehydroalanines and one dehydrobutyrine (Figure 5-4). *In vivo* and *in vitro* conjugation is observed between TS and thiolo groups on two proteins whose expression is induced by the presence of the antibiotic, TipAL and TipAS in *Streptomyces* sp. [239].

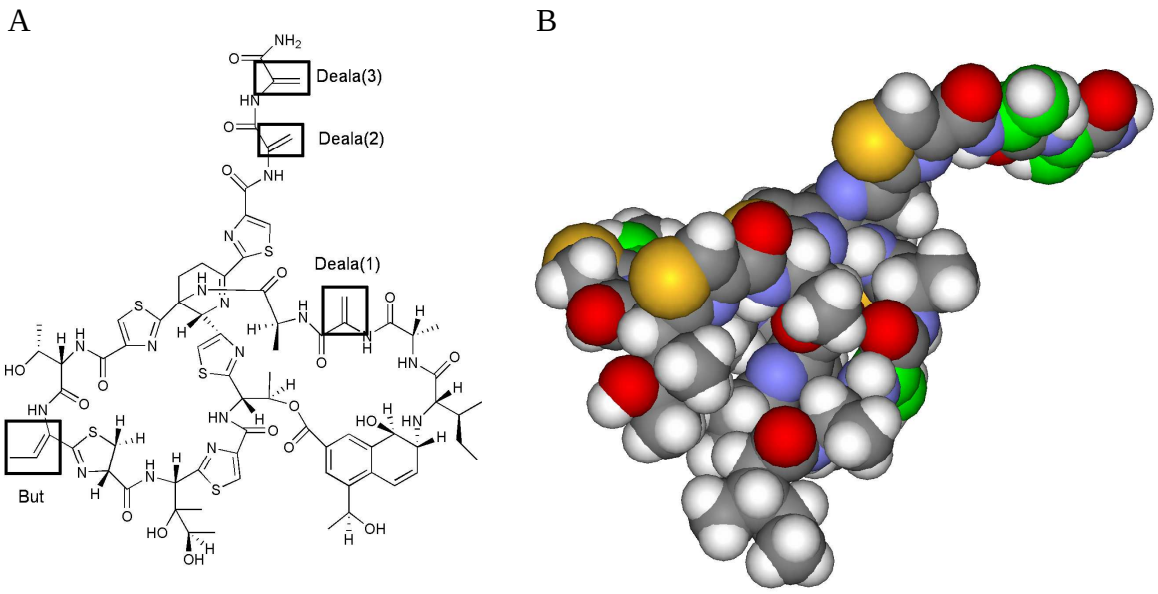

Figure 5. 4: Reactive groups on the antibiotic thiostrepton.
(A) Thiostrepton has four sites of potential chemical modification by Michael addition. The three dehydroalanines (Deala1-3) and one dehydrobutyrine (But) are shown in black boxes. **(B)** Space filling model of TS with green atoms indicating the sites of unsaturation.

Blocking experiments of the cysteine residues on TipAS with *N*-ethylmaleimide prevented the formation of covalent bond between the protein and antibiotic. Likewise, when the dehydroalanine and dehydrobutyrine residues of TS were blocked with cysteines, no adduct resulted. This indicates that the formation of this complex requires the cysteine residues of TipAS and the dehydroalanine/dehydrobutryine residues of TS. The protein-antibiotic complex formation was analyzed using mass spectrometry and SDS-PAGE gel analysis and was found to have a 1:1 stoichiometric ratio in spite of the multiple sites available on TS for modification [240]. Nonetheless, it was reported by the same group that reaction with free cysteine and other thiols (β-mercaptoethanol and dithiothreitol) gave additions of three or four molecules to the thiostrepton. However, these thiol adducts had an antibiotic activity that was reduced 1000-fold [240].

5.1.3 Plan of Action

TS is an extraordinarily complex macrocyclic peptide antibiotic containing thiazoline and quinaldic acid moieties along with a didehydroalanine tail. The complexity of its molecular architecture underlines the need to characterize its electronic and conformational properties, which should provide the opportunity to extend our insight into its possible modes of binding to the ribosomal RNA.

This chapter presents a detailed study on the structure of TS. The TS crystal structure was geometry optimized using molecular mechanics and semi-empirical methods. Information acquired from these computations were then utilized for detailed calculations including conformation searches and electron density calculations at the AM1 and *ab initio* levels to obtain partial charges of atoms that will be important in future modeling efforts. Our findings of this study, discussed later in this chapter, were published in Bioorganic Medicinal Chemistry Letters [241].

Results of the preliminary studies on the modification of the antibiotic utilizing an approach similar to the semi-synthesis of nocathiacin analogues will also be presented and discussed. The previous study by Chiu *et al*. [240] was taken into consideration, and we limited ourselves to in performing *single site* modifications of the antibiotic to avoid any reduction of antibacterial activity. Single modifications also permit us to investigate which sites of unsaturation play a biologically significant role. In addition, modification with compounds bearing a polar functionality may increase the water solubility of TS.

The antibiotic was modified successfully, purified and tested against various Gram-positive bacterial species and provides a good scaffold for future modification processes to increase the solubility of the drug.

5.2. Materials and Methods

5.2.1. Reagents and Materials

The following reagents and materials were obtained from the following companies:

Caledon Laboratories (Georgetown, ON): dimethylformamide (DMF), HPLC grade acetonitrile (ACN)

EMD Pharmaceuticals (Durham, NC): chloroform, triethylamine (TEA)

Sigma Chemical Company (St. Louis, MO): 2-mercaptoethanesulfonic acid (2-MESNA), Thiostrepton from *Streptomyces azureus* (>90%)

5.2.2. General Equipment

5.2.2.1. Computational Hardware and Software

All calculations were performed on a Silicon Graphics Inc. (SGI, Mountain View, CA) O_2 workstation (named “Violin”) or Flexor, the University of Waterloo’s multi-CPU SGI Origin 3800 system. Violin hardware specifications: IRIX 3.5X operating system, MIPS R10000 processor chip, MIPS R10010 floating point chip, 195 MHz IP32 processor, 750 MB RAM. Flexor hardware specifications: 64-bit IRIX 6.5.27f operating system and is a system comprised of forty 400 MHz MIPS R12000 CPUs and twelve 500 MHz MIPS R14000 CPUs with 52 GB of RAM.

Structures were visualized using Maestro 5.1 (Schrödinger Inc, Portland, OR) or WebLab Viewer Pro 3.7 (MSI). Force field assessment, conformational searching and stochastic dynamics studies were carried out using MacroModel 8.0 (Schrödinger Inc, Portland, OR) [242]. Geometry optimizations and detailed electronic calculations were performed using Gaussian '03, Revision B.05 (Gaussian Inc., Wallingford, CT) [243].

5.2.2.2. Chromatographic Equipment

Modified TS derivatives were purified by using a Waters (Mildford, MA, USA) μBondapak C_{18} reverse phase radial compression column (25 × 100 mm). All HPLC purifications were carried out on a Waters HPLC system (Mildford, MA, USA) consisting of the following components: Waters 600 controller, Waters 600 Gradient Pump, Waters 996 Photodiode Array Dectector with Waters Empower software, Build 1152. All aqueous solvents were filtered through a 0.2 μm membrane filter (Pall Life Sciences, East Hills, NY) and all organic solvents were filtered through a 0.45 μm membrane filter (Millipore Corp., Billerica, MA). All solvents were degassed prior to use.

5.2.2.3. Mass Spectrometer

The nano-electrospray mass spectrometer that was used was a Micromass Q-TOF Ultima™ Global and supplied by the Waterloo Chemical Analysis Facility, University of Waterloo.

5.2.2.4. Nuclear Magnetic Resonance (NMR) Spectrometer

^{1}H Nuclear magnetic resonance spectra were obtained using a Bruker 500 MHz NMR spectrometer using deuterated solvents manufactured by Cambridge Isotopes Laboratories

(Andover, MA). All samples were prepared by dissolving the compound in $CDCl_3$ or $CDCl_3$: CD_3OD (4:1). The number of scans ranged from 48 to 1056 with a sweep width of -0.5 ppm to 11 ppm.

5.2.2.5. Incubators

Growth of liquid bacterial cultures employed either a Series 25 controlled environment incubator shaker (New Brunswick Scientific Co., Inc., Edison, NJ) or Innova™ 4330 refrigerated incubator shaker (New Brunswick Scientific) both shaking ~ 200 rpm. For standing or plated bacterial cultures, growth was done in a Precision® gravity convection incubator from Precision Scientific, Inc (Chicago, IL).

5.2.2.6. Spectrophotometry

Optical density (λ = 600 nm) measurements on bacterial cultures were performed on one of the following instruments: Varian Cary 3 UV-Visible Spectrophotometer (Mississauga, ON) spectrophotometer with the CaryWinUV Advanced Reads Application Software 3.00 (182); Ultrospec 2100 pro UV/Visible spectrophotometer (Amersham Biosciences, Uppsala, Swedan); Molecular Devices Spectramax® Plus 384 (Union City, CA, USA), SoftmaxPro v. 501 Software.

5.2.3. Computational Methods

5.2.3.1. Experimental TS Structure

The recently reported crystal structure of TS (PDB: 1E9W) [211] was imported into WebLab ViewerPro 3.7 (MSI) where bond types and hydrogen atoms were added to produce the complete structure used for analysis. One of the proton additions was a secondary amine

(N^{15}) linked to the quinaldic acid moiety of TS. Secondary amines are known to pyramidalize and the heavy atom data for the crystal structure does not indicate the orientation of the proton. A number of steric interactions were visually observed when the proton was pointed inwards to the centre of the TS antibiotic, hence the proton was added such that it pointed outwards with a dihedral angle (H^{175}-C^{164}-N^{15}-H^{33}) of 65.1°. As well, the water of hydration bound to TS was removed. This TS structure, with all required hydrogens, was utilized as the starting structure for the series geometry optimizations outlined below.

It is interesting to note that the structure of TS (PDB: 1E9W) was not the first reported crystal structure. It was first reported in 1970 by Anderson and co-workers in Nature, however the coordinates were never reported nor deposited in the Cambridge Structural Database [210].

5.2.3.2. Geometry Optimizations of Thiostrepton

Molecular Mechanics Geometry Optimization

An assessment of various available force fields in MacroModel 8.0 (Schrödinger Inc, Portland, OR) [242] was undertaken to determine if an appropriate force field might be found without the need for the development of new force field parameters. The following force fields were surveyed: AMBER, AMBER94, MM2*, MM3*, MMFF, MMFFS, OPLS and OPLS-AA using the TS crystal structure. Minimizations of TS in these force fields gave the number and quality of high, medium and the low bond stretch/bend/torsional parameters, which were then evaluated. The OPLS-AA force field was determined to be the best of the available force fields. Final geometry optimizations of TS were performed *in vacuo* and in water using the Generalized Born/Surface Area (GB/SA) implicit solvation model [244] as implemented by MacroModel [242].

Semi-empirical Geometry Optimization

Geometry optimization calculations of TS were carried out with semi-empirical methods at the AM1 level [245] of theory using Gaussian ’03 (Gaussian Inc., Wallingford, CT) [243]. Structures obtained were compared with the starting experimental TS crystal and OPLS-AA derived structures and visualized in Maestro (Schrödinger Inc, Portland, OR).

5.2.3.3. Molecular Orbital and *Ab Initio* Charge Calculations

Molecular orbital calculations to determine the highest occupied molecular orbital (HOMO) and the lowest unoccupied molecular orbital (LUMO) were implemented at the semi-empirical AM1 level (Gaussian ’03), using the AM1 minimized structure obtained previously (see above). *Ab initio* Mulliken [246,247] and ChelpG [248] charge calculations using the AM1 minimized structure were performed on the B3LYP [249,250] functional using the 631-G(d) basis set. These calculations were performed *in vacuo* with Gaussian ’03.

5.2.3.4. Investigation into Conformational Flexibility of Thiostrepton

Low Mode (LMOD) Conformational Searching

The OPLS-AA minimized structures (*in vacuo* and implicit water) were used as the starting structures for Low Mode (LMOD) [251] conformational searches as implemented by MacroModel 8.0 [242]. The chirality of the 17 chiral centres present in the TS structure were held fixed during the conformation search, with the exception of the secondary amine (N^{15}). At each step, the new starting structure was selected from the previous set of low energy structures saved. Maximum iterations was set to 20 000 with 1000 steps. All other parameters were used at their default settings. Heavy atoms were used for comparison of similarity. All steps were repeated until conformations reached convergence.

Stochastic Dynamics Studies

OPLS-AA derived structures were utilized as starting structures in stochastic dynamics studies in their respective phases (*in vacuo* and implicit GB/SA water solvation). One nanosecond dynamics experiments (MacroModel 8.0 [242]) were carried out at constant temperature of 300 K, with an equilibration time of 1.0 ps and 1.5 fs time steps. The following segments of the antibiotic were monitored during the 1 ns timespan: the dihedral angle of the internal lactone (C^{142}-O^{144}-C^{153}-C^{154}), the dihedral angle of secondary amine (H^{175}-C^{164}-N^{15}-H^{33}) and the atomic distance between the two loops (C^{2}-N^{155}).

5.2.4. Modification of Thiostrepton with 2-Mercaptoethanesulfonic Acid Methods

5.2.4.1. General Procedure for the Michael Addition of 2-Mercaptoethanesulfonic acid (2-MESNA) to Thiostrepton

Initial Screening of Reaction Conditions

The addition reaction of the thiol, 2-MESNA, was performed in different organic solvents and in water. Reactions were carried out as a simple one pot semi-synthesis: to a stirring solution of TS and triethylamine (TEA; varied equivalents), one equivalent of thiol was added, and the reaction was allowed to proceed at either room temperature (23 °C) or low temperature (-20 °C). Reactions conducted at room temperature were placed in -20 °C for an additional night. The progress of reactions was monitored with thin layer chromatography (TLC) with $CHCl_3$: MeOH (4:1) and visualized with UV light as well as phosphomolybdic acid:0.4% in ethanol stain. Rf values: *2MESNA:* 0.2; *TS:* 0.9 and 0.75; *mTS-2MESNA:* 0.2.

Optimized Reaction Procedure for Michael Addition of 2-MESNA to TS

To a stirred solution of TS (30 mg) in DMF (755 μL) was added 10 equivalents of TEA at room temperature under argon. One equivalent of 2-MESNA (150 mM stock solution, deoxygenated) was then added to the pale orange-yellow solution to a final volume of 1 mL and stirred overnight at 4 °C. Thin layer chromatography was used to monitor the progress of the reaction. The solvent and excess TEA were removed by rotary evaporation and subsequently dried under high vaccum over night to remove any residual solvent to give an orange-yellow solid. Yield: 95%-100%

5.2.4.2. Purification of Modified Thiostrepton (mTS-2MESNA)

Method 1: Silca Gel Flash Chromatography Column

The orange-yellow product was dissolved in a minimum amount of solvent (chloroform with a few drops of methanol) and dried on silica gel (mesh size: 40-63 μm). The sample was applied onto a silica flash column. Then 5-8% methanol in chloroform was used to elute TS starting material and impurities. The compound of interest was eluted with 15% methanol in chloroform. All fractions were monitored by TLC and fractions containing the TS derivative were then combined and dried *in vacuo*. Yield: 73%.

Method 2: C_{18} Reverse Phase Sep-Pak

The crude product was dissolved in 20%/80% acetonitrile (ACN)/methanol and loaded onto a Waters C18 Sep Pak cartridge, which had been pre-conditioned with methanol and water. The column was washed with water followed by elution of mTS-2MESNA with 30%/70% ACN/H_2O, while the parent compound was obtained with 40%/60% ACN/H_2O.

All fractions were analyzed by TLC and fractions containing the TS derivative were then combined and dried *in vacuo*. Yield: 51%.

Method 3: Reversed-Phase HPLC

The orange-yellow powder of modified TS (25-30 mg) and 2-MESNA conjugate (mTS-2MESNA) was dissolved in milli-Q water (MQW). The mTS-2MESNA was sparingly soluble in water and extensive sonication and vortexing was required to prepare the sample prior to injection. The sample was filtered through a 0.2 μm polyethersulfone filter (VWR International, Mississauga, ON) to remove any particulate matter and undissolved compound. The column was equilibrated with 100% MilliQ Water (MQW), and the sample loaded at 5 mL/min. The column was washed extensively with MQW until an absorbance reached baseline at 220 nm (~10min).

Different elution gradients were performed to optimize for maximal separation, and were as follows:

- A gradient of 100% MQW to 100% ACN over 50 min (2%/min)
- A gradient of 100% MQW to 100% ACN over 100 min (1%/min)
- A gradient of 90%:10% MQW/ACN to 50%/50% MQW/ACN over 100 min (0.4%/min)

The large peak obtained from the last gradient was isolated and characterized by NMR and mass spectrometry and found contain a monoaddition product of 2-MESNA to TS. Yield: 13%. ^{1}H NMR spectra showed elimination of dehydroalanine peaks at 6.82 ppm, 6.72 ppm, 5.59 ppm, 5.49 ppm, indicating two modifications occurring at the tail portion of the parent antibiotic. Positive electrospray mass spectrometry confirmed a single successful

conjugation was made. Molecular weight determined: 1806 Da; expected molecular weight: 1807 Da. Thus, a mixture of products was isolated.

5.2.4.3. *In vitro* Susceptibility Test

Two different Gram-positive species were tested for antibiotic susceptibility to mTS-2MESNA. *Bacillus subtilis* ATCC E308 (strain 168) was a generous gift from Dr. Guy Guillemette (University of Waterloo) and the *Staphylococcus aureus* ATC 6538P was a kind contribution by Karen Pike (University of Waterloo). All microbiological manipulations were performed on Luria-bertani broth (LB ; per liter: 10 g tryptone, 5 g yeast extract, 10 g NaCl, pH 7.0) and LB agar (LB broth plus 1.5% agar) for *B. subtillis* and trypticase soy (TSB; per liter: 30 g trypticase, 3 g yeast extract, pH 7.0) broth and agar (TSB plus 1.5% agar) for *S. aureus*. Details of bacterial culture growth and tests are described below.

Kirby-Bauer Disc Diffusion Method [252,253]

A single colony was picked from an overnight bacterial re-streak grown on suitable agar plates and then inoculated into the appropriate broth (3 mL) as a small scale starter culture, and shaken overnight at 37°C. The actively growing culture (1 mL) was then diluted (1:100) in its respective media and grown at 37°C with constant agitation (~200 rpm) until both sets of cells reached a mid-log phase (A_{600} = 0.5-0.8). The densities of the bacterial suspensions were adjusted by addition of fresh sterile broth to give final optical densities of A_{600} = 0.5. These solutions were used immediately to inoculate agar plates. The inoculum (~200 μL) was spread evenly over the entire surface of the agar plate (100 × 15 mm plate) and allowed to dry (no more than 15 min) before application of discs.

The parent TS and the modified drug (mTS-2MESNA) were dissolved in MQW and DMF at various concentrations (Table 5.2). Sterile discs were firmly applied to the surface of the agar plate. Afterwards, 20 μL of each antimicrobial solution was added to the discs, and the plates were inverted and placed in a 37°C incubator immediately. After 16 h of incubation, each plate and disc was examined and the diameters of zones of inhibition were measured with a ruler.

Table 5. 2: Concentrations Utilized for Kirby-Bauer Disc Diffusion Test for Thiostrepton and its Analogue.

DMF		**H_2O (MQW)**	
TS (μg/mL)	**mTS-2MESNA (μg/mL)**	**TS (μg/mL)**	**mTS-2MESNA (μg/mL)**
0	0	0	0
0.03	0.03	0.03	0.03
0.3	0.3	0.3	0.3
3	3	3	3
		10	10
		25	25
		50	50

In vitro Susceptibility Curve

A small scale starter culture (3 mL) was inoculated with a single colony picked from an overnight re-streak grown from a suitable agar plate and grown overnight at 37°C with aeration. An aliquot of the starter culture (1 mL) was removed and its optical density adjusted to A_{600} = 0.5 with addition of fresh sterile broth. A series of fresh broths were prepared (5 mL) and the antibiotics, previously prepared in DMF or MQW, were added at various concentrations (Table 5.3). The cultures were incubated at 37°C with constant agitation. Samples of 200 μL were withdrawn at one hour intervals for 5-7 h and their optical densities at 600 nm were determined.

Table 5. 3: Concentrations Used for Antibacterial Susceptibility Testing for Thiostrepton and its Analogue.

DMF		H_2O (MQW)	
TS (μg/mL)	**mTS-2MESNA (μg/mL)**	**TS (μg/mL)**	**mTS-2MESNA (μg/mL)**
0	0	0	0
0.1	0.1	1	1
0.3	0.3	5	5
3	3	50	50

5.3. Results and Discussion

5.3.1. Geometry Optimizations of Thiostrepton

Using the crystal structure of TS with all the required hydrogens added as the starting structure, a survey of force fields available in Macromodel 8.0 [242] was performed to determine the best force field suited to model the antibiotic. From the information returned regarding the quality and number of stretch, bend and torsional parameters available in each forced field, it determined that the OPLS-AA was the best force field with which to model TS in (Table 5.4).

Table 5. 4: The number of bonds of high, medium and low quality bonds calculated for stretch/bend/torsional parameters in each force field available in MacroModel 8.0.

Force Field	**Stretch**			**Bend**			**Torsional**		
	H[a]	M[b]	L[c]	H[a]	M[b]	L[c]	H[a]	M[b]	L[c]
MM2* [1]	138	77	0	215	142	31	181	254	120
MM3* [2]	145	35	19	194	93	55	207	100	19
Amber* [3]	111	30	16	264	71	21	265	219	15
OPLS [4]		Error			Error			Error	
Amber94 [5]		Error			Error			Error	
MMFF [6]	195	0	13	301	0	62	318	0	217
MMFFS [7]	195	0	13	301	0	62	318	0	217
OPLS-AA [8‡]	200	8	0	348	15	0	435	98	2

[a]High quality; [b]Medium quality; [c]Low quality; 1. Allinger, N. L. *J Am Chem Soc* **1977**, *99*, 8127-8134. 2. Allinger, N. L.; Yuh, Y. H.; Lii, J. H. *J Am Chem Soc* **1989**, *111*, 8551-8566. 3. Ferguson, D. M.; Kollman, P. A. *J Comput Chem* **1991**, *12*, 620-626. 4. Jorgensen, W. L.; Tiradorives, J. *J Am Chem Soc* **1988**, *110*, 1657-1666. 5. Cornell, W. D.; Cieplak, P.; Bayly, C. I.; Gould, I. R.; Merz, K. M.; Ferguson, D. M.; Spellmeyer, D. C.; Fox, T.; Caldwell, J. W.; Kollman, P. A. *J Am Chem Soc* **1995**, *117*, 5179-5197. 6. Halgren, T. A. *J Comput Chem* **1996**, *17*, 490-519. 7. Halgren, T. A. *J Comput Chem* **1999**, *20*, 720-729. 8. Jorgensen, W. L.; Maxwell, D. S.; TiradoRives, J. *J Am Chem Soc* **1996**, *118*, 11225-11236. ; ‡This force field is a greatly expanded version of the OPLS force field.; MM2*, MM3* and Amber* are MacroModel's version of the three force fields originating from the above listed references.

Two low quality torsional parameters for the following angles were noted: N^{98}-C^{96}-S^{93}-C^{94} and N^{179}-C^{178}-C^{191}-S^{193} (Figure 5.5). These torsion angles are found in the ring of the dihydrothiazole group (N^{98}-C^{96}-S^{93}-C^{94}) and the bond attaching the thiazole of the tail to the piperidine group (N^{179}-C^{178}-C^{191}-S^{193}) (Figure 5.6, Red). Due to the ring constraints of the dihydrothiazole, these low quality torsional angles would not be expected to greatly affect the conformational studies. The tail with the piperidine group was expected to freely rotate in solution. This view was taken into account when evaluating the generated conformers for relatedness (see below). It is important to note that although we utilized OPLS-AA as the molecular mechanics for this particular problem, more detailed studies may require the development of force field parameters for these particular torsional rotations.

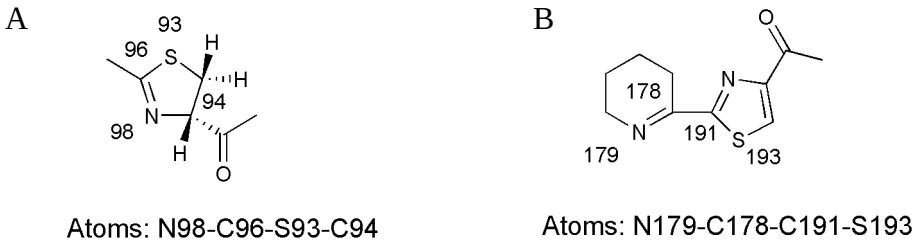

Figure 5. 5: Low quality torsion angles of thiostrepton found in OPLS-AA. **(A)** Torsion angle between atoms N^{98}-C^{96}-S^{93}-C^{94} on the dihydrothiazole. **(B)** Torsion angle between atoms N^{179}-C^{178}-C^{191}-S^{193} in the tail region of thiostrepton.

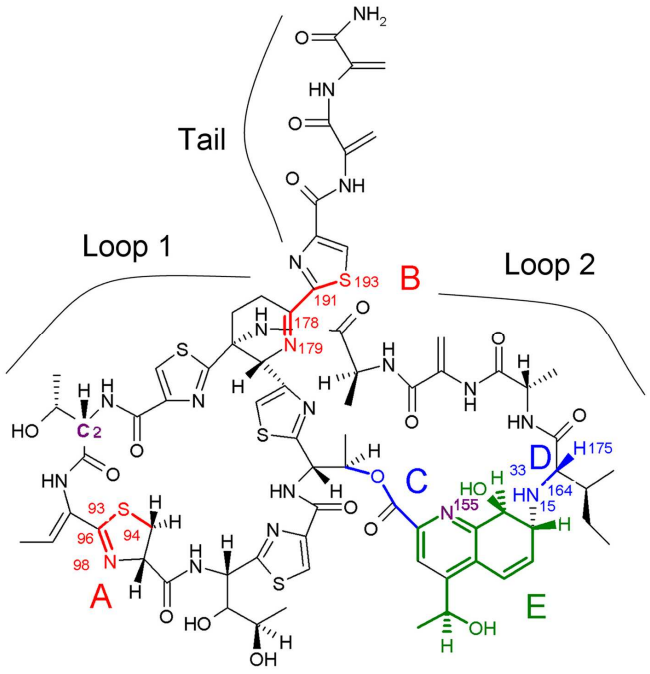

Figure 5. 6: A closer examination of the thiostrepton (TS) structure.
(A) The dihydrothiazole moiety; **(B)** linkage between tail and body of thiostrepton; **(C)** ester linkage; **(D)** secondary amine (N^{15}); (E) quinaldic acid moiety. Red: two low quality torsion angles found using the OPLS-AA force field. Blue: dihedral angles used to monitor the stochastic dynamics run. Purple: distance monitored during the stochastic dynamics run between N^{155} and C^{2}.

OPLS-AA energy minimizations were performed *in vacuo* and in water, utilizing the implicit GB/SA methodology [244]. The GB/SA implicit solvation model is based on two popular continumm solvation models: the Generalized Born (GB) and Solvent Accessible Surface Area (SA) model; solvation free energies (G_{sol}) are calculated based on the sum of a solvent-solvent cavity term (G_{cav}), a solute-solvent van der Waals term (G_{wdW}) and a solute-solvent electrostatics polarization term (G_{pol}) [244,254]. The minimized structures obtained had energies of: -827.83 kcal/mol (vacuum) and -1014.75 kcal/mol (water). Superimposition of non-hydrogen atoms of the TS crystal structure with these two energy minimized structures revealed low RMS values of 0.4380 and 0.5431, respectively, suggesting that the two low quality torsional angle parameters discussed earlier do not appear to be major obstacles in modelling TS (Figure 5.7). The dihedral angles were determined to be -11.7°

(N^{98}-C^{96}-S^{93}-C^{94}) and 0.4° (N^{179}-C^{178}-C^{191}-S^{193}) in the gas phase. The didehydroalanine tail showed the largest difference with RMS values 1.797 and 1.820 for the gas and liquid phase, respectively.

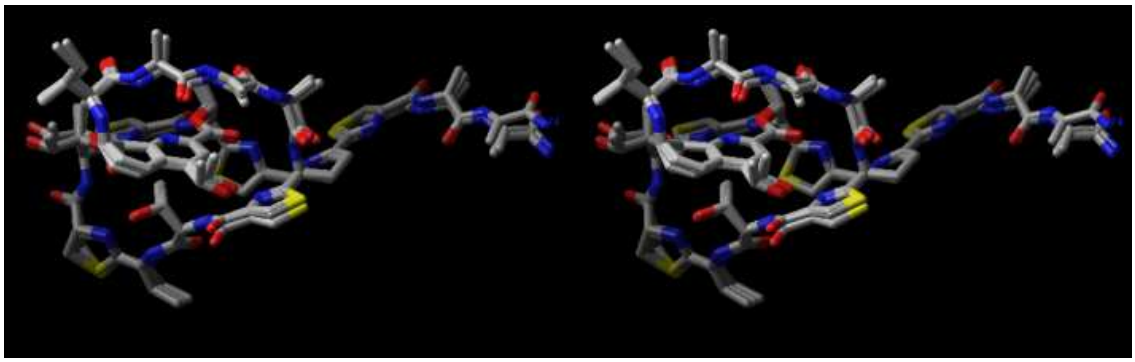

Figure 5. 7: Relaxed stereoview of thiostrepton starting crystal structure with OPLS-AA energy-minimized structure *in vacuo* and water and hydrogens eliminated for clarity [241].

A second approach was undertaken to determine the energy-minimized structure of TS by utilizing semi-empirical AM1 calculations. The AM1 structure (vacuum) obtained from the starting crystal structure was minimized to a low energy structure that had no negative frequencies based on frequency calculations. When superimposed on the starting crystal structure, the RMS difference obtained was 0.9623 (Figure 5.8). Additional comparisons of the AM1 structure to the OPLS-AA structures determined *in vacuo* and in water resulted in RMS differences of 1.0433 and 0.9904, respectively (Figure 5.9 and 5.10). The two torsion angles, N^{98}-C^{96}-S^{93}-C^{94} and N^{179}-C^{178}-C^{191}-S^{193} in the AM1 structure were determined to be 0.8° and 12.0°, respectively.

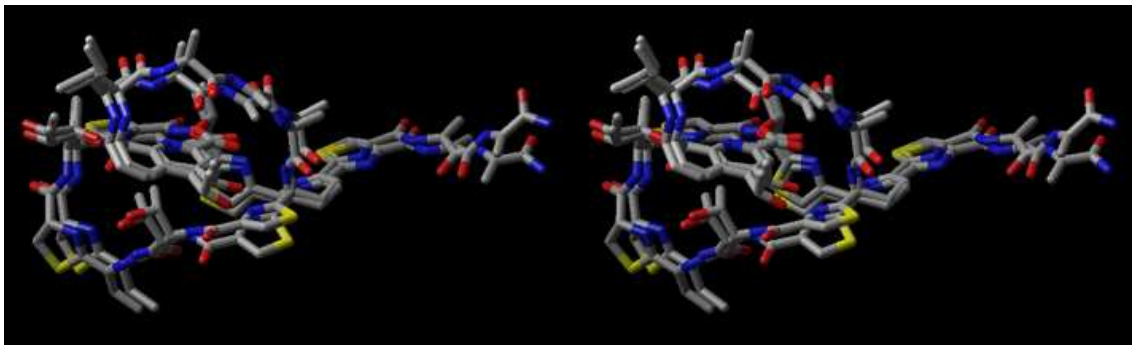

Figure 5. 8: Relaxed stereoview of superimposed structures of the thiostrepton crystal structure with the AM1-minimized structure (RMS = 0.9623) and hydrogens eliminated for clarity [241].

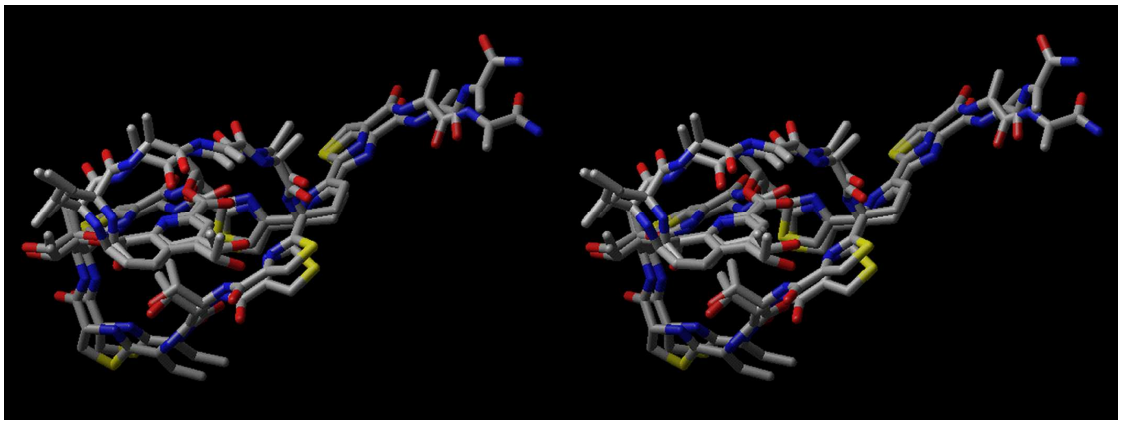

Figure 5. 9: Overlay of the OPLS-AA minimized thiostrepton structure *in vacuo* with the AM1-minimized structure (RMS = 1.0433) in relaxed stereo mode with hydrogens eliminated for clarity [241].

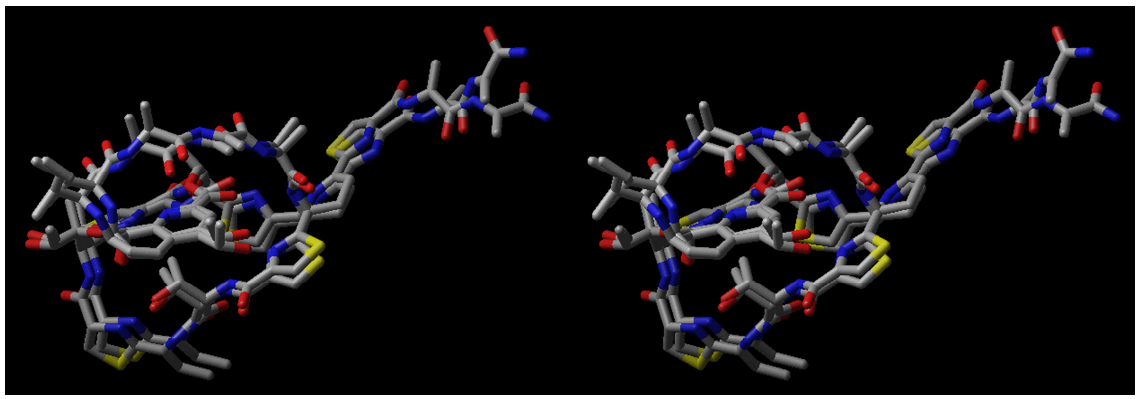

Figure 5. 10: Overlay of the OPLS-AA minimized thiostrepton structure in water with the AM1-minimized structure (RMS = 0.9904) in relaxed stereo mode with hydrogens eliminated for clarity [241].

5.3.2. Molecular Orbital and Ab initio Charge Calculations

The highest occupied molecular orbital (HOMO) and the lowest unoccupied molecular orbital (LUMO) at the AM1 level of calculation were determined to be localized

on the dihydrothiazole and quinaldic acid moieties, respectively (Figure 5.11). The HOMO and LUMO could be important in contributing to the interaction of TS with ribosomal RNA. It was previously suggested that the quanaldic acid and the thiazole moieties of TS engage in pi-stacking interactions with adenosine 1067 and 1095, respectively; this was confirmed by a recent NMR model by Jonker and coworkers [106].

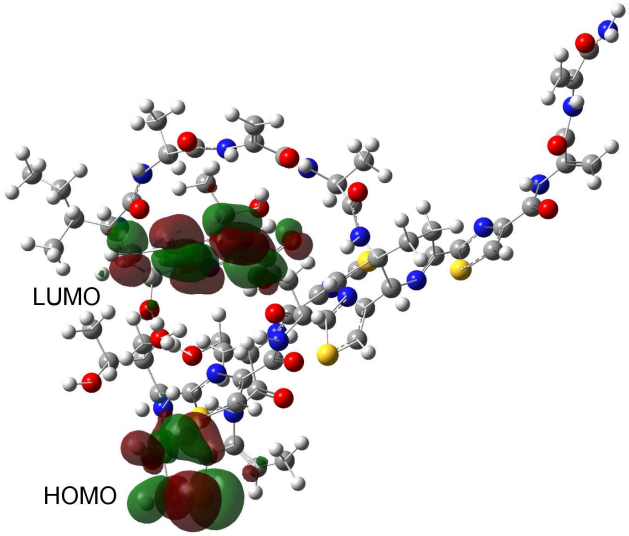

Figure 5. 11: The HOMO and LUMO of thiostrepton.
The highest unoccupied molecular orbital (HOMO) and the lowest unoccupied molecular orbital (LUMO) diagram at the AM1 level were overlapped, and were calculated to be localized on the dihydrothiazole and quinaldic acid moieties of thiostrepton, respectively [241].

Additionally, the AM1 minimized structure was utilized as the geometry for a single point energy calculation at the B3LYP/631-G(d)//AM1 level. The calculation led to a detailed analysis of the electronic structure of TS. The Mulliken charges were determined by AM1 and B3LYP/6-31(d) calculations and the CHelpG (B3LYP/6-31(d)) electrostically fit charges on the AM1 geometry-optimized structure are shown in Figure 5.12.

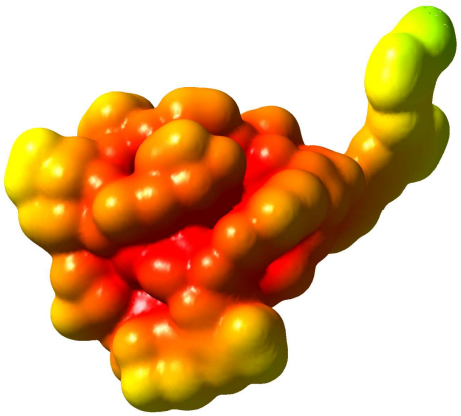

Figure 5. 12: Electrostatic potentials (-2.000e^{1} [red]-1.00e^{1} [blue]) mapped onto electron density (Density = SCF) for AM1 energy-minimized structure. Isovalue for isosurface: 0.0004 electrons/au^{3}.

5.3.3. Conformational Flexibility of Thiostrepton

5.3.3.1. LMOD Conformational Search

Although the semi-empirical and *ab initio* calculations provide partial charges for the atoms on this large drug molecule, it is also important to realize that the crystal structure and the minimized structures directly obtained from it, are each but one structure on the energy potential surface. Such a large molecule such as TS should exhibit a multiplicity of conformations in spite of the fact that is restricted by two internal loops. In order to explore this in a computationally efficient manner, we utilized the energy-minimized OPLS-AA (vacuum and water) structures for a series of conformational searches.

There are 39 rotatable bonds in the TS structure, not including methyl group rotations. This number precludes approaches that utilized dihedral angle drive-based search protocols. We therefore applied the highly efficient low mode (LMOD) [251] conformational search protocol implemented in MacroModel 8.0 [242]. This method explores the low frequency eigenvectors of the molecular system and is expected to follow “soft” degrees of freedom, such as those found in torsional rotations. Due to the aggressive search protocol utilized in this approach, the chirality of the 17 chiral centres were held fixed during the

conformational search. Only the secondary amine (N^{15}) was not fixed, as it was believed that pyramidalization of this nitrogen, in addition to it inherent flexibility might be a contributing factor to the conformational flexibility of TS. Both vacuum and water phase OPLS-AA minimized structures were used in separate calculations using LMOD.

LMOD calculations performed *in vacuo* found a total of 158 conformations within ~10.0 kcal/mol of the global minimum (-908.1 kcal/mol), 31 of which are within 3 kcal/mol of the global minimum. In the case of water (GB/SA), 293 unique conformations were found, 76 of which were within 3 kcal/mol of the global minimum (-1133.8 kcal/mol). Overlaying the two global minimum structures (vacuum and water) with the starting TS crystal structure (Figure 5.13), reveal that Loop 2 and the tail region are more opened and exposed *in vacuo*, whereas the structure obtained in implicit water forms a more tightly packed architecture. The secondary amine (N^{15}) was observed to have pyramidalized and faces inwards towards the TS core in the LMOD structure *in vacuo*. This suggests that the binding interactions of TS could potentially involve significant conformational changes of Loop 2 that may be facilitated by the pyramidalization and torsional flexibility of N^{15}.

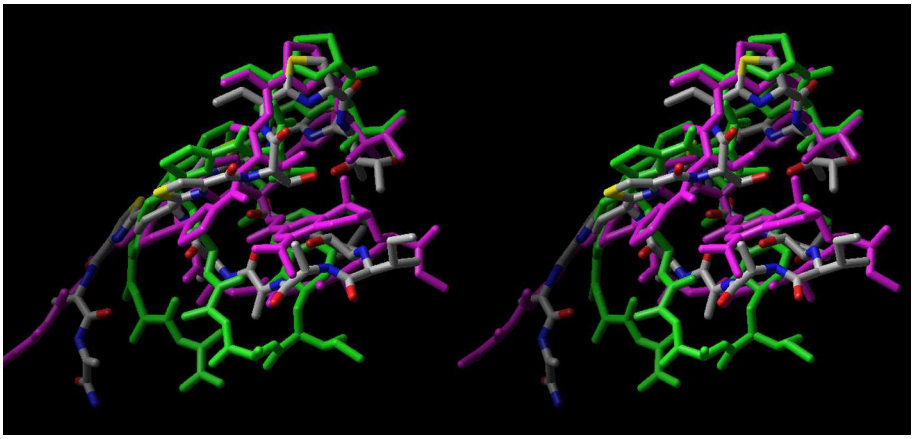

Figure 5. 13: Superimposed global minimized energy structures calculated from LMOD in vacuum (green) and water (CPK) and the starting thiostrepton structure (magenta) [241].

Although by no means exhaustive, the above approaches did find a number of conformations lower in energy than the OPLS-AA minimized crystal structure. A number of the conformations found in the LMOD searches showed N^{15} pyramidalization, where approximately 16% and 13% of the LMOD-generated vacuum and water conformation (1000) had the amine proton pointed inward. Hence this process may play an important role in defining the conformation ensemble of TS. In order to gain some insight into the frequency of this possible pyramidalization process, as well as to explore further the conformational mobility of the loop regions of TS, stochastic dynamics studies were undertaken.

5.3.3.2. Stochastic Dynamics Studies

One nanosecond dynamics experiments were undertaken at 300 K *in vacuo* and in implicit water (GB/SA). The dihedral angles around the internal lactone (C^{142}-O^{144}-C^{153}-C^{154}), the secondary amine (H^{175}-C^{164}-N^{15}-H^{33}), and the atomic distance between the two internal loops (C^{2}-N^{155}) (Figure 5.6) were also monitored to gain additional information as to the conformational changes over the one nanosecond time frame.

Results from the stochastic dynamics studies performed *in vacuo* indicate that early in the run, the N15 proton orientates itself inwards (steps 17-74, 130-167) periodically, while no such behaviour was observed in the water run (Figure 5.14). The region of the internal lactone ring does not appear to change significantly in both cases, although conformation of the opposite orientation was sampled frequently throughout the duration of the analysis (Figure 5.15). The distance between the two loops was found to increase over the duration of the dynamics run (both vacuum and water), thereby expanding the core of TS (Figure 5.16).

Data from these stochastic dynamics runs suggest that TS exhibits a conformational flexibility, a 'breathing' dynamic for binding interactions.

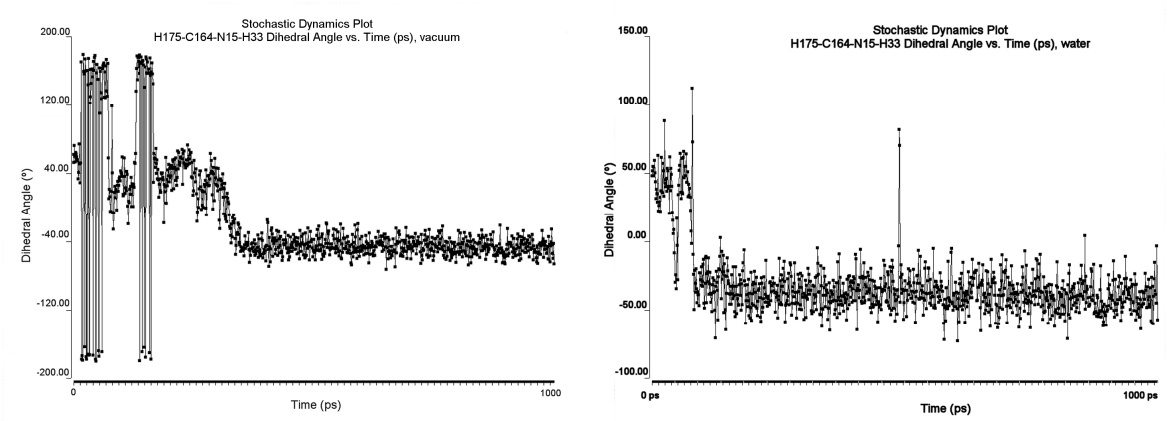

Figure 5. 14: Stochastic dynamics plot (*in vacuo* and water) of the dihedral angle (H^{175}-C^{164}-N^{15}-H^{33}) of the N^{15} secondary amine (D, Figure 5.5) over time (1 ns) [241].

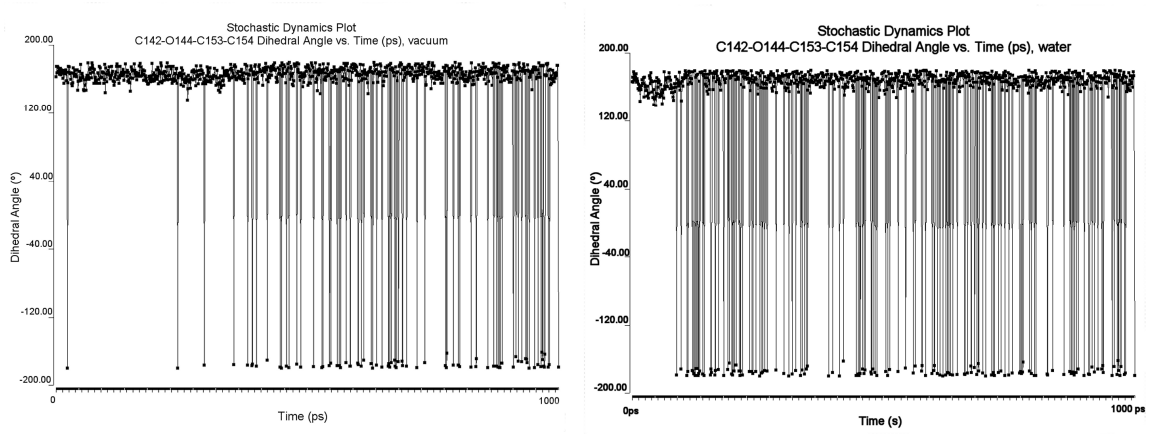

Figure 5. 15: Stochastic dynamics plot (*in vacuo* and water) of the dihedral angle (C^{142}-O^{144}-C^{153}- C^{154}) of the internal lactone ring (C, Figure 5.5) over time (1 ns) [241].

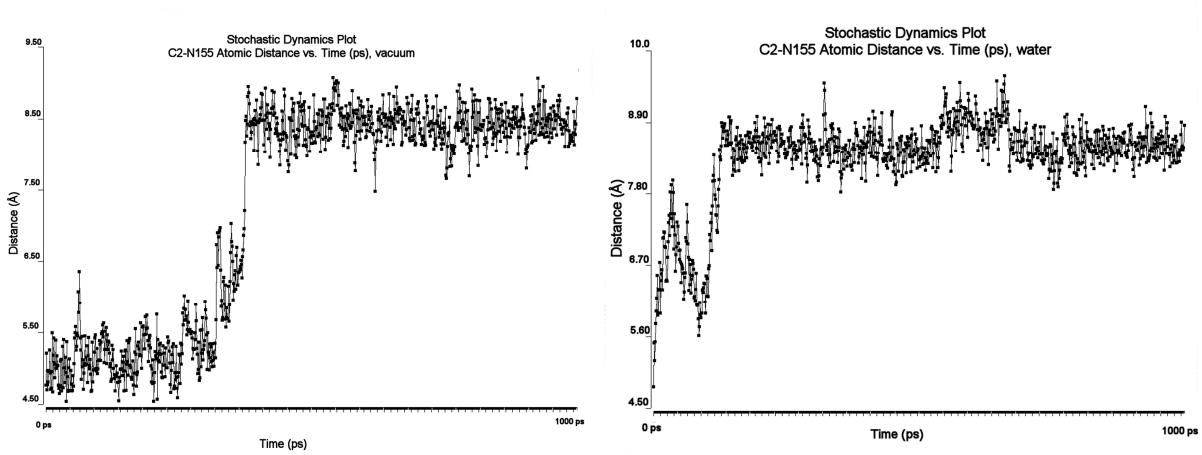

Figure 5. 16: Stochastic dynamics plots (*in vacuo* and water) of the distance between the two macrocyclic rings (Loop 1 and 2, Figure 5.5) between C^2 amd N^{155} over time (1 ns) [241].

5.3.4. Modification of Thiostrepton

5.3.4.1. Reaction of Thiostrepton with 2-Mercaptoethanesulfonic Acid

With the recent success of the development of nocathiacin analogues from Michael addition reactions [231,233,236], we commenced our modification of TS in a similar fashion (Table 5.5 and 5.6). Nocathiacins only have a single double bond for modification, and is a good scaffold for which to base our reactions on. Therefore, a single site modification with TS should not be a problem. With the goal of a single site modification, only one equivalent of thiol (2-mercaptoethanesulfonic acid; 2MESNA) was added under aqueous conditions. Although nocathiacins have poor solubility in water, it was found that successful conjugation with thiols was made possible with the addition of the weak base, triethylamine (TEA). It is believed that the TEA aided in improving the solubility of the nocathiacins in addition to acting as a general base catalyst for the Michael addition [233], however we did not observe this for TS.

The TS starting material remained insoluble throughout the entire length of reaction. Increasing the amount of organic solvent in the reaction mixture and trying two different temperatures with varying equivalents of base allowed for evaluation of the effects of solvent temperature and base on the thiol addition. For conditions that were largely aqueous (80% H_2O/20% DMF), no improvement in solubility of starting material was observed. On the other hand, when solvent was composed of 20% H_2O/80% DMF, the cloudy reaction mixture was stirred for two hours before turning into a clear homogeneous solution, and product was observed by TLC. With fully organic conditions, Michael addition occurred much more rapidly and product was observed as early as one hour. Side reactions were minimal and did not discriminate between either set of conditions (100% DMF vs. 20% H_2O/80% DMF). In addition, it did not appear that temperature (-20°C) eliminated side reactions as it did for the nocathiacins [231,233,236]. Nonetheless, it was later noticed that performing the reaction in 100% DMF at 4 °C gave a crude product that was slightly less orange compared to when performed at 23°C (room temperature). Therefore, all subsequent reactions were executed at 4 °C in 100% DMF.

Table 5. 5: Summary of Reactions Conditions Attempted for the Michael Addition of 2-MESNA to TS at Room Temperature (23 °C).

Solvent	Equiv. TEA	Time (h)				
		0	***1***	***2***	***O/N***	***O/N* (-20 ℃)***
DMF	0	—[a]	—[a]	—[a]	—[a]	—[a]
	1	—[a]	Product/thiol[b]	Product/thiol[b]	Product	No change[c]
	10	—[a]	Product/thiol[b]	Product	Product	No change[c]
80% DMF/20% H_2O	0	—[a]	—[a]	—[a]	—[a]	—[a]
	1	—[a]	—[a]	—[a]	Product/thiol[b]	No change[c]
	10	—[a]	—[a]	Product/thiol[b]	Product	No change[c]
20% DMF/80% H_2O	0	—[a]	—[a]	—[a]	—[a]	—[a]
	1	—[a]	—[a]	—[a]	—[a]	—[a]
	10	—[a]	—[a]	—[a]	—[a]	—[a]
H_2O	0	—[a]	—[a]	—[a]	—[a]	—[a]
	1	—[a]	—[a]	—[a]	—[a]	—[a]
	10	—[a]	—[a]	—[a]	—[a]	—[a]

*Reaction vessel was placed in -20 °C for an additional overnight

[a]Only starting material was observed on the TLC plate or nothing was observed as TS starting material was not soluble in solvent condition

[b]The emergence of the product was observed, along with the thiol and TS starting material

[c]No observable difference from placing reaction vessel from RT to -20°C

Table 5. 6: Summary of Reactions Conditions Attempted for the Michael Addition of 2-MESNA to TS at -20 °C

Solvent	Equiv. TEA	Time (h)			
		0	***1***	***2***	***O/N***
DMF	0	—[a]	—[a]	—[a]	—[a]
	1	—[a]	Product/thiol[b]	Product/thiol[b]	Product
	10	—[a]	Product/thiol[b]	Product	Product
80% DMF/20% H_2O	0	—[a]	—[a]	—[a]	—[a]
	1	—[a]	—[a]	—[a]	Product/thiol[b]
	10	—[a]	—[a]	Product/thiol[b]	Product
20% DMF/80% H_2O	0	—[a]	—[a]	—[a]	—[a]
	1	—[a]	—[a]	—[a]	—[a]
	10	—[a]	—[a]	—[a]	—[a]
H_2O	0	—[a]	—[a]	—[a]	—[a]
	1	—[a]	—[a]	—[a]	—[a]
	10	—[a]	—[a]	—[a]	—[a]

[a]Only starting material was observed on the TLC plate or nothing was observed as TS starting material was not soluble in solvent condition

[b]The emergence of the product was observed, along with the thiol and TS starting material

5.3.4.2. Purification of Thiostrepton Derivative (mTS-2MESNA)

Initial efforts at purifying the crude modified TS antibiotic were carried out using flash chromatography and purification by using a precolumn of C18 (Sep Pak). In both purification processes, although the majority of the starting material was removed, there was

still a residual amount that remained. Mass spectrometric analysis indicated a single addition had successfully occurred (please see below). No clear NMR spectra were obtained due to the presence of contaminants such as silica from the flash chromatography purification or side products.

Isolation of mTS-2MESNA was then pursued by analytical HPLC methods. Sample preparation encountered difficulties as the modified TS analogue still remained sparingly soluble in water. The sample was sonicated and vortexed to facilitate dissolution, however insoluble compound remained and was centrifuged and filtered away prior to purification. Different elution gradients from water to acetonitrile (ACN) were applied: 2%/min (100% H_2O to 100% ACN; Figure 5.17), 1%/min (100% H_2O to 100% ACN ; Figure 5.18) and 0.4%/min (90% H_2O:10% ACN to 50% H_2O:50% ACN Figure 5.19) and it was found to remove the majority of side products and starting thiostrepton. Fractions collected from the 0.4%/min run were assessed for biological activity relative to the parent compound (see *Section 5.3.4.3*).

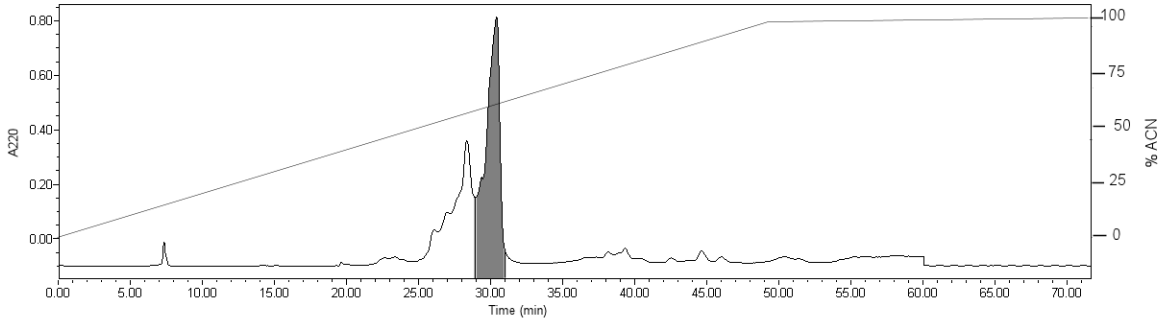

Figure 5. 17: Chromatogram showing the separation of mTS-2MESNA.
A gradient of 100% water to 100% acetonitrile was employed over 50 min (2%/min). First major peak (shaded) corresponds to the modified antibiotic.

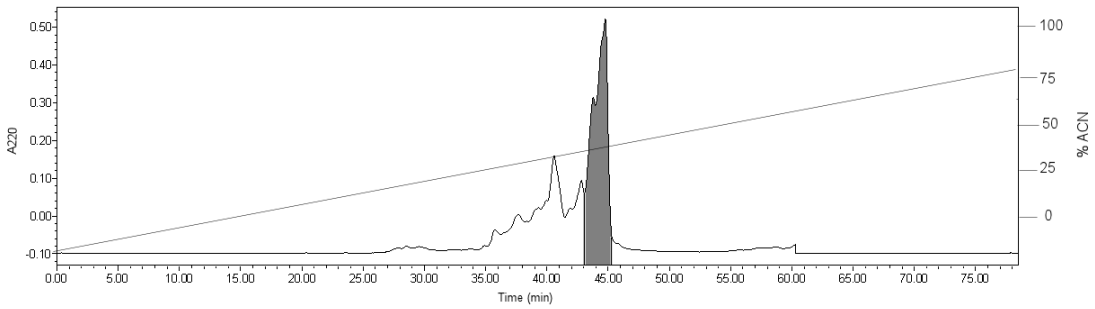

Figure 5. 18: Section of elution profile of the purification of mTS-2MESNA with 1%/min gradient. The gradient went from 100% water to 100% acetonitrile over 100 min. The area shaded indicates the fractions that contained the modified mTS-MESNA as shown with TLC.

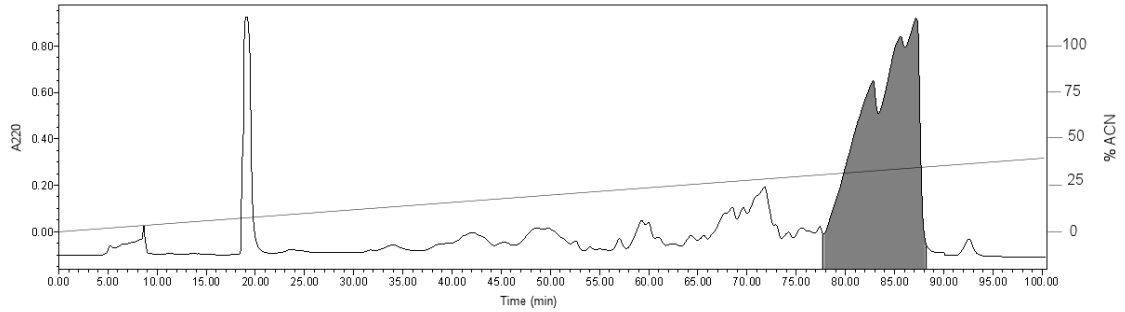

Figure 5. 19: Further separation was achieved with a slower gradient of 0.4%/min. The gradient went from 10% acetonitrile:90%water to 50% acetonitrile:50% water over 100 min. Area under shaded peak was collected and used for antibiotic susceptibility testing.

Mass spectrometric analysis of all purified samples showed a single successful modification (Figure 5.20). However, it remained unclear whether the modification had occurred at a single location or whether it was a mixture of singly modified products. NMR spectroscopy was used to further provide insight into the location of the conjugation. The NMR data was obtained and compared to the TS starting material (Figure 5.21) and peak assignments were based on previous ^{1}H NMR assignments published by in the literature by the groups of Anderson [255] and Floss [256].

Peaks corresponding to the dehydrobutyrine (Figure 5.4A; But) and the internal dehydroalanine (Figure 5.4A and Figure 5.21; Deala(1)) were still present. However, the peak intensity of signals corresponding to the dehydroalanine residues in the tail region (Figure 5.4A and Figure 5.21; Deala(2), Deala(3)) were reduced significantly. The lack of

presence of proton shifts for both Deala(2) and Deala(3) shows that successful single site modification has been achieved, although the product isolated is composed of both products modified at the different sites of the tail (Figure 5.20). This mixture of products was then tested for its biological activity.

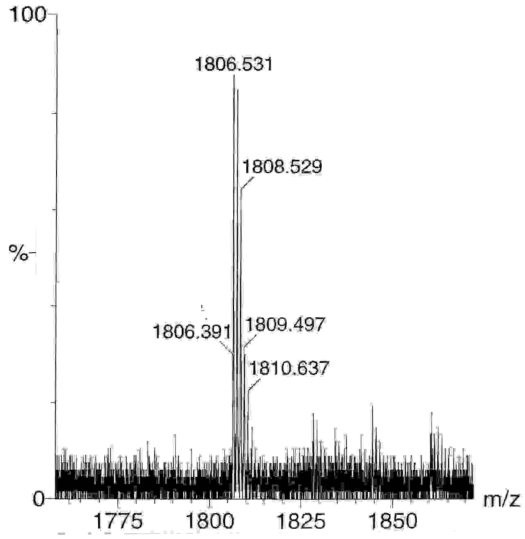

Figure 5. 20: Positive ion mode electrospray mass spectrum of mTS-2MESNA.
The expected molecular weight is calculated to be 1807 Da .The major peak indicates molecular weight corresponding to a mono-adduct.

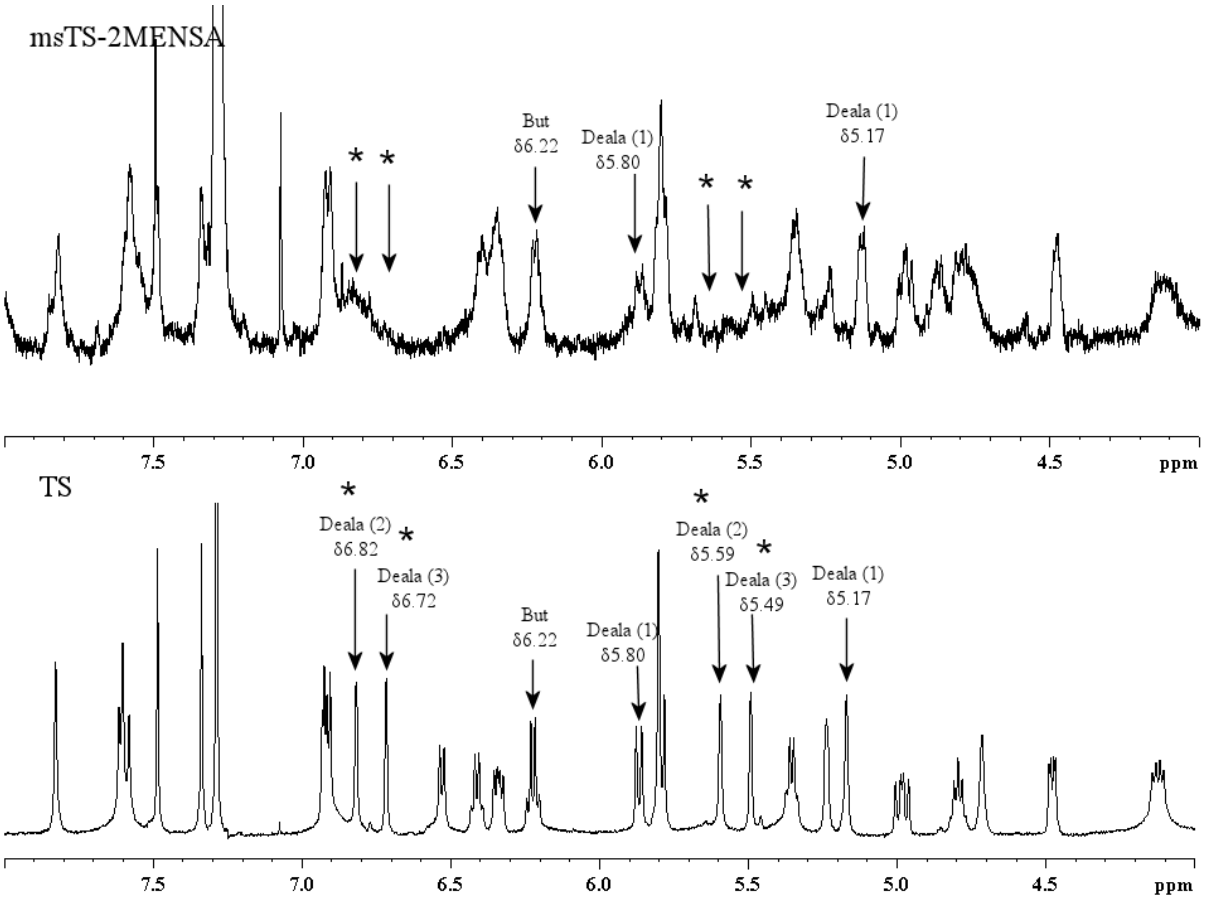

Figure 5. 21: Comparison of partial ^{1}H NMR spectrum of the modified TS (top) and the original TS (bottom) in $CDCl_3$.
Arrows show peaks corresponding to different protons in the four potential sites of modification. Asterisks (*) indicate the singles arising from protons of the dehydroalanine tails. Peaks corresponding to Deala(2) and Deala(3) were no longer present in the modified antibiotic.

5.3.4.3. Susceptibility Testing of mTS-2MESNA

Two Gram-positive species were used to evaluate the antibacterial activity of the TS derivative and compared to that of parent compound, namely *Staphylococcus aureus* and *Bacillus subtilis*. Both the TS and the TS derivative were dissolved in organic solvent (DMF) and in MQW with varying concentrations (Table 5.2 and Table 5.3). The activity of the antibiotic solutions was tested using disc diffusion methods and broth dilution methods.

Kirby-Bauer Disc Diffusion Tests

Antibiotic and antibiotic analogue impregnated discs were put on the surface of the agar medium that had been previously inoculated with a pure bacterial suspension of either *S. aureus* or *B. subtilis*. After incubation of 16 h, zones of inhibition were measured and compared (Table 5.7).

Table 5. 7: Inhibition Zone Diameters of Thiostrepton and its Derivative on *B. subtilis* and *S. aureus*.

	Diameter of Growth Inhibition Zone (mm)								
	DMF					**H_2O**			
	B. subtilis		***S. aureus***			***B. subtilis***		***S. aureus***	
Conc (μg/mL)	**TS**	**mTS-2MESNA**	**TS**	**mTS-2MESNA**	**Conc (μg/mL)**	**TS**	**mTS-2MESNA**	**TS**	**mTS-2MESNA**
0	6.5	6.5	6.5	6.5	0	6.5	6.5	6.5	6.5
0.03	7.1	6.5	7.0	6.5	10	6.5	6.5	6.5	6.5
0.3	7.2	7.0	8.0	6.7	25	7.2	8.8	10.0	10.2
3	12.0	8.0	12.7	8.0	50	10.5	11.0	10.5	12.6

At all concentrations in organic solvent, it was found that the unmodified compound exhibited similar or slightly larger zones of growth inhibition for both bacterial species. However, at the same concentrations (0, 0.03, 03 and 3 μg/mL) in water, it was found that there was no effect on bacterial growth. This is very likely due to the inherent low water solubility for both the native TS and the modified compound. Similar difficulties in dissolving the mTS-2MESNA during purification (*section 5.3.4.2*) and the parent TS were encountered. Concentrations three to one thousand times higher (10, 25, 50 μg/mL) were also examined and slightly larger diameters of inhibition zones were observed for the mTS-2MESNA. This indicates that although the parent compound has a higher overall activity in organic solvent, in an aqueous environment, the modified TS was shown to have higher activity, therefore, correlating to higher water solubility.

In vitro Susceptibility Curve

The effect of the TS derivative on bacterial growth curves of both *B. subtilis* and *S. aureus* were studied. Initial growth curve studies were performed with liquid media with concentrations of antibiotic solutions that gave the largest clearing zone in the disc diffusion tests (3 μg/mL in DMF and 50 μg/mL in H_2O), however, complete inhibition was observed and antibiotic concentrations were reduced to 0.3 μg/mL and 0.1 μg/mL in DMF and 5 μg/mL and 1 μg/mL in H_2O (Figure 5.22).

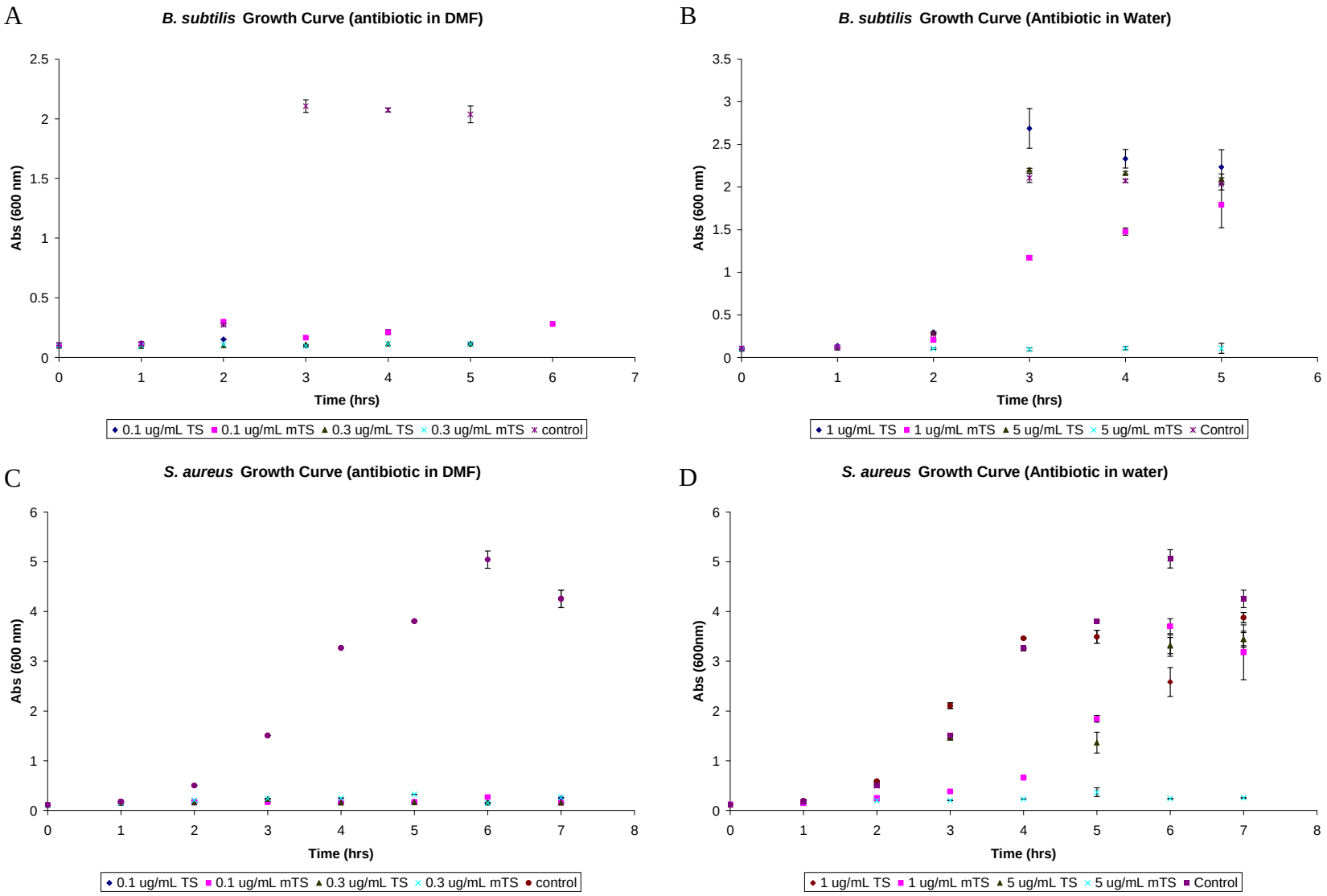

Figure 5. 22: Bacterial growth curves for *B. subtilis* (A and B) and *S. aureus* (C and D) in the presence of antibiotic in aqueous or organic solvent.

For both *B. subtilis* and *S. aureus*, TS and its modified counterpart inhibited growth completely at concentrations as low as 0.1 μg/mL and 0.3 μg/mL (Figure 5.22 A and C). However when the solutions of antibiotics were made in water, bacterial growth was observed for all antibiotics with concentrations of 0.1 μg/mL. It was only at a higher concentration of antibiotic (5 μg/mL) that inhibition was observed by only mTS-2MESNA. Thus, similar to the disc diffusion results, the modified thiostrepton is more active when administered in aqueous solution.

5.4. Conclusions and Future Work

Two approaches were utilized in studying the structure-activity relationship of TS, a representative of a major class of thiazole peptide antibiotics. First, a detailed molecular mechanics-based conformational search, stochastic dynamics, semi-empirical and *ab initio* studies on TS yielded a number of insights into its structure including the potential pyramidalization of the secondary amine and aspects of the mobility of the TS loops. In addition, the focus has provided detailed electronic structure parameters on the antibiotic, including providing knowledge of the position of the HOMO or LUMO orbitals and the electrostatic charges of TS. This information should serve as an important basis for future studies on TS and other thiazole peptide antibiotic and their interaction with biological samples.

Second, a single addition of 2-mercaptoethanesulfonic acid (2-MESNA) to the TS didehydroalanine tail has been successfully made. A mixture of the didehydroalanine addition product can be attained using a C_{18} reverse phase column on the HPLC. It was demonstrated through Kirby-Bauer disc diffusion and *in vitro* susceptibility growth tests that

the thiostrepton-2MESNA conjugates were more active than the parent TS compound in aqueous solution. Further information on the activity of the modified compound could be obtained by measuring the minimal inhibitory concentrations (MIC) of the antibiotics.

Given that there are two sites that are possible for the modification of the TS tail, each position can give two different enantiomeric products (R and S) for a total of four products. Therefore, the aforementioned modified antibiotic in fact is a mixture two conjugation products, and further separation is required to separate these chemical species.

Further resolution can be achieved by employing a gradient of 0.17% /min (25% ACN: 75% H_2O to 35% ACN: 65% H_2O over 78 min) on the major peak collected from previous gradient of 0.4%/min (10% ACN: 90% H_2O to 50% ACN: 50% H_2O over 100 min, Figure 5.19), and can be seen in Figure 5.23.

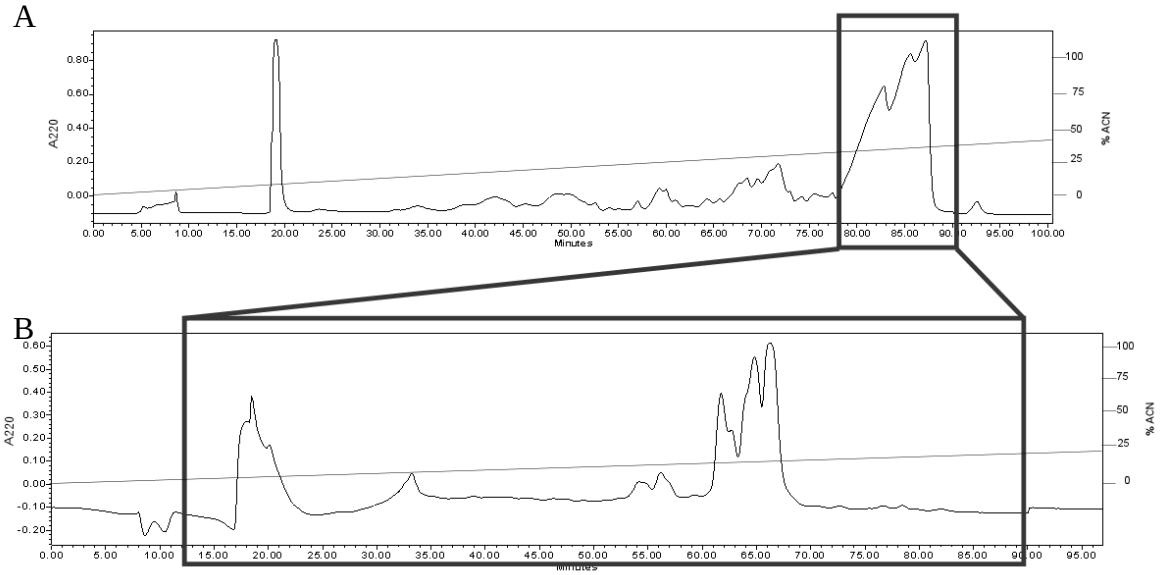

Figure 5. 23: Further purification of mTS-2MESNA.
(A) Purification of mTS-2MESNA with a 0.4%/min (10% acetonitrile:90%water to 50% acetonitrile:50% water over 100 min). Peak highlighted was pooled, and further resolution was achieved with a 0.17% gradient from 25% ACN:75% H_2O to 38% ACN:65% H_2O over 78 min **(B)**.

Therefore, collection of peaks can be further discriminated to optimize separation and discrete peaks can collected, isolated and characterized before testing against for biological activity in the future.

REFERENCES

1. Jones RS, Gelbart WM: **The Drosophila Polycomb-group gene Enhancer of zeste contains a region with sequence similarity to trithorax**. *Mol Cell Biol* 1993, **13**:6357-6366.
2. Cantoni GL: **The nature of the active methyl donor formed enzymatically from l-methionine and adenosinetriphosphate**. *J. Am. Chem. Soc* 1952, **74**:2942-2943.
3. Cantoni GL: **Biological methylation: selected aspects**. *Annu Rev Biochem* 1975, **44**:435-451.
4. Lu SC: **S-Adenosylmethionine**. *Int J Biochem Cell Biol* 2000, **32**:391-395.
5. Kotb M, Geller AM: **Methionine adenosyltransferase: structure and function**. *Pharmacol Ther* 1993, **59**:125-143.
6. Fontecave M, Atta M, Mulliez E: **S-adenosylmethionine: nothing goes to waste**. *Trends Biochem Sci* 2004, **29**:243-249.
7. Roje S: **S-Adenosyl-L-methionine: beyond the universal methyl group donor**. *Phytochemistry* 2006, **67**:1686-1698.
8. Chiang PK, Gordon RK, Tal J, Zeng GC, Doctor BP, Pardhasaradhi K, McCann PP: **S-Adenosylmethionine and methylation**. *Faseb J* 1996, **10**:471-480.
9. Loenen WA: **S-adenosylmethionine: jack of all trades and master of everything?** *Biochem Soc Trans* 2006, **34**:330-333.
10. Schubert HL, Blumenthal RM, Cheng X: **Many paths to methyltransfer: a chronicle of convergence**. *Trends Biochem Sci* 2003, **28**:329-335.
11. Deguchi T, Barchas J: **Inhibition of transmethylations of biogenic amines by S-adenosylhomocysteine. Enhancement of transmethylation by adenosylhomocysteinase**. *J Biol Chem* 1971, **246**:3175-3181.
12. Martin JL, McMillan FM: **SAM (dependent) I AM: the S-adenosylmethionine-dependent methyltransferase fold**. *Curr Opin Struct Biol* 2002, **12**:783-793.
13. Cheng X, Kumar S, Klimasauskas S, Roberts RJ: **Crystal structure of the HhaI DNA methyltransferase**. *Cold Spring Harb Symp Quant Biol* 1993, **58**:331-338.
14. Rao ST, Rossmann MG: **Comparison of super-secondary structures in proteins**. *J Mol Biol* 1973, **76**:241-256.
15. Cheng X, Blumenthal RM: *S-Adenosylmethionine-Dependent Methyltransferases: Strucure and Functions*. Singapore: World Scientific Publishing; 1999.
16. Vidgren J, Svensson LA, Liljas A: **Crystal structure of catechol O-methyltransferase**. *Nature* 1994, **368**:354-358.
17. Kagan RM, Clarke S: **Widespread occurrence of three sequence motifs in diverse S-adenosylmethionine-dependent methyltransferases suggests a common structure for these enzymes**. *Arch Biochem Biophys* 1994, **310**:417-427.
18. Kozbial PZ, Mushegian AR: **Natural history of S-adenosylmethionine-binding proteins**. *BMC Struct Biol* 2005, **5**:19.
19. Posfai J, Bhagwat AS, Posfai G, Roberts RJ: **Predictive motifs derived from cytosine methyltransferases**. *Nucleic Acids Res* 1989, **17**:2421-2435.
20. Schluckebier G, O'Gara M, Saenger W, Cheng X: **Universal catalytic domain structure of AdoMet-dependent methyltransferases**. *J Mol Biol* 1995, **247**:16-20.

21. Malone T, Blumenthal RM, Cheng X: **Structure-guided analysis reveals nine sequence motifs conserved among DNA amino-methyltransferases, and suggests a catalytic mechanism for these enzymes**. *J Mol Biol* 1995, **253**:618-632.
22. Dixon MM, Huang S, Matthews RG, Ludwig M: **The structure of the C-terminal domain of methionine synthase: presenting S-adenosylmethionine for reductive methylation of B12**. *Structure* 1996, **4**:1263-1275.
23. Schubert HL, Wilson KS, Raux E, Woodcock SC, Warren MJ: **The X-ray structure of a cobalamin biosynthetic enzyme, cobalt-precorrin-4 methyltransferase**. *Nat Struct Biol* 1998, **5**:585-592.
24. Vevodova J, Graham RM, Raux E, Schubert HL, Roper DI, Brindley AA, Ian Scott A, Roessner CA, Stamford NP, Elizabeth Stroupe M, et al.: **Structure/function studies on a S-adenosyl-L-methionine-dependent uroporphyrinogen III C methyltransferase (SUMT), a key regulatory enzyme of tetrapyrrole biosynthesis**. *J Mol Biol* 2004, **344**:419-433.
25. Wada K, Harada J, Yaeda Y, Tamiaki H, Oh-Oka H, Fukuyama K: **Crystal structures of CbiL, a methyltransferase involved in anaerobic vitamin B biosynthesis, and CbiL in complex with S-adenosylhomocysteine--implications for the reaction mechanism**. *Febs J* 2007, **274**:563-573.
26. Nureki O, Shirouzu M, Hashimoto K, Ishitani R, Terada T, Tamakoshi M, Oshima T, Chijimatsu M, Takio K, Vassylyev DG, et al.: **An enzyme with a deep trefoil knot for the active-site architecture**. *Acta Crystallogr D Biol Crystallogr* 2002, **58**:1129-1137.
27. Tkaczuk KL, Dunin-Horkawicz S, Purta E, Bujnicki JM: **Structural and evolutionary bioinformatics of the SPOUT superfamily of methyltransferases**. *BMC Bioinformatics* 2007, **8**:73.
28. Gustafsson C, Reid R, Greene PJ, Santi DV: **Identification of new RNA modifying enzymes by iterative genome search using known modifying enzymes as probes**. *Nucleic Acids Res* 1996, **24**:3756-3762.
29. Anantharaman V, Koonin EV, Aravind L: **SPOUT: a class of methyltransferases that includes spoU and trmD RNA methylase superfamilies, and novel superfamilies of predicted prokaryotic RNA methylases**. *J Mol Microbiol Biotechnol* 2002, **4**:71-75.
30. Tschiersch B, Hofmann A, Krauss V, Dorn R, Korge G, Reuter G: **The protein encoded by the Drosophila position-effect variegation suppressor gene Su(var)3-9 combines domains of antagonistic regulators of homeotic gene complexes**. *Embo J* 1994, **13**:3822-3831.
31. Stassen MJ, Bailey D, Nelson S, Chinwalla V, Harte PJ: **The Drosophila trithorax proteins contain a novel variant of the nuclear receptor type DNA binding domain and an ancient conserved motif found in other chromosomal proteins**. *Mech Dev* 1995, **52**:209-223.
32. Dillon SC, Zhang X, Trievel RC, Cheng X: **The SET-domain protein superfamily: protein lysine methyltransferases**. *Genome Biol* 2005, **6**:227.
33. Yeates TO: **Structures of SET domain proteins: protein lysine methyltransferases make their mark**. *Cell* 2002, **111**:5-7.
34. Qian C, Zhou MM: **SET domain protein lysine methyltransferases: Structure, specificity and catalysis**. *Cell Mol Life Sci* 2006, **63**:2755-2763.

35. Kurowski MA, Sasin JM, Feder M, Debski J, Bujnicki JM: **Characterization of the cofactor-binding site in the SPOUT-fold methyltransferases by computational docking of S-adenosylmethionine to three crystal structures**. *BMC Bioinformatics* 2003, **4**:9.
36. Borchardt RT, Huber JA, Wu YS: **Potential inhibitors of S-adenosylmethionine-dependent methyltransferases. 4. Further modifications of the amino and base portions of S-adenosyl-L-homocysteine**. *J Med Chem* 1976, **19**:1094-1099.
37. Borchardt RT, Shiong Y, Huber JA, Wycpalek AF: **Potential inhibitors of S-adenosylmethionine-dependent methyltransferases. 6. Structural modifications of S-adenosylmethionine**. *J Med Chem* 1976, **19**:1104-1110.
38. Borchardt RT, Wu YS: **Potential inhibitors of S-adenosylmethionine-dependent methyltransferases. 1. Modification of the amino acid portion of S-adenosylhomocysteine**. *J Med Chem* 1974, **17**:862-868.
39. Borchardt RT, Huber JA, Wu YS: **Potential inhibitor of S-adenosylmethionine-dependent methyltransferases. 2. Modification of the base portion of S-adenosylhomocysteine**. *J Med Chem* 1974, **17**:868-873.
40. Borchardt RT, Wu YS: **Potential inhibitors of S-adenosylmethionine-dependent methyltransferases. 3. Modifications of the sugar portion of S-adenosylhomocysteine**. *J Med Chem* 1975, **18**:300-304.
41. Borchardt RT, Wu YS, Wu BS: **Potential inhibitors of S-adenosylmethionine-dependent methyltransferases. 7. Role of the ribosyl moiety in enzymatic binding of S-adenosyl-L-homocysteine and S-adenosyl-L-methionine**. *J Med Chem* 1978, **21**:1307-1310.
42. O'Dea RF, Pons G, Hansen JA, Mirkin BL: **Characterization of protein carboxyl-O-methyltransferase in the spontaneous in vivo murine C-1300 neuroblastoma**. *Cancer Res* 1982, **42**:4433-4436.
43. Glick JM, Leboy PS: **Purification and properties of tRNA(adenine-1)-methyltransferase from rat liver**. *J Biol Chem* 1977, **252**:4790-4795.
44. Johnson BA, Aswad DW: **Kinetic properties of bovine brain protein L-isoaspartyl methyltransferase determined using a synthetic isoaspartyl peptide substrate**. *Neurochem Res* 1993, **18**:87-94.
45. Heady JE, Kerr SJ: **Purification and characterization of glycine N-methyltransferase**. *J Biol Chem* 1973, **248**:69-72.
46. Yokochi T, Robertson KD: **Preferential methylation of unmethylated DNA by Mammalian de novo DNA methyltransferase Dnmt3a**. *J Biol Chem* 2002, **277**:11735-11745.
47. Baudry M, Chast F, Schwartz JC: **Studies on S-adenosylhomocysteine inhibition of histamine transmethylation in brain**. *J Neurochem* 1973, **20**:13-21.
48. Hamil RL, Hoehn MM: **A9145, a new adenine-containing antifungal antibiotic. I. Discovery and isolation**. *J Antibiot (Tokyo)* 1973, **26**:463-465.
49. Borchardt RT, Eiden LE, Wu B, Rutledge CO: **Sinefungin, a potent inhibitor or S-adenosylmethionine: protein O-methyltransferase**. *Biochem Biophys Res Commun* 1979, **89**:919-924.
50. Pugh CS, Borchardt RT, Stone HO: **Sinefungin, a potent inhibitor of virion mRNA(guanine-7-)-methyltransferase, mRNA(nucleoside-2'-)-methyltransferase, and viral multiplication**. *J Biol Chem* 1978, **253**:4075-4077.

51. Ueland PM: **Pharmacological and biochemical aspects of S-adenosylhomocysteine and S-adenosylhomocysteine hydrolase**. *Pharmacol Rev* 1982, **34**:223-253.
52. Vedel M, Lawrence F, Robert-Gero M, Lederer E: **The antifungal antibiotic sinefungin as a very active inhibitor of methyltransferases and of the transformation of chick embryo fibroblasts by Rous sarcoma virus**. *Biochem Biophys Res Commun* 1978, **85**:371-376.
53. Shlaes DM: **The abandonment of antibacterials: why and wherefore?** *Curr Opin Pharmacol* 2003, **3**:470-473.
54. Yoneyama H, Katsumata R: **Antibiotic resistance in bacteria and its future for novel antibiotic development**. *Biosci Biotechnol Biochem* 2006, **70**:1060-1075.
55. Sigerist HE: *The Great Doctors*. New York: Cover Publications; 1971.
56. Davies J: **Bacteria on the rampage**. *Nature* 1996, **383**:219-220.
57. Neu HC: **The crisis in antibiotic resistance**. *Science* 1992, **257**:1064-1073.
58. McDermott PF, Walker RD, White DG: **Antimicrobials: modes of action and mechanisms of resistance**. *Int J Toxicol* 2003, **22**:135-143.
59. Walsh C: **Where will new antibiotics come from?** *Nat Rev Microbiol* 2003, **1**:65-70.
60. Walsh C: **Molecular mechanisms that confer antibacterial drug resistance**. *Nature* 2000, **406**:775-781.
61. Poole K: **Mechanisms of bacterial biocide and antibiotic resistance**. *J Appl Microbiol* 2002, **92 Suppl**:55S-64S.
62. Cloutier MJ: **Antibiotics: Mechanisms of Action and the Acquisition of Resistance - When Magic Bullets Lose Their Magic**. *Am J Pharm Educ* 1995, **59**.
63. Tenover FC: **Mechanisms of antimicrobial resistance in bacteria**. *Am J Med* 2006, **119**:S3-10; discussion S62-70.
64. Watve MG, Tickoo R, Jog MM, Bhole BD: **How many antibiotics are produced by the genus Streptomyces?** *Arch Microbiol* 2001, **176**:386-390.
65. Cundliffe E: **How antibiotic-producing organisms avoid suicide**. *Annu Rev Microbiol* 1989, **43**:207-233.
66. Auerbach T, Bashan A, Harms J, Schluenzen F, Zarivach R, Bartels H, Agmon I, Kessler M, Pioletti M, Franceschi F, et al.: **Antibiotics targeting ribosomes: crystallographic studies**. *Curr Drug Targets Infect Disord* 2002, **2**:169-186.
67. Nakajima Y: **Mechanisms of bacterial resistance to macrolide antibiotics**. *J Infect Chemother* 1999, **5**:61-74.
68. McGuire JM, Bunch RL, Anderson RC, Boaz HE, Flynn EH, Powell HM, Smith JW: **Ilotycin, a new antibiotic.** *Antibiot Chemother* 1952, **2**:281-283.
69. Oleinick NL: **The Erythromycins**. In *Mechanism of Action of Antimicrobial and Antitumor Agents*. Edited by Corcoran JW, Hanh FE: Springer; 1975. vol III.]
70. Contreras A, Vazquez D: **Cooperative and antagonistic interactions of peptidyl-tRNA and antibiotics with bacterial ribosomes**. *Eur J Biochem* 1977, **74**:539-547.
71. Yonath A: **Antibiotics targeting ribosomes: resistance, selectivity, synergism and cellular regulation**. *Annu Rev Biochem* 2005, **74**:649-679.
72. Hansen LH, Mauvais P, Douthwaite S: **The macrolide-ketolide antibiotic binding site is formed by structures in domains II and V of 23S ribosomal RNA**. *Mol Microbiol* 1999, **31**:623-631.
73. Ban N, Nissen P, Hansen J, Moore PB, Steitz TA: **The complete atomic structure of the large ribosomal subunit at 2.4 A resolution**. *Science* 2000, **289**:905-920.

74. Xiong L, Shah S, Mauvais P, Mankin AS: **A ketolide resistance mutation in domain II of 23S rRNA reveals the proximity of hairpin 35 to the peptidyl transferase centre**. *Mol Microbiol* 1999, **31**:633-639.
75. Douthwaite S, Champney WS: **Structures of ketolides and macrolides determine their mode of interaction with the ribosomal target site**. *J Antimicrob Chemother* 2001, **48 Suppl T1**:1-8.
76. Davydova N, Streltsov V, Wilce M, Liljas A, Garber M: **L22 ribosomal protein and effect of its mutation on ribosome resistance to erythromycin**. *J Mol Biol* 2002, **322**:635-644.
77. Hansen JL, Ippolito JA, Ban N, Nissen P, Moore PB, Steitz TA: **The structures of four macrolide antibiotics bound to the large ribosomal subunit**. *Mol Cell* 2002, **10**:117-128.
78. Schlunzen F, Zarivach R, Harms J, Bashan A, Tocilj A, Albrecht R, Yonath A, Franceschi F: **Structural basis for the interaction of antibiotics with the peptidyl transferase centre in eubacteria**. *Nature* 2001, **413**:814-821.
79. Denoya C, Dubnau D: **Mono- and dimethylating activities and kinetic studies of the ermC 23 S rRNA methyltransferase**. *J Biol Chem* 1989, **264**:2615-2624.
80. Denoya CD, Dubnau D: **Site and substrate specificity of the ermC 23S rRNA methyltransferase**. *J Bacteriol* 1987, **169**:3857-3860.
81. Weisblum B: **Erythromycin resistance by ribosome modification**. *Antimicrob Agents Chemother* 1995, **39**:577-585.
82. Leclercq R, Courvalin P: **Bacterial resistance to macrolide, lincosamide, and streptogramin antibiotics by target modification**. *Antimicrob Agents Chemother* 1991, **35**:1267-1272.
83. Doi Y, Arakawa Y: **16S ribosomal RNA methylation: emerging resistance mechanism against aminoglycosides**. *Clin Infect Dis* 2007, **45**:88-94.
84. Beauclerk AA, Cundliffe E: **Sites of action of two ribosomal RNA methylases responsible for resistance to aminoglycosides**. *J Mol Biol* 1987, **193**:661-671.
85. Treede I, Jakobsen L, Kirpekar F, Vester B, Weitnauer G, Bechthold A, Douthwaite S: **The avilamycin resistance determinants AviRa and AviRb methylate 23S rRNA at the guanosine 2535 base and the uridine 2479 ribose**. *Mol Microbiol* 2003, **49**:309-318.
86. Kehrenberg C, Schwarz S, Jacobsen L, Hansen LH, Vester B: **A new mechanism for chloramphenicol, florfenicol and clindamycin resistance: methylation of 23S ribosomal RNA at A2503**. *Mol Microbiol* 2005, **57**:1064-1073.
87. Bagley MC, Dale JW, Merritt EA, Xiong X: **Thiopeptide antibiotics**. *Chem Rev* 2005, **105**:685-714.
88. Donovick R, Pagano JF, Stout HA, Weinstein MJ: **Thiostrepton, a new antibiotic. I. In vitro studies**. *Antibiot Annu* 1955, **3**:554-559.
89. Jambor WP, Steinberg BA, Suydam LO: **Thiostrepton, a new antibiotic. III. In vivo studies**. *Antibiot Annu* 1955, **3**:562-565.
90. Cron MJ, Whitehead DF, Hooper IR, Heinemann B, Lein J: **Braymycin, a new antibiotic**. *Antibiot Chemother* 1956, **6**:63-67.
91. Trejo WH, Dean LD, Pluscec J, Meyers E, Brown WE: **Streptomyces laurentii, a new species producing thiostrepton**. *J Antibiot (Tokyo)* 1977, **30**:639-643.

92. Cundliffe E: **Thiostrepton and Related Antibiotics**. In *Mechanism of Action of Antibacterial Agents*. Edited by Hanh FE: Springer; 1979. vol V.]
93. Clough B, Strath M, Preiser P, Denny P, Wilson IR: **Thiostrepton binds to malarial plastid rRNA**. *FEBS Lett* 1997, **406**:123-125.
94. Cundliffe E, Thompson J: **Ribose methylation and resistance to thiostrepton**. *Nature* 1979, **278**:859-861.
95. Egebjerg J, Douthwaite S, Garrett RA: **Antibiotic interactions at the GTPase-associated centre within Escherichia coli 23S rRNA**. *Embo J* 1989, **8**:607-611.
96. Porse BT, Leviev I, Mankin AS, Garrett RA: **The antibiotic thiostrepton inhibits a functional transition within protein L11 at the ribosomal GTPase centre**. *J Mol Biol* 1998, **276**:391-404.
97. Thompson J, Cundliffe E, Stark M: **Binding of thiostrepton to a complex of 23-S rRNA with ribosomal protein L11**. *Eur J Biochem* 1979, **98**:261-265.
98. Thompson J, Cundliffe E: **The binding of thiostrepton to 23S ribosomal RNA**. *Biochimie* 1991, **73**:1131-1135.
99. Xing Y, Draper DE: **Cooperative interactions of RNA and thiostrepton antibiotic with two domains of ribosomal protein L11**. *Biochemistry* 1996, **35**:1581-1588.
100. Conn GL, Draper DE, Lattman EE, Gittis AG: **Crystal structure of a conserved ribosomal protein-RNA complex**. *Science* 1999, **284**:1171-1174.
101. Xing Y, Guha Thakurta D, Draper DE: **The RNA binding domain of ribosomal protein L11 is structurally similar to homeodomains**. *Nat Struct Biol* 1997, **4**:24-27.
102. Cundliffe E: **Involvement of specific portions of rRNA in defined ribosoma fuctions: a study utilizing antibiotics.** In *Structure, Function and Genetics of Ribosomes*. Edited by Hardesty B, Kramer G: Springer-Verlag; 1986:586-604.
103. Cameron DM, Thompson J, March PE, Dahlberg AE: **Initiation factor IF2, thiostrepton and micrococcin prevent the binding of elongation factor G to the Escherichia coli ribosome**. *J Mol Biol* 2002, **319**:27-35.
104. Agrawal RK, Linde J, Sengupta J, Nierhaus KH, Frank J: **Localization of L11 protein on the ribosome and elucidation of its involvement in EF-G-dependent translocation**. *J Mol Biol* 2001, **311**:777-787.
105. Wimberly BT, Guymon R, McCutcheon JP, White SW, Ramakrishnan V: **A detailed view of a ribosomal active site: the structure of the L11-RNA complex**. *Cell* 1999, **97**:491-502.
106. Jonker HR, Ilin S, Grimm SK, Wohnert J, Schwalbe H: **L11 domain rearrangement upon binding to RNA and thiostrepton studied by NMR spectroscopy**. *Nucleic Acids Res* 2007, **35**:441-454.
107. Harms JM, Wilson DN, Schluenzen F, Connell SR, Stachelhaus T, Zaborowska Z, Spahn CM, Fucini P: **Translational regulation via L11: molecular switches on the ribosome turned on and off by thiostrepton and micrococcin**. *Mol Cell* 2008, **30**:26-38.
108. Lee D, Walsh JD, Yu P, Markus MA, Choli-Papadopoulou T, Schwieters CD, Krueger S, Draper DE, Wang YX: **The structure of free L11 and functional dynamics of L11 in free, L11-rRNA(58 nt) binary and L11-rRNA(58 nt)-thiostrepton ternary complexes**. *J Mol Biol* 2007, **367**:1007-1022.

109. Savelsbergh A, Mohr D, Kothe U, Wintermeyer W, Rodnina MV: **Control of phosphate release from elongation factor G by ribosomal protein L7/12**. *Embo J* 2005, **24**:4316-4323.
110. Thompson J, Cundliffe E: **Resistance to thiostrepton, siomycin, and sporangiomycin in actinomycetes that produce them**. *J Bacteriol* 1980, **142**:455-461.
111. Cundliffe E: **Mechanism of resistance to thiostrepton in the producing-organism Streptomyces azureus**. *Nature* 1978, **272**:792-795.
112. Thompson J, Schmidt F, Cundliffe E: **Site of action of a ribosomal RNA methylase conferring resistance to thiostrepton**. *J Biol Chem* 1982, **257**:7915-7917.
113. Bechthold A, Floss HG: **Overexpression of the thiostrepton-resistance gene from Streptomyces azureus in Escherichia coli and characterization of recognition sites of the 23S rRNA A1067 2'-methyltransferase in the guanosine triphosphatase center of 23S ribosomal RNA**. *Eur J Biochem* 1994, **224**:431-437.
114. Thompson J, Cundliffe E: **Purification and Properties of an RNA Methylase Produced by Streptomyces azureus and Involved in Resistance to Thiostrepton**. *J. Gen. Micro.* 1981, **124**:291-297.
115. Watanabe K, Nureki O, Fukai S, Ishii R, Okamoto H, Yokoyama S, Endo Y, Hori H: **Roles of conserved amino acid sequence motifs in the SpoU (TrmH) RNA methyltransferase family**. *J Biol Chem* 2005, **280**:10368-10377.
116. Virnau P, Mirny LA, Kardar M: **Intricate knots in proteins: Function and evolution**. *PLoS Comput Biol* 2006, **2**:e122.
117. Arnau J, Lauritzen C, Petersen GE, Pedersen J: **Current strategies for the use of affinity tags and tag removal for the purification of recombinant proteins**. *Protein Expr Purif* 2006, **48**:1-13.
118. Hearn MT, Acosta D: **Applications of novel affinity cassette methods: use of peptide fusion handles for the purification of recombinant proteins**. *J Mol Recognit* 2001, **14**:323-369.
119. Lichty JJ, Malecki JL, Agnew HD, Michelson-Horowitz DJ, Tan S: **Comparison of affinity tags for protein purification**. *Protein Expr Purif* 2005, **41**:98-105.
120. Sun QM, Chen LL, Cao L, Fang L, Chen C, Hua ZC: **An improved strategy for high-level production of human vasostatin120-180**. *Biotechnol Prog* 2005, **21**:1048-1052.
121. Chen H, Xu Z, Xu N, Cen P: **Efficient production of a soluble fusion protein containing human beta-defensin-2 in E. coli cell-free system**. *J Biotechnol* 2005, **115**:307-315.
122. Kou G, Shi S, Wang H, Tan M, Xue J, Zhang D, Hou S, Qian W, Wang S, Dai J, et al.: **Preparation and characterization of recombinant protein ScFv(CD11c)-TRP2 for tumor therapy from inclusion bodies in Escherichia coli**. *Protein Expr Purif* 2007, **52**:131-138.
123. Tang W, Sun ZY, Pannell R, Gurewich V, Liu JN: **An efficient system for production of recombinant urokinase-type plasminogen activator**. *Protein Expr Purif* 1997, **11**:279-283.
124. Chant A, Kraemer-Pecore CM, Watkin R, Kneale GG: **Attachment of a histidine tag to the minimal zinc finger protein of the Aspergillus nidulans gene regulatory protein AreA causes a conformational change at the DNA-binding site**. *Protein Expr Purif* 2005, **39**:152-159.

125. Goel A, Colcher D, Koo JS, Booth BJ, Pavlinkova G, Batra SK: **Relative position of the hexahistidine tag effects binding properties of a tumor-associated single-chain Fv construct**. *Biochim Biophys Acta* 2000, **1523**:13-20.
126. Kim KM, Yi EC, Baker D, Zhang KY: **Post-translational modification of the N-terminal His tag interferes with the crystallization of the wild-type and mutant SH3 domains from chicken src tyrosine kinase**. *Acta Crystallogr D Biol Crystallogr* 2001, **57**:759-762.
127. Terpe K: **Overview of tag protein fusions: from molecular and biochemical fundamentals to commercial systems**. *Appl Microbiol Biotechnol* 2003, **60**:523-533.
128. Waugh DS: **Making the most of affinity tags**. *Trends Biotechnol* 2005, **23**:316-320.
129. Rais-Beghdadi C, Roggero MA, Fasel N, Reymond CD: **Purification of recombinant proteins by chemical removal of the affinity tag**. *Appl Biochem Biotechnol* 1998, **74**:95-103.
130. Banki MR, Wood DW: **Inteins and affinity resin substitutes for protein purification and scale up**. *Microb Cell Fact* 2005, **4**:32.
131. Porath J, Carlsson J, Olsson I, Belfrage G: **Metal chelate affinity chromatography, a new approach to protein fractionation**. *Nature* 1975, **258**:598-599.
132. Wray W, Boulikas T, Wray VP, Hancock R: **Silver staining of proteins in polyacrylamide gels**. *Anal Biochem* 1981, **118**:197-203.
133. Sambrook J, Fritsch E, Maniatis T: *Molecular Cloning: A laboratory Manual*. Plainsview, NY: Cold Spring Harbour Laboratory Press; 1989.
134. Bradford MM: **A rapid and sensitive method for the quantitation of microgram quantities of protein utilizing the principle of protein-dye binding**. *Anal Biochem* 1976, **72**:248-254.
135. Wilkinson DL, Harrison RG: **Predicting the solubility of recombinant proteins in Escherichia coli**. *Biotechnology (N Y)* 1991, **9**:443-448.
136. Georgiou G, Valax P: **Expression of correctly folded proteins in Escherichia coli**. *Curr Opin Biotechnol* 1996, **7**:190-197.
137. Georgiou G, Valax P: **Isolating inclusion bodies from bacteria**. *Methods Enzymol* 1999, **309**:48-58.
138. Chi EY, Krishnan S, Randolph TW, Carpenter JF: **Physical stability of proteins in aqueous solution: mechanism and driving forces in nonnative protein aggregation**. *Pharm Res* 2003, **20**:1325-1336.
139. Shimizu S, McLaren WM, Matubayasi N: **The Hofmeister series and protein-salt interactions**. *J Chem Phys* 2006, **124**:234905.
140. Priev A, Almagor A, Yedgar S, Gavish B: **Glycerol decreases the volume and compressibility of protein interior**. *Biochemistry* 1996, **35**:2061-2066.
141. Bondos SE, Bicknell A: **Detection and prevention of protein aggregation before, during, and after purification**. *Anal Biochem* 2003, **316**:223-231.
142. Sprules T, Green N, Featherstone M, Gehring K: **Nickel-induced oligomerization of proteins containing 10-histidine tags**. *Biotechniques* 1998, **25**:20-22.
143. Mosbacher TG, Bechthold A, Schulz GE: **Structure and function of the antibiotic resistance-mediating methyltransferase AviRb from Streptomyces viridochromogenes**. *J Mol Biol* 2005, **345**:535-545.

144. Graham DE, Kramer G: **Identification and characterization of archaeal and fungal tRNA methyltransferases**. *Methods Enzymol* 2007, **425**:185-209.
145. Oldham KG: **Radiometric Assays**. In *Enzyme Assays: A Practical Approach*. Edited by Eisenthal R, Danson M: Oxford University Press; 1992:93-122.
146. Bollum FJ: **Filter Paper Disk Techniques for Assaying Radioactive Macromolecules**. *Methods Enzymol* 1968, **12B**:169-173.
147. Hart HE, Greenwald EB: **Scintillation proximity assay (SPA)--a new method of immunoassay. Direct and inhibition mode detection with human albumin and rabbit antihuman albumin**. *Mol Immunol* 1979, **16**:265-267.
148. Dorgan KM, Wooderchak WL, Wynn DP, Karschner EL, Alfaro JF, Cui Y, Zhou ZS, Hevel JM: **An enzyme-coupled continuous spectrophotometric assay for S-adenosylmethionine-dependent methyltransferases**. *Anal Biochem* 2006, **350**:249-255.
149. Hendricks CL, Ross JR, Pichersky E, Noel JP, Zhou ZS: **An enzyme-coupled colorimetric assay for S-adenosylmethionine-dependent methyltransferases**. *Anal Biochem* 2004, **326**:100-105.
150. Collazo E, Couture JF, Bulfer S, Trievel RC: **A coupled fluorescent assay for histone methyltransferases**. *Anal Biochem* 2005, **342**:86-92.
151. Wang C, Leffler S, Thompson DH, Hrycyna CA: **A general fluorescence-based coupled assay for S-adenosylmethionine-dependent methyltransferases**. *Biochem Biophys Res Commun* 2005, **331**:351-356.
152. Capdevila A, Burk RF, Freedman J, Frantzen F, Alfheim I, Wagner C: **A simple rapid immunoassay for S-adenosylhomocysteine in plasma**. *J Nutr Biochem* 2007, **18**:827-831.
153. Woo YH, Rajagopalan PT, Benkovic SJ: **A nonradioactive DNA methyltransferase assay adaptable to high-throughput screening**. *Anal Biochem* 2005, **340**:336-340.
154. Farrell Jr RE: *RNA Methodologies: A Laboratory Guide for Isolation and Characterization*. Columbia: Academic Press; 1993.
155. Jones P, Qiu J, Rickwood D: *RNA: Isolation and Analysis*. Oxford: BIOS Scientific Publishers Ltd.; 1994.
156. Wilson KW, Walker J: *Principles and Techniques of Practical Biochemistry* edn 5th. Cambridge: Cambridge Univerisity Press; 2000.
157. Lentzen G, Klinck R, Matassova N, Aboul-ela F, Murchie AI: **Structural basis for contrasting activities of ribosome binding thiazole antibiotics**. *Chem Biol* 2003, **10**:769-778.
158. Pyle AM, Green JB: **RNA folding**. *Curr Opin Struct Biol* 1995, **5**:303-310.
159. Macarron R, Mensah L, Cid C, Carranza C, Benson N, Pope AJ, Diez E: **A homogeneous method to measure aminoacyl-tRNA synthetase aminoacylation activity using scintillation proximity assay technology**. *Anal Biochem* 2000, **284**:183-190.
160. Lai YL, Yen SC, Yu SH, Hwang JK: **pKNOT: the protein KNOT web server**. *Nucleic Acids Res* 2007, **35**:W420-424.
161. Taylor WR: **Protein knots and fold complexity: some new twists**. *Comput Biol Chem* 2007, **31**:151-162.

162. Misaghi S, Galardy PJ, Meester WJ, Ovaa H, Ploegh HL, Gaudet R: **Structure of the ubiquitin hydrolase UCH-L3 complexed with a suicide substrate**. *J Biol Chem* 2005, **280**:1512-1520.
163. Wallin S, Zeldovich KB, Shakhnovich EI: **The folding mechanics of a knotted protein**. *J Mol Biol* 2007, **368**:884-893.
164. Murzin AG, Brenner SE, Hubbard T, Chothia C: **SCOP: a structural classification of proteins database for the investigation of sequences and structures**. *J Mol Biol* 1995, **247**:536-540.
165. Michel G, Sauve V, Larocque R, Li Y, Matte A, Cygler M: **The structure of the RlmB 23S rRNA methyltransferase reveals a new methyltransferase fold with a unique knot**. *Structure* 2002, **10**:1303-1315.
166. Wallner B, Elofsson A: **All are not equal: a benchmark of different homology modeling programs**. *Protein Sci* 2005, **14**:1315-1327.
167. Yu H: **Extending the size limit of protein nuclear magnetic resonance**. *Proc Natl Acad Sci U S A* 1999, **96**:332-334.
168. Tramontano A: *Protein Structure Predictions*. Weinheim, Germany: Wiley-VCH Verlag Gmbh & Co. KGaA; 2006.
169. Nayeem A, Sitkoff D, Krystek S, Jr.: **A comparative study of available software for high-accuracy homology modeling: from sequence alignments to structural models**. *Protein Sci* 2006, **15**:808-824.
170. Arnold K, Bordoli L, Kopp J, Schwede T: **The SWISS-MODEL workspace: a web-based environment for protein structure homology modelling**. *Bioinformatics* 2006, **22**:195-201.
171. Xiang Z: **Advances in homology protein structure modeling**. *Curr Protein Pept Sci* 2006, **7**:217-227.
172. Marti-Renom MA, Stuart AC, Fiser A, Sanchez R, Melo F, Sali A: **Comparative protein structure modeling of genes and genomes**. *Annu Rev Biophys Biomol Struct* 2000, **29**:291-325.
173. Sanchez R, Sali A: **Advances in comparative protein-structure modelling**. *Curr Opin Struct Biol* 1997, **7**:206-214.
174. Ginalski K, Grishin NV, Godzik A, Rychlewski L: **Practical lessons from protein structure prediction**. *Nucleic Acids Res* 2005, **33**:1874-1891.
175. Bernstein FC, Koetzle TF, Williams GJ, Meyer EF, Jr., Brice MD, Rodgers JR, Kennard O, Shimanouchi T, Tasumi M: **The Protein Data Bank: a computer-based archival file for macromolecular structures**. *J Mol Biol* 1977, **112**:535-542.
176. Altschul SF, Gish W, Miller W, Myers EW, Lipman DJ: **Basic local alignment search tool**. *J Mol Biol* 1990, **215**:403-410.
177. Pearson WR: **Empirical statistical estimates for sequence similarity searches**. *J Mol Biol* 1998, **276**:71-84.
178. Altschul SF, Madden TL, Schaffer AA, Zhang J, Zhang Z, Miller W, Lipman DJ: **Gapped BLAST and PSI-BLAST: a new generation of protein database search programs**. *Nucleic Acids Res* 1997, **25**:3389-3402.
179. Ginalski K: **Comparative modeling for protein structure prediction**. *Curr Opin Struct Biol* 2006, **16**:172-177.
180. Chung SY, Subbiah S: **A structural explanation for the twilight zone of protein sequence homology**. *Structure* 1996, **4**:1123-1127.

181. Baker D, Sali A: **Protein structure prediction and structural genomics**. *Science* 2001, **294**:93-96.
182. Laskowski RA, McArthur MW, Moss DS, Thornton JM: **PROCHECK: a program tocheck the stereochemical quality of protein structures**. *J. Appl. Crystalogr.* 1993, **26**:631-639.
183. Luthy R, Bowie JU, Eisenberg D: **Assessment of protein models with three-dimensional profiles**. *Nature* 1992, **356**:83-85.
184. Guex N, Peitsch MC: **SWISS-MODEL and the Swiss-PdbViewer: an environment for comparative protein modeling**. *Electrophoresis* 1997, **18**:2714-2723.
185. Schwede T, Kopp J, Guex N, Peitsch MC: **SWISS-MODEL: An automated protein homology-modeling server**. *Nucleic Acids Res* 2003, **31**:3381-3385.
186. Jeanmougin F, Thompson JD, Gouy M, Higgins DG, Gibson TJ: **Multiple sequence alignment with Clustal X**. *Trends Biochem Sci* 1998, **23**:403-405.
187. Corpet F: **Multiple sequence alignment with hierarchical clustering**. *Nucleic Acids Res* 1988, **16**:10881-10890.
188. Melo F, Feytmans E: **Assessing protein structures with a non-local atomic interaction energy**. *J Mol Biol* 1998, **277**:1141-1152.
189. Laskowski RA, Watson JD, Thornton JM: **ProFunc: a server for predicting protein function from 3D structure**. *Nucleic Acids Res* 2005, **33**:W89-93.
190. Laskowski RA, Watson JD, Thornton JM: **Protein function prediction using local 3D templates**. *J Mol Biol* 2005, **351**:614-626.
191. Scott WRP, Hunenberger PH, Tironi IG, Mark AE, Billeter SR, Fennen J, Torda AE, Huber T, Kruger P, van Gunsteren WF: **The GROMOS Biomolecular Simulation Program Package**. *J. Phys. Chem. A* 1999, **103**:3596-3607.
192. Colovos C, Yeates TO: **Verification of protein structures: patterns of nonbonded atomic interactions**. *Protein Sci* 1993, **2**:1511-1519.
193. Wiederstein M, Sippl MJ: **ProSA-web: interactive web service for the recognition of errors in three-dimensional structures of proteins**. *Nucleic Acids Res* 2007, **35**:W407-410.
194. Kabsch W: **Evaluation of single crystal X-ray diffraction data from a position senstive detector**. *J Appl Crystallogr* 1988, **21**:916-924.
195. Collaborative Computational Project N: **The CCP4 Suite: Programs for protein crystallography**. *Acta Crystallogr D Biol Crystallogr* 1994, **50**:760-763.
196. Vagin A, Teplyako A: **MOLREP: an automated program for molecular replacement**. *J Appl Crystallogr* 1997, **30**:1022-1025.
197. Nureki O, Watanabe K, Fukai S, Ishii R, Endo Y, Hori H, Yokoyama S: **Deep knot structure for construction of active site and cofactor binding site of tRNA modification enzyme**. *Structure* 2004, **12**:593-602.
198. Sippl MJ: **Recognition of errors in three-dimensional structures of proteins**. *Proteins* 1993, **17**:355-362.
199. Ramachandran GN, Ramakrishnan C, Sasisekharan V: **Stereochemistry of polypeptide chain configurations**. *J Mol Biol* 1963, **7**:95-99.
200. Morris AL, MacArthur MW, Hutchinson EG, Thornton JM: **Stereochemical quality of protein structure coordinates**. *Proteins* 1992, **12**:345-364.

201. Guillen Schlippe YV, Hedstrom L: **Is Arg418 the catalytic base required for the hydrolysis step of the IMP dehydrogenase reaction?** *Biochemistry* 2005, **44**:11700-11707.
202. Hedstrom L, Gan L: **IMP dehydrogenase: structural schizophrenia and an unusual base**. *Curr Opin Chem Biol* 2006, **10**:520-525.
203. Holm L, Sander C: **Protein structure comparison by alignment of distance matrices**. *J Mol Biol* 1993, **233**:123-138.
204. Chao JA, Williamson JR: **Joint X-ray and NMR refinement of the yeast L30e-mRNA complex**. *Structure* 2004, **12**:1165-1176.
205. Mao H, White SA, Williamson JR: **A novel loop-loop recognition motif in the yeast ribosomal protein L30 autoregulatory RNA complex**. *Nat Struct Biol* 1999, **6**:1139-1147.
206. Klimasauskas S, Kumar S, Roberts RJ, Cheng X: **HhaI methyltransferase flips its target base out of the DNA helix**. *Cell* 1994, **76**:357-369.
207. Priyakumar UD, MacKerell AD, Jr.: **Computational approaches for investigating base flipping in oligonucleotides**. *Chem Rev* 2006, **106**:489-505.
208. Nicolaou KC, Safina BS, Zak M, Lee SH, Nevalainen M, Bella M, Estrada AA, Funke C, Zecri FJ, Bulat S: **Total synthesis of thiostrepton. Retrosynthetic analysis and construction of key building blocks**. *J Am Chem Soc* 2005, **127**:11159-11175.
209. Nicolaou KC, Zak M, Safina BS, Estrada AA, Lee SH, Nevalainen M: **Total synthesis of thiostrepton. Assembly of key building blocks and completion of the synthesis**. *J Am Chem Soc* 2005, **127**:11176-11183.
210. Anderson B, Hodgkin DC, Viswamitra MA: **The structure of thiostrepton**. *Nature* 1970, **225**:233-235.
211. Bond CS, Shaw MP, Alphey MS, Hunter WN: **Structure of the macrocycle thiostrepton solved using the anomalous dispersion contribution of sulfur**. *Acta Crystallogr D Biol Crystallogr* 2001, **57**:755-758.
212. Pascard C, Ducruix A, Lunel J, Prange T: **Highly modified cysteine-containing antibiotics. Chemical structure and configuration of nosiheptide**. *J Am Chem Soc* 1977, **99**:6418-6423.
213. Prange T, Ducruix A, Pascard C, Lunel J: **Structure of nosipeptide, a polythiazole-containing antibiotic**. *Nature* 1977, **265**:189-190.
214. Heffron SE, Jurnak F: **Structure of an EF-Tu complex with a thiazolyl peptide antibiotic determined at 2.35 A resolution: atomic basis for GE2270A inhibition of EF-Tu**. *Biochemistry* 2000, **39**:37-45.
215. Holtje HD, Sippl W, Rognan D, Folkders G: *Molecular Modeling: Basic Principles and Applications* edn 2nd. Weinheim: Wiley-VCH GmbH & Co KGaA; 2003.
216. Bowen JP, Allinger NL: *Molecular Mechanics: The Art and Science of Parameterization*, vol 2. Edited by Lipkowitz KB, Boyd DB. New York: VCH Publishers; 1991.
217. Stewart JJP: *Semiempirical Molecular Orbital Methods*, vol 2. Edited by Lipkowitz KB, Boyd DB. New York: VCH Publishers; 1990.
218. Leach AR: *Molecular Modelling: Principles and Applications* edn 2nd. Harlow, Essex, England: Prentice Hall; 2001.
219. Cramer CJ: *Essentials of Computational Chemistry* edn 2nd. West Sussex: John Wiley and Sons LTd; 2004.

220. Young DC: *Computational Chemistry: A Practical Guide for Applying Techniques for Real World Problems*. New York: Wiley Interscience; 2001.
221. Feller D, Davidson ER: *Basis Sets for Ab Initio Molecular Orbital Calculations and Intermolecular Interactions*, vol 1. Edited by Lipkowitz KB, Boyd DB. New York: VCH Publishers; 1990.
222. Reynolds CH: **Semiempirical MO methods: the middle ground in molecular modelling**. *J. Mol. Struct. (Theochem)* 1997, **401**:267-277.
223. von Ragué Schleyer P: **Application of semi-empirical and ab intio quantum mechanial calculations**. *J. Comput. Aided Mol. Des* 1988, **2**:223-224.
224. Dennis SM, Nagaraja TG, Dayton AD: **Effect of lasalocid, monensin and thiopeptin on rumen protozoa**. *Res Vet Sci* 1986, **41**:251-256.
225. Barrett CT, Barrett JF: **Antibacterials: are the new entries enough to deal with the emerging resistance problems?** *Curr Opin Biotechnol* 2003, **14**:621-626.
226. Kurath P, Jones PH, Egan RS, Perun TJ: **Acid degradation of erythromycin A and erythromycin B**. *Experientia* 1971, **27**:362.
227. Ackermann G, Rodloff AC: **Drugs of the 21st century: telithromycin (HMR 3647)--the first ketolide**. *J Antimicrob Chemother* 2003, **51**:497-511.
228. Leet JE, Li W, Ax HA, Matson JA, Huang S, Huang R, Cantone JL, Drexler D, Dalterio RA, Lam KS: **Nocathiacins, new thiazolyl peptide antibiotics from Nocardia sp. II. Isolation, characterization, and structure determination**. *J Antibiot (Tokyo)* 2003, **56**:232-242.
229. Li W, Leet JE, Ax HA, Gustavson DR, Brown DM, Turner L, Brown K, Clark J, Yang H, Fung-Tomc J, et al.: **Nocathiacins, new thiazolyl peptide antibiotics from Nocardia sp. I. Taxonomy, fermentation and biological activities**. *J Antibiot (Tokyo)* 2003, **56**:226-231.
230. Pucci MJ, Bronson JJ, Barrett JF, DenBleyker KL, Discotto LF, Fung-Tomc JC, Ueda Y: **Antimicrobial evaluation of nocathiacins, a thiazole peptide class of antibiotics**. *Antimicrob Agents Chemother* 2004, **48**:3697-3701.
231. Naidu BN, Li W, Sorenson ME, Connolly TP, Wichtowski JA, Zhang Y, Kim OK, Matiskella JD, Lam KS, Bronson JJ, et al.: **Organic reactions in frozen water: Michael addition of amines and thiols to the dehydroalanine side chain of nocathiacins**. *Tetrahedron Lett* 2004, **45**:1059-1063.
232. Naidu BN, Sorenson ME, Bronson JJ, Pucci MJ, Clark JM, Ueda Y: **Synthesis, in vitro, and in vivo antibacterial activity of nocathiacin I thiol-Michael adducts**. *Bioorg Med Chem Lett* 2005, **15**:2069-2072.
233. Naidu BN, Sorenson ME, Connolly TP, Ueda Y: **Michael addition of amines and thiols to dehydroalanine amides: a remarkable rate acceleration in water**. *J Org Chem* 2003, **68**:10098-10102.
234. Naidu BN, Sorenson ME, Hudyma T, Zheng X, Zhang Y, Bronson JJ, Pucci MJ, Clark JM, Ueda Y: **Synthesis and antibacterial activity of O-substituted nocathiacin I derivatives**. *Bioorg Med Chem Lett* 2004, **14**:3743-3746.
235. Naidu BN, Sorenson ME, Matiskella JD, Li W, Sausker JB, Zhang Y, Connolly TP, Lam KS, Bronson JJ, Pucci MJ, et al.: **Synthesis and antibacterial activity of nocathiacin I analogues**. *Bioorg Med Chem Lett* 2006, **16**:3545-3549.
236. Naidu BN, Sorenson ME, Zhang Y, Kim OK, Matiskella JD, Wichtowski JA, Connolly TP, Li W, Lam KS, Bronson JJ, et al.: **Nocathiacin I analogues: synthesis, in vitro**

and in vivo biological activity of novel semi-synthetic thiazolyl peptide antibiotics. *Bioorg Med Chem Lett* 2004, **14**:5573-5577.
237. Regueiro-Ren A, Naidu BN, Zheng X, Hudyma TW, Connolly TP, Matiskella JD, Zhang Y, Kim OK, Sorenson ME, Pucci M, et al.: **Novel semi-synthetic nocathiacin antibiotics: synthesis and antibacterial activity of bis- and mono-O-alkylated derivatives**. *Bioorg Med Chem Lett* 2004, **14**:171-175.
238. Grieco PA: *Organic Synthesis in Water*. London: Blackie Academic and Professional; 1998.
239. Murakami T, Holt TG, Thompson CJ: **Thiostrepton-induced gene expression in Streptomyces lividans**. *J Bacteriol* 1989, **171**:1459-1466.
240. Chiu ML, Folcher M, Griffin P, Holt T, Klatt T, Thompson CJ: **Characterization of the covalent binding of thiostrepton to a thiostrepton-induced protein from Streptomyces lividans**. *Biochemistry* 1996, **35**:2332-2341.
241. Hang PC, Honek JF: **Electronic structure calculations on the thiazole-containing antibiotic thiostrepton: molecular mechanics, semi-empirical and ab initio analyses**. *Bioorg Med Chem Lett* 2005, **15**:1471-1474.
242. Mohamadi F, Richards NGJ, Guida WC, Liskamp R, Lipton M, Cauleld C, Chang G, Hendrickson T, Still WG: **MacroModel—An integrated software system for modeling organic and bioorganic molecules using molecular mechanics**. *J. Comput. Chem.* 1990, **11**:440-467.
243. Frisch MJ, Trucks GW, Schlegel HB, Scuseria GE, Robb MA, Cheeseman JR, Montgomery J, J. A., Vreven T, Kudin KN, Burant JC, et al.: **Gaussian '03 Revision B05**. Edited by. Pittsburgh, PA; 2003.
244. Qiu D, Shenkin PS, Hollinger FP, Still WC: **The GB/SA continuum model for solvation: a fast analytical method for the calculation of approximate born radii**. *J. Phys. Chem. A* 1997, **101**:3005-3014.
245. Dewar MJS, Zoebisch EG, Healy EF, Stewart JJP: **AM1: a new general purpose quantum mechanical model**. *J. Am. Chem. Soc.* 1985, **107**:3902-3909.
246. Mulliken RS: **Electronic Population Analysis on LCAO[Single Bond]MO Molecular Wave Functions. I** *J. Chem. Phys* 1955, **23**:1833-1840
247. Mulliken RS: **Electronic Population Analysis on LCAO[Single Bond]MO Molecular Wave Functions. II. Overlap Populations, Bond Orders, and Covalent Bond Energies**. *J. Chem. Phys* 1955, **23**:1841-1846
248. Breneman CM, Wiberg KB: **Determining atom-centred monopoles from molecular electrostatic potentials—the need for high sampling density in formamide conformational-analysis**. *J Comput Chem*
1990, **11**:361-373.
249. Becke AD: **A new mixing of Hartree--Fock and local density-functional theories**. *The Journal of Chemical Physics* 1993, **98**:1372-1377.
250. Becke AD: **Density-functional exchange-energy approximation with correct asymptotic behavior**. *Physical Review A* 1988, **38**:3098.
251. Kolossvary I, Guida WC: **Low Mode Search. An Efficient, Automated Computational Method for Conformational Analysis: Application to Cyclic and Acyclic Alkanes and Cyclic Peptides**. *J. Am. Chem. Soc.* 1996, **118**:5011-5019.
252. Andrews JM: **BSAC standardized disc susceptibility testing method (version 5)**. *J Antimicrob Chemother* 2006, **58**:511-529.

253. Bauer AW, Kirby WMM, Sherris JC, Turck M: **Antibiotic susceptibility testing by a standardized single disk method.** *Am J Clin Pathol* 1966, **45**:493-496.
254. Still WC, Tempczyk A, Hawley RC, Hendrickson T: **Semianalytical treatment of solvation for molecular mechanics and dynamics**. *J. Am. Chem. Soc.* 1990, **112**:6127-6129.
255. Hensens OD, Albers-Schonberg G, Anderson BF: **The solution conformation of the peptide antibiotic thiostrepton: a 1H NMR study**. *J Antibiot (Tokyo)* 1983, **36**:799-813.
256. Mocek U, Beale JM, Floss HG: **Reexamination of the 1H and 13C NMR spectral assignments of thiostrepton**. *J Antibiot (Tokyo)* 1989, **42**:1649-1652.
257. Terwilliger TC: **Automated side-chain model building and sequence assignment by template matching**. *Acta Crystallogr D Biol Crystallogr* 2003, **59**:45-49.
258. He Y, Yao DQ, Gu YX, Lin ZJ, Zheng CD, Fan HF: **OASIS and molecular-replacement model completion**. *Acta Crystallogr D Biol Crystallogr* 2007, **63**:793-799.
259. Brunger AT, Adams PD, Clore GM, DeLano WL, Gros P, Grosse-Kunstleve RW, Jiang JS, Kuszewski J, Nilges M, Pannu NS, et al.: **Crystallography & NMR system: A new software suite for macromolecular structure determination**. *Acta Crystallogr D Biol Crystallogr* 1998, **54**:905-921.
260. Emsley P, Cowtan K: **Coot: model-building tools for molecular graphics**. *Acta Crystallogr D Biol Crystallogr* 2004, **60**:2126-2132.
261. Ho SN, Hunt HD, Horton RM, Pullen JK, Pease LR: **Site-directed mutagenesis by overlap extension using the polymerase chain reaction**. *Gene* 1989, **77**:51-59.

APPENDIX 1: RADIOMETRIC ASSAY SUPPLEMENTARY INFORMATION

A1.1. Reducing the Specific Activity of *S*-Adenosyl-L-[methyl-^{3}H]-methionine

The specific activity (S_A) of commercially available *S*-adenosyl-L-[methyl-^{3}H]-methionine ([^{3}H]-AdoMet*) is typically reduced for storage or assay conditions. This is achieved by "cutting" the S_A (Ci/mmol) with a non-radiolabelled ("cold") compound. Therefore, the amount of radioactivity ("hotness") remains unchanged while the total amount of compound increases. For radiometric assays discussed in *Chapter 3*, [^{3}H]-AdoMet* was typically stored at 500 Ci/mmol. This section shows a sample calculation of calculations involved in reducing the S_A of [^{3}H]-AdoMet* from the manufacturer from 61 Ci/mmol to 500 mCi/mmol for storage.

A1.1.1. Calculating How Much Non-radiolabelled AdoMet is Required

Table A1. 1: Information on radiolabelled and non-radiolabelled AdoMet

^{3}H-AdoMet*$_{commercial}$	AdoMet
• Specific activity = 61 Ci/mmol • [Radioactive] = 1.0 mCi/mL • Volume = 250 µL • Total radioactivity = 250 µCi • MW = 405 g/mol	• in *p*-toluenesulfonate salt form with hydration • $C_{15}H_{22}N_5O_5 \cdot xC_7H_8O_3S \cdot y\ H_2O$* • MW = 959.26 g/mol

* x and y are obtained by manufacterer's product sheet. In this example x = 3.1 and y = 1.5

Using the information for both "hot" and "cold" AdoMet (Table A1.1), the following equation [156] can be used to calculate how much non-radiolabelled AdoMet is needed to cut the specific activity down to 500 mCi/mmol:

$$W = Ma \times \left[\frac{1}{A'} - \frac{1}{A} \right]$$

Where W = weight (in mg) of unlabelled "cold" compound to be added (mg)
M = molecular weight of radiolabelled compound (g/mol)
a = total activity (GBQ, mCi) in sample
A = molar specific activity (GBq/mmol, mCi/mmol of compound as supplied)
A′ = molar specific activity (GBq/mmol, mCi/mmol) of the desired diluted compound

$$W = Ma \times \left[\frac{1}{A'} - \frac{1}{A} \right]$$

$$W = (959.275\ g/mol) \times (0.250\ mCi) \times \left[\frac{1}{500\ Ci/mmol} - \frac{1}{61000\ Ci/mmol} \right]$$

$$W = 239.82 \times (0.002 - 1.63 \times 10^{-5})$$

$$W = 0.4757\ mg = 475.7\ \mu g \quad \textbf{(1)}$$

Therefore, 475.7 µg of non-radiolabelled AdoMet must be added to reduce the specific activity. However, this mass was too small, making it not possible to measure out. Therefore, a stock solution of cold AdoMet was made (10 µg/µL).

A1.1.2. Using the Cold AdoMet Stock Solution to Reduce Specific Activity

Making the cold AdoMet stock solution:

2.5 mg (2500 µg) of cold AdoMet into 250 µL of Assay buffer*:

$$c = \frac{2500\ \mu g}{250\ \mu L} = 10\ \mu g/\mu L \quad \textbf{(2)}$$

*Assay buffer: 50 mM HEPES pH 7.5, 7.4 mM MgCl2, 73.5 mM NH4Cl, 3 mM mercaptoethanol, 10% glycerol

How much cold AdoMet stock to add to reduce S_A:

$$c = \frac{m}{v} \Rightarrow v = \frac{m}{c}$$ Substitute (1) and (2)

$$v = \frac{475.5\ \mu g}{10\ \mu g/\mu L} = 47.5\ \mu L$$

$\therefore$ **47.5 µL** of the cold AdoMet stock solution is to be added to commercial ^{3}H-AdoMet* bottle to reduce the S_A to 500 mCi/mmol

A.1.3. How Much ^{3}H-AdoMet$_{Reduced}$ to Be Added to Each Assay Tube*

If the total amount of radioactivity desired for each assay reaction tube (total volume of 100 µL) is 2.5 µCi, given the radioactive concentration, one should be able to calculate how much hot compound to add. The original commercial [^{3}H]-AdoMet* had a radioactive concentration of 1.0 mCi/mL or 1.0 µCi/mL. The amount of [^{3}H]-AdoMet* that is needed to be added to each assay tube can be calculated:

$$\frac{1.0\ \mu Ci}{\mu L} = \frac{2.5\ \mu Ci}{x} \Rightarrow x = 2.5\ \mu L$$

Therefore, 2.5 µL of [^{3}H]-AdoMet* is to be added to each assay. However, the radioactive concentration was changed upon the addition of the cold AdoMet that was used to cut down the S_A (to give [^{3}H]-AdoMet*$_{reduced}$). Thus, the amount added must be corrected as follows:

$$\text{Adjusted volume} = 2.5\ \mu L \times \frac{47.5\ \mu L + 250\ \mu L}{250\ \mu L} = 2.975\ \mu L$$

Therefore, for each 100 µL assay, the amount of ^{3}H-AdoMet*$_{reduced}$ to be added is 2.975 µL.

A.1.4. Calculating the Concentration of [^{3}H]-AdoMet$_{reduced}$*

Number of moles of [^{3}H]-AdoMet*$_{commercial}$:

-The bottle has a SA of 61000 mCi/mmol
-In each assay (100 µL), has 2.5 µCi

$\therefore$ Number of moles of hot [^{3}H]-AdoMet$_{commerical}$ in each assay tube is:

2.5 µCi = 0.0025 mCi

$$0.0025\ mCi \times \frac{1\ mmol}{61000\ mCi} = 4.1\times10^{-8}\ mmol$$

Number of Moles of AdoMet$_{cold}$:

-Recall we had reduced S_A down to 500 mCi/mmol

$$\frac{61000\ mCi/mmol}{500\ mCi/mmol} = 122$$

-We added 122 fold more AdoMet$_{cold}$

$\therefore$ Number of mole of AdoMet$_{cold}$ is:

$$122\times4.098\times10^{-8}\ mmol = 5.0\times10^{-6}\ mmol$$

Therefore, the TOTAL amount of AdoMet in each assay reaction tube:
[^{3}H]-AdoMet$_{commercial}$ + AdoMet$_{cold}$ = ~**5.0×10^{-6} mmol.**

Concentration of [^{3}H]-AdoMet*$_{reduced}$:

$$c = \frac{n}{v} = \frac{5.0\times10^{-9}\,mol}{2.975\times10^{-6}\,L} = 1.68mM$$

Final concentration of [^{3}H]-AdoMet*$_{reduced}$ in each assay tube:

$$c = \frac{n}{v} = \frac{5.0\times10^{-9}\,mol}{1\times10^{-4}\,L} = 0.05mM$$

A1.2. Conversion of Disintegrations Per Minute to a Mole Quantity

The data collected using the liquid scintillation counter instrument gives methylation in disintegrations per min (dpm). In order to calculate kinetic parameters, the signal first must be converted to a molar quantity as seen below:

$$1\ dpm\times\frac{Ci}{2.2\times10^{12}\,dpm}\times\frac{1}{S_A} = \frac{Ci}{2.2\times10^{12}\,dpm}\times\frac{1}{0.5\,Ci} = 9.1\times10^{-13}\,mmol$$

$$\text{Note: } dpm = \frac{cpm}{efficiency}$$

After this conversion is performed, calculations to obtain kinetic values can proceed.

APPENDIX 2: *S.AZUREUS* TSR PROTEIN STRUCTURE

The *S. azureus* TSR protein crystal structure and TSR-RNA modelling interactions were carried out by by Dr. Mark Dunstan and Dr. Graeme Conn at the University of Manchester. A summary of methodology used and structure data are provided here.

A2.1. X-ray Diffraction Data Collection, Structure Determination and Refinement

Crystallization trials and optimizations were done with the JBScreen HTS1 screen (Jenabioscience) on an Innovadyne 96 crystallization robot. Protein crystals grew with the vapour diffusion hanging drop method. Diffraction-quality crystals grew within the first two to three days in 4 μL drops containing 27% PEG 4K, 0.2 sodium acetate and 0.1 M Tris buffer pH 8.0 with an equal volume of protein. An additional five days after their intial appearance, crystals produced reached their maximum size of $800 \times 150 \times 80$ μm. Crystals with the *S*-adenosyl-L-methionine (AdoMet) cosubstrate bound was achieved by soaking the crystal in the same solution supplemented with 5 mM AdoMet for 24 hours.

Crystals were cryoprotected by passing through perfluoropolyether (PFPE) prior to flash-cooling with liquid nitrogren. Diffraction data sets were collected at the European Synchrotron Radiation Facility (ESRF) on the ID23-1 beamline and processed using X-ray Dectector Software (XDS) [194]. Molecular replacement (MR) was performed using the MOLREP program [195,196] of the CCP4 package with a poly-serine model of the C-terminal domain of the SpoUT MTase RrmA (1IPA: 27% sequence identity) as a search template. MOLREP determined that asymmetric unit contains two molecules which

confirms the number estimated by the Matthews coefficient (VM =2.12, solvent content = 42%).

Manual model building of the missing N-terminal domain was conducted with the program RESOLVE [257] and was initially difficult due to the poor electron density; the program only placed 280 of the amino acid residues into the electron density, most of which belong to the C-terminal domain. To improve the model quality, the dual-space MR model completion method was executed. After several rounds of phase calculation with OASIS06 [258] and density modification with DM [195], followed by more automated model building with RESOLVE and structure refinement with CNS [259], over 470 residues (including side chains) were placed by RESOLVE into the electron density. The final steps of manual building was completed by Coot [260] and refinement of the model was achieved by translation, liberation, screw (TLS) refinement using Pheix.refine. The completed structure contains residues 8-268 for each TSR monomer in the asymmetric unit (Table A2.1 and Figure A2.1).

Table A2. 1: X-ray data collection and refinement statistics for the TSR-AdoMet complex.

		TSR-AdoMet complex
Space group		$P2_12_12_1$
Resolution (Å)		2.45
Unit cell	a,b,c (Å)	40.80, 56.20, 213.90
	α,β,γ (°)	90.0, 90.0, 90.0
Redundancy		4.4 (4.5)
Reflections	Total	85388
	Unique	18568
Completeness (%)		95.8 (90.0)
R_{meas} (%)		10.9 (67.0)
<I/σI>		10.2 (2.36)
Solvent molecules		43
Rwork (%)		21.9
Rfree (%)		26.6
Overall B-factor ($Å^2$)		57.9
Ramachandran plot (%)		
Favourable		84.6
Allowed		11.8
Generous		1.8
Disallowed		1.8
RMS deviations from ideal geometry		
Bond lengths (Å)		0.022
Bond angles (°)		2.007

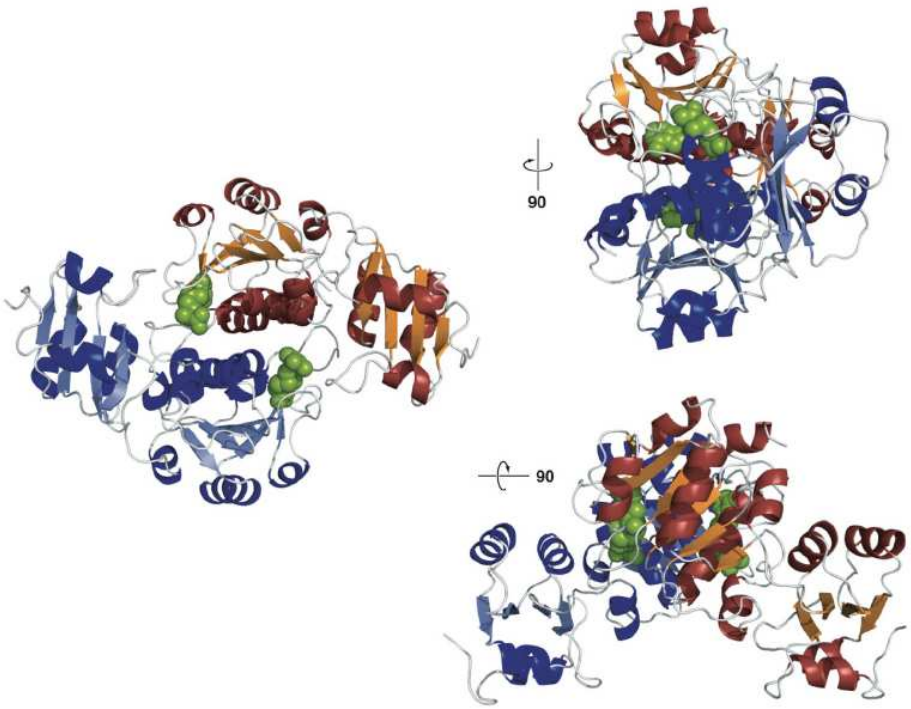

Figure A2. 1: X-ray crystal structure of TSR-AdoMet complex in three orthogonal views. AdoMet is represented by the green space-fill figure. Figure courtesy of Drs. Mark Dunstan and Graeme Conn.

A2.2. Modelling TSR-RNA Interactions

The coordinates for the 58 nucleotide L11 binding domain rRNA (PDB: 1HC8) was modified at position 1061 to the wild type *E. coli* sequence (U1061). Docking experiments were carried out using the Hex program (http://www.csd.abdn.ac.uk/hex). Rigid-body prediction of the RNA ('ligand') was applied and oriented towards the cleft formed by the conserved C-terminal domains of the TSR dimer ('receptor'). Both shape-only and shape-electrostatics correalation algorithms were used with a search radius of N-30 and the top 10 docking solutions inspected visually in Coot.

In *Chapter 4*, the non-conserved N-terminal recognition domain has a striking similarity to the yeast L30e-mRNA, an autoregulatory complex [204,205]. A critical Phe residue engages in aromatic ring stacking interaction and is proposed for TSR (Figure A2.2). For more details, please refer to *Chapter 4* of the thesis.

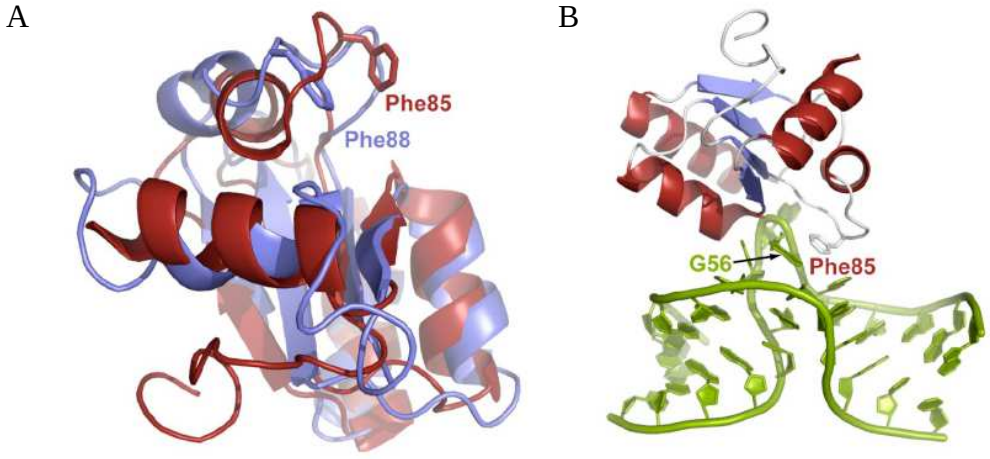

Figure A2. 2: Yeast L30e domain structure with RNA binding.
(A) Alignment of L30e (red) and the TSR NTD (blue). **(B)** Structure of L30e-mRNA complex including the interaction between Phe85 and nucleotide G56. The equivalent position is found in Phe88 of TSR and is believed to play a role in RNA recognition. Figure courtesy of Drs. Mark Dunstan and Graeme Conn.

APPENDIX 3: GEOMETRIC DISTORTIONS IN HOMOLOGY MODELS

A3.1. Geometric Distortions for *TSRMonomer2*

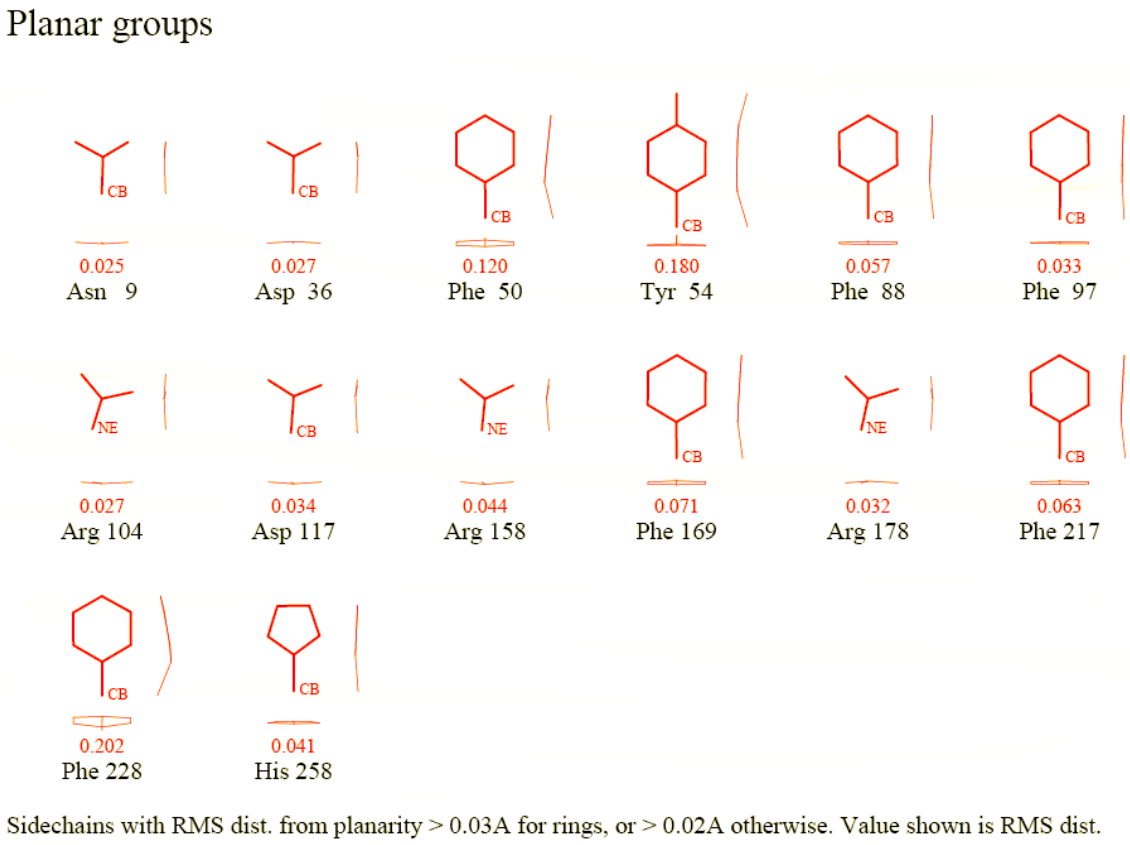

Figure A3. 1: Geometric distortions for the homology model *TSRMonomer2*.
Figure obtained from PROCHECK.

A3.2. Geometric Distortions for *PrimeTSR*

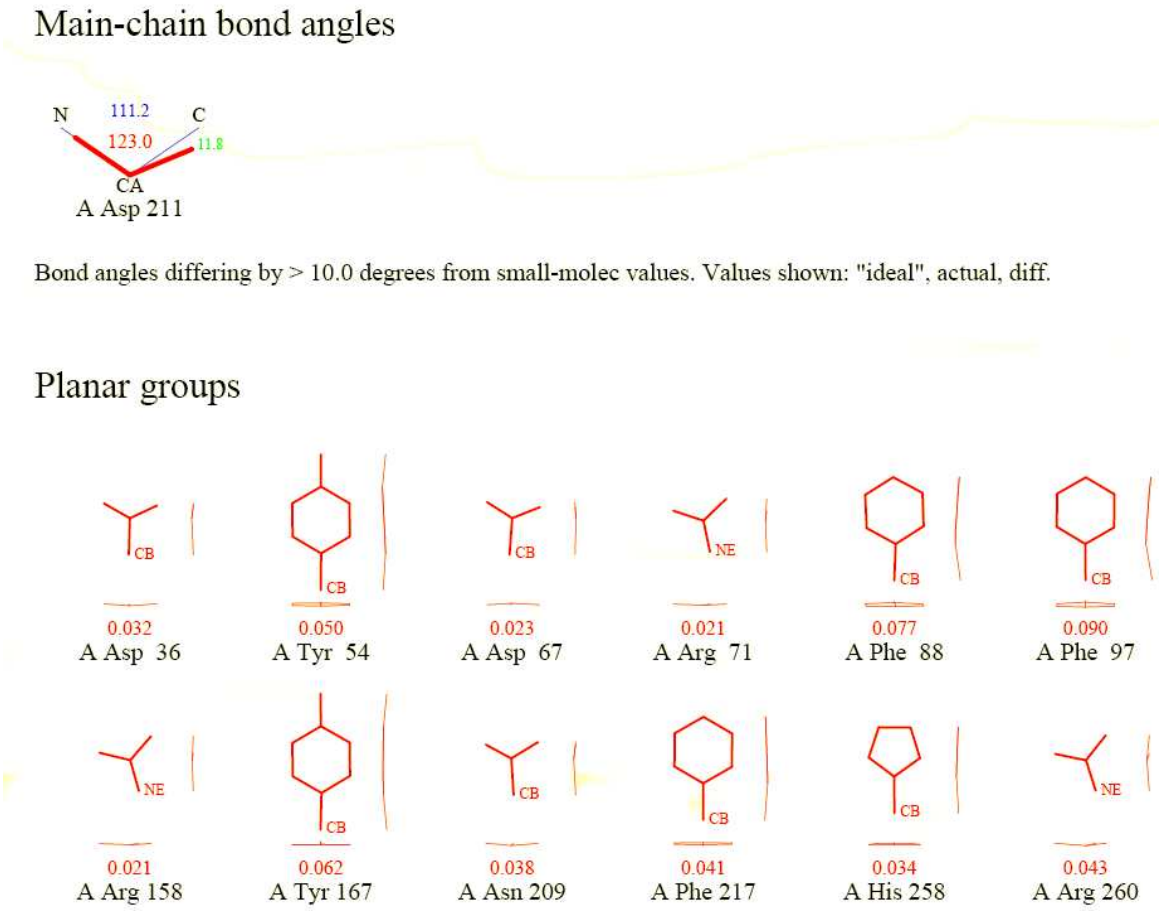

Figure A3. 2: Geometric distortions for the homology model *PrimeTSR*.
Figure obtained from PROCHECK.

A3.3. Geometric Distortions for TSRDimer

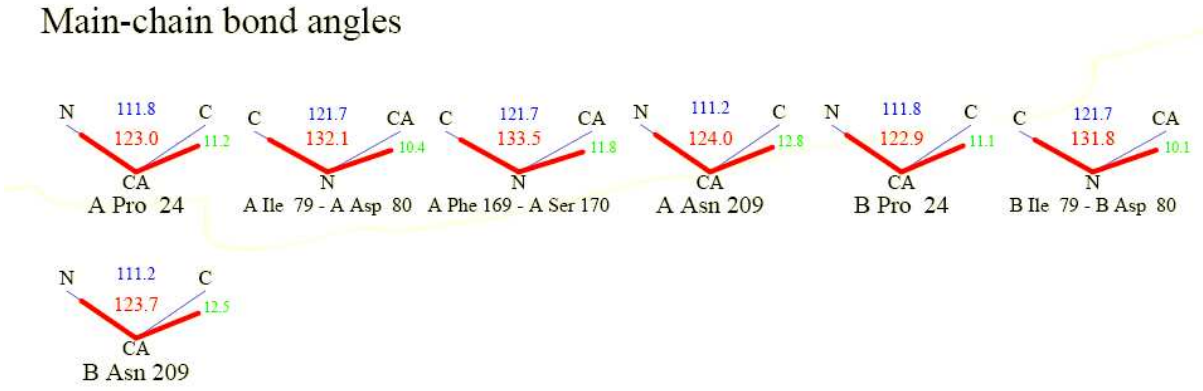

Bond angles differing by > 10.0 degrees from small-molec values. Values shown: "ideal", actual, diff.

Planar groups

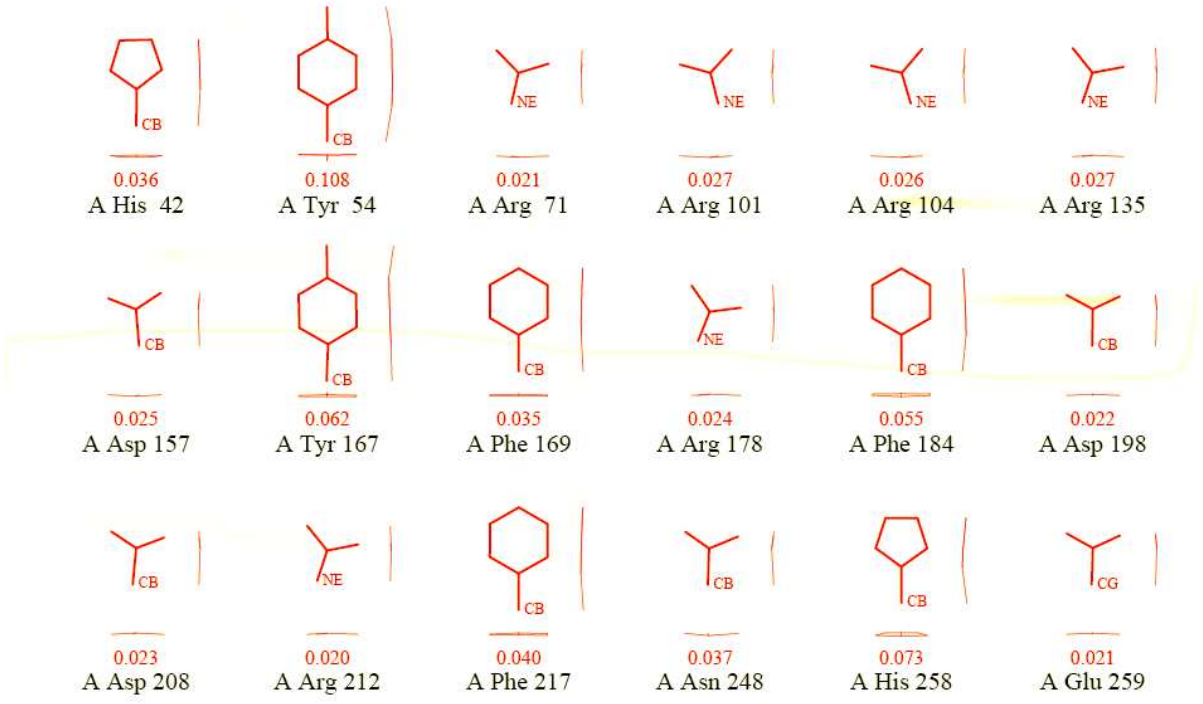

Figure A3. 3: Geometric distortions for the homology model *TSRDimer*.
Figure obtained from PROCHECK.

APPENDIX 4: MUTAGENESIS

Two different mutagenesis methods were utilized to obtain the mutants discussed in *Chapter 4*. Below is an overview of these two techniques.

A4.1. QuikChange™ Site-Directed Mutagenesis

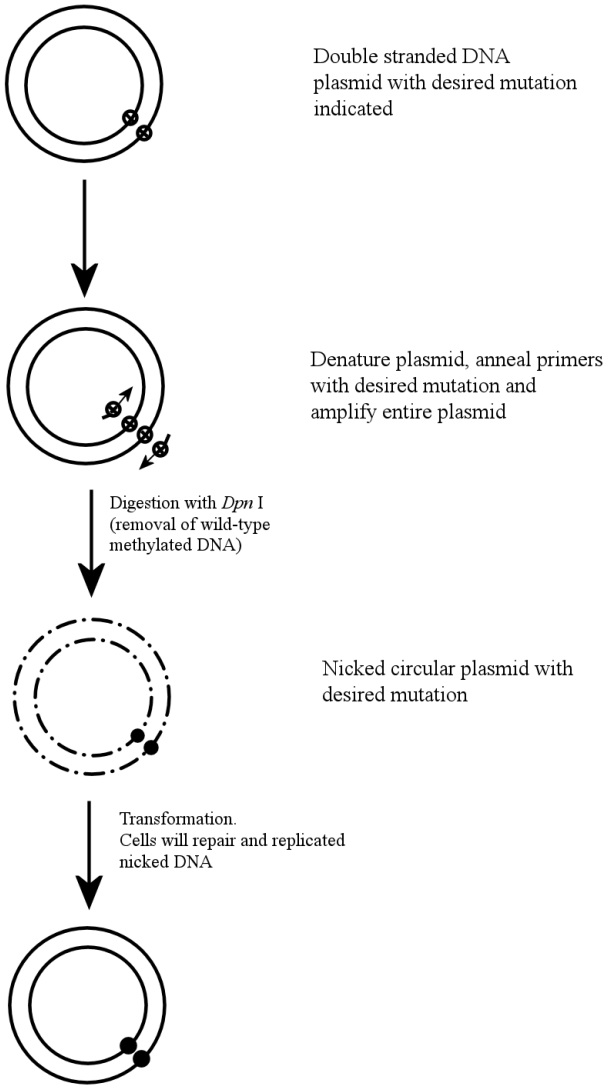

Figure A4. 1: Overview of the QuikChange™ site directed mutagenesis method. Adapted from Stratagene Closing Systems Quikchange™ Site-Directed Mutagenesis Kit Manual.

A4.2. Splicing Overlap Extension Mutagenesis

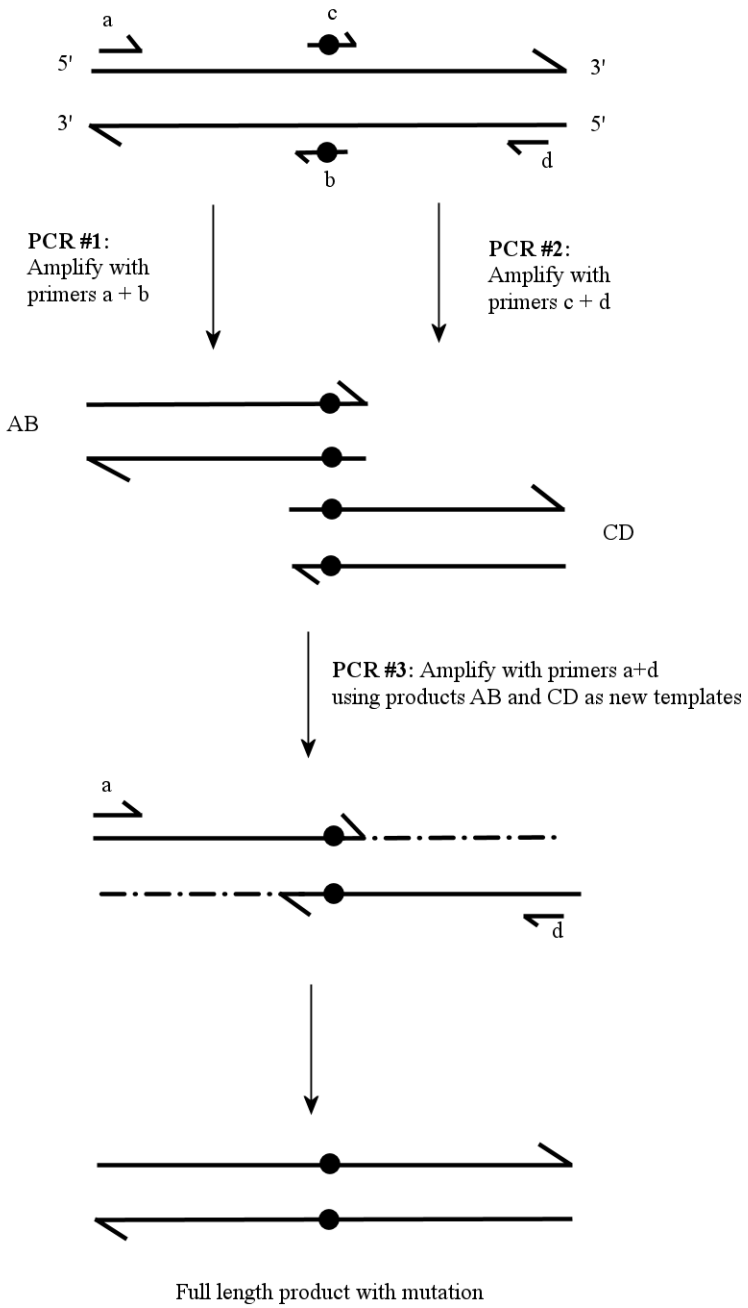

Figure A4. 2: Overview of splicing overlap extension site-mutagenesis method.
Primers a and b are the external primers (T7 forward and reverse) and the internal primers contain the mutation. After the first two PCR amplifications, two pairs of separate strands. These strands are complementary at their 3′ ends such that they can act as primers for one another and be extended by polymerase to give the full length product with the desired mutation. Adapted from: [261].

A4.3. Mass Spectra of TSR Mutants

All molecular weights of TSR mutants were determined by positive ion electrospray mass spectrometry. In conjunction with sequencing results, the success of the mutation was confirmed.

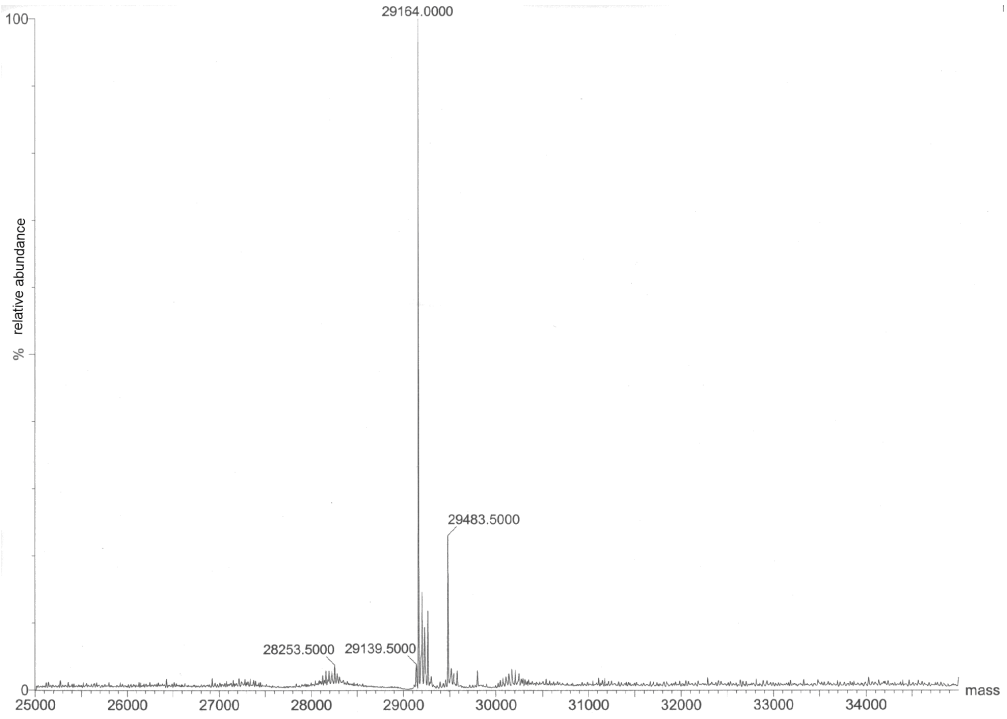

Figure A4. 3: Positive ion mode electrosrapy of S246A TSR′.
The expected molecular weight is 29162 Da and the major peak indicates a monomeric weight of 29164 Da. The secondary peak with a mass of 29483 Da is S246A TSR′ is most likely two tris adducts bound to the protein.

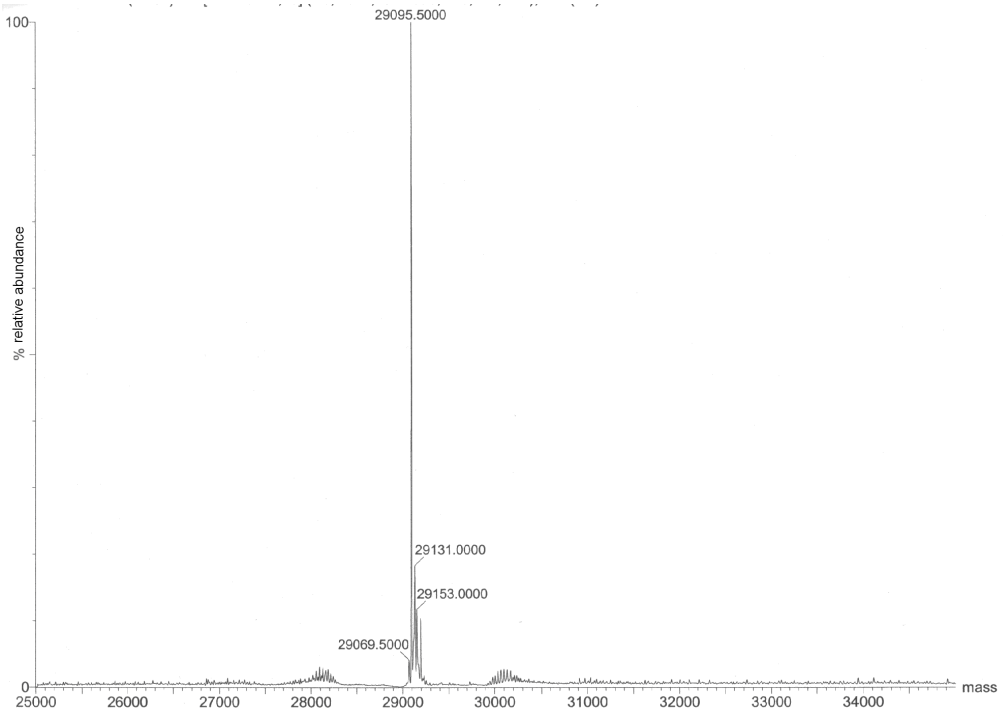

Figure A4. 4: Positive ion mode electrosrapy of R135A TSR′.
The expected molecular weight is 29097 Da and the major peak indicates a monomeric weight of 29095 Da.

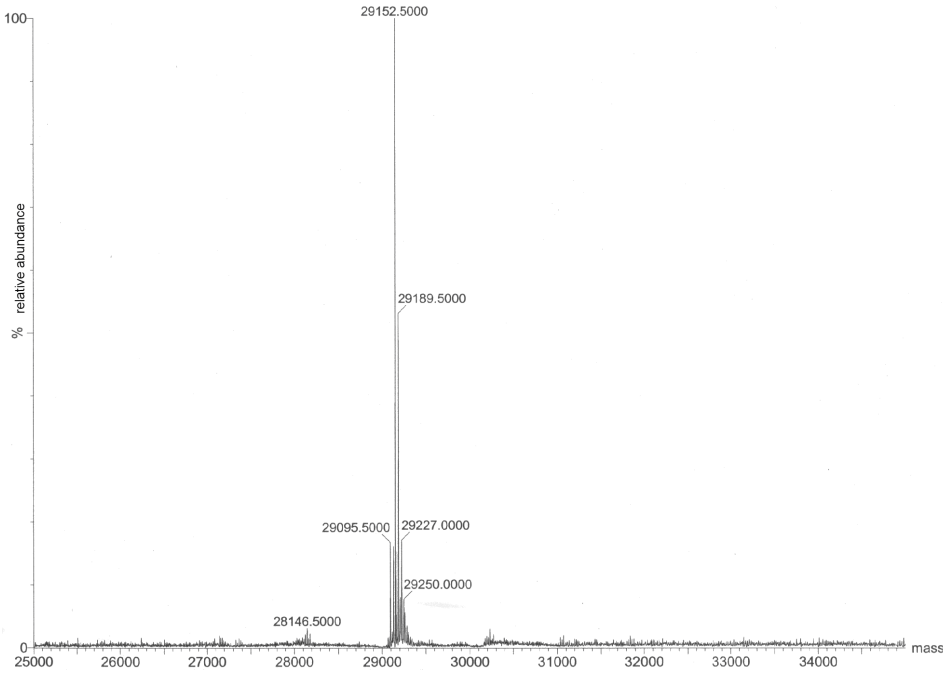

Figure A4. 5: Positive ion mode electrosrapy of R135K TSR′.
The expected molecular weight is 29154 Da and the major peak indicates a monomeric weight of 29152 Da.

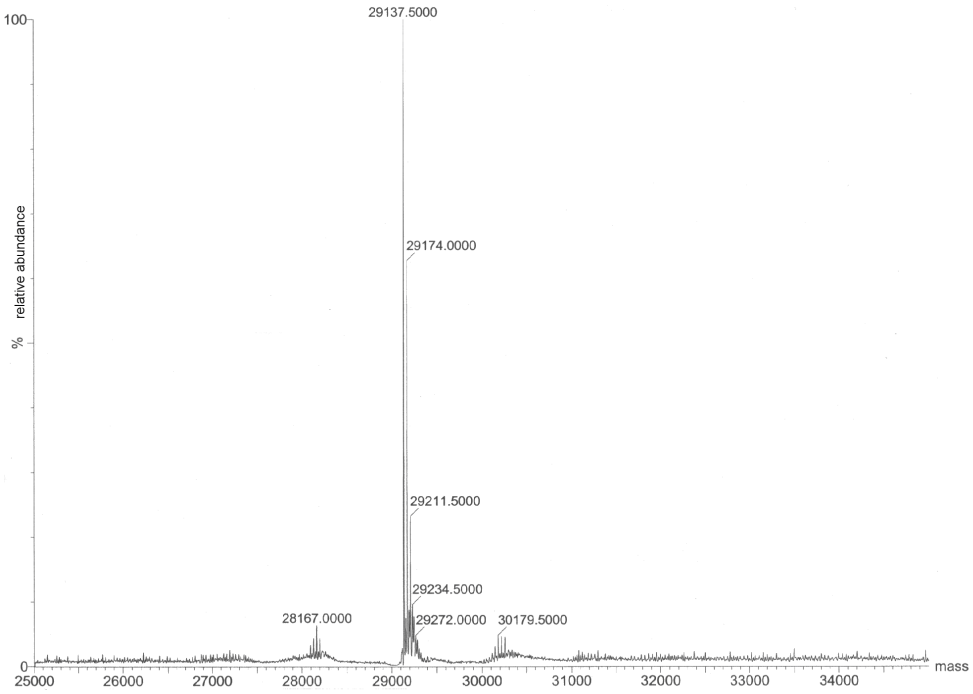

Figure A4. 6: Positive ion mode electrosrapy of N248A TSR′.
The expected molecular weight is 29139 Da and the major peak indicates a monomeric weight of 29137 Da.

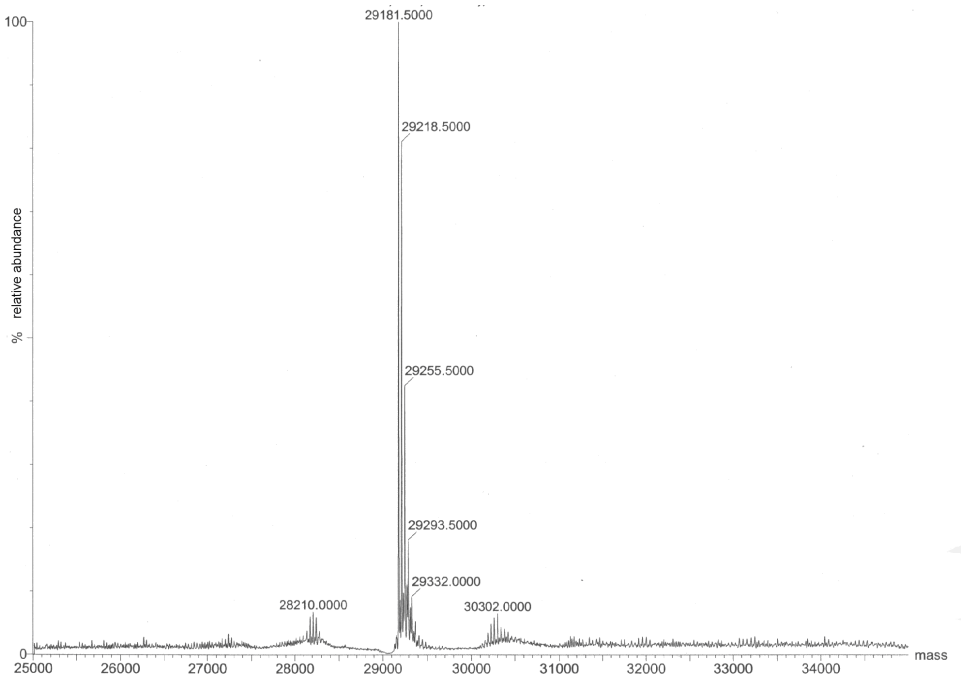

Figure A4. 7: Positive ion mode electrosrapy of N248D TSR′.
The expected molecular weight is 29183 Da and the major peak indicates a monomeric weight of 29181 Da.

A4.3. Preliminary CD and DSC of TSR Mutants

Circular dichroism (CD) and differential scanning calorimetry (DSC) were applied to TSR′ and some of the mutants created.

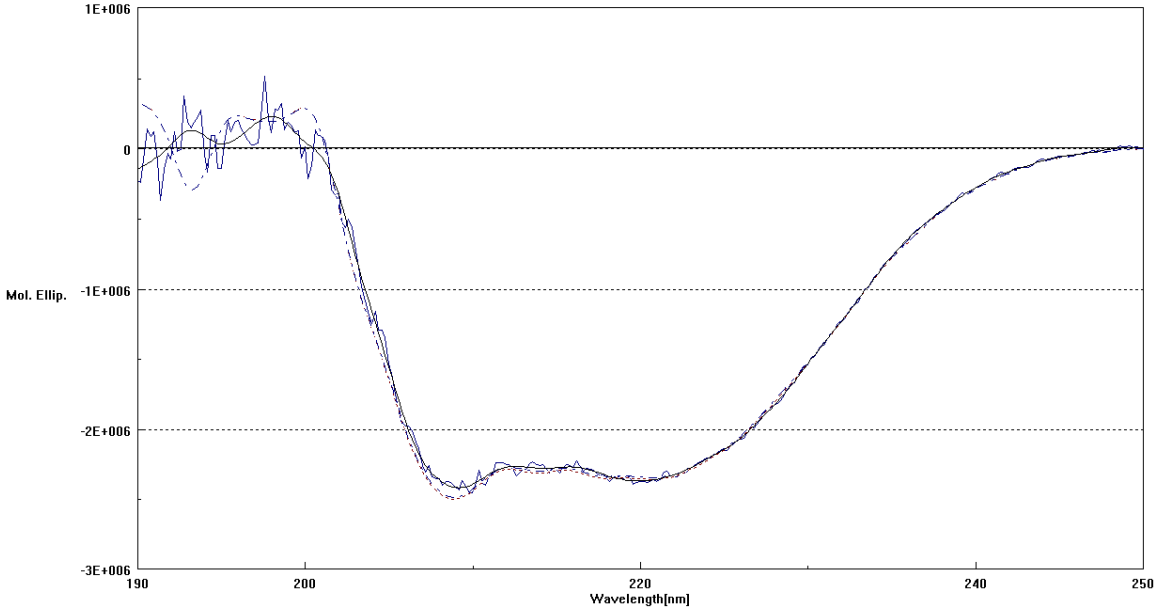

Figure A4.8: CD spectra of mutants S246A, R135A and R135K compared to the wildtype TSR′.

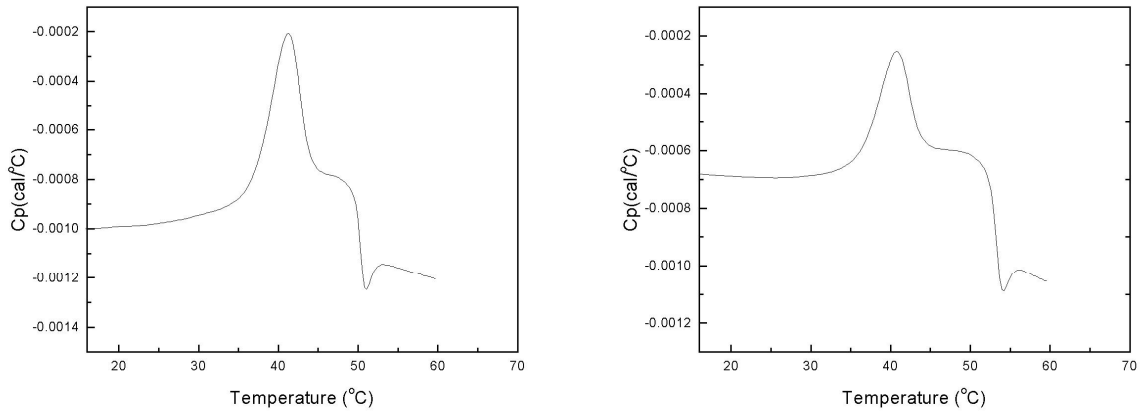

Figure A4.9: Raw DSC data for a representative scan of wildtype TSR′ and S246A.
The differences in the melting temperature was negligible (Tm = 42 °C). All scans were performed at 1 °C per minute in 20 mM Tris pH 7.5, 75 mM KCl, 10% glycerol.

APPENDIX 5: TS MODELLING SUPPLEMENT

Please refer to Chapter 5 for full description of the methods used as well as discussion of these results.

A5.1. Conformational Flexiblity of Thiostrepton

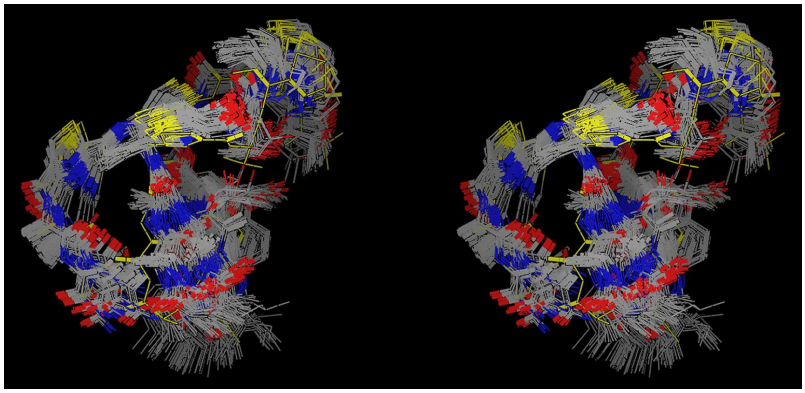

Figure A5. 1: Superimposition of the 158 conformations determined *in vacuo* by LMOD calculations. 31 structures are within 3 kcal/mol of the global minimum (yellow) [241].

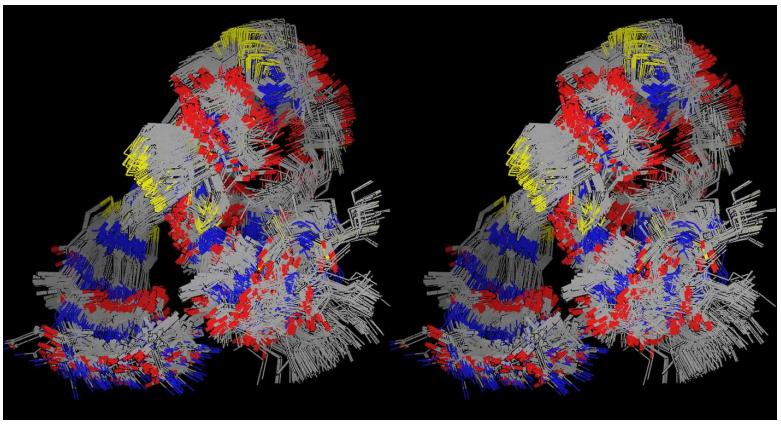

Figure A5. 2: Superimposition of the 293 conformations determined in water by LMOD calculations. 76 structures were within 3 kcal/mol of the global minimum the global minimum (yellow) [241].

A5.2. Electronic Structure of Thiostrepton

Table A5. 1: Mulliken charges determined by AM1 and B3LYP/6-31G(d), and B3LYP/6-31G(d) CHelpG[¥] electrostatic fit charges on the AM1 geometry-optimized structure.
These calculations were performed using Gaussian ’03γ, Revision B.05 (Gaussian Inc., Carnegie, Pennsylvania, USA).

Atom	AM1	B3LYP/6-31G(d)//AM1	
		Mulliken	CHelpG
1 N	-0.352167	-0.619568	-0.563028
2 C	0.006034	-0.075297	0.305248
3 C	0.289517	0.58477	0.432976
4 O	-0.370304	-0.525672	-0.42032
5 C	0.022375	0.139182	0.276134
6 O	-0.351363	-0.655566	-0.756127
7 C	-0.256556	-0.506569	-0.17378
8 H	0.228686	0.414575	0.467268
9 H	0.084999	0.134171	0.045535
10 H	0.09852	0.183527	0.002156
11 H	0.091529	0.144382	0.056838
12 H	0.252561	0.367186	0.223853
13 H	0.163622	0.208362	0.060864
14 H	0.097144	0.143858	-0.00819
15 N	-0.331103	-0.585358	-1.117211
16 C	-0.023976	-0.074879	0.151235
17 C	0.305118	0.616213	0.668707
18 O	-0.3792	-0.538112	-0.575322
19 C	-0.129165	-0.072546	0.135886
20 C	-0.160893	-0.267452	0.11856
21 C	-0.214305	-0.466023	-0.214814
22 C	-0.210464	-0.441187	-0.284545
23 H	0.123475	0.154224	0.002167
24 H	0.077027	0.143471	0.064636
25 H	0.073647	0.144927	0.07286
26 H	0.079594	0.150967	0.070961
27 H	0.075099	0.122773	-0.014265
28 H	0.088221	0.132074	-0.008621
29 H	0.117159	0.149345	-0.001124
30 H	0.084484	0.146212	0.05262
31 H	0.070102	0.137847	0.054952
32 H	0.077237	0.160619	0.03253
33 H	0.181	0.313428	0.385495
34 N	-0.350785	-0.588068	-0.7216
35 C	0.013755	-0.045128	0.379551
36 C	0.286223	0.612792	0.446957
37 O	-0.371745	-0.526963	-0.479551
38 C	-0.22442	-0.438573	-0.195089
39 H	0.087966	0.150571	0.025855
40 H	0.09229	0.1598	0.062797

41	**H**	0.09747	0.167124	0.064395
42	**H**	0.135631	0.178097	0.025056
43	**H**	0.246037	0.341645	0.340361
44	**N**	-0.311574	-0.683237	-0.412663
45	**C**	-0.007911	0.342595	0.143375
46	**C**	-0.226751	-0.405154	-0.365006
47	**C**	0.336281	0.558196	0.517567
48	**O**	-0.380973	-0.54657	-0.491196
49	**H**	0.258435	0.356162	0.259858
50	**H**	0.129155	0.151623	0.12567
51	**H**	0.153782	0.192305	0.187783
52	**N**	-0.353819	-0.610375	-0.461184
53	**C**	0.028262	0.008151	0.005989
54	**C**	0.299581	0.599133	0.707109
55	**O**	-0.387686	-0.545067	-0.532253
56	**C**	-0.232591	-0.454256	-0.174515
57	**H**	0.141593	0.1868	0.134987
58	**H**	0.08629	0.147363	0.020476
59	**H**	0.091289	0.159493	0.063423
60	**H**	0.10291	0.177281	0.079174
61	**H**	0.248515	0.347774	0.27917
62	**N**	-0.303021	-0.703014	-0.270373
63	**C**	-0.010164	0.33687	0.031916
64	**C**	-0.228916	-0.399543	-0.336149
65	**C**	0.336442	0.527427	0.5868
66	**O**	-0.352551	-0.510952	-0.48756
67	**H**	0.126931	0.147695	0.111132
68	**H**	0.16526	0.20552	0.196307
69	**H**	0.266893	0.364916	0.211037
70	**N**	-0.309434	-0.678436	-0.434442
71	**C**	-0.008502	0.343192	0.138967
72	**C**	-0.230499	-0.403302	-0.397183
73	**C**	0.329352	0.508971	0.65651
74	**N**	-0.423287	-0.734575	-0.88364
75	**O**	-0.372061	-0.516054	-0.52706
76	**H**	0.123189	0.142454	0.127831
77	**H**	0.163324	0.204566	0.200818
78	**H**	0.261355	0.3594	0.276388
79	**H**	0.236064	0.352084	0.417318
80	**H**	0.229187	0.342803	0.379947
81	**C**	-0.31887	0.085217	0.077324
82	**N**	-0.074595	-0.482419	-0.387723
83	**S**	0.574442	0.30574	0.015414
84	**C**	-0.143395	0.235038	0.155826
85	**C**	-0.410601	-0.355633	-0.185523
86	**C**	0.388457	0.57239	0.512506
87	**O**	-0.373793	-0.54517	-0.544602
88	**H**	0.203081	0.207832	0.178943
89	**C**	-0.08876	-0.146898	-0.183873
90	**C**	-0.201014	-0.503346	0.047626

91	**C**	0.009845	0.336852	0.171093
92	**N**	-0.295758	-0.677927	-0.470627
93	**S**	0.148371	0.159361	-0.326665
94	**C**	-0.302612	-0.465707	0.368807
95	**O**	-0.374402	-0.519918	-0.551217
96	**C**	-0.091292	0.073604	0.213686
97	**C**	0.31514	0.613653	0.480743
98	**N**	-0.195312	-0.453253	-0.33744
99	**C**	-0.067565	-0.059643	0.023003
100	**H**	0.140467	0.175963	0.042732
101	**H**	0.153914	0.218809	-0.004192
102	**H**	0.127163	0.18204	-0.038015
103	**H**	0.141771	0.174844	0.147858
104	**H**	0.081908	0.145606	0.015107
105	**H**	0.096383	0.166518	0.011053
106	**H**	0.122977	0.210227	0.027394
107	**H**	0.256745	0.369643	0.320041
108	**C**	0.071754	-0.026359	-0.019104
109	**N**	-0.349417	-0.605611	-0.288052
110	**C**	0.102522	0.292235	0.435062
111	**C**	-0.246569	-0.509138	-0.323818
112	**O**	-0.359267	-0.674945	-0.621238
113	**C**	0.03468	0.139831	0.278114
114	**C**	-0.24927	-0.490755	-0.255528
115	**O**	-0.331386	-0.625805	-0.649792
116	**H**	0.156812	0.210534	0.126883
117	**H**	0.096796	0.167802	0.114104
118	**H**	0.109218	0.182663	0.077056
119	**H**	0.087219	0.163367	0.048583
120	**H**	0.238733	0.431409	0.338772
121	**H**	0.090438	0.126554	-0.017905
122	**H**	0.208462	0.400763	0.416956
123	**H**	0.075016	0.138158	0.061511
124	**H**	0.091035	0.160542	0.077863
125	**H**	0.097272	0.178222	0.075543
126	**H**	0.255496	0.3645	0.130111
127	**C**	-0.334784	0.077851	0.287098
128	**N**	-0.108977	-0.509019	-0.338946
129	**S**	0.607985	0.330382	0.041959
130	**C**	-0.1436	0.238941	0.06528
131	**C**	-0.411414	-0.352448	-0.168427
132	**C**	0.378648	0.57787	0.465063
133	**O**	-0.359372	-0.531487	-0.513624
134	**H**	0.20771	0.21824	0.187066
135	**C**	-0.066237	0.360793	0.108345
136	**N**	-0.108769	-0.490191	-0.44439
137	**C**	-0.460659	-0.382445	-0.147586
138	**C**	-0.325172	0.066449	0.284981
139	**S**	0.612102	0.314244	-0.014194
140	**C**	0.076371	-0.028693	-0.036867

141	**N**	-0.355136	-0.639769	-0.263541
142	**C**	0.015808	0.101609	0.602063
143	**C**	-0.22965	-0.445658	-0.433883
144	**O**	-0.257377	-0.492454	-0.406104
145	**H**	0.184049	0.184694	0.154269
146	**H**	0.156057	0.212638	0.091631
147	**H**	0.247939	0.371067	0.128706
148	**H**	0.150063	0.203895	-0.06366
149	**H**	0.095655	0.165414	0.119103
150	**H**	0.088757	0.151827	0.109747
151	**H**	0.095706	0.159696	0.097631
152	**O**	-0.36768	-0.503129	-0.515478
153	**C**	0.375883	0.626964	0.572422
154	**C**	-0.056883	0.215722	0.264367
155	**N**	-0.097484	-0.557185	-0.626767
156	**C**	-0.08693	-0.190749	-0.260902
157	**C**	-0.045166	0.275997	0.474352
158	**C**	0.082633	0.015267	0.137451
159	**O**	-0.344105	-0.666863	-0.821057
160	**C**	-0.032887	0.102097	0.232055
161	**O**	-0.327255	-0.630239	-0.611948
162	**C**	-0.033188	0.101916	-0.19967
163	**C**	0.064281	0.078707	0.288101
164	**C**	0.020869	-0.001433	0.888636
165	**C**	-0.252933	-0.475406	-0.247186
166	**C**	-0.104973	-0.140642	0.002639
167	**C**	-0.141172	-0.151248	-0.309694
168	**H**	0.231511	0.447755	0.540543
169	**H**	0.141464	0.152046	0.083856
170	**H**	0.135675	0.14335	0.101497
171	**H**	0.208786	0.399641	0.400296
172	**H**	0.075399	0.129607	0.05921
173	**H**	0.093315	0.15295	0.045215
174	**H**	0.115845	0.198136	0.073792
175	**H**	0.086028	0.127358	-0.12007
176	**H**	0.114023	0.159946	0.022336
177	**H**	0.088904	0.137828	0.000981
178	**C**	0.064245	0.331943	0.275663
179	**N**	-0.175111	-0.447054	-0.550133
180	**C**	-0.14907	-0.340031	-0.032554
181	**C**	0.045553	-0.069485	0.334722
182	**C**	0.147805	0.160264	0.475772
183	**C**	-0.191678	-0.347358	0.117068
184	**N**	-0.346008	-0.645303	-0.635003
185	**H**	0.125125	0.183731	0.027389
186	**H**	0.12109	0.183925	0.003618
187	**H**	0.091053	0.152016	-0.063189
188	**H**	0.136802	0.21317	-0.008683
189	**H**	0.119882	0.158546	-0.044486
190	**H**	0.273633	0.400005	0.245325

191	**C**	-0.296514	0.030295	0.235025
192	**N**	-0.083721	-0.502695	-0.411808
193	**S**	0.676178	0.349872	0.033063
194	**C**	-0.14796	0.242795	0.086123
195	**C**	-0.435118	-0.345172	-0.116866
196	**C**	0.388806	0.595199	0.495742
197	**O**	-0.358482	-0.533198	-0.516732
198	**H**	0.208311	0.21848	0.168987
199	**H**	0.18885	0.203411	0.130667

[¥]Breneman, C. M.; Wiberg, K. B. *J Comput Chem* **1990**, *11*, 361-373. [ɣ]Frisch, M. J.; Trucks, G. W.; Schlegel, H. B.; Scuseria, G. E.; Robb, M. A.; Cheeseman, J. R.; Montgomery, J., J. A.; Vreven, T.; Kudin, K. N.; Burant, J. C.; Millam, J. M.; Iyengar, S. S.; Tomasi, J.; Barone, V.; Mennucci, B.; Cossi, M.; Scalmani, G.; Rega, N.; Petersson, G. A.; Nakatsuji, H.; Hada, M.; Ehara, M.; Toyota, K.; Fukuda, R.; Hasegawa, J.; Ishida, M.; Nakajima, T.; Honda, Y.; Kitao, O.; Nakai, H.; Klene, M.; Li, X.; Knox, J. E.; Hratchian, H. P.; Cross, J. B.; Adamo, C.; Jaramillo, J.; Gomperts, R.; Stratmann, R. E.; Yazyev, O.; Austin, A. J.; Cammi, R.; Pomelli, C.; Ochterski, J. W.; Ayala, P. Y.; Morokuma, K.; Voth, G. A.; Salvador, P.; Dannenberg, J. J.; Zakrzewski, V. G.; Dapprich, S.; Daniels, A. D.; Strain, M. C.; Farkas, O.; Malick, D. K.; Rabuck, A. D.; Raghavachari, K.; Foresman, J. B.; Ortiz, J. V.; Cui, Q.; Baboul, A. G.; Clifford, S.; Cioslowski, J.; Stefanov, B. B.; Liu, G.; Liashenko, A.; Piskorz, P.; Komaromi, I.; Martin, R. L.; Fox, D. J.; Keith, T.; Al-Laham, M. A.; Peng, C. Y.; Nanayakkara, A.; Challacombe, M.; Gill, P. M. W.; Johnson, B.; Chen, W.; Wong, M. W.; Gonzalez, C.; Pople, J. A.; B.05 ed.; **2003**: Pittsburgh PA, 2003.

A5.3. AM1-Geometry Optimized Thiostrepton Coordinates

Table A5. 2: Coordinates for the AM1-geometry optimized structure of thiostrepton.

Center Number	Atomic Number	Atomic type	Coordinate (Å)		
			X	***Y***	***Z***
1	7	0	-1.3897	-2.00276	3.033206
2	6	0	-2.80567	-2.20288	3.185295
3	6	0	-3.22718	-3.65405	2.833889
4	8	0	-2.43404	-4.46175	2.313412
5	6	0	-3.6183	-1.20595	2.307403
6	8	0	-4.90463	-1.1391	2.911417
7	6	0	-3.70689	-1.63914	0.858382
8	1	0	-5.37196	-0.40374	2.49414
9	1	0	-4.22802	-0.85834	0.250213
10	1	0	-4.27682	-2.59409	0.758512
11	1	0	-2.68196	-1.78557	0.440159
12	1	0	-0.97219	-2.37429	2.209875
13	1	0	-3.08623	-2.00297	4.267723
14	1	0	-3.13773	-0.18583	2.366572
15	7	0	-5.0132	4.966454	0.70799
16	6	0	-5.31902	5.175837	-0.68729
17	6	0	-4.05363	5.607467	-1.47818
18	8	0	-3.92521	5.21949	-2.65669
19	6	0	-6.46665	6.160048	-1.00943
20	6	0	-6.38112	7.46743	-0.23731
21	6	0	-7.79701	5.477615	-0.76105
22	6	0	-7.12803	8.579338	-0.93116
23	1	0	-5.61118	4.190975	-1.17057

24	1	0	-7.05324	9.520885	-0.33491
25	1	0	-8.20837	8.321808	-1.04836
26	1	0	-6.70062	8.769778	-1.94544
27	1	0	-6.80329	7.328056	0.793733
28	1	0	-5.30833	7.772964	-0.11985
29	1	0	-6.38293	6.38842	-2.11156
30	1	0	-8.63533	6.149519	-1.06621
31	1	0	-7.9204	5.230676	0.32143
32	1	0	-7.87178	4.529077	-1.34942
33	1	0	-5.29174	5.745708	1.272049
34	7	0	-3.12432	6.432447	-0.88067
35	6	0	-1.80885	6.633214	-1.4401
36	6	0	-0.72053	6.3387	-0.36832
37	8	0	-0.87426	6.708202	0.812497
38	6	0	-1.5626	8.065381	-1.91901
39	1	0	-0.53741	8.131301	-2.35597
40	1	0	-1.64232	8.789015	-1.07286
41	1	0	-2.30727	8.342294	-2.703
42	1	0	-1.69727	5.936997	-2.32747
43	1	0	-3.21328	6.655389	0.086341
44	7	0	0.412235	5.68397	-0.80632
45	6	0	1.526781	5.36373	-0.01129
46	6	0	1.872186	5.983146	1.133009
47	6	0	2.37336	4.245405	-0.59242
48	8	0	2.491454	4.111781	-1.82986
49	1	0	0.454567	5.364694	-1.75234
50	1	0	2.769246	5.701873	1.697741
51	1	0	1.280416	6.80145	1.567679
52	7	0	2.975685	3.386566	0.292626
53	6	0	3.710389	2.230817	-0.16859
54	6	0	3.843178	1.191778	0.977846
55	8	0	4.303565	1.54292	2.083375
56	6	0	5.13323	2.540051	-0.6389
57	1	0	3.132741	1.798188	-1.04469
58	1	0	5.611768	1.595322	-0.99207
59	1	0	5.745734	2.966107	0.191166
60	1	0	5.10082	3.269239	-1.48433
61	1	0	2.905597	3.530548	1.273217
62	7	0	11.02277	-1.74683	-1.28445
63	6	0	12.40456	-1.51018	-1.2966
64	6	0	13.30789	-2.04824	-2.13782
65	6	0	12.85768	-0.57053	-0.19178
66	8	0	12.43507	-0.69739	0.972583
67	1	0	14.37456	-1.80164	-2.06754
68	1	0	13.03847	-2.75983	-2.93148
69	1	0	10.55013	-1.49068	-0.44171
70	7	0	13.75807	0.40802	-0.57228
71	6	0	14.30599	1.387168	0.270003

72	6	0	13.87948	1.700006	1.508332
73	6	0	15.45591	2.145081	-0.36409
74	7	0	16.51897	2.473258	0.433223
75	8	0	15.44726	2.451095	-1.57461
76	1	0	14.35901	2.490455	2.098237
77	1	0	13.03207	1.196737	1.995692
78	1	0	13.99689	0.485696	-1.54058
79	1	0	17.27711	2.980277	0.048626
80	1	0	16.54463	2.21325	1.38508
81	6	0	2.765874	-1.29564	2.69111
82	7	0	1.444195	-1.41962	2.568628
83	16	0	3.317496	-1.18059	4.324473
84	6	0	0.865348	-1.43515	3.833992
85	6	0	1.76862	-1.31232	4.891535
86	6	0	-0.59894	-1.5577	4.073553
87	8	0	-1.08378	-1.24942	5.182304
88	1	0	1.466543	-1.29464	5.940361
89	6	0	-4.74854	-6.43622	3.097092
90	6	0	-3.61695	-6.73692	3.987537
91	6	0	-5.14109	-5.18852	2.736549
92	7	0	-4.52203	-4.00537	3.198194
93	16	0	-7.30629	-6.45579	1.541404
94	6	0	-8.3875	-5.53785	0.45849
95	8	0	-8.39145	-4.1043	-1.90741
96	6	0	-6.3124	-5.04551	1.839102
97	6	0	-7.73926	-3.56395	-0.99167
98	7	0	-6.67152	-3.94094	1.253584
99	6	0	-7.87892	-4.0785	0.455125
100	1	0	-8.6643	-3.41238	0.929598
101	1	0	-8.36929	-5.98047	-0.56653
102	1	0	-9.43121	-5.58856	0.843562
103	1	0	-5.29149	-7.3089	2.68865
104	1	0	-3.57465	-7.82836	4.222271
105	1	0	-3.70136	-6.16834	4.948119
106	1	0	-2.65314	-6.43672	3.495198
107	1	0	-5.14713	-3.24671	3.395509
108	6	0	-6.82579	-1.86932	-2.529
109	7	0	-6.9734	-2.4407	-1.21124
110	6	0	-6.72254	-0.30534	-2.47635
111	6	0	-6.4584	0.25163	-3.86671
112	8	0	-5.72268	0.105509	-1.55127
113	6	0	-8.0497	0.270281	-1.90848
114	6	0	-8.00723	1.780904	-1.76897
115	8	0	-9.07093	-0.13691	-2.81202
116	1	0	-7.76169	-2.10818	-3.1273
117	1	0	-6.29789	1.355592	-3.80115
118	1	0	-7.3405	0.051394	-4.52179
119	1	0	-5.54857	-0.2028	-4.32365

120	1	0	-4.86132	0.005659	-1.97697
121	1	0	-8.24264	-0.18311	-0.89535
122	1	0	-9.89614	0.236289	-2.48075
123	1	0	-8.91044	2.138463	-1.21835
124	1	0	-7.98728	2.272557	-2.7708
125	1	0	-7.09322	2.0773	-1.19642
126	1	0	-6.33384	-2.11788	-0.51853
127	6	0	-5.64377	-2.46562	-3.25871
128	7	0	-4.37299	-2.26003	-2.90559
129	16	0	-5.83895	-3.52756	-4.59633
130	6	0	-3.53425	-2.95987	-3.76312
131	6	0	-4.19835	-3.70335	-4.7421
132	6	0	-2.0485	-2.88295	-3.68852
133	8	0	-1.34791	-3.35968	-4.60374
134	1	0	-3.68145	-4.30433	-5.49338
135	6	0	2.279703	-2.81244	0.076696
136	7	0	1.857378	-2.06101	-1.00952
137	6	0	1.375611	-3.79475	0.483822
138	6	0	0.63915	-2.46892	-1.38746
139	16	0	0.010852	-3.76773	-0.46036
140	6	0	-0.10795	-1.86599	-2.55266
141	7	0	-1.48676	-2.30468	-2.56066
142	6	0	0.036793	-0.31609	-2.55701
143	6	0	-0.42292	0.276448	-3.87567
144	8	0	-0.82417	0.226783	-1.53298
145	1	0	1.531461	-4.48377	1.311801
146	1	0	0.397116	-2.2367	-3.50238
147	1	0	-2.08262	-1.82058	-1.92269
148	1	0	1.11199	-0.04344	-2.36753
149	1	0	-0.23561	1.377263	-3.87978
150	1	0	-1.51461	0.106699	-4.03241
151	1	0	0.145057	-0.1933	-4.71384
152	8	0	0.963241	1.102618	-0.50331
153	6	0	-0.26517	0.987711	-0.55007
154	6	0	-1.22048	1.617008	0.405624
155	7	0	-2.53964	1.711484	0.106488
156	6	0	-0.66332	2.129447	1.594495
157	6	0	-3.34094	2.304862	1.011517
158	6	0	-4.81089	2.462329	0.656464
159	8	0	-5.55325	1.353764	1.147286
160	6	0	-1.50331	2.739476	2.535072
161	8	0	0.426183	2.911557	3.897083
162	6	0	-2.87972	2.800199	2.265591
163	6	0	-0.9321	3.334474	3.790302
164	6	0	-5.43761	3.718556	1.32797
165	6	0	-1.01691	4.853846	3.766436
166	6	0	-3.85612	3.334571	3.200075
167	6	0	-5.06296	3.746772	2.788703

168	1	0	-5.55349	0.685511	0.448329
169	1	0	-3.57126	3.356822	4.264589
170	1	0	-5.82395	4.130736	3.481214
171	1	0	0.779285	3.329015	4.691461
172	1	0	-0.56988	5.273125	4.699272
173	1	0	-2.08375	5.174583	3.698742
174	1	0	-0.46581	5.269572	2.885869
175	1	0	-6.56146	3.576278	1.246741
176	1	0	-4.92495	2.515885	-0.46521
177	1	0	-1.5009	2.929632	4.679418
178	6	0	5.833975	-2.25461	-0.06958
179	7	0	4.682952	-2.8262	-0.22305
180	6	0	6.224301	-1.31161	1.034696
181	6	0	3.618424	-2.61093	0.731677
182	6	0	3.736203	-1.24272	1.526492
183	6	0	5.171762	-1.25266	2.120887
184	7	0	3.516294	-0.10951	0.654335
185	1	0	7.200589	-1.63492	1.484892
186	1	0	6.380038	-0.29144	0.588619
187	1	0	5.263454	-2.15233	2.78596
188	1	0	5.334681	-0.33619	2.750209
189	1	0	3.713796	-3.42266	1.521147
190	1	0	2.851818	-0.23337	-0.08243
191	6	0	6.873534	-2.52664	-1.08109
192	7	0	8.166961	-2.19942	-0.94401
193	16	0	6.492875	-3.30619	-2.56597
194	6	0	8.855399	-2.59672	-2.07791
195	6	0	8.062614	-3.21729	-3.05349
196	6	0	10.31861	-2.40099	-2.28221
197	8	0	10.85496	-2.80843	-3.3315
198	1	0	8.467836	-3.58124	-4.00095
199	1	0	0.42206	2.049002	1.7774